

**STRUCTURAL ELECTROCHEMISTRY AND BIOMIMETIC
SENSING CHARACTERISTICS OF POLYINDOLE AND
POLY(3,4-ETHYLENEDIOXYTHIOPHENE) BASED
MATERIALS**

*Thesis Submitted to
the University of Calicut for the
Award of*

DOCTOR OF PHILOSOPHY IN CHEMISTRY

By

LIJIN RAJAN

Under the Supervision of

Dr. YAHYA A. I.



DEPARTMENT OF CHEMISTRY

UNIVERSITY OF CALICUT

KERALA-673 635

MAY 2024

CERTIFICATE

This is to certify that the thesis entitled “**Structural Electrochemistry and Biomimetic Sensing Characteristics of Polyindole and Poly(3,4-ethylenedioxythiophene) Based Materials**” submitted by **Lijin Rajan** to the University of Calicut for the award of the degree of Doctor of Philosophy in Chemistry, is an authentic record of research work carried out at the Department of Chemistry, of the University of Calicut under my guidance and supervision. The contents of the thesis have been checked for plagiarism using the software ‘iThenticate’ and the similarity index falls under permissible limit, and I further certify that the thesis or part has not previously formed the basis for the award of any degree/diploma/ associate ship of any other University or Institute. The corrections/suggestions recommended by the adjudicators have been incorporated in the thesis and the content in the thesis and the soft copy are one and the same.

University of Calicut

Dr. Yahya A.I.

Associate Professor

Department of Chemistry

University of Calicut

DECLARATION

I, **Lijin Rajan**, hereby declare that thesis entitled “**Structural Electrochemistry and Biomimetic Sensing Characteristics of Polyindole and Poly(3,4-ethylenedioxythiophene) Based Materials**” submitted to the University of Calicut by me, is a bonafide record of my research work done under the supervision and guidance of **Dr. Yahya A. I.**, Associate Professor, Department of Chemistry, University of Calicut, for the award of the degree of Doctor of Philosophy in Chemistry under the Faculty of Sciences, University of Calicut, Kerala. The contents of this thesis have not been presented previously for the award of any Degree/Diploma in any other University or Institution. I also declare that the thesis is free from A. I. generated contents.

University of Calicut

Lijin Rajan

Dedicated to...

***All martyrs who gave their life for the human
liberation***

ACKNOWLEDGEMENT

Throughout these research days, I was never alone. As I reach the successful completion of this thesis, I am deeply appreciative of those who supported me with their care, guidance, and encouragement. Their presence has been invaluable, and I cherish the memories of their support with profound love and gratitude. First and foremost, I would like to express my deep gratitude to my dear research guide Dr. Yahya A I for his immense support, guidance, patience, love and friendship. His mentorship significantly shaped my research and perspective. I owe a great deal to his expertise, encouragement, and insightful feedback. I deeply appreciate the freedom and resources he provided for my research endeavors. He exemplifies how a guide can transform the research journey into a more enjoyable experience. I recall his humility with utmost gratitude. Without a supervisor like him, this journey wouldn't have been as smooth.

I would like to express my hearty thanks to Dr. Rajeev S Menon, the Head of the Department of Chemistry, and the former HODs of the department for providing me with all the facilities to carry out my research work. I would also like to express my sincere gratitude to Prof. P Raveendran, Prof. Abraham Joseph and Prof. N K Renuka for their valuable suggestions and encouragement. I would also extend my gratitude to all faculty members of the department. I extend my appreciation to the lab assistants, and other non-teaching staff members in this department for their invaluable assistance and support. I also reflect with gratitude on my past teachers,

appreciating the invaluable life lessons and knowledge they imparted to me.

I remember with gratitude the present and former office staff, including Jinson Chetan, Sathi Chechi, Beenechi, Shiny Chechi, Premetan, and Rajani Chechi, whose love and support have transcended the boundaries of mere work.

I am extremely thankful to Dr. Mohamed Shahin Thayyil, Professor, Department of Physics, University of Calicut and his research group for providing me necessary arrangement and help for electrical characterization.

I thank KSCSTE for the financial assistance availed during my Ph.D. I would also like to acknowledge CSIF, University of Calicut, CeNS Bengaluru, IIT Madras, STIC CUSAT and NIT Calicut for the analysis facilities used for the completion of this research work. I express my sincere gratitude to Prof. Toribio F. Otero, Prof. Edwin Jager, Dr. Jose G. Martinez for their guidance and support. I want to take this moment to express my heartfelt appreciation and gratitude to Dr. Shabeeba, Dr. Sidheekha, Siva, Roopasri, Razana, Afeefa, and Sivettan, my group members for their unwavering support, love and care throughout my research period. I am also thankful to Madhav, Anu and Athira for fostering a friendly atmosphere in the lab and offering extensive support with this thesis work.

I am extremely thankful to Jijiletan for his valuable suggestions, love and friendship. I am so thankful for the friendship and brotherhood shared with Sankar and Krishnaraj. My heart is overwhelmed with gratitude and love as I think of Sowmya, Akhilechi, Anjitha, Tanu,

Harsha and, my friends who turned into my family. I remember with gratitude Vibi and Shyvindettan for their support and love. Also, I extend my sincere thanks to my lab mates Dr. Varsha, Anjali, Nidhisha, Amrutha, and Arya. I am thankful to Sruthi, Neethu, Amrutha, Nimisha, Dany, Haritha, Aparna, and Jai for their love and care. Their friendship and moments with them made my life more beautiful.

I am forever grateful to my comrades of AKRSA, SFI, DYFI Eruvatty east, and Rakthasakshi mandhiram Kuttian Bazar for their immense love support, care and comradeship. I would like to extend my gratitude to Chunk Broz for their support and love. I would like to convey my heartfelt appreciation and affection to Anju, Nikil, Sangeetha and Roshima for their love and support. I am indebted to all the researchers of the Department of Chemistry for their kind words and generosity. I would like to announce my fondness and thankfulness to every individual, whose kind words or gestures influenced me throughout my entire life.

I cannot complete this thesis without remembering the name of Deepak who supported me through every crisis during my research period. I remember him with much love, care and gratitude for being with me, for sharing tea time together, for being by my side day and night and most importantly, for being a brother to me. Along with that two names I remember with love and gratitude are Siva and Dheeraj. I remember them with a lot of love for making my days happy and laughing, and de-stressing with jokes and playful slaps, more so than any specific events in my research career. Athira is the

name that I remember with the fondest gratitude of my research life. Dear Kanjan, thank you for being love, for being with me, and for being a sister. I am forever grateful to dear vellya for her care, love and support.

“This Journey would never have been complete without my other half accompanying me on the never-ending journey of life. Dear Ammu there are no words to express my gratitude or appreciation for you- just a thousand kisses”.

During this research period, I experienced two biggest losses of my life. My dear Kunja and my Pothandi. Not a single moment passes without remembering you both. Your memeories will keep me strong.

On this occasion, I fondly remember my beloved brother, Appu. Hugging you with love, for ensuring my absence was not felt as a deficiency by our parents and for diligently managing my responsibilities even in my absence.

“Above all, Amma and Achan. I dedicate this life to you. The sweat you shed on the soil and the paths you trod have made me who I am today. Kisses of love to you, for giving me freedom in my ways, for being with me and for being my greatest refuge on earth”

Finally, I would like to convey my deepest gratitude to everybody whose kind words and support led to the completion of this thesis.

Lijin Rajan

TABLE OF CONTENTS

	Page No.
<i>Preface</i>	i
<i>List of tables</i>	vi
<i>List of figures</i>	vii
<i>List of abbreviations</i>	xx
Chapter 1	1 -
Introduction	74
1.1. Conducting polymers	1
1.1.1. Doping in CPs	4
1.1.2. Example of CPs	6
1.1.3. The mechanism of charge transport in CPs	8
1.1.4. The influencing factors on CP conductivity	11
1.1.5. Polymerization initiation	12
1.1.5.1. Electrochemical initiation	12
1.1.5.2. Chemical initiation	13
1.1.6. Applications of CPs	14
1.1.7. Limitations of CPs	16
1.2. Hydrogels an overview- introduction	18
1.2.1. CP/ hydrogel hybrid system	19
1.2.2. Fabrication methods of CP/hydrogel hybrid materials	21
1.2.2.1. In situ chemical polymerization	21
1.2.2.2. Physical mixing and crosslinking	22
1.2.2.3. Layer-by-Layer assembly	22
1.2.2.4. Electrochemical deposition	22
1.2.2.5. Template-assisted synthesis	23
1.2.2.6. Covalent crosslinking method	23
1.2.3. Applications of CP/hydrogel hybrid materials	24
1.2.3.1. Flexible electronics and wearable devices	24
1.2.3.2. Sensors and biosensors	24
1.2.3.3. Drug delivery systems	25

1.2.3.4.	Tissue engineering and regeneration	25
1.2.3.5.	Artificial muscles	25
1.2.3.6	Supercapacitors	26
1.3.	Polyindole (PIN)-introduction	26
1.3.1.	Molecular structure of PIN	28
1.3.2.	Synthesis of PIN	30
1.3.2.1.	Chemical oxidative synthesis	30
1.3.2.2.	Electrochemical synthesis	30
1.3.2.3.	Interfacial synthesis	31
1.3.3.	Mechanism of oxidative polymerization	32
1.3.4.	Application of PIN	34
1.3.4.1.	Electrochromics	34
1.3.4.2.	Sensors	34
1.3.4.3.	Electrocatalysis	35
1.3.4.4.	Batteries	36
1.3.4.5	Supercapacitors	36
1.3.5.	Limitations of PIN	37
1.4	Poly(3,4-ethylenedioxythiophene) (PEDOT) - introduction	41
1.4.1.	Molecular structure	42
1.4.2.	Synthesis of PEDOT	43
1.4.2.1.	The coupling of halogen derivatives of EDOT mediated by transition metals	43
1.4.2.2.	Electrochemical polymerization	44
1.4.2.3.	Chemical oxidative polymerization	44
1.4.3.	Applications of PEDOT	46
1.5.	Supercapacitors	49
1.5.1.	Electrical double layer capacitor	50
1.5.2.	Pseudocapacitor	52
1.5.3.	Hybrid supercapacitor	53
1.6.	Electrochemistry of CPs-introduction	55
1.6.1.	Oxidation (p-doping)	56

1.6.2.	Reduction (n-doping)	59
1.7	CPs as reversible multi-step macromolecular motors	59
1.8	Biomimetic properties of CPs	61
1.9	The present work	63
	References	66
 Chapter 2		77
Materials and methods		-
		101
2.1.	Materials	77
2.2.	Synthesis and fabrication methods	78
2.2.1.	Synthesis of polyindole	78
2.2.1.1.	Working electrode fabrication using PIN	79
2.2.2.	Fabrication of PIN/Polyvinyl alcohol film	79
2.2.2.1.	Working electrode preparation using PIN/Polyvinyl alcohol film	80
2.2.3.	Synthesis of Poly (3, 4-ethylenedioxythiophene)	80
2.2.3.1.	Working electrode fabrication using Poly (3, 4-ethylenedioxythiophene)	81
2.2.4.	Fabrication of Poly(3, 4-ethylenedioxythiophene) /Polyvinyl alcohol film	82
2.2.4.1.	Working electrode fabrication using Poly (3, 4-ethylenedioxythiophene) /Polyvinyl alcohol film	83
2.2.4.2.	Fabrication of solid-state Poly (3, 4-ethylenedioxythiophene) /Polyvinyl alcohol device	83
2.3.	Characterization techniques	84
2.3.1.	Fourier Transform Infrared Spectroscopy	85
2.3.2.	UV-Visible Spectroscopy	86
2.3.3.	Thermo Gravimetric Analysis	87

2.3.4.	Field Emission Scanning Electron Microscope	87
2.3.5.	High Resolution Transmission Electron Microscopy	88
2.3.6.	Energy Dispersive X-ray Spectroscopy	89
2.3.7.	Universal Testing Machine	90
2.3.8.	Electrical Conductivity Studies	91
2.4.	Electrochemical Characterizations	93
2.4.1.	Cyclic voltammetry	94
2.4.2.	Chronopotentiometry	96
2.4.3.	Galvanostatic Charge-Discharge	98
2.4.4.	Electrochemical Impedance Spectroscopy	99
	References	100
Chapter 3		102
Electrochemical characterization of polyindole with a special emphasis on its structural electrochemistry		- 129
3.1.	Introduction	102
3.2.	Results and Discussion	103
3.2.1.	FTIR spectra	103
3.2.2.	UV-VIS Spectra	104
3.2.3.	Morphological characterization-FE-SEM	105
3.2.4.	Thermal characterization- TGA	106
3.2.5.	Electrochemical characterization	107
3.2.5.1.	Cyclic voltammetry	107
3.2.5.2.	Coulovoltammogram	111
3.2.5.3.	Structural faradaic process in PIN	113
3.2.5.4.	Influence of cathodic potential limit on voltammetric and coulovoltammetric responses	119
3.2.5.5.	The influence of anodic potential limit on voltammetric and coulovoltammetric response	124
3.3.	Conclusion	127
	References	128

Chapter 4	130
Polyindole as Biomimetic sensors of electrical, chemical, and thermal working environment	- 157
4.1. Introduction	130
4.2. Results and Discussion	132
4.2.1. Reactive sensing ability of PIN towards the working electrical, chemical, and thermal ambient; chronopotentiometry	132
4.2.1.1. Sensing of electrical working condition- current sensor	133
4.2.1.2. Sensing chemical working condition- concentration sensor	134
4.2.1.3 Sensing of thermal working condition- temperature sensor	136
4.2.2. Reaction-driven sensing characteristics of PIN: A voltammetric investigation	140
4.2.2.1. Sensing electrical working condition	140
4.2.2.2. Sensing of chemical working conditions- concentration sensor	145
4.2.2.3. Sensing thermal working condition- Temperature sensor	148
4.3. Conclusions	154
References	156
Chapter 5	158
Cooperative actuation of polyindole/polyvinyl alcohol hybrid film and their applicability as a free standing electrode material for self-sensing their working ambient	- 196
5.1. Introduction	158
5.2. Results and Discussion	160
5.2.1. FTIR-ATR spectra	160

5.2.2.	Thermo Gravimetric Analysis	161
5.2.3.	FE-SEM and elemental analysis	162
5.2.4.	High-resolution transmission electron microscopy-(HRTEM)	163
5.2.5.	Mechanical characterization-UTM analysis	164
5.2.6.	Electrical Conductivity	166
5.2.7.	Electrochemical characterization	166
5.2.7.1.	Cyclic voltammetry	166
5.2.7.2.	Reaction-driven sensing characteristics of PIN/PVA hybrid film: Chronopotentiometric study	169
5.2.7.2.1.	Sensing electrical working conditions: Current Sensor	169
5.2.7.2.2.	Sensing chemical working conditions- Concentration sensing	171
5.2.7.2.3.	Sensing thermal working condition-Temperature sensing	172
5.2.7.3.	Cooperative actuation induced working ambient sensing ability of PIN/PVA film: Voltammetric study	175
5.2.7.3.1.	Cooperative actuation of PIN/PVA film senses the electrical working condition	176
5.2.7.3.2.	Cooperative actuation of PIN/PVA film senses chemical working condition	182
5.2.7.3.3.	Cooperative actuation of PIN/PVA film senses the	187

	thermal working condition	
5.3.	Conclusion	191
	References	193
Chapter 6		
	Electrochemical characterization of Poly(3, 4-ethylene dioxithiophene) with a special emphasis on its structural electrochemistry and their biomimetic sensing characteristics	197
		-
		249
6.1.	Introduction	197
6.2.	Results and Discussion	198
6.2.1.	FTIR spectra	198
6.2.2.	TGA	199
6.2.3.	FE-SEM	200
6.2.4.	HR-TEM	201
6.2.5.	Electrical Conductivity	201
6.2.6.	Electrochemical characterization	202
6.2.6.1.	Voltammetric analysis	202
6.2.6.2.	Coulovoltammogram	206
6.2.7.	Structural Faradaic Processes in PEDOT	207
6.2.7.1.	Influence of cathodic potential limit on voltammetric and coulovoltammetric responses	211
6.2.7.2.	Influence of anodic potential limit on voltammetric and coulovoltammetric responses	216
6.2.8.	Sensing ability of PEDOT electrode material towards the working electrical, chemical, and thermal ambient using voltammetric study	219
6.2.8.1.	Sensing electrical working condition	220
6.2.8.2.	Chemical working condition sensing - concentration sensor	226

6.2.8.3.	Sensing Thermal working condition - Temperature sensor	230
6.2.9.	Reaction-driven sensing characteristics of PEDOT towards the working ambient (electrical, chemical, and thermal): Chronopotentiometric investigation	236
6.2.9.1.	Sensing electrical working conditions: Current Sensor	236
6.2.9.2.	Sensing chemical working conditions: Concentration Sensor	238
6.2.9.3.	Sensing thermal working conditions: Temperature Sensor	239
6.3.	Conclusion	244
	References	247

Chapter 7		250
Cooperative actuation of PEDOT/PVA hybrid film and their applicability as a sensing macromolecular motor: fabrication of sensing supercapacitor device		- 303
7.1.	Introduction	250
7.2.	Results and discussion	253
7.2.1.	FTIR-ATR spectra	253
7.2.2.	FE-SEM and EDX analysis	254
7.2.3.	TGA analysis	255
7.2.4.	Mechanical characterization- UTM analysis	256
7.2.5.	Electrochemical characterization	257
7.2.5.1.	Voltammetric analysis	257
7.2.5.2	Coulovoltammogram	260
7.2.5.3.	Sensing capability of PEDOT/PVA film electrode towards the working ambient using chronopotentiometry	262
7.2.5.3.1.	Sensing of electrical working condition- current sensor	262

7.2.5.3.2.	Sensing of chemical working condition - concentration sensor	264
7.2.5.3.3.	Sensing of thermal working condition-temperature sensor	267
7.2.5.4.	Cooperative actuation induced sensing ability of PEDOT/PVA film towards the working electrical, chemical and thermal ambient using voltammetric study	269
7.2.5.4.1.	Cooperative actuation of PEDOT/PVA film senses the electrical working condition	270
7.2.5.4.2.	Cooperative actuation of PEDOT/PVA film senses the chemical working condition	274
7.2.5.4.3.	Cooperative actuation of PEDOT/PVA film senses the thermal working condition	279
7.2.5.5.	Sensing supercapacitor based on PEDOT/PVA hybrid film	283
7.2.5.5.1.	Super capacitance performance of PEDOT/PVA film	284
7.2.5.5.1.1.	PEDOT/PVA film as sensing supercapacitor	288
7.2.5.6.	Symmetric supercapacitor device based on PEDOT/PVA film	289

7.2.5.6.1.	Reactive sensing characteristics of the PEDOT/PVA supercapacitor device	294
7.2.5.6.2.	PEDOT/PVA supercapacitor device as a simultaneous sensing supercapacitor	296
7.3.	Conclusion	298
	References	301
	Chapter 8	304
	Summary and Future Outlook	-
		309
	List of publications and presentations	312

Preface

For the last three decades conducting polymers (CPs) have garnered considerable interest among the scientific community because of their fascinating electrical and electrochemical characteristics, which have spurred a wide range of applications. Majority of their applications were focused on considering them as dry materials where their composition remains constant. In the wet state CPs behave like gel and their properties are largely governed by their composition. This thesis focuses on investigating the composition-dependent, giant non-stoichiometric properties of CPs, aiming to demonstrate their inherent biomimetic reactive sensing characteristics under various electrochemical reaction controls. The ultimate goal is to contribute to the realization of engineers' aspirations in fabricating a device or a self-sensing motor capable of simultaneously sensing their surrounding conditions while working, without the need of additional connectivities. While our research group has previously established the reactive sensing capabilities of polypyrrole and polyaniline, this study aims to validate the generalizability of this self-sensing properties of two prominent CPs: polyindole (PIN) and poly(3,4-ethylenedioxythiophene) (PEDOT). The thesis delves into the fundamental structural electrochemistry and explores the conformational changes during the electrochemical reaction of these two CPs, a subject that has been not extensively explored to date.

This thesis is divided into eight chapters

Chapter 1 provides brief physical and chemical characteristics and applications of CPs and their hydrogel systems. This chapter also provides a brief description of the synthesis, properties and applications of PIN and PEDOT. Special emphasis is given to describing the electrochemistry of CPs and their biomimetic reactive sensing capabilities. A brief introduction to supercapacitor application is also present.

Chapter 2 offers an overview of the experimental procedures and methodologies employed in the present investigation. This chapter also provides the details of the chemicals used and the characterization techniques. Additionally, this chapter offers a detailed explanation of different electrochemical techniques employed for the present study such as cyclic voltammetry (CV), chronopotentiometry, galvanostatic charge-discharge (GCD) and electrochemical impedance spectroscopy (EIS).

Chapters 3 to 7 are the working chapters focusing on our research objectives.

Chapter 3 entitled *Electrochemical characterization of polyindole with a special emphasis on its structural electrochemistry* explores the basic characterization and electrochemistry of PIN. Further, this chapter investigates the structural electrochemistry and electrochemical-induced conformational changes in chemically polymerized PIN. For the first time, we have applied the coullovoltammetric technique to explore the structural Faradaic processes occurring during the electrochemical redox reaction of PIN. Additionally, this chapter examines the consumed charge during

each structural process and optimizes the potential window for the electrochemical reactions of PIN without having any parallel irreversible process.

Chapter 4: *Polyindole as Biomimetic sensors of electrical, chemical and thermal working environment.* This chapter deals with the reactive sensing ability of PIN towards the working environmental variables such as electrical, chemical and thermal ambient, and is explored using CV and chronopotentiometry. The redox charge and the electrical energy consumed during the reaction were proved as the sensing parameters. A theoretical foundation for validating the sensing characteristics of PIN is also developed in this chapter.

Chapter 5: *Cooperative actuation of polyindole/polyvinyl alcohol hybrid film and their applicability as a free-standing electrode material for self-sensing working ambient.* This chapter explains the fabrication of a free-standing electrode material based on PIN using PVA as a template and their electrochemical characteristics leading to their potential application as a biomimetic reactive sensor of their working ambient (electrical, chemical and thermal conditions). The reactive sensing characteristics of the PIN/PVA film are explored and using QV and chronopotentiometry. This chapter also introduces a novel concept, cooperative actuation (involving reversible conformational movement) of the macromolecular motors formed by the polymer chain of the hybrid film. Additionally, the chapter provides a comprehensive explanation of how the working variables influence the cooperative actuation of the film.

Chapter 6: *Electrochemical characterization of Poly(3, 4-ethylene dioxythiophene) with a special emphasis on its structural electrochemistry and biomimetic sensing characteristics* provides insight into the fact that reactive sensing property is a general property of all CPs by taking PEDOT as an example. The structural Faradaic process of the chemically synthesized PEDOT was explored for the first time, along with it this chapter also explores the biomimetic reactive sensing capabilities of PEDOT using QV and chronopotentiometry. The chapter also includes calculations of consumed redox charge and consumed electrical energy based on voltammetry and chronopotentiometry respectively. Additionally, we have optimized the actual potential window for the redox reaction of PEDOT by utilizing the QV technique.

Chapter 7: *Cooperative actuation of PEDOT/PVA hybrid film and its applicability as a biomimetic sensing macromolecular motor.*

This chapter addresses the possibilities of designing a self-sensing motor specifically a sensing supercapacitor based on the fabricated PEDOT/PVA flexible hybrid films. This chapter also explores the biomimetic reactive sensing characteristics of PEDOT/PVA film using chronopotentiometry. In addition, this chapter also has a look into cooperative actuation and examines how the working environment influences the conformational movement of the PEDOT chains during its electrochemical reaction. Additionally, the charge storage capability of the hybrid film and simultaneous sensing

ability of the fabricated supercapacitor device (self-sensing motor) is also explored.

Chapter 8: *Summary and future outlook* presents an overview of the key discoveries and significant aspects of the current study. It also addresses the future outlook of the present research carried out. This chapter also have a look into the possibility of developing biomimetic sensing artificial muscles, proprioceptive devices, sensing robots, artificial synaptic devices etc. by using fabricated hybrid films.

LIST OF TABLES

Table No.	Table caption	Page No.
1.1	Examples of CPs	7
2.1	List of materials/chemicals used for the entire study and their manufacturer	77
3.1	Structural Faradaic process in PIN, potential ranges and the consumed electrical charges	118
3.2	Charges consumed during different cathodic potential limit	123
3.3	Charge consumed during different anodic potential limit	126
5.1	The Mechanical properties of the bare PVA and PIN/PVA film in dry and wet state.	165
6.1	Structural faradaic processes in PEDOT, potential ranges and corresponding electrical charges	211
6.2	Charge consumed at various cathodic potential limits	214
6.3	Charge consumed at each anodic potential limits	218
7.1	The Mechanical properties of the bare PVA and PEDOT/PVA film in dry and wet state.	256
7.2	Areal capacitance of PEDOT/PVA film at different scan rates	285
7.3	Areal capacitance of PEDOT/PVA film at different current densities	286
7.4	Areal capacitance of the supercapacitor device at different scan rates	290
7.5	Specific capacitance of supercapacitor device at different current densities	291

LIST OF FIGURES

Figure No.	Figure captions	Page No.
1.1	Tunable conductivity of CPs	3
1.2	Charge transfer mechanism in polyacetylene	9
1.3	The band structure of polypyrrole	10
1.4	The technological applications of CPs	16
1.5	The doped and de-doped structures of PIN	30
1.6	The schematic representation of polymerization of PIN	33
1.7	The molecular structure of PEDOT	43
1.8	The schematic representation of chemical oxidative polymerization of PEDOT	45
1.9	The chemical structure of PEDOT: PSS	45
1.10	The schematic representation of charging-discharging in EDLC	51
1.11	The schematic representation of charging-discharging in pseudocapacitor	53
1.12	The schematic representation of the prevailing anion exchange mechanism in CP	57
1.13	The schematic representation of the prevailing cation exchange mechanism in CP	58
1.14	The conformational movement during redox reaction in CP	60
1.15	The composition-dependent properties and corresponding biomimetic applications of CP	61
1.16	Schematic representation of biomimicking property of CPs	63
2.1	Synthesis method of PIN	78
2.2	Schematic representation of fabrication of PIN/PVA hybrid film	80

2.3	Schematic representation of Synthesis of PEDOT	81
2.4	Schematic representation employed for the Fabrication method of PEDOT/PVA hybrid film	82
2.5	Schematic representation of fabrication of PEDOT/PVA-based symmetric solid-state device	83
2.6	a) Square current waves applied to the material. b) Anodic and cathodic potential evolution with respect to time (chronopotentiogram or charge-discharge).	97
3.1	FTIR spectrum of PIN	104
3.2	UV-VIS spectrum of PIN	105
3.3	(a) FE-SEM image of PIN. (b) EDX data of PIN	106
3.4	TGA curve of PIN	106
3.5	CV curve of PIN	107
3.6	Schematic representation of polyindole oxidation mechanism	108
3.7	(a) CVs of PIN at different scan rates. (b) Linear fit of anodic and cathodic peak current with square root of scan rate	110
3.8	Swelling and de-swelling of PIN during oxidation and reduction	111
3.9	QV of PIN	112
3.10	Different structural processes during the electrochemical reaction from QV in 1 M HCl at 25 mVs ⁻¹	115
3.11	(a) CVs obtained for PIN in 1 M HCl at 25 mVs ⁻¹ from different cathodic potential limits. (b) QVs obtained by integration of the CVs	120
3.12	(a) Charge consumed in the oxidation and reduction of PIN and (b) irreversible reduction	123

	charge obtained for different cathodic potential limits	
3.13	(a) CVs obtained for PIN in 1 M HCl at 25 mVs ⁻¹ from different anodic potential limits. (b) QVs obtained by integration of the CVs from (a)	124
3.14	QV obtained in 1 M HCl at the scan rate 25 mVs ⁻¹ (a) at the anodic potential limit 0.75 V and (b) at the anodic potential limit 1.1 V	125
3.15	(a) Charge consumed in the oxidation and reduction of PIN and (b) irreversible reduction charge obtained for different anodic potential limits	126
4.1	Chronopotentiograms obtained when different constant (a) anodic and (b) cathodic currents were applied to PIN by passing a constant charge of 3 mC in 1 M HCl solution (c) Electrical energy consumed by the PIN as a function of applied current	134
4.2	Chronopotentiogram obtained from different concentrations of HCl when (a) 0.05 mA and (b) -0.05 mA of current were applied to the PIN for 60s. (c) Electrical energy (U) consumed by the PIN	135
4.3	Chronopotentiogram obtained from different experimental temperatures when (a) +0.1 mA and (b) -0.1 mA of current were applied to the PIN for 60s. (c) The variation of electrical energy (U) consumed during anodic and cathodic processes with temperature	137
4.4	(a) CVs obtained from different scan rates in forward (5 mVs ⁻¹ to 200 mVs ⁻¹) in 1 M HCl at room temperature within the potential window of -0.2 V to 0.75 V. (b) Corresponding coul voltammogram obtained by integrating	141

	the CVs obtained in(a). (c) Linear fit of anodic and cathodic peak current with the square root of scan rate. (d) Logarithmic relation of redox charge consumed during the reaction of PIN obtained from the QV with the scan rate	
4.5	Schematic representation of the extension of reaction at lower and higher scan rates	142
4.6	(a) CVs obtained in different concentrations of aqueous solution of HCl between -0.2 V and 0.75 V at a scan rate of 25mVs ⁻¹ . (b) QV obtained by integrating the voltammograms obtained in (a). (c) logarithmic relation of the charge consumed during the redox reaction of PIN with the electrolyte concentration of aqueous HCl	146
4.7	Schematic representation of extension of reaction at lower and higher concentrations of electrolyte	147
4.8	(a) CVs obtained from experimental temperatures in (20° C to 55° C) in 1 M HCl at 25 mVs ⁻¹ between -0.2 to 0.75 V. (b) Corresponding QV obtained by integrating the CVs (a). (c) Semi-logarithmic relation of redox charge consumed during the reaction of PIN obtained from the QV with the inverse of temperature in Kelvin scale	150
4.9	Schematic representation of the extension of reaction at lower and higher working temperatures	151
5.1	Schematic representation of H-bonding in PIN/PVA hybrid film	160
5.2	FTIR spectrum of PIN and PIN/PVA film	161
5.3	Thermograms of PVA and PIN/PVA films	162

5.4	FE-SEM images of a) PVA film b) PIN/PVA film and EDX of c) PVA film d) PIN/PVA film	163
5.5	HRTEM image of PIN/PVA film	164
5.6	Stress-strain curve of the films (a) in the dry state. (b) In wet state	165
5.7	I-V characteristic of bare PVA film and PIN/PVA hybrid film	166
5.8	a) CV obtained from PIN/PVA film in 1 M HCl against Ag/AgCl electrode at the scan rate of 25 mVs ⁻¹ at room temperature. b) Corresponding QV	168
5.9	a) CVs obtained at different scan rates in 1 M HCl, at room temperature b) Relation of anodic and cathodic peak currents with the square root of scan rates	169
5.10	Chronopotentiograms obtained when different constant (a) anodic and (b) cathodic currents were applied to PIN/PVA hybrid film by passing a constant charge of 3 mC in 1 M HCl solution (c) Electrical energy consumed by the film as a function of applied current (R^2 is the correlation factor)	170
5.11	Chronopotentiogram obtained from different concentrations of HCl when (a) 0.05 mA and (b) -0.05 mA of current were applied to the PIN/PVA hybrid film for 60s. (c) The electrical energy consumed by the film during the reaction is a semi-logarithmic function of electrolyte concentration at room temperature	172
5.12	Chronopotentiogram obtained from different experimental temperatures when (a) +0.1 mA and (b) -0.1 mA of current were applied to the PIN/PVA hybrid film for 60s. (c) The variation	173

	of electrical energy consumed during anodic and cathodic processes with temperature	
5.13	Experimental procedure adopted for the study of cooperative actuation of PIN/PVA film at different electrical working conditions (scan rate)	177
5.14	(a) CVs obtained from different experimental scan rates in increasing (5 mVs^{-1} to 200 mVs^{-1}) and decreasing (200 mVs^{-1} to 5 mVs^{-1}) scan rate direction between 0 V to 0.6 V in 1 M HCl at room temperature. (b) Corresponding QVs	178
5.15	a) CVs obtained in a control scan rate (50 mVs^{-1}) in 1 M HCl between 0 and 0.6 V at room temperature. b) Corresponding QVs	179
5.16	(a) Logarithmic relation of redox charge consumed during the reaction of PIN/PVA film by increasing (forward) and decreasing (backward) the scan rates. (b) Bar diagram of corresponding consumed redox charge during the process	180
5.17	Schematic representation of the reaction extension based on cooperative actuation of the PIN/PVA hybrid film and corresponding QVs	181
5.18	(a) CVs obtained in different concentrations of aqueous solution of HCl for increasing and decreasing the concentration at a scan rate of 25 mVs^{-1} . (b) Corresponding QVs	183
5.19	(a) CVs obtained from the control solution of HCl (0.1 M) between 0 V and 0.6 V at a scan rate of 25 mVs^{-1} . (b) corresponding QVs	184
5.20	A schematic representation of the extension of reaction of PIN/PVA hybrid film in 0.01 M HCl and 1 M HCl	186

5.21	Logarithmic relation of the charge consumed during the redox reaction of PIN/PVA hybrid film with the electrolyte concentration of aqueous HCl	186
5.22	(a) CVs obtained from increasing (10° C to 60° C) and decreasing (60° C to 10° C) the temperature in 1 M HCl at 25 mVs ⁻¹ (b) Corresponding QVs	188
5.23	(a) Semi-logarithmic relation of redox charge consumed during the reaction of PIN/PVA hybrid film by increasing (forward) and decreasing (backward) the temperature (b) Bar diagram of redox charge consumed during the reaction	189
5.24	Schematic representation of the extension of reaction of the PIN/PVA film at 60°C and 10°C and corresponding QV responses	190
5.25	(a) CV obtained in a control temperature (30°C) in 1 M HCl at 25 mVs ⁻¹ . (b) Corresponding QV responses	191
6.1	FTIR spectrum of PEDOT	198
6.2	Thermogram of PEDOT	199
6.3	The FE-SEM image of PEDOT a) at 1 µm b) at 100nm c) EDX data of the PEDOT	200
6.4	a) HR-TEM image of PEDOT b) secondary electron image in EDS elemental mapping of PEDOT c) Carbon in PEDOT d) Oxygen in PEDOT e) Sulphur in PEDOT and APS dopant.	201
6.5	Log-log plot of the frequency dependence of the AC conductivity data of the PEDOT	202
6.6	CV plot of PEDOT	203
6.7	(a) CVs of PEDOT at different scan rates. (b) Linear fit of anodic and cathodic peak currents with the square root of scan rate	205

6.8	QV of PEDOT	206
6.9	Different structural processes during the electrochemical reaction from QV in 1 M NaCl at 25 mVs ⁻¹	208
6.10	(a) Stationary CVs obtained for PEDOT in 1 M NaCl at a scan rate of 25 mVs ⁻¹ from different cathodic potential limits. (b) Corresponding QVs. (c) QVs obtained at the cathodic potential limits of -0.6 V and -1.1 V	212
6.11	(a) Charge consumed in the oxidation and reduction of PEDOT as a function of the cathodic potential limit and (b) irreversible reduction charge obtained for different cathodic potential limits	215
6.12	(a) CVs obtained for PEDOT in 1 M NaCl at a scan rate of 25 mVs ⁻¹ from different anodic potential limits. (b) Corresponding QVs (c) Charge consumed in the oxidation and reduction of PEDOT and (d) irreversible oxidation charge obtained for different anodic potential limits	217
6.13	(a) QVs obtained by integrating the corresponding CVs from 6.5(a). (b) Double logarithmic relation of redox charge consumed during the reaction of PEDOT with the scan rate	221
6.14	Schematic representation of extension of reaction at different scan rates	222
6.15	(a) CVs obtained in different concentrations of an aqueous solution of NaCl at a scan rate of 25 mVs ⁻¹ . (b) Corresponding QVs (c) Double logarithmic relation of the charge consumed during the redox reaction of PEDOT with the electrolyte concentration of aqueous NaCl	228

6.16	Schematic representation of extension of reaction at different concentrations of NaCl	229
6.17	(a) CVs obtained from experimental temperatures (20°C to 55°C) in 1 M NaCl at 25 mVs ⁻¹ (b) Corresponding QVs (c) calibration curve showing the Semi logarithmic relation of redox charge consumed with the inverse of temperature	231
6.18	Schematic representation of extension of reaction at different working temperatures	232
6.19	Chronopotentiograms obtained when different constant (a) anodic and (b) cathodic currents were applied to PEDOT by passing a constant charge of 6 mC in 1 M NaCl solution (c) Electrical energy consumed by the as a function of applied current (R^2 is the correlation factor)	237
6.20	Chronopotentiogram obtained from different concentrations of NaCl when (a) 0.1 mA and (b) -0.1 mA of current were applied to the PEDOT for 60 s. (c) Electrical energy consumed by during the reaction as a logarithmic function of electrolyte concentration	238
6.21	Chronopotentiogram obtained from different experimental temperatures when (a) +0.1 mA and (b) -0.1 mA of current were applied to the PEDOT for 60 s. (c) The variation of electrical energy consumed during anodic and cathodic processes with temperature	241
7.1	FTIR-ATR spectra of PVA and PEDOT/PVA hybrid films	253
7.2	FE-SEM images of a) PVA b) PEDOT/PVA and EDX of c) PVA d) PEDOT/PVA	254
7.3	TGA of PVA and PEDOT/PVA films	255

7.4	Stress-strain relation curve of the films (a) in dry state. (b) In wet state	257
7.5	CV of PEDOT/PVA film	257
7.6	(a) CVs of PEDOT/PVA film at different scan rates (b) Linear fit of anodic and cathodic peak currents with the square root of scan rates	260
7.7	Coulovoltammogram of PEDOT/PVA	261
7.8	Chronopotentiograms obtained when different constant (a) anodic and (b) cathodic currents were applied to PEDOT/PVA hybrid film by passing a constant charge of 6mC in 1 M NaCl solution (c) Electrical energy consumed by the film as a function of applied current (R^2 is the correlation factor)	263
7.9	Chronopotentiogram obtained from different concentrations of aq. NaCl when (a) 0.1 mA and (b) -0.1 mA of current were applied to the PEDOT/PVA film for 60s. (c) Electrical energy consumed during the reaction as a logarithmic function of electrolyte concentration	265
7.10	Chronopotentiogram obtained from different experimental temperatures when (a) +0.1 mA and (b) -0.1 mA of current were applied to the PEDOT/PVA film for 60s. (c) The variation of electrical energy consumed during anodic and cathodic processes with temperature	268
7.11	(a) CVs obtained from PEDOT/PVA film at different experimental scan rates in increasing (5 mVs^{-1} to 200 mVs^{-1}) and decreasing (200 mVs^{-1} to 5 mVs^{-1}) scan rate in 1 M NaCl at room temperature. (b) Corresponding QVs	270
7.12	a) CVs obtained from PEDOT/PVA film in a control scan rate (50 mVs^{-1}) in 1 M NaCl at room temperature. b) Corresponding QVs	271

7.13	Logarithmic relation of redox charge consumed during the forward and backward reaction of PEDOT/PVA film obtained from the coulovoltammogram with the scan rate	273
7.14	Schematic representation of the redox reaction extension based on the cooperative actuation of the PEDOT/PVA film at 10 mVs ⁻¹ and at 200 mVs ⁻¹	274
7.15	(a) CVs obtained in different electrolyte concentrations of NaCl at a scan rate of 25 mVs ⁻¹ (b) corresponding QV	275
7.16	Logarithmic relation of the charge consumed during the redox reaction of PEDOT/PVA hybrid film with the electrolyte concentration of aqueous NaCl	276
7.17	(a) CVs obtained in a control solution of NaCl (0.1 M) at a scan rate of 25 mVs ⁻¹ . (b) Corresponding QVs	277
7.18	Schematic representation of the redox reaction extension based on the cooperative actuation of the PEDOT/PVA film in 0.01 M NaCl and in 1 M NaCl	278
7.19	(a) CVs obtained from PEDOT/PVA film for increasing and decreasing the temperatures in 1 M NaCl at 25 mVs ⁻¹ (b) Corresponding QV obtained	279
7.20	(a) CVs obtained in a control temperature (30°C) in 1 M NaCl at 25 mVs ⁻¹ . (b) Corresponding QV responses	280
7.21	Semi-logarithmic relation of redox charge consumed during the forward and backward reaction of PEDOT/PVA film obtained from the coulovoltammogram with the inverse of temperature.	281

7.22	Schematic representation of the extension of the redox reaction based on cooperative actuation of the PEDOT/PVA film at 55° C and 20° C	282
7.23	Schematic representation of charging and discharging in PEDOT/PVA film-based supercapacitor	283
7.24	(a) CVs of PEDOT/PVA film at different scan rates. (b) GCD of PEDOT/PVA film at different current densities. (c) Variation of areal capacitance to the scan rates. (d) Variation of specific capacitance with the current densities obtained	284
7.25	Cyclic stability of PEDOT/PVA film for 1500 cycle	287
7.26	(a) Normalized discharge curve from GCD of PEDOT/PVA film for different current densities (b) consumed electrical energy as a function of applied current (R^2 is the correlation factor)	288
7.27	(a) CVs of supercapacitor device at different scan rates. (b) GCD curves at different current densities. (c) Variation of specific capacitance with respect to the scan rates (d) Variation of specific capacitance with respect to different current densities	290
7.28	Nyquist plot of solid-state device	292
7.29	Cyclic stability of solid-state device for 1700 cycle	293
7.30	Chronopotentiograms obtained when different constant (a) anodic and (b) cathodic currents were applied to the supercapacitor device by passing a constant charge of 6 mC (c) Electrical energy consumed by the device as a function of applied current (R^2 is the correlation factor)	294

7.31	Chronopotentiogram obtained from different experimental temperatures when (a) +0.1 mA and (b) -0.1 mA of current were applied to the supercapacitor device for 60s. (c) The variation of electrical energy consumed during the anodic and cathodic processes with temperature	295
7.32	(a) Normalized discharge curve from GCD of the PEDOT/PVA supercapacitor device of PEDOT/PVA film for different current densities (b) Electrical energy consumed by the supercapacitor device as a function of applied current (R^2 is the correlation factor). (c) Logarithmic relation of specific capacitance with consumed electrical energy	297

LIST OF ABBREVIATIONS

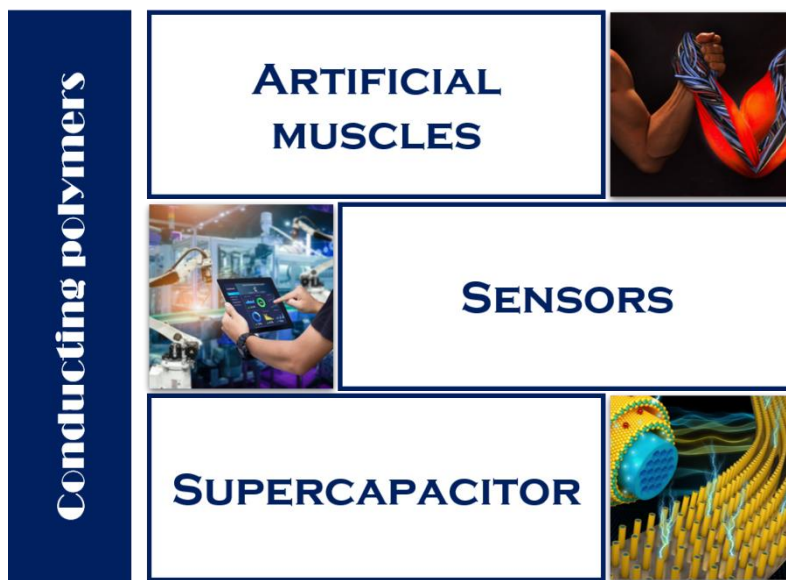
<i>AC</i>	<i>Alternating Current</i>
<i>APS</i>	<i>Ammonium persulphate</i>
<i>ATR</i>	<i>Attenuated Total Reflectance</i>
<i>BDS</i>	<i>Broadband Dielectric Spectroscopy</i>
<i>BIPV</i>	<i>Building-integrated photovoltaic</i>
<i>BTfEE</i>	<i>Boron trifluoride diethyletherate</i>
<i>CB</i>	<i>Conduction Band</i>
<i>CE</i>	<i>Counter Electrode</i>
<i>CNFs</i>	<i>Cellulose Nanofibers</i>
<i>CNT(s)</i>	<i>Carbon Nanotube(s)</i>
<i>CP(s)</i>	<i>Conducting Polymer(s)</i>
<i>CPF</i>	<i>Chitosan/PANI hybrid film</i>
<i>CPH(s)</i>	<i>Conducting Polymer Hydrogel(s)</i>
<i>Cs</i>	<i>Chitosan</i>
<i>CTAB</i>	<i>Cetyl trimethylammonium bromide</i>
<i>CV(s)</i>	<i>Cyclic Voltammogram(s)</i>
<i>DBSA</i>	<i>Dodecylbenzene sulphonic acid</i>
<i>DC</i>	<i>Direct Current</i>
<i>EDCLs</i>	<i>Electrical Double Layer Capacitors</i>
<i>EDOT</i>	<i>Ethylenedioxythiophene</i>
<i>EDX</i>	<i>Energy Dispersive X-ray Spectroscopy</i>
<i>EIS</i>	<i>Electrochemical Impedance Spectroscopy</i>
<i>EMI</i>	<i>Electromagnetic Interference</i>
<i>ES</i>	<i>Emeraldine Salt</i>
<i>ESCR</i>	<i>Electrochemically Stimulated Conformational Relaxation</i>
<i>ESR</i>	<i>Equivalent Series Resistance</i>
<i>FED</i>	<i>Field Emitting Diodes</i>
<i>FESEM</i>	<i>Fourier Transform Scanning Electron Microscopy</i>
<i>FTIR</i>	<i>Fourier Transform Infra-red spectroscopy</i>

<i>GCD</i>	<i>Galvanostatic Charge-Discharge</i>
<i>GCE</i>	<i>Glassy Carbon Electrode</i>
<i>HDL</i>	<i>Helmholtz double layer</i>
<i>HOMO</i>	<i>Highest Occupied Molecular Orbital</i>
<i>HR-TEM</i>	<i>High-Resolution Transmission Electron Microscope</i>
<i>ICM</i>	<i>Intercellular Matrices</i>
<i>ICP(s)</i>	<i>Intrinsic Conducting Polymer(s)</i>
<i>ITO</i>	<i>Indium tin oxide</i>
<i>LE</i>	<i>Leucoemeraldine</i>
<i>LED(s)</i>	<i>Light Emitting Diode(s)</i>
<i>LUMO</i>	<i>Lowest Unoccupied Molecular Orbital</i>
<i>MDOT</i>	<i>Methylenedioxythiophene</i>
<i>MWCNT</i>	<i>Multi-walled carbon nanotubes</i>
<i>NMP</i>	<i>N-methyl-2-pyrrolidone</i>
<i>NMR</i>	<i>Nuclear Magnetic Resonance</i>
<i>NLO</i>	<i>Non-Linear Optics</i>
<i>OCV</i>	<i>Open Circuit Voltage</i>
<i>OLEDs</i>	<i>Organic light-emitting diodes</i>
<i>OPVs</i>	<i>Organic photovoltaic cells</i>
<i>OTFTs</i>	<i>Organic thin film transistors</i>
<i>OFETs</i>	<i>Organic field-effect transistors</i>
<i>PAA</i>	<i>Polyacrylic acid</i>
<i>PANI</i>	<i>Polyaniline</i>
<i>PEDOT</i>	<i>Poly(3,4-ethylenedioxythiophene)</i>
<i>PHE</i>	<i>Polymer Hydrogel Electrolyte</i>
<i>PHEA</i>	<i>Poly (N-hydroxyethyl acrylamide)</i>
<i>PIN</i>	<i>Polyindole</i>
<i>PLA</i>	<i>Polylactic acid.</i>
<i>PN</i>	<i>Pernigraniline</i>
<i>POT</i>	<i>Polytoluidine</i>
<i>PP</i>	<i>PVA/PANI hybrid film</i>
<i>PPV</i>	<i>Polyphenylene vinylenes</i>

<i>Ppy</i>	<i>Polypyrrole</i>
<i>PSS</i>	<i>Polystyrene sulfonate</i>
<i>PTh</i>	<i>Polythiophene</i>
<i>PTSA</i>	<i>p-Toluene sulfonic acid</i>
<i>PVA</i>	<i>Polyvinyl alcohol</i>
<i>QV</i>	<i>Coul voltammogram</i>
<i>RE</i>	<i>Reference Electrode</i>
<i>rGO</i>	<i>Reduced Graphene Oxide</i>
<i>SWCNT</i>	<i>Single-Walled Carbon Nanotube</i>
<i>TGA</i>	<i>Thermogravimetric Analysis</i>
<i>UTM</i>	<i>Universal Testing Machine</i>
<i>VB</i>	<i>Valence Band</i>
<i>VOC</i>	<i>Volatile Organic Compounds</i>
<i>WE</i>	<i>Working Electrode</i>

Chapter 1

Introduction



This chapter discusses a general introduction to conducting polymer (CP) research. CPs have gained considerable attention in the scientific community due to their tunable electrical conductivity, intriguing electrochemical characteristics, ease of synthesis, capacity to form composites/hybrid materials etc. These materials have opened up new avenues for research and find diverse applications in modern science and technology. The chapter also presents brief literature on CPs and their hydrogel composites, particularly focusing on the hybrid systems derived from polyvinyl alcohol (PVA) with polyindole (PIN) and poly(3,4-ethylenedioxythiophene) (PEDOT). It then provides a brief description of electrochemical properties, as well as biomimetic characteristics of CPs.

1.1. Conducting polymers

Scientists were exploited the insulating ability of organic polymers for various applications until the discovery of the polyacetylene in the mid-twentieth century. This groundbreaking discovery of polyacetylene in 1958 brought about the emergence of CPs in late 1970s by Hideki Shirakawa, Alan MacDiarmid, and Alan Heegar. They observed a huge shift in its electrical conductivity spanning multiple orders of magnitude from insulator to metal^[1] through doping with iodine^[2]. CPs are considered as new generation materials that led to revolutionary advances in the scientific world from the end of the 20th century to the present day and resulted in the creation of the electronic age itself^[3]. This historical revelation led to their recognition with the Nobel Prize in Chemistry in 2000. Never previously had science encountered the ability to manipulate a material's optical, electrical, mechanical, or magnetic attributes across such a vast spectrum^[4].

CPs represent a remarkable class of materials with unique properties that bridge the gap between traditional insulating polymers and metallic conductors. These polymers exhibit the ability to conduct electricity while retaining the inherent flexibility and processability of organic polymers. In recent decades, CPs have garnered increasing interest due to their significant potential as viable alternatives to inorganic semiconductors^[5]. This has prompted extensive research efforts both in terms of fundamental understanding and practical applications.

As soon as the electronic structure of CPs was studied, scientists realized that the main reason for their conductivity is the π conjugated system located along the backbone of the polymer chain, where π the electrons are overlapped and delocalized throughout the backbone of the polymer chain [6]. This electron delocalization not only controls the conductivity of CPs but also controls their chemical redox processes. By precisely modulating this redox process, it is possible to control all the electrical and optical properties of CP. CPs with desired conductivity and optical properties can be designed by exploiting this unique redox property and used as versatile materials for electronic and electrochemical and other technology applications.

Several key factors determine electronic conduction in CPs. (i) The presence of charge carriers is essential for electronic conduction, introduced through a process called doping, and these carriers have a substantial impact on the material's electrical properties. (ii) The overlap of molecular orbitals is critical for facilitating carrier mobility within the polymer structure, allowing smoother movement of charge carriers. (iii) The mobility of π -electrons is involved in electronic conduction. (iv) Charge hopping between polymer chains is a significant mechanism that influences the overall conductivity of CPs. Together, these factors contribute collectively to the electronic conduction in CPs. The insulating nature of the undoped CPs can be converted to conducting, through the doping process. Modifying synthetic conditions allows CPs to exhibit its unique capability in finely tuning their electrical conductivity across

a broad spectrum. The dopant anion concentration in the electrolyte/solvent can be varying in the electrochemical/chemical polymerization that helps this tunable conductivity of CPs. The conductivity of the CPs increases by increasing the dopant concentration, enabling them to attain the metallic range. Consequently, heavily doped CPs are commonly termed "synthetic metals". The tunable conductivity ranges of CPs are illustrated in Figure 1.1.

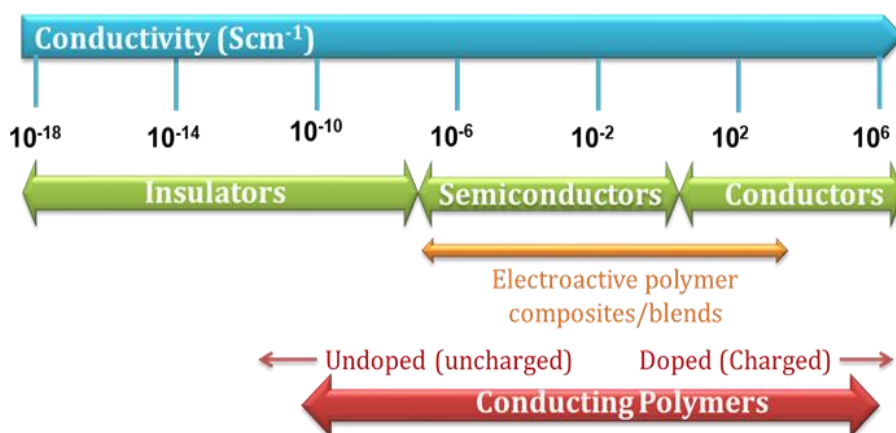


Figure 1.1 Tunable conductivity of CPs

It has already been said that the physical and chemical properties of CPs can be determined and tuned during their synthesis. Therefore, by varying the various synthesis parameters, like synthesis time, synthesis temperature, concentration of the monomer, concentration of the dopant, type of the dopant, and pH of the medium of synthesis, it is possible to vary their various properties such as dielectric, morphological, chemical, thermal and electrochemical and change them according to our needs.

Despite their remarkable ability to adjust various properties, CPs faced setbacks in their initial commercial application due to their poor solubility/processability, and poor mechanical strength. Scientists in this field aimed to overcome these limitations. Enhancing processability could involve adding functional groups to the polymer backbone to create derivatives or using surfactants during dissolution in solvents. Mechanical properties are superior in crystalline polymers compared to amorphous or semi-crystalline ones. CPs lack crystallinity and their overall mechanical behavior relies on minute shifts in the molecular mobility of their macromolecules. Molecular mobility hinges on factors such as the conformational structure of branching polymers and macroscopic conditions like temperature and pressure. The disordered arrangement of monomers in amorphous polymers fosters greater molecular motion within them. Consequently, scientists have extensively researched methods to improve CPs' mechanical strength, such as crafting composites/hybrids/blends with processable polymers, integrating metallic nanoparticles, or using polymeric/hydrogel nano-fibers and microfibers as templates.

1.1.1. Doping in CPs

Doping in CPs are crucial process that involves introducing foreign molecules or ions into the polymer matrix to modify its electrical conductivity or that changes a π -conjugated polymer from being unable to conduct electricity to becoming a semiconductor or conductor. This manipulation enables us to manage and improve the electronic characteristics of the polymer. The undoped CPs are

insulators in nature and it can be converted in to conducting by doped with oxidizing or reducing agents that increases the charge carrier concentration in CPs.

Doping can be achieved mainly through chemical and electrochemical methods. Chemical doping involves the incorporation of dopants into the polymer during synthesis or through post-treatment processes, altering the polymer's electronic structure either by redox or non-redox method. Electrochemical doping, on the other hand, utilizes electrochemical reactions to introduce dopants into the polymer, often via redox reactions at the polymer-electrolyte interface. Two types of redox doping are observed in CPs.

p-type doping: p-doping is generally known as oxidation, which produce a positive charge or holes along the polymer chain by the extraction of electrons from the polymer chain using an electron acceptors. This type of mechanism is most common in CPs^[7].

n-type doping: here the doping in CPs is attained through reduction. The introduction of electrons to the polymer chain by an electron donor imparts a negative charge to the polymer chain^[8].

The **de-doping** is a process that converts the CPs in the conducting state to insulators or neutral state. The oxidized polymers (p-type) are de-doped by treating with the electron donors whereas the reduced (n-type) are de-doped by treating with electron acceptors^[9]. The choice of dopant and doping method significantly influences the conductivity, stability, and other properties of CPs, making doping a vital aspect of their synthesis and application.

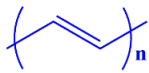
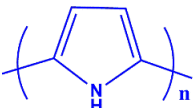
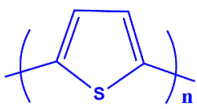
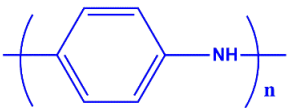
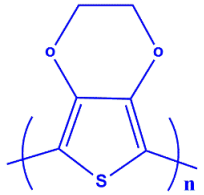
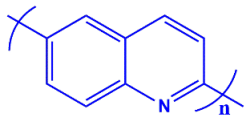
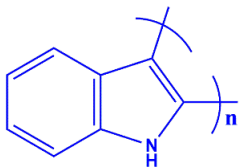
Another type of doping is non-redox doping, which is described in the case of polyaniline. This type of doping is based on acid-base chemistry. The protonation of the polyaniline chain by treating with an acid converts the semi-conducting emeraldine base into highly conducting emeraldine salt. The number of electrons in the polymer chain does not change in this type of doping. The de-doping takes place by the treatment of any base with the protonated polymer^[10]. Apart from this chemical and electrochemical doping methods photo-doping^[11], charge-injection were also reported^[12].

1.1.2. Example of CPs

Following the initial discovery of the first CP, polyacetylene, subsequent exploration extended to polypyrrole, polyaniline, polythiophene, and poly (3,4-ethylenedioxythiophene). The polyacetylene was invented in 1958 as an insulator, later in 1977 Shirakawa et al., reported as the iodine-doped polyacetylene with conductivity in the range of 10^4 Scm^{-1} ^[3a, 13] (Siemens per centimeter). The limitations such as poor processability, solubility and environmental stability of polyacetylene make it a non-suitable candidate for technological applications. To overcome these limitations, new families of CPs are invented; they are Polypyrrole (PPY)^[14], Polyaniline (PANI)^[15], Polythiophene (PTh)^[16] and Polyquilonine etc. Among these, PANI and PPV are six-membered rings where as PPY and PTh are five-membered hetero cyclic ring families. The derivatives of these families also invented later; they are ortho and para Polytoluidine (POT and PPT respectively) which is a derivative of PANI, PIN is considered as a fused ring structure of

PPY and benzene rings and finally Poly(3,4-ethylenedioxythiophene) (PEDOT) is derived from PTh. The list of some important CPs is listed below in Table 1.1.

Table 1 *Examples of CPs*

Structure	Name	Conductivity Scm^{-1}
	Polyacetylene	1.5×10^5
	Polypyrrole	600
	Polythiophene	100
	Polyaniline	200
	Poly(3,4-ethylenedioxythiophene)	400
	Polyquilonine	300
	Polyindole	80

1.1.3. The mechanism of charge transport in CPs

The electrical conductivity of any system is determined by the product of charge density, the charge carried by each carrier and the mobility of the charge carriers. Conductivity of CPs is defined as the migration of holes or electrons along the polymer chain in the guise of various electronic states or quasi-particles such as solitons, polarons, and bipolarons^[17].

Solitons are free radicals or delocalized unpaired electrons on a degenerate conjugate polymer chain. The positive solitons are formed by the loss of one electron from the neutral polymer chain and the negative solitons are formed by the gain of one electron. The solitons possess $\frac{1}{2}$ spins, whereas no spin for positive and negative solitons. In solitons, the charge is transported as the solitons hops along the carbon chain.

The major charge carriers of the degenerate and non-degenerate CPs are the polarons. It can be positive (P^+) or negative (P^-), formed after the oxidation or reduction of the polymer backbone respectively and characterized by a spin value $\pm 1/2$. Some of the atoms along the chain acquire a formal positive charge when CP is doped with a negative dopant. The polaron is formed by the coupling of this positive charge with the unpaired electron of the solitons and the length of polaron can be determined by the number of monomer units which contains the delocalized positive charges along the chain and the length of the polarons decreased by increasing the number of polarons which takes place by increasing the concentration of the dopant.

When the concentration of the dopant increases beyond a critical point, two polarons coupled together to form another quasi particle named as bipolarons which has quantum spin values 0 or 1 and have a charge of $\pm 2e$. The length of bipolarons also determined as in the case of polarons^[18]. The charge transfer mechanisms in polyacetylene (via solitons, polarons and bipolarons) are showcased in Figure 1.2.

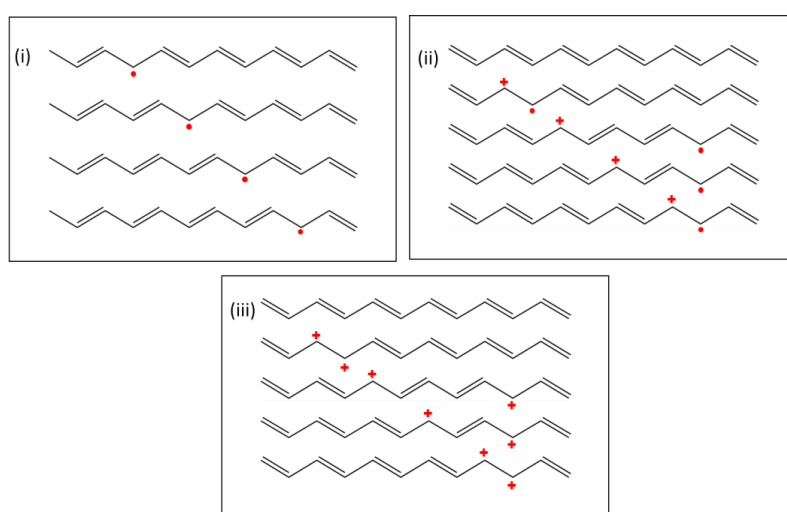


Figure 1.2 Charge transfer mechanism in polyacetylene

According to band theory, CP can be considered as a semiconductor and has a narrow band gap (E_g), which means that electrons have at least enough energy to independently jump from the valence band (VB) to the conduction band (CB)^[19]. The band structure of polypyrrole has previously been documented^[20]. In its pristine and undoped form, polypyrrole acts as an insulator, exhibiting a large band gap. When doped with a p-type material, the polymer backbone undergoes oxidation, leading to the loss of a π electron. This electron loss prompts a shift in the polymer's structure by

rearrangement of π electrons, resulting in the formation of a polaron along the polymer chain. In this polaron mechanism, the valence band is raised and conduction band is lowered by a value corresponding to the polaron's binding energy. This generates a localized electronic level within the band structure, subsequently leading to the development of bipolarons through the loss of additional π electrons from the polaronic structure. The conversion from benzenoid to quinoid structure is expedited in the case of bipolarons. The energy bands between the original conduction and valence bands allow for a greater population of electrons to carry charge via this new array of available energy levels. As a result, the band energy reduces from 3.16 eV to 1.4 eV (as illustrated in the polypyrrole band diagram, Figure 1.3). This transformation signifies

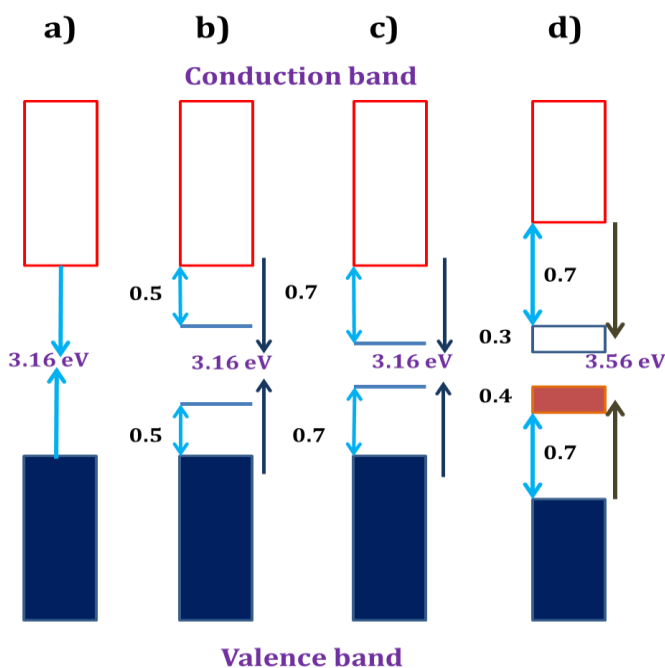


Figure 1.3 *The band structure of polypyrrole*

the transition of the semiconductor polypyrrole to a metallic form, thereby enhancing the material conductivity^[21].

The CPs are characterized by a high degree of disorder and primarily polycrystalline or amorphous in nature. Apart from the polaron-bipolarons-based conduction mechanism hopping or tunneling conduction is commonly encountered. Based on the various models the conduction mechanism in CP is comprehended.

Variable range hopping conduction: Instead of band conduction the charge transport occurs via phonon-assisted hopping between localized sites in CP when the charge carriers are localized due to random electric fields. Activation energy is essential for each hop since the localized states have quantized energies that encompass a specific range^[22].

Charging energy-limited tunnelling: The electron tunnelling is takes place in CP between small areas, when the insulating barrier between two conducting region is thin enough. The charging energy is negligible and the conduction takes place by the fluctuation-induced tunnelling when the conducting segments are large^[23].

1.1.4. The influencing factors on CP conductivity

There are some factors which influence the conductivity of the CPs. They are listed below.

Dopant effect: the nature of the dopant and the degree of doping will influence the conductivity of the polymer. The molecular structure of the dopants defines the conductivity and if the concentration of the dopant (degree of doping) increases the conductivity also increases^[24].

Structure of the backbone chain: conductivity increases by increasing the chain length of the polymer backbone and the extent of conjugation also directly depends on the conductivity of the CP. The straight chain instead of a branched chain is preferred for better conductivity.

Polymerization condition: the concentrations of the monomer, dopant, oxidant, polymerization time and temperature are directly proportional to the conductivity of the CP. But there is a critical point, if the temperature and the polymerization time is beyond that the over oxidation is occurs and the double bonds must convert into single bonds which stops the conjugation and that affects the conductivity of the polymer^[25].

1.1.5. Polymerization initiation

A widely acknowledged method for initiating polymerization involves creating radical cations or anions, which are then followed by the polycondensation of these radical ions. The synthesis process varies based on how radical anions are initiated through electrochemical, chemical, or photochemical oxidation of the monomer. Each of these approaches necessitates an initial solution containing the monomer, solvent, and salt. The presence of salt is crucial as it facilitates current flow, leading to conductivity and supplying the necessary anions for doping during the polymerization process.

1.1.5.1. Electrochemical initiation

The polymer growth by the electrochemical oxidation of the monomer is followed when a metal working electrode in a monomer

solution is submitted to consecutive potential sweeps using reference electrode to control the potential of the working electrode and the counter electrode to support the current flow. The potential window of the solution must be large enough to allow maximum extension of the oxidation/reduction reaction of the generated polymer inside this window. The monomer oxidation initiates the polymerization; a progressive color change at the electrode is occurred. The polymerization will stop when the potential is reversed. So the flow of previous anodic current drives two reactions; the monomeric oxidation-polymerization and the oxidation of the electro generated polymer. The newly generated polymer will deposit on the metal surface during each potential sweep^[26].

The polymer also can be generated by under constant polymerization rate by the constant flow of anodic current through the clean electrode. The potential evolution in the chronopotentiometric response indicates the potential approaches to that of parallel electrolyte discharge. The deposited polymer film morphology also can be control by the square current waves^[27].

1.1.5.2. Chemical initiation

The process of initiating the synthesis of CPs chemically involves employing various chemical initiators to start the polymerization process. One commonly applied approach is oxidative polymerization, where a monomer, like aniline or thiophene, experiences oxidation while in the presence of an oxidizing agent or initiator. Initiators such as ammonium persulfate, ferric chloride, or

ferric tosylate aid in producing radicals, kick starting the polymerization of the monomer and resulting in the formation of a conductive polymer. These radicals facilitate the bonding of monomer units, allowing the polymer chains to grow with a conjugated structure, vital for electron movement and thereby conferring electrical conductivity to the material. The selection of the initiator and the conditions of the reaction significantly impact the properties and conductivity of the resulting CP. This underscores the pivotal role of chemical initiation in the controlled synthesis of these materials for diverse technological applications^[28].

1.1.6. Applications of CPs

The adaptable characteristics of CPs have resulted in their adoption across a broad spectrum of applications, causing significant transformations in numerous industries. These polymers, characterized by their distinct blend of electrical conductivity and polymer flexibility, have unlocked opportunities for creative resolutions.

In the field of electronics, CPs are utilized in supple and lightweight electronic gadgets, such as wearable sensors, and even organic solar cells. Their adjustable conductivity permits customized performance, broadening prospects in this arena^[29].

Within the scope of energy storage and conversion, CPs are employed in supercapacitors and batteries, offering high energy density and moderate power density. They also contribute to fuel cells and other devices converting energy^[30].

In medical contexts, CPs are integral to biosensors and drug delivery systems. They empower the creation of biosensors with the capability to identify specific biological molecules, thereby facilitating the early detection of diseases. Their capacity for controlled release enhances the efficacy of drug delivery techniques^[31].

CPs have left an imprint on protective coatings against **corrosion for metals**, prolonging the lifespan of structures and equipment^[32].

Furthermore, they serve in actuators and synthetic muscles, finding application in robotics and prosthetics by virtue of their capacity to change shape through electrical stimulation.

In the environmental sphere, they are used in sensors to detect pollutants and toxins, contributing to environmental monitoring endeavors. Additionally, they are being explored for water purification and treating wastewater, underscoring their potential to address critical global challenges^[33].

From electronics to healthcare, energy to the environment, the array of applications for CPs is continuously expanding, offering inventive solutions and advancements across diverse domains^[34].

Actuators, applying potential across the CP-based materials prompts ions to move within the polymer, resulting in its expansion or contraction and subsequent motion. This characteristic renders conducting polymer actuators well-suited for various uses including artificial muscles, microfluidic devices, and drug delivery systems^[35]. When subjected to different triggers like gases, chemicals, or biological elements, the conductivity of the polymer

film changes, allowing for the identification and measurement of the specific substance. This feature renders conducting polymer **sensors** useful across a wide array of fields including environmental surveillance, industrial management, medical analysis, and wearable devices^[36].

Some technological applications are illustrated in Figure 1.4.

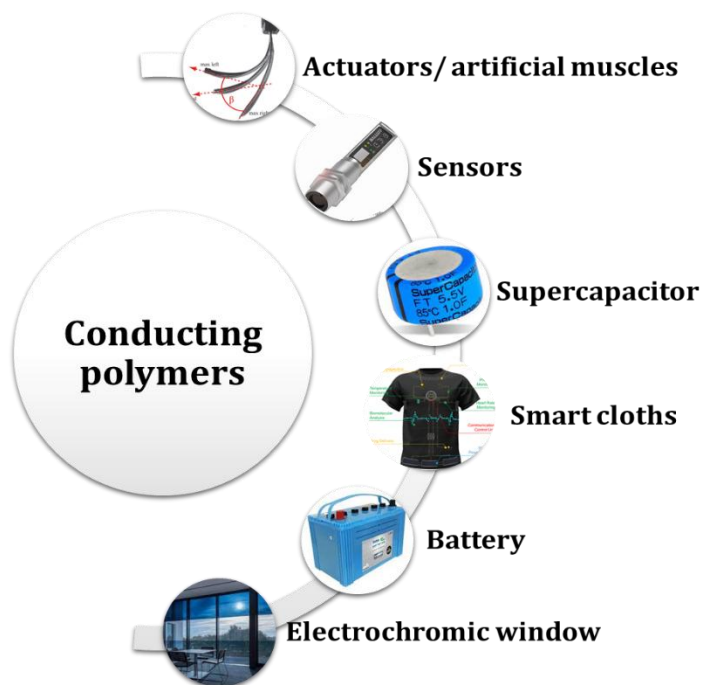


Figure 1.4 *The technological applications of CPs*

1.1.7. Limitations of CPs

There are some inherent limitations associated with CPs which may hinder their applicability in device fabrication. Some of them are detailed below.

- **Poor Mechanical stability:** Many CPs are brittle, making them prone to cracking or breaking under stress. The mechanical stability of a material is essential for device fabrication.

- **Environmental Sensitivity:** CPs can be sensitive to environmental factors like moisture, oxygen, and temperature, leading to degradation over time.
- **Doping Reversibility:** Some CPs exhibit limited reversibility in their doping and de-doping processes, affecting their long-term stability and performance.
- **Processing Challenges:** The fabrication and processing of CP can be complex and may require specific conditions to achieve desired properties.
- **Color Fading:** CPs that exhibit color changes due to doping and de-doping can experience fading of the color over time.
- **Low Electrical Stability:** CPs can experience changes in their electrical properties over extended periods, affecting their reliability in electronic applications.
- **Poor Solubility:** Some CPs have limited solubility in common solvents, making their processing and incorporation into devices more challenging.
- **Poor Thermal Stability:** Some CPs might have relatively low thermal stability, restricting their use in high-temperature applications.

Despite these limitations, ongoing research and advancements continue to address these issues and expand the potential applications of CPs.

Approaches to tackle these challenges

Several methods exist to overcome the above-mentioned shortcomings and have been mentioned in the literature. Some of them are listed below.

Different approaches are there to overcome the poor mechanical stability and thermal stability of CPs are proposed

- **Polymer blending** method helps mix CPs with other polymers, hydrogels or additives to enhance mechanical strength and stability^[37].
- Incorporating **nanoparticles** to improve mechanical properties and provide better structural integrity^[38].
- **Chemical modification:** Altering the polymer's chemical structure to enhance mechanical properties while retaining electrical conductivity^[39].
- **Cross-linking:** Introducing crosslinks between polymer chains to increase overall strength and durability^[40].
- **Making composites/ hybrid materials** with metal oxides^[41], other polymers, and hydrogels^[42].

The poor solubility is a barrier to good processability. The solubility can be improved by using surfactant. Water-soluble polyanilines are also reported in the literature^[43].

1.2. Hydrogels an overview- introduction

Hydrogels are materials that have gained substantial attention across various fields due to their unique properties and diverse applications. Their three-dimensional networks is capable of absorbing and retaining a significant amount of water, leading to gel-like characteristics. One of the most remarkable features of

hydrogels is their ability to swell substantially upon absorbing water or other fluids, often resembling natural tissues in terms of water content^[44]. The cross-linking takes place between the polymer backbones with ionic, covalent and hydrogen bonding interaction^[45]. This characteristic renders them particularly useful in applications ranging from medical and pharmaceutical fields to agriculture, cosmetics, and beyond^[46].

Hydrogels exhibit a wide range of properties that can be fine-tuned through the selection of polymer types, crosslinking methods, and other formulation factors. They can vary in their mechanical strength, porosity, responsiveness to environmental changes (such as pH or temperature variations), and release kinetics for encapsulated substances. The versatile nature of hydrogels, combined with their biocompatibility and controllable properties, have spurred ongoing research and innovation^[47]. The swelling characteristics of hydrogels depend on the degree of cross-linking, their chemical composition and the interaction between the network and surrounding liquid. The hydrophilic groups that present in the hydrogels are responsible for high water retention; hydrophilic groups like carboxylic acids, amides, and alcohols etc., in their polymer backbone^[48] are responsible for high water retention.

1.2.1. CP/ hydrogel hybrid system

A CP/hydrogel system is an exceptional and adaptable material that merges the characteristics of CPs and hydrogels. CPs are renowned for their electrical conductivity, while hydrogels form three-dimensional networks capable of soaking up and retaining water

and other electrolyte ion. When these constituents are united, they generate a composite like substance that demonstrates both electrical conductivity and water absorption/swelling-deswelling characteristics and remarkable mechanical properties etc.^[49]

This hybrid material presents a wide array of potential uses owing to its dual attributes. The CP component contributes electrical conductivity, enabling the material to conduct charges and react to electrical stimuli. Meanwhile, the hydrogel component offers mechanical stability and water absorption capacity, potentially resulting in alterations in the material's dimensions and response to environmental stimuli^[50]. CP/hydrogels system can experience alterations, either physical or chemical when subjected to shifts in environmental stimuli like electric fields, temperature, pH, changes in ionic concentration, diverse types of salts, modifications in solvent, external mechanical forces, and light exposure, or a combination of these factors^[51]. This amalgamation of traits renders CP/hydrogel systems suitable for a variety of applications, including sensors^[52], actuators^[53], drug delivery mechanisms^[54], scaffolds for tissue engineering^[55], energy storage devices (battery and supercapacitors)^[56] and pliable electronics^[57]. Their ability to respond to both electrical and environmental signals opens the door to designing intelligent and adaptable materials capable of fulfilling specific functions based on external inputs. Moreover, both demonstrate responsiveness to stimuli and are potential contenders for applications involving sensing and actuation. Developing CP/hydrogel systems necessitates meticulous design of the polymer

and hydrogel elements, along with the techniques employed to blend them. They possess remarkable processability, enabling easy casting into thin films, fibers, or desired forms during the gelation phase.

1.2.2. Fabrication methods of CP/hydrogel hybrid materials

The techniques for fabricating CP/hydrogel materials encompass the amalgamation of CPs and hydrogels, resulting in a composite material that capitalizes on the distinctive characteristics of each constituent. Below are outlined several comprehensive approaches to fabricating these hybrid materials:

1.2.2.1. In situ chemical polymerization

In this approach, the CP is fabricated within the hydrogel framework. For instance, the monomers of the CP can be generated into a solution containing hydrogel precursors, and then polymerization is initiated under suitable conditions. The resulting, CP networks become interwoven with the structure of the hydrogel. The formed CP/ hydrogel hybrid mixture can be coagulated using a coagulating medium and then dried it^[42b]. An alternate in situ fabrication technique is the coating approach. In this method, a pre-made hydrogel film or fiber is allowed to expand in a solution containing monomers. The hydrogel absorbs both monomer and solvent molecules within its internal structure. Subsequently, polymerization of the monomer occurs within both the hydrogel's interior and its surface, achieved by introducing an oxidant solution after certain duration. As a result, a hybrid material comprising CP uniformly coated on the hydrogel film or fiber is produced^[58].

1.2.2.2. Physical mixing and crosslinking

This approach signifies a versatile strategy for fabricating CP/hydrogel hybrid materials with unique characteristics. The method entails mixing CPs and hydrogels, followed by a subsequent crosslinking procedure to link the entities together. The particles of CPs can be distributed within a solution containing hydrogel precursors, after which a crosslinking agent is introduced to foster the connection between the CP and hydrogel^[59].

1.2.2.3. Layer-by-Layer assembly

In this technique, consecutive layers of CPs and hydrogel components are successively applied onto a substrate. The layer-by-layer assembly approach permits meticulous management of layer thickness and composition, culminating in a precisely defined hybrid structure^[60].

1.2.2.4. Electrochemical deposition

The electrochemical deposition technique proves to be a versatile method for crafting tailored CP/hydrogel hybrid materials. This strategy involves carefully placing CPs onto conductive substrates through controlled electrochemical deposition, followed by introducing hydrogel precursors to form a composite. For instance, CPs like PPY or PEDOT can be electrodeposited onto conductive surfaces such as indium tin oxide (ITO) electrodes. Following the formation of the CP layer, hydrogel precursors like acrylamide or N-isopropyl acrylamide can be introduced onto the surface. Subsequent polymerization of the hydrogel precursors results in a hydrogel layer enveloping the CP, yielding a composite of CP and

hydrogel. This method allows meticulous control over the deposition process, enabling manipulation of layer thickness and composition for both the CP and hydrogel components^[61].

1.2.2.5. Template-assisted synthesis:

The Template-Assisted Synthesis technique presents an inventive method for crafting CP/hydrogel hybrid materials with finely tuned attributes. This strategy involves the utilization of porous templates as frameworks in the fabrication process. For example, CP precursors can be infused within the pores of these templates, succeeded by the introduction of a solution containing hydrogel precursors. As polymerization and gelation transpire, the template serves as a scaffold, enabling the formation of CP and hydrogel hybrid material. Once the composite material solidifies, the template can be extracted, yielding a CP/hydrogel hybrid material featuring a precisely structured porous arrangement^[62].

1.2.2.6. Covalent crosslinking method:

The Covalent Crosslinking Method emerges as a significant approach to tailor CP/hydrogel hybrid materials. This technique involves establishing covalent bonds between the CP and hydrogel constituents, resulting in a resilient and unified composite. For example, CPs like PPy or PEDOT can be synthesized alongside the functional groups present in the hydrogel precursor. During polymerization, covalent bonds are formed between the CPs and the hydrogel, effectively merging their distinct attributes^[63].

An example for this the material developed by is Wang et al., in which they showcased the covalent crosslinking of PEDOT and a

hydrogel through the integration of acrylamide groups into the hydrogel precursor. The co-polymerization procedure resulted in the development of a CP/hydrogel hybrid material that displayed improved electrical and mechanical characteristics^[64].

1.2.3. Applications of CP/hydrogel hybrid materials

1.2.3.1. Flexible electronics and wearable devices

CP/ hydrogel hybrids are widely employed in flexible electronics and wearable devices. These composite materials possess unique attributes such as high stretchability, biocompatibility, and mechanical robustness, making them suitable for conformal contact with the human body. They can be employed in various wearable technologies, including health monitoring devices, smart textiles, and soft robotics. Their capability to conform to irregular shapes or stretch with movements, along with their biocompatibility, makes them promising candidates for next-generation electronics designed to seamlessly integrate with the human body, enhancing comfort and usability in various applications within healthcare, fitness, and beyond. Moreover, their compatibility with bioelectronics interfaces enables diverse functionalities, such as bio-sensing or drug delivery systems, marking a significant advancement in the realm of wearable technology^[65].

1.2.3.2. Sensors and biosensors

CP/hydrogel hybrids function as exceptional bases for sensors and biosensors, thanks to their capacity to respond to both electrical and environmental signals. Their capability spans the detection of various analytes, encompassing biomolecules, ions, gases, and

contaminants. By tailoring the hydrogel component, specific molecule absorption can be achieved, while the CP component reacts to altered conductivity upon interaction with the analyte. These sensors exhibit remarkable sensitivity to various stimuli, including pH changes, temperature fluctuations, and specific biomolecules. They offer a high surface area and tunable properties, enabling close interaction with biological systems^[66].

1.2.3.3. Drug delivery systems

CP/hydrogel hybrids find application in drug delivery systems due to their capacity to encase and administer pharmaceutical compounds in a regulated fashion. The hydrogel can absorb water and expand, enabling the gradual dispensation of medicines, while the CP can react to external triggers, prompting the release of drugs as required^[54].

1.2.3.4. Tissue engineering and regeneration

The integration of CP hydrogel hybrids is pivotal in the realm of tissue engineering, as they furnish a foundation that facilitates cell proliferation, specialization, and tissue revitalization. The CP facet contributes electrical stimuli that enhance cellular communication, while the hydrogel delivers a three-dimensional framework akin to the inherent extracellular matrix^[67].

1.2.3.5. Artificial muscles

The application of CP/ hydrogel hybrid materials in the realm of artificial muscles offers promising avenues for the creation of responsive and adaptable biomimetic systems. These materials can replicate the contraction and expansion mechanisms observed in

natural muscles, and sensing of working conditions (chemical, electrical and thermal) while working making them suitable for applications in robotics and medical devices. Notably, Yahya et al., introduced an innovative approach by developing an artificial muscle utilizing a CP hydrogel hybrid system^[58]. The CP/ hydrogel hybrid system contributed electrical responsiveness, and volume changes upon stimulation, resulting in muscle-like contractions and extensions^[68].

1.2.3.6. Supercapacitors

CP hydrogel hybrid materials present a promising pathway to enhance the efficiency of supercapacitors, devices crafted for efficient energy storage. These materials exhibited higher capacitance and cyclic stability, attributed to the synergistic interplay between the CP and hydrogel components. The 3D porous composites of CP and hydrogel for use as supercapacitor electrodes are also reported^[69]. The distinctive structure of these materials facilitated efficient charge transport and elevated energy storage capabilities^[70].

1.3. Polyindole (PIN) - introduction

PIN, which belongs to the fused-ring family, has garnered considerable attention over the past few decades due to its distinctive chemical and electrochemical characteristics. PIN holds a significant position in the realm of CPs due to its ease of synthesis, cost-effectiveness of the monomer, structural versatility, environmental stability, and the ability to fine-tune its physical properties. The polymerization of indole monomers to form PIN

through chemical oxidative methods was first reported in 1976^[71]. Electrochemical polymerization for PIN synthesis was introduced by Tourillon and Garnier in 1982, employing a platinum electrode as the working electrode and LiClO₄ in acetonitrile as the electrolyte^[72]. Their work involved methyl-substituted indole monomers at the second position, catalyzed by an acid. However, this initial polymer was not conductive. The absence of the N-H stretching vibration peak in the IR spectrum, suggests coupling occurred via 1, 1 coupling through the N atom. The exact site of polymerization remained unclear until subsequent studies. Waltman et al., conducted spin density calculations at the fifth position and explored electron-donating and accepting substituents at that site, proposing that indole polymerization primarily took place via the 1 and 3 positions^[73]. Zotti et al., suggested another polymerization site, drawing an analogy to polyaniline^[74]. They proposed a stereoregular coupling at the 2-2 and 3-3 positions. Addressing these contradictory findings, H. Talbi et al., delved into the vibrational properties of doped and undoped PIN and concluded that the polymerization of indole to form highly conductive PIN primarily occurred through the C 2 and C 3 positions^[75].

The various benefits of PIN, such as its relatively robust thermal stability compared to polypyrrole and polyaniline, its remarkable redox stability, rapid-switching electrochromic capabilities, and strong conductivity when doped, have attracted significant interest across various applications. To date, approximately 20 derivatives of indole have been polymerized to form the PIN family, captivating

the attention of scientists for in-depth exploration. This group of PIN materials offers adjustable properties, including tunable conductivity, photoluminescence, and redox activity.

The conductivity of PIN arises from the presence of delocalized π electrons; although it exhibits slightly lower conductivity compared to major CPs like polypyrrole and polyaniline. What makes it particularly attractive is its ability to be chemically synthesized at room temperature, whereas other prominent CPs often require lower temperatures for longer chain lengths. Similar to polyaniline, the doping and de-doping mechanism has also been observed in PIN, as reported by Phasukom et al., PIN shares similarities with conducting polyaniline, which can be identified through cyclic voltammetry (CV)^[76]. In an acid electrolyte, the CV of PIN displays two oxidation and corresponding reduction peaks, similar to polyaniline. However, PIN exhibits electrochemical responsiveness in salt solutions (such as NaCl, LiClO₄, etc.) similar to polypyrrole. In such solutions, a single oxidation and reduction peak can be observed in the CV. Therefore, PIN can function like polyaniline in acidic environments and similar to polypyrrole in salt solutions.

1.3.1. Molecular structure of PIN

PIN exhibits a complex molecular structure, and there has been debate regarding the exact site of polymerization. As previously discussed, achieving good conductivity with more delocalized π electrons is possible only when the polymerization occurs at the 2 and 3 positions of the indole monomer. The chemical structure of PIN is predominantly confirmed through FTIR spectral analysis of

the polymer. Notably, the peak due to the deformation C-H bond is absent and there is peak due to the stretching vibrations of the benzene ring and the N-H vibration in the polymer.

This indicates the existence of free benzene ring and N-H bond in the pyrrole ring of PIN. These observations collectively establish that polymerization does not occur at the N site or the benzene ring. Therefore, the FTIR data of PIN indicates that polymerization primarily transpires at the C 2 and C 3 positions of the pyrrole ring. Similarly, proton NMR data and UV-Vis data further corroborate this finding^[77].

The process of doping and de-doping in PIN is similar to that of polyaniline. When FeCl_3 is employed as the oxidizing agent, Cl^- ions act as dopants, and de-doping can be achieved through treatment with a 2 M NaOH solution. Furthermore, when the reduced PIN undergoes a reaction with HCl for 10 minutes, it results in the re-doping of the polymer.

An alternative structural representation of PIN is depicted in figure 1.5. Existing literature strongly suggests that FeCl_3 is a more potent oxidizing agent compared to others. The incorporation of the 2p orbital of chlorine into the polymer backbone supports the self-doping of PIN. The presence of Cl 2p originates from the anionic component of the HCl solvent used in conjunction with the oxidant FeCl_3 .

The chloride ion interacts with the oxidized PIN backbone through electrostatic forces to neutralize the charge. Figure 1.5 illustrates both the oxidized (doped) and reduced (undoped) structures of PIN.

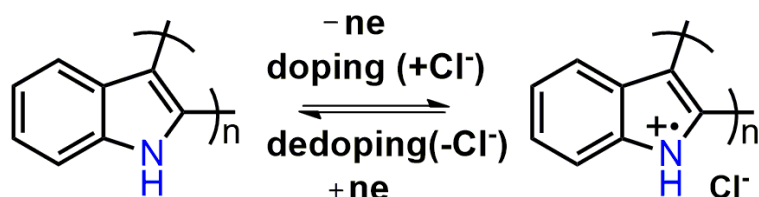


Figure 1.5 The doped and de-doped structures of PIN

1.3.2. Synthesis of PIN

1.3.2.1. Chemical oxidative synthesis

One of the primary techniques for synthesizing conducting PIN involves a chemical oxidative polymerization process where indole monomers are dissolved in a suitable solvent along with an oxidizing and doping agent. Common oxidizing agents used include ferric chloride, copper perchlorate hydrate, potassium iodate), ammonium persulfate, and hydrogen peroxide. Typical solvents employed are acetonitrile, chloroform, methanol, ethanol, and phenylethanol, a mixture of ethanol and water, and surfactant-containing water. The success of the chemical polymerization of indole depends on factors such as the type of oxidizing agent, solvent choice, reaction temperature, and the concentration of reagents^[78].

1.3.2.2. Electrochemical synthesis

Electrochemical methods are commonly employed for the production of PIN and are typically carried out in a three-electrode system using potentiostatic, galvanostatic, or potentiodynamic techniques.

The solutions utilized in these processes include acetonitrile, dichloromethane, benzonitrile, ethanol, ethyl acetate, perchloric

acid, ionic liquids, and boron trifluoride diethyl etherate (BTfEE). PINs synthesized through electrochemical means exhibit notable attributes such as high thermal stability, improved redox activity, and enhanced stability when compared to PANI and PPY^[79]. These materials also demonstrate slow degradation over time.

The electrical conductivity of electrochemically synthesized PIN can be significantly enhanced and approach levels close to 0.1 Scm^{-1} when doped with ions like ClO_4^- or BF_4^- . Furthermore, the position of substitution at 1, 2, 4, 5, 6, or 7 on the indole ring can influence the rate of electro-polymerization^[80].

1.3.2.3. Interfacial synthesis

Interfacial synthesis involves the chemical oxidative polymerization occurring at the boundary of two phases, one being an organic phase containing the monomer and the other being an aqueous phase containing the oxidant. This setup leads to self-assembly phenomena that trigger polymerization at the interface. Koiry and colleagues successfully synthesized lengthy PIN fibers at the stable interface between FeCl_3 aqueous solution and an organic phase containing indole in dichloromethane solution.

Interestingly, they discovered that by agitating the interface with a stirring solution, spherical PIN structures could be produced. Another study by Nurulla and associates involved the interfacial polymerization of an $(\text{NH}_4)_2\text{S}_2\text{O}_8$ aqueous solution and a solution of indole in chloroform solution, resulting in the formation of uniformly sized PIN nanoparticles with diameters ranging from 100 to 200 nm^[81].

1.3.3. Mechanism of oxidative polymerization

In the case of PIN two types of oxidation mechanisms are discussed. They are the radical-radical mechanism and the radical-monomer mechanism.

In the radical-radical mechanism, a neutral molecule undergoes oxidation, resulting in the formation of a cation radical. Subsequently, two radical cation species combine to create dihydro-dimer dications, which further transform into a neutral dimer through the loss of two protons. This dimerization process is repeated, involving oxidation to generate a radical cation and subsequent combination, ultimately leading to deprotonation. The final product of this sequence is the polymer.

This mechanism was initially confirmed in the case of polypyrrole. Due to the structural similarities between PIN and polypyrrole, research expanded to include PIN as well. Yurtsever and colleagues employed DFT calculations to elucidate the oxidation mechanisms in PIN^[82].

In the radical-monomer pathways, the generated radical interacts with the neutral indole monomer, resulting in an exothermic reaction.

However, it's important to note that the second ionization step in this pathway requires significantly more energy compared to the radical-radical mechanism. As a result, the radical-radical mechanism is favored as the preferred oxidation mechanism for PIN^[83].

In 2006, a comprehensive examination utilizing ^1H NMR spectroscopy was conducted to precisely determine the polymerization sites of indole. The presence of the N-H bond within the polymer serves as confirmation that polymerization did not take place at the 1 and 3 positions, but rather occurred at the 2 and 3 positions^[84]. Both electrochemical and chemical polymerization of indole was found to transpire at the 2 and 3 positions, as elucidated

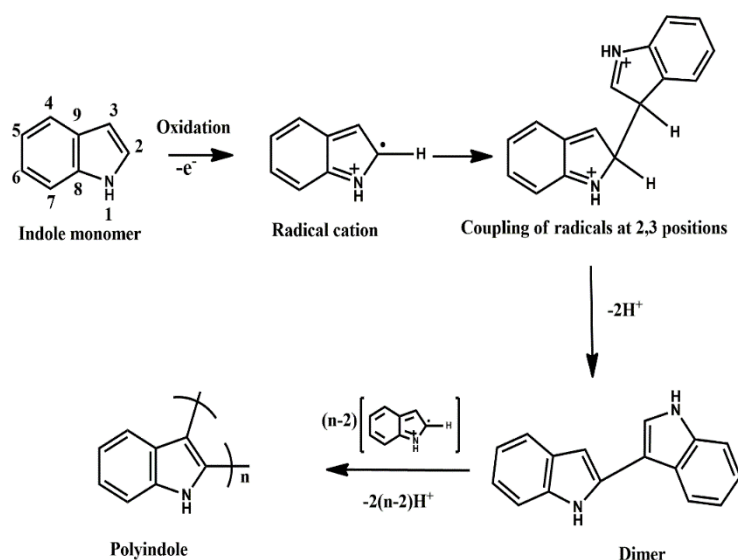


Figure 1.6 The schematic representation of polymerization of PIN

by Goel et. al.,^[85]. The schematic representation in Figure 1.6 illustrates the oxidation process, the formation of radical cations leading to dimerization, and subsequent polymerization. Additionally, it has been substantiated that 5-substituted indole undergoes polymerization primarily at the 2 and 3 positions, while 2-substituted indole tends to polymerize at the 3 and 6 positions, and 3-substituted indole favors polymerization at the 2, 5, or 2, 6 positions.

1.3.4. Application of PIN

The considerable amount of research on PIN has been greatly driven by the possible technological uses of PINs. These potential applications encompass areas like electrochromic devices, sensing technologies, electrocatalytic processes, catalyst applications, diode devices, supercapacitors, and battery technologies.

1.3.4.1. Electrochromics

PIN's electrochromic characteristics have unveiled intriguing possibilities in the realm of intelligent windows and displays. When incorporated into electrochromic devices, PIN undergoes reversible color alterations in response to an external voltage or potential. This electrochromic phenomenon is a result of the redox reactions taking place within the polymer structure, enabling it to shift between different oxidation states and, consequently, display varying colors. Lately, there has been progress in constructing electrochromic devices (EDs) using PIN derivatives as the materials for the anode and either poly (3,4-(2,2-dimethylpropylenedioxy)thiophene) (PProDOTMe₂) or PEDOT for the cathode^[86].

1.3.4.2. Sensors

PIN's distinct electrical and chemical characteristics have garnered interest in diverse sensor applications. Below are several sensing categories where PIN assumes a noteworthy role.

Gas Sensors

Volatile Organic Compounds (VOCs): PIN-derived sensors have the capability to identify VOCs, including ethanol, methanol, and

acetone. Such sensors are utilized in breath analysis, monitoring air quality, and ensuring industrial safety^[87].

Toxic Gases: Sensors made from PIN exhibit sensitivity to harmful gases such as ammonia (NH₃), nitrogen dioxide (NO₂), and hydrogen sulfide (H₂S). These sensors are of great importance in tasks involving environmental surveillance and industrial safety^[88].

Biosensors

Glucose Sensors: Biosensors utilizing PIN have been developed for glucose detection, primarily aimed at aiding diabetes management. These sensors provide rapid and precise glucose assessments for individuals^[89].

DNA Sensors: PIN can be modified to generate DNA sensors, enabling the identification of particular DNA sequences. These serve as vital instruments in genetic investigations and medical screening^[90].

Chemical Sensors

pH Sensors: PIN can be employed to produce pH sensors that track shifts in acidity or alkalinity. These sensors are applied in diverse fields, such as environmental surveillance and biotechnology^[91].

Ion-Selective Sensors: PIN can be adapted to fabricate ion-selective sensors with the ability to identify particular ions such as potassium, sodium, or chloride. These sensors have uses in clinical diagnostic procedures and environmental assessments^[92].

1.3.4.3. Electrocatalysis

PIN-based electrocatalysis has emerged as a significant development in enhancing electrocatalytic reactions involving compounds such as ascorbate^[93], NADH^[78], methanol^[94], and formic

acid^[95]. PIN, owing to its conductive and catalytic properties, serves as an effective electrocatalyst. In the case of ascorbate and NADH, PIN-based electrocatalysis plays a crucial role in the oxidation of these biomolecules, which is integral in various biochemical processes. Additionally, in the electrocatalytic oxidation of methanol and formic acid, PIN serves as a catalyst, facilitating the conversion of these organic compounds into carbon dioxide and water, (fuel cell technology). The utilization of PIN-based electrocatalysts in these reactions showcases its potential in diverse fields contributing to more efficient and sustainable technological advancements.

1.3.4.4. Batteries

PIN-based materials are attracting considerable interest in the realm of battery technology. Its excellent qualities, such as moderately good electrical conductivity and stability in electrochemical processes make it a good fit for different battery parts.

Researchers in various laboratories have investigated PIN as a potential electrode material for batteries. For instance, a cell system was developed using Zn/1 M ZnSO₄/PIN, which demonstrated a remarkable maximum capacity of 90 Ah kg⁻¹ and an open-circuit potential of 1.45 V. Additionally, Cai and Hou assembled another cell, Zn/1 M ZnCl₂/PIN, with PIN serving as the cathode^[96].

1.3.4.5. Supercapacitors

Supercapacitors incorporating PIN as a key component mark a notable stride in energy storage technology. PIN's distinct blend of electrical conductivity and electrochemical characteristics renders it

a valuable choice for supercapacitor electrodes. These supercapacitors harness PIN's electrical conductivity, enabling swift charge and discharge processes. Furthermore, the robust electrochemical stability of PIN contributes to the prolonged lifespan of supercapacitors, ultimately lowering maintenance and replacement expenses^[97].

Furthermore, scientists have investigated different strategies to boost the efficacy of PIN in supercapacitors. These methods encompass structural adjustments, the integration of nanomaterials, hydrogels, metal oxides, and carbon-based materials, as well as the optimization of electrode design. These endeavors have resulted in the development of supercapacitors based on PIN that exhibits enhanced energy density, power density, and overall effectiveness^[98].

1.3.5. Limitations of PIN

Limited Solubility: PIN typically exhibits poor solubility in aqueous solvents and commonly used organic solvents, leading to difficulties in processing. Because of its low solubility, PIN can pose challenges when attempting to shape it into different formats, like films or fibers, thereby restricting its applicability in specific use cases.

Mechanical Properties: While PIN exhibits favorable electrical conductivity, its mechanical characteristics may not be as good as those of other CPs for certain applications. This can limit their application that demands a combination of electrical conductivity and mechanical resilience.

Poor cyclic stability during energy storage: PIN encounters a primary drawback related to its limited cyclic stability when employed as an energy storage material. This limitation arises from the expansion and contraction of the polymer chain during the redox process. Prolonged swelling can compromise the material's stability.

Approaches to tackle these challenges

Efforts have been taken by the scientific community to overcome the drawbacks of PIN, through synthesizing composites, copolymers, and hybrid materials by combining it with other polymers such as hydrogels, both in film and fiber forms.

PIN/metal composites: PIN/metal composites are a captivating category of materials that combine the distinct qualities of PIN, with the advantageous properties of various metal components. These composites are carefully crafted to leverage PIN's electrical conductivity and the versatile attributes of metals, opening up a wide array of potential applications such as catalysts, sensors, or integral components in electronic devices. Furthermore, when PIN is integrated with metals like gold, silver, palladium, or platinum, it can enhance the stability and sensitivity of sensors, making them valuable tools in various analytical and diagnostic applications^[99].

PIN/metal oxide composites: PIN/metal oxide composites offer a promising category of hybrid materials that merge the distinctive traits of PIN, with the unique attributes of metal oxide nanoparticles. For instance, when metal oxides like titanium dioxide, zinc oxide, or iron oxide are integrated into PIN matrices, the resulting materials exhibit heightened photoelectrochemical and photo-catalytic

properties^[100]. These composites find utility across various domains including photovoltaic, water purification, and environmental remediation. The collaborative influence of PIN and metal oxide constituents leads to improved charge transport and photo-catalytic performance, rendering them invaluable for solar energy utilization and addressing environmental concerns^[101]. The PIN/metal oxide composites are also used for supercapacitor applications^[97].

PIN/carbon composites: Carbon materials, including carbon fibers, single-walled carbon nanotubes (SWCNT), multi-walled carbon nanotubes (MWCNT), graphene, and reduced graphene oxide (rGO), have been incorporated into PIN through chemical or electrochemical techniques. This integration involves the formation of covalent bonds, such as C-N bonds, between the nitrogen in PIN and the carbon atoms in materials like SWCNT. When combined with MWCNT, PIN gains carboxy substitutions that enable the formation of nanowires^[102]. Joshi and colleagues introduced an in-situ chemical polymerization method to create tubular PIN^[102]. Moreover, the inclusion of rGO in PIN composites effectively addresses the issue of poor cyclic stability, resulting in improved energy storage capacity and cyclic stability^[103].

PIN/polymer and PIN/ hydrogel composite: The challenge of forming flexible films with PIN has somewhat restricted its potential applications. To enhance the mechanical properties, processability, and controllable conductivity of PIN, considerable research has been dedicated to incorporate PIN into other polymers like poly (vinyl acetate) ^[104], polyethylene, poly(vinyl chloride) ^[105], and

polydimethylsiloxane^[106]. As the proportion of PIN doped with Cl⁻ ions in these composites increases, so does the thermal stability. Additionally, the conductivity steadily rises. However, it is important to note that as the quantity of PIN in the composite increases the maximum mechanical strain that the composite films can endure decreases.

PIN/hydrogel hybrids, particularly when combined with materials like chitosan and polyvinyl alcohol (PVA) ^[107], stand out as excellent options for enhancing mechanical strength and flexibility, crucial for manufacturing devices across various applications. These hybrid materials also offer improved cyclic stability when employed in energy storage applications. PIN/PVA and PIN/chitosan hybrid films and fibers are very recently utilized in electrochemical sensing and charge storage applications^[52a, 108]. Moreover, these hydrogel-based hybrid materials are biocompatible, making them suitable for biomimetic purposes and drug delivery systems.

Copolymerization: Copolymerization presents a viable approach to modify the structure and characteristics of CPs. Copolymers typically exhibit properties that lie between those of homopolymers but differ significantly from composites and blends. Copolymers are formed by combining indole with other monomers like aniline^[109], pyrrole^[110], N-methyl pyrrole^[111], thiophene^[112], 3-methylthiophene^[113], 3,4-ethylenedioxythiophene (EDOT)^[114], and carbazole^[115] have primarily been synthesized using electrochemical copolymerization techniques. These copolymers demonstrate enhanced electrochemical, thermal, optical, and

electronic properties, positioning them as promising materials for applications in the realm of organic electronic devices.

1.4. Poly(3,4-ethylenedioxythiophene)-introduction

PEDOT stands as an incredibly adaptable CP that has garnered significant attention in the fields of materials science and electronics. Due to its unique chemical composition consisting of a thiophene ring and two ethylenedioxy (EDOT) side groups, PEDOT demonstrates remarkable electrical conductivity, and thermal stability. The PEDOT has relatively good processability. It is part of a group of CPs celebrated for their capability to carry electrical charge while preserving the flexibility and manageable properties typical of regular polymers.

The German Bayer Central Research Department has actively engaged in the pursuit of durable CPs suitable for industrial use. While initial efforts to stabilize polyacetylene and work on polypyrrole proved unsuccessful, they redirected their focus towards enhancing stability using mono alkoxy and 3,4-dialkoxy substituted thiophenes, and exploring bicyclic ring structures to reduce steric hindrance. Early attempts to synthesize 3,4-methylenedioxythiophene (MDOT) fell short due to the inability to isolate a usable quantity of the monomer^[116]. Consequently, attention turned to 3,4-ethylenedioxythiophene (EDOT), which yielded immediate success. Upon polymerization with an oxidative agent like iron (III) chloride, the resulting PEDOT marked a breakthrough in CP research, especially for its stability in the doped state and exhibited conductivities reaching up to 200 Scm⁻¹. This

synthesized PEDOT found immediate applications in capacitors. Following the initial oxidative polymerization of PEDOT reported by Bayer AG researchers in 1988, they also explored the first electro-polymerized PEDOT in the same year. Although PEDOT displays intriguing electrical conductivity, air and water stability, chemically synthesized PEDOT is black, insoluble, and non-meltable, whereas electrochemically synthesized PEDOT can solely be formed on conductive surfaces.

This exceptional trait, i.e., remarkable very high electrical conductivity combined with its ability to be easily synthesized using both chemical and electrochemical approaches, makes PEDOT a valuable material in various electronic applications. Its applications span in diverse fields such as organic electronics, sensor technology, actuator development, and energy storage systems. PEDOT's exceptional properties support the development of electronic components that are both pliable and lightweight, solidifying its significance in the burgeoning domain of flexible and wearable electronics. The distinctive combination of electrical performance and ease of processing inherent in this CP remains a driving force for innovation, catalyzing pioneering advancements in materials science and electronics^[117].

1.4.1. Molecular structure

The molecular structure of PEDOT involves repetitive units, which can be symbolically represented as $[(-C_4H_2O_2^-)_n]$. This notation denotes the replicated part that constitutes the polymer chain. PEDOT consists of multiple of these recurring units connected to

create an elongated polymer chain (Figure 1.7). The specific chemical configuration of PEDOT encompasses a thiophene ring with two ethylenedioxy side groups attached to it, as previously mentioned^[118].

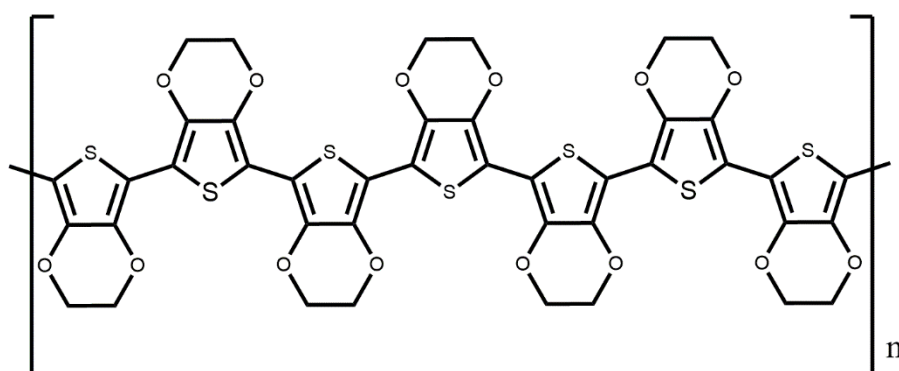


Figure 1.7 *The molecular structure of PEDOT*

1.4.2. Synthesis of PEDOT

PEDOT can be synthesized through three different polymerization routes.

1.4.2.1. The coupling of halogen derivatives of EDOT mediated by transition metals.

In this method, PEDOT predominantly appears in its more stable oxidized p-doped state, making it challenging to de-dope due to the stabilizing influence of the electron-donating dialkoxy groups. Investigating the neutral form of PEDOT, Yamamoto et al., conducted a polycondensation of 2,5-dichloro-3,4 ethylenedioxythiophene. This involved a reaction with a Ni(0) reagent, as outlined in Figure 1.8. However, the resultant dark purple product was insoluble, preventing the determination of its molecular weight, similar to other doped forms of PEDOT^[119].

1.4.2.2. Electrochemical polymerization

EDOT or its derivatives can undergo electrochemical polymerization in an electrolyte solution, and in presence of an oxidizing agent, often introduced as salts in a three-electrode system. The formation of PEDOT takes place on the surface of the anode, typically utilizing materials such as indium tin oxide plate (ITO), carbon cloth, or gold (Au). The process is rapid, yielding both supported and independent films. The resulting product's appearance varies from transparent blue to dark blue and can exhibit excellent electrical conductivities [120].

1.4.2.3. Chemical oxidative polymerization

In chemical oxidative polymerization the most common oxidizing agents used are complexes involving Fe^{3+} , such as ferric chloride (FeCl_3), ferric para-toluenesulfonate or tosylate ($\text{Fe}(\text{Tos})_3$) where $\text{Tos} = (\text{CH}_3\text{C}_6\text{H}_4\text{SO}_3^-)$, ferric camphor sulfonate ($\text{Fe}(\text{C}_7\text{H}_7\text{OSO}_3)_3$), ferric methanesulfonate or mesylate ($\text{Fe}(\text{CH}_3\text{SO}_3)_3$), and ferric trifluoromethanesulfonate or triflate ($\text{Fe}(\text{OTf})_3$) with $\text{OTf} = (\text{CF}_3\text{SO}_3^-)$. Among these, $\text{Fe}(\text{Tos})_3$ is the most commonly employed. In this process, Fe^{3+} oxidizes EDOT and is subsequently reduced to Fe^{2+} , while two oxidized EDOT units combine to form a dimer. This dimer is further deprotonated by surrounding water molecules and undergoes repetition to create polymer chains. The remaining Fe^{3+} ions function to dope the resulting PEDOT and Tos^- ions are incorporated as counter-anions to stabilize the doped PEDOT [121]. A schematic representation of the common oxidative polymerization method is shown in Figure 1.8.

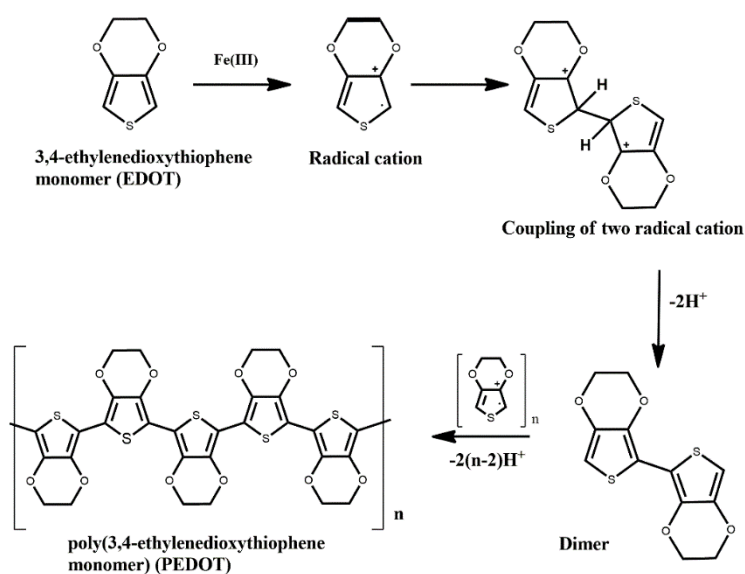


Figure 1.8 The schematic representation of chemical oxidative polymerization of PEDOT

Bayer et al., established the most widely used method for synthesizing PEDOT, which entailed adding the oxidizing agent to a mixture of the monomer and solvent. This process resulted in the

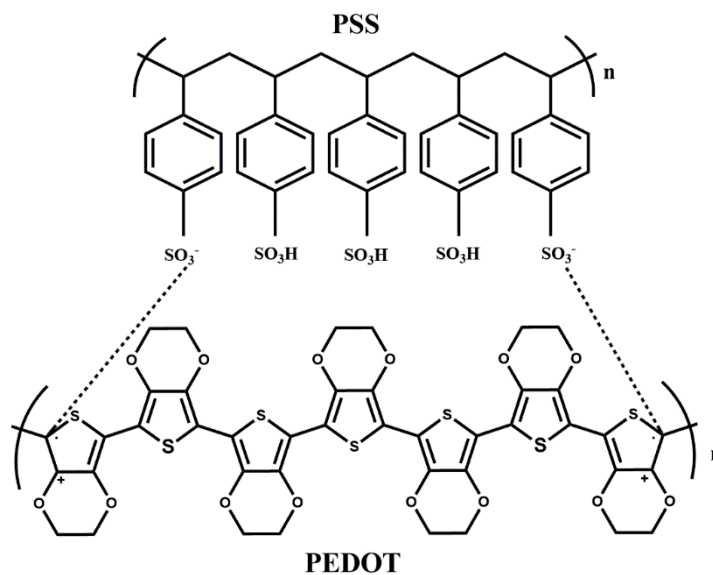


Figure 1.9 The chemical structure of PEDOT:PSS

formation of a dark, insoluble precipitate, marking the initial discovery of PEDOT. In the second method introduced by Bayer AG in 1990, EDOT is polymerized in an aqueous polyelectrolyte, typically PSS, using $\text{Na}_2\text{S}_2\text{O}_8$ as an oxidizing agent. Following this reaction, PEDOT was stabilized by the counter-anion PSS, resulting in a blue dispersion known as PEDOT: PSS (Figure 1.9).

1.4.3. Applications of PEDOT

PEDOT based materials have been extensively applied across various fields owing to their exceptional blend of electrical conductivity, durability and stability, and adaptability. A few noteworthy uses of PEDOT-based materials encompass:

Organic Electronics: PEDOT-based materials find application in organic electronics, including organic light-emitting diodes (OLEDs), organic photovoltaic cells (OPVs), organic thin film transistors (OTFTs), and organic field-effect transistors (OFETs). Their usefulness in these contexts stems from their electrical conductivity and film-forming characteristics^[122].

Transparent Conductive Films: PEDOT: PSS is frequently used in creating transparent conductive films for touchscreens, displays, and solar cells because of its excellent combination of high conductivity and optical transparency^[123].

Supercapacitors: PEDOT-derived materials serve as electrode components in supercapacitors, leveraging their exceptional electrical conductivity and electrochemical characteristics to rapidly store and discharge electrical energy^[124].

Electrochromic Devices: PEDOT-derived materials find application in electrochromic windows and displays, enabling alterations in optical characteristics like color or transparency due to their reversible redox reactions triggered by an applied voltage^[125].

Sensors: PEDOT-based materials are utilized in diverse sensor types, encompassing gas sensors and biosensors, leveraging their electrical conductivity and compatibility with biological systems. In the realm of **biosensors**, they are used in detecting biological molecules like glucose, DNA, and proteins, being instrumental in healthcare for purposes like monitoring blood glucose, disease diagnostics, and environmental surveillance^[126]. In **gas sensors**, PEDOT-based materials detect gases such as ammonia, nitrogen dioxide, and volatile organic compounds (VOCs), finding use in environmental monitoring, industrial safety, and air quality management^[127]. Moreover, these materials are adaptable for use as flexible wearable **temperature sensors**^[128]. Within **electrochemical sensors**, they play a role in identifying specific analytes like heavy metals in water and soil. Customizable to detect precise chemicals, PEDOT-based materials hold value in an array of applications, from ensuring food safety and water quality to controlling chemical processes^[129].

Biomedical Devices: PEDOT demonstrates compatibility with living tissues and has been applied in neural interfaces and various biomedical tools to record and stimulate neural activity^[130].

Conductive Textiles: PEDOT-infused materials can be integrated into textile production to fabricate conductive fabrics, serving

purposes in wearable electronics, intelligent garments, and health monitoring^[131].

Corrosion Protection: Studies have explored PEDOT-centered coatings for their ability to safeguard metals against corrosion, providing a substitute for conventional anti-corrosion coatings^[132].

Photovoltaic Windows: PEDOT-derived materials can be incorporated into windows to capture sunlight and produce electricity, making them well-suited for building-integrated photovoltaic (BIPV) systems^[133].

Printed Electronics: PEDOT-based inks and solutions are used in inkjet and screen printing for flexible and cost-effective printed electronic applications^[134].

Electrodes for Tissue Engineering: PEDOT-derived materials have been utilized as conductive frameworks in tissue engineering to stimulate cell growth and aid in tissue regeneration^[135].

The adaptable characteristics of PEDOT-based materials, alongside ongoing exploration and advancement, persistently pave the way for novel and inventive uses in diverse sectors, spanning electronics, energy, healthcare, and materials science.

Similar to PIN powder, PEDOT possesses several limitations. Its poor solubility and lack of mechanical durability hinder its practical application, restricting the fabrication of devices for diverse uses and the development of independent electrodes solely using PEDOT. This limitation is a common issue with CPs for fabricating flexible, stand-alone electrodes with enhanced mechanical strength. Different PEDOT composites are employed to fabricate

supercapacitors with improved cyclic stability, among which PEDOT: PSS is notably crucial.

1.5. Supercapacitors

Supercapacitors, also known as ultra-capacitors, represent a unique class of energy storage systems that markedly differ from conventional batteries concerning charge storage, energy density, and power density. Although both serve the purpose of storing electrical energy, their fundamental operating mechanisms differentiate them^[136].

Batteries store energy through chemical processes within their electrodes and electrolytes, enabling them to achieve high energy density. This characteristic allows batteries to store a significant amount of energy, making them well-suited for applications that need sustained power over a longer duration, such as smartphones or electric vehicles. Nonetheless, batteries have slower charging and discharging rates due to the chemical reactions involved, constraining their ability to rapidly deliver power^[137].

In contrast, supercapacitors accumulate energy through electrostatic and electrochemical means. This process empowers supercapacitors with exceptionally high power density, enabling swift delivery of energy when required. Their rapid charging and discharging capabilities make supercapacitors well-suited for scenarios where rapid bursts of power are crucial, like regenerative braking in hybrid vehicles or peak load management in industrial systems. Yet, supercapacitors generally exhibit lower energy density in comparison to batteries. This indicates their inability to store as

much overall energy as batteries, often requiring more frequent recharging or sometimes necessitating their use alongside batteries to ensure an uninterrupted power supply.

Essentially, supercapacitors and batteries play complementary roles in energy storage. Batteries are proficient in delivering high energy density for long-term power, whereas supercapacitors excel in scenarios needing quick power supply and high power density. Scientists are consistently seeking methods to unite these technologies, creating hybrid systems that merge their advantages, thereby enhancing energy storage solutions for a variety of applications^[30b].

Working principle: A supercapacitor consists of two electrodes separated by an ion-permeable layer known as a separator, while they remain ionically linked through an electrolyte. The electrolyte serves as a medium holding both positive and negative ions. To connect the electrodes to the electronic circuit, a thin metallic film called a collector is applied on the outer surface of the electrodes. Supercapacitors are categorized into three types, depending on the charge storage mechanism: electrical double-layer capacitors, pseudo capacitors, and hybrid supercapacitors^[138].

1.5.1. Electrical double-layer capacitor

Electrical double-layer capacitors (EDLCs), also known as supercapacitors or ultra-capacitors, are advanced energy storage devices that store electrical energy by creating an electrical double layer at the interface between the electrode and electrolyte. Unlike standard capacitors, EDLCs do not rely on chemical reactions for

charge storage; instead, they use high-surface-area electrodes typically made of activated carbon or porous materials to achieve a large surface area for charge accumulation (Figure 1.10). When a voltage is applied across the supercapacitor's electrodes, charges accumulate, creating a potential difference across the electrolyte^[139]. This potential difference causes positive and negative ions to move towards the oppositely charged electrodes. Simultaneously, solvent molecules become polarized and adhere to the electrode surfaces, preventing oppositely charged ions from combining with the electrodes. Consequently, an electrostatic double layer, referred to as a Helmholtz double layer (HDL), forms at the electrode surfaces. Each HDL behaves like a standard capacitor, with polarized solvent molecules acting as a dielectric medium^[140].

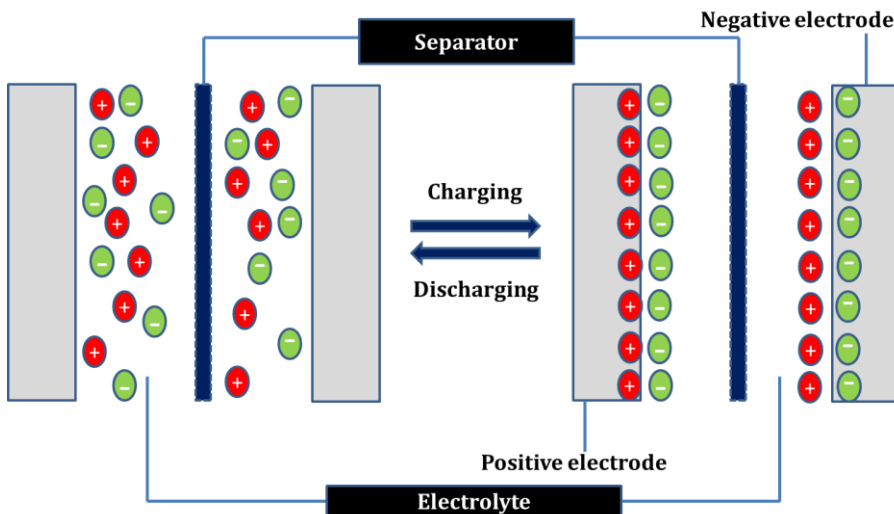


Figure 1.10 *The schematic representation of charging-discharging in EDLC*

The EDLCs are highly efficient in scenarios demanding high power density and frequent cycles of charging and discharging. These applications include hybrid vehicles, renewable energy systems, and portable electronics. Despite their benefits like extended cycle life and swift response times, EDLCs possess much lower energy density compared to batteries. Consequently, they are well-suited to complement battery systems across a range of applications.

1.5.2. Pseudocapacitor

A pseudocapacitor stores electrical energy through a reversible faradaic charge transfer process occurring between the electrode and the electrolyte, as illustrated in Figure 1.11. Typically, when a voltage is applied to the two electrodes of a supercapacitor, electrolyte ions migrate towards electrodes with opposite charges, creating a double layer at the interface between the electrolyte and the electrode. In the case of a pseudocapacitor, certain adsorbed electrolyte ions penetrate the double layer, transferring their charge to the electrodes. This charge transfer results from highly reversible redox reactions, intercalation, and electrosorption processes. Pseudocapacitance occurs concurrently with electrostatic double-layer capacitance but exhibits a significantly larger specific capacitance compared to EDLC. This is due to fact that charge storage in a pseudocapacitor occurs through redox reactions throughout the bulk of the electrode material, not just at the surface, as observed in EDLC. The magnitude of pseudocapacitance depends on the nature and distribution of porosity in the electrode utilized. A

pseudocapacitor stores a larger charge than an EDLC, thereby providing relatively higher specific energy^[141].

1.5.3. Hybrid supercapacitor

A hybrid supercapacitor merges both EDLC and pseudocapacitor technologies, featuring two dissimilar electrodes, one with high pseudocapacitance and the other with high electrostatic double-layer capacitance. The electrode with pseudocapacitance boosts the specific capacitance, working voltage, and specific energy of the supercapacitor, while the double-layer capacitive electrode enhances cyclic stability and specific power. This amalgamation

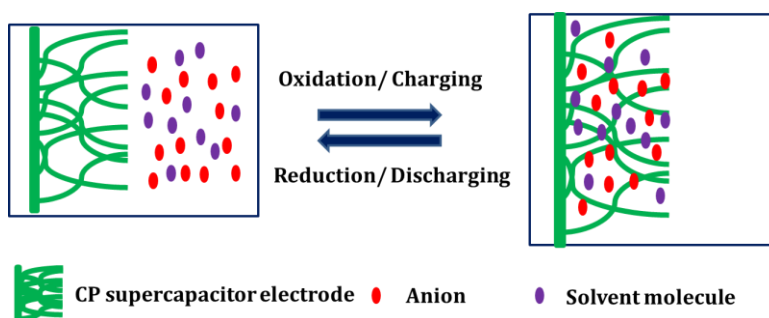


Figure 1.11 *The schematic representation of charging-discharging in pseudocapacitor*

results in a hybrid supercapacitor showing improved electrochemical performance. Consequently, researchers predominantly focus on exploring various types of hybrid supercapacitors. These hybrid supercapacitors can also be produced by blending composites of pseudocapacitive materials with double-layer capacitive materials^[142].

CP based supercapacitor

The effectiveness of a supercapacitor heavily relies on the electrode material used. To enhance supercapacitors, numerous electrode

materials, including carbon-based substances, transition metal oxides/sulfides, CPs, and others, have been studied by various researchers^[143].

Lately, CPs and their combinations have gained significant attention among researchers because of their notable characteristics such as high conductivity (when doped), excellent charge storage capability, broad voltage range, ease of synthesis, cost-effectiveness, and environmentally friendly nature. These attributes render CPs as favorable materials for constructing supercapacitor electrodes^[70b, 144].

PANI, PPY, PTh, PEDOT, and PIN stand out as the most thoroughly researched CPs for creating supercapacitor electrodes owing to their good conductivity, significant porosity, broad potential range, ease of synthesis, and minimal environmental impact^[145]. Each CP presents certain advantages and drawbacks. Reviewing specific capacitance values in existing literature indicates that PANI leads among these polymers in terms of the theoretical gravimetric specific capacitance. It showcases impressive environmental and thermal stability, yet its relatively cyclic stability is not so promising which restricts its applications.

However, PEDOT demonstrates remarkable conductivity and exceptional stability^[117b]. It can be easily fashioned into thin films. Nevertheless, its limitations in terms of low specific capacitance, power density, and energy density hinder its extensive use in supercapacitors. In contrast, PPY, as a denser material, exhibits higher volumetric specific capacitance (400–500 F/cm³), good

electrical conductivity, and greater chemical and thermal stability. Additionally, it boasts outstanding mechanical flexibility, crucial for developing future foldable, squeezable, twistable, stretchable, and flexible electronic devices. Like other CPs, PPY struggles with cyclic stability due to the breakage of polymer chains during continuous charge-discharge cycles. PIN, a relatively novel and less researched CP, faces challenges due to its low electrical conductivity and specific capacitance^[146]. However, its advantageous properties, including high redox activity, cost-effectiveness, superior thermal stability, and ease of synthesis, attract the attention of various researchers. Additionally, PIN degrades slowly compared to other CPs, prolonging its cyclic life and making it suitable for long-lasting energy storage devices. Consequently, PPY and PIN have recently emerged as highly regarded CPs for creating energy storage devices. As CP-based electrodes undergo continuous swelling and contracting during charge and discharge cycles due to ion movement within the polymer, this process ultimately leads to electrode degradation and decreased cyclic stability.

Enhancing cyclic stability and specific capacitance can be achieved by synthesizing composite of CPs with various substances such as metal oxides, nanoparticles, hydrogels, etc., effectively minimizing the swelling of the polymer chain when counter anions are inserted.

1.6. Electrochemistry of CPs-introduction

The groundbreaking discovery in the late 1970s revealed the distinctive reversible redox reaction in CPs, an achievement that led to the Nobel Prize in 2000. These polymers, through either chemical

or electrochemical processes, undergo redox reaction, triggering an ion exchange with the surrounding electrolyte, known as the doping-de-doping mechanism^[147]. This exchange of ions continuously alters the composition of the CPs, influencing various properties such as conductivity, color, and volume. CPs, owing to their capacity for reversible oxidation and reduction from a neutral state, hold significant importance for various applications. The osmotic pressure generated during the redox reaction is balanced by the exchange of solvent molecules to or from the electrolyte. This reversible electrochemical redox reaction induces changes in the conformation of the polymer chain by converting the quinoid structure to benzenoid and vice versa^[148]. As a result, CPs are considered reactive materials, and their fundamental electrochemical reactions are elucidated here.

1.6.1. Oxidation (p-doping)

p-doping stands as a significant mechanism in CPs. Oxidation of the material occurs through the application of the polymer's ionization potential. The oxidation of the CPs chain through p-doping involves the removal of n consecutive electrons from every polymer chain facilitated by an applied potential that generates positive charges or "holes" along the chain. The transformation from a neutral to a positively charged material can occur in two different ways.

Prevailing anion exchange

Here, during oxidation, the stimulated conformational changes in the polymer chains create additional space, allowing anions from the solution to enter and balance the positive charges on the polymer

chains. The elevated concentration of positive charges within the oxidized polymer chain prompts the entry of solvent from the solution to sustain the osmotic pressure.

Consequently, the polymer expands during oxidation (volume increases). Conversely, during neutralization, observed in reaction 1.1, a reverse process occurs, leading to a shrinking of the polymer chain (decrease in volume).

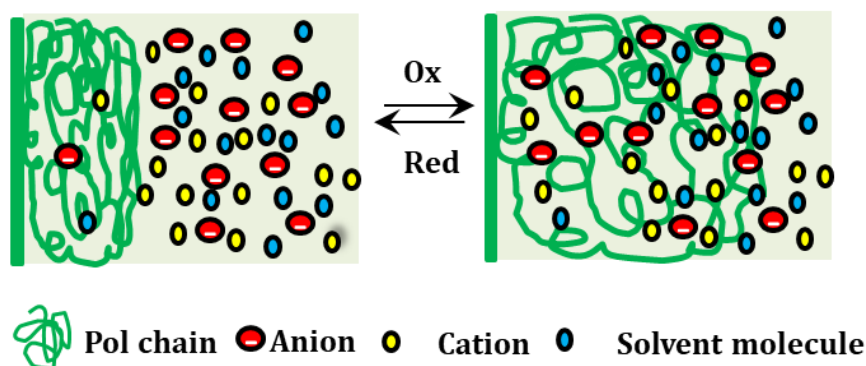
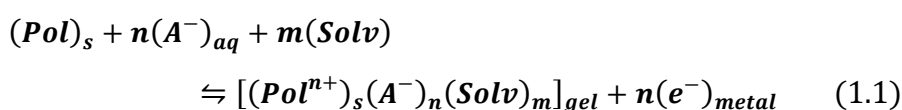


Figure 1.12 The schematic representation of prevailing anion exchange mechanism in CP

The variables *pol*, A^- , *Solv* represent the reactive centers of the polymer, counter anions, and solvent molecules, respectively. The subscripts 's' and 'aq' stand for solid and aqueous solutions, respectively.

Anion insertion causes an increase in the volume of the polymer chain, transforming the densely packed solid state of the polymer

into a gel structure, leading to swelling during oxidation. In contrast, reduction leads to a decrease or shrinking, as depicted in Figure 1.12.

Prevailing cation exchange

When the polymer is synthesized in the presence of larger anions, these anions are confined within the polymer structure, regardless of the oxidation state of the CPs. In such cases, the positive charge that emerges during the oxidation process is offset by expelling cations from the polymer chain, as indicated in the reaction. As a result, the volume of the polymer structure decreases during oxidation, causing shrinking.

Conversely, during reduction, the opposite process, i.e., the polymer expands during reduction, as depicted in Figure 1.13.

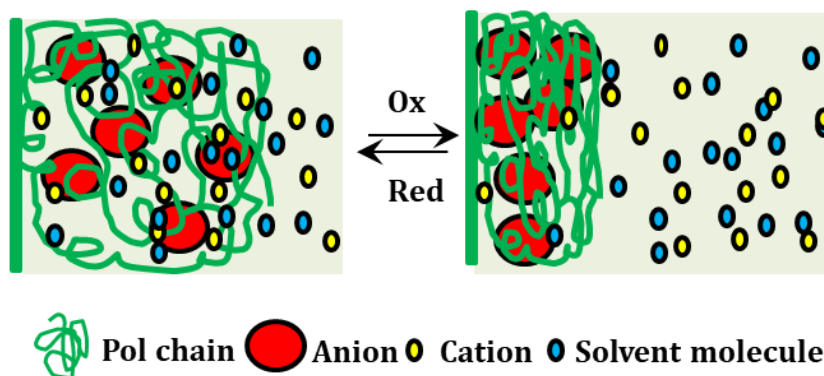
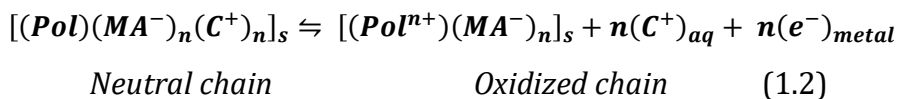


Figure 1.13 The schematic representation of prevailing cation exchange mechanism in CP



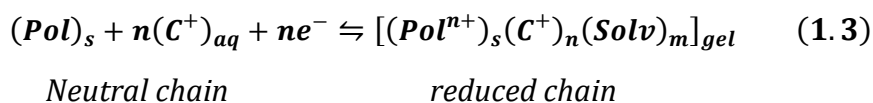
MA⁻ signifies any macroscopic anion (organic, polymeric, or inorganic) confined within the CP during polymerization, while C⁺ denotes a cation. In this scenario, the function of the solvent

molecule remains ambiguous due to the existence of ionic species within the material that exhibit a robust interaction with the solvent dipole, irrespective of the oxidation state.

1.6.2. Reduction (n-doping)

Certain CPs like PEDOT, polythiophene, or polyfluorenes possess a significant electronic affinity, allowing them to transform from a neutral state to a reduced state. This transition permits the storage of negative charges by injecting electrons into the chains at high cathodic potentials.

To execute this reaction (1.3), extremely stable solvents and salts are necessary as electrolytes. As a result of reduction, the material expands, while during neutralization, it contracts.



1.7. CPs as reversible multi-step macromolecular motors

During oxidation of CPs, a series of n consecutive steps, each involving the extraction of one electron, occurs gradually (each step representing an energetic conformational state). As the polymer chain oxidizes, it generates extra space to accommodate anions and solvent molecules from the electrolyte to balance the charge and osmotic pressure. This process leads to an expansion/swelling of the polymer structure and prompts structural alterations.

When the available free volume is limited, meaning that the distance between adjacent polymer chains is similar to the diameter of the counter anions, the reaction rate is sluggish. Significant force is

necessary to diffuse the anions from the solvent to the polymer chain.

Consequently, the effective insertion of anions and solvent molecules is impeded, although minor structural changes may still occur^[149].

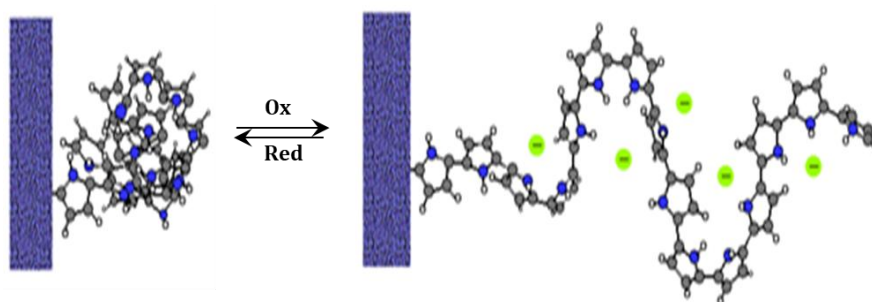


Figure 1.14 *The conformational movement during redox reaction in CP*

The reversible oxidation/reduction process involves rearrangements of σ and π bonds. During oxidation, there is a rearrangement of π bonds to a certain degree leading to conformational movements, as depicted in Figure 1.14.

The flexible, coiled structure experiences restricted rotation as it converts to a planar form upon the creation of bipolarons. Conversely, during reduction, a reverse conformational change occurs. Consequently, CPs are regarded as reversible macromolecular motors.

This process involves the ejection and insertion of electrons in 'n' consecutive steps, which characterizes them as reversible, multistep macromolecular motors^[150].

1.8. Biomimetic properties of CPs

When wet, CPs manifest as reactive gels, and within their structures, the combination of CPs, water, and ions represents the most basic material system capable of mimicking biological functions^[151]. The electrochemical reactions of CPs in aqueous solutions involve electron, ion, and water molecules which flow between the CP/electrolyte interface, leading to reorganization (breaking and formation) of double bonds along the chains, resulting in conformational movements, and macroscopic processes, i.e., expansion or contraction^[147]. These steps resemble the sequential events occurring in functioning biological organs. The continuous alteration in the composition of the polymer's active center influences various properties of CPs responsible for the biomimicking applications depicted in Figure 1.15.

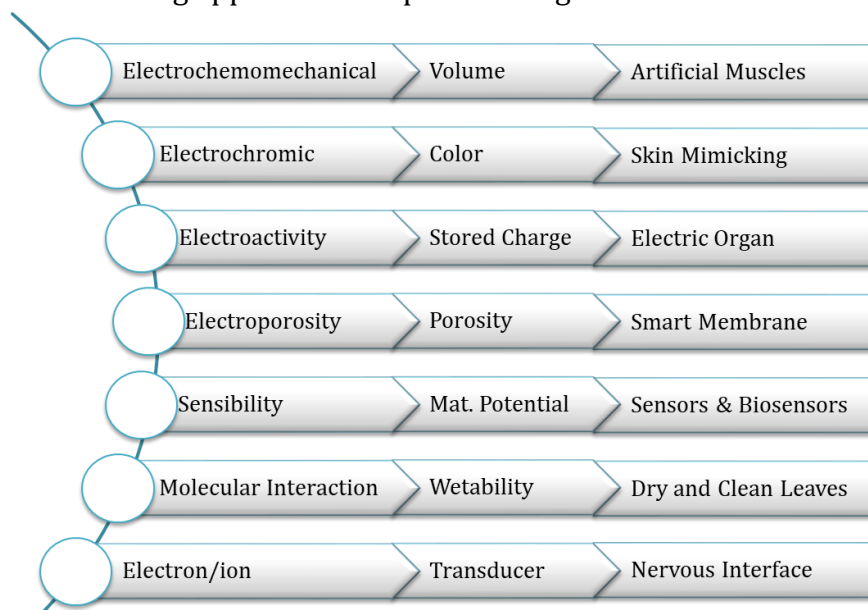


Figure 1.15 *The composition-dependent properties and corresponding biomimetic applications of CP*

Biological systems communicate with their environment through electrical signals transmitted through nerves to the brain via a single connectivity. Muscles within biological entities possess the capability to perceive various energetic conditions, including temperature, pressure, muscle potential, and chemical potential during operation. They function as macromolecular machines, activated by electrical signals from the brain via neurons, which in turn send feedback impulses back to the brain, known as the brain-muscle interface^[152]. Replicating these sequential reactions observed in biological muscles using a model material was a significant challenge for the scientific community.

CPs can serve as a material model replicating the sequential reactions akin to those occurring in biological muscles. In this thesis, our focus lies on investigating the reactive sensing attributes of CPs, imitating the sensing capabilities of biological muscles. The polymer chain functions akin to a molecular machine, operating through the cooperative actuation initiated by the reversible redox reaction, which results in volume expansion to accommodate anions and solvent, followed by contraction to expel them. This movement within the polymer chain mirrors the cooperative actuation seen in the sarcomere within the cellular matrix, responsible for energy transfer in muscles. In this context, CPs convert mechanical energy to electrical energy or charge, communicating variations in operational parameters to the computer via two connecting wires, similar to the biological muscle-nerve-brain interface. As a result, CPs operate as reversible biomimetic macromolecular motors.

Figure 1.16 represents the schematic representation of the biomimicking property of CPs.

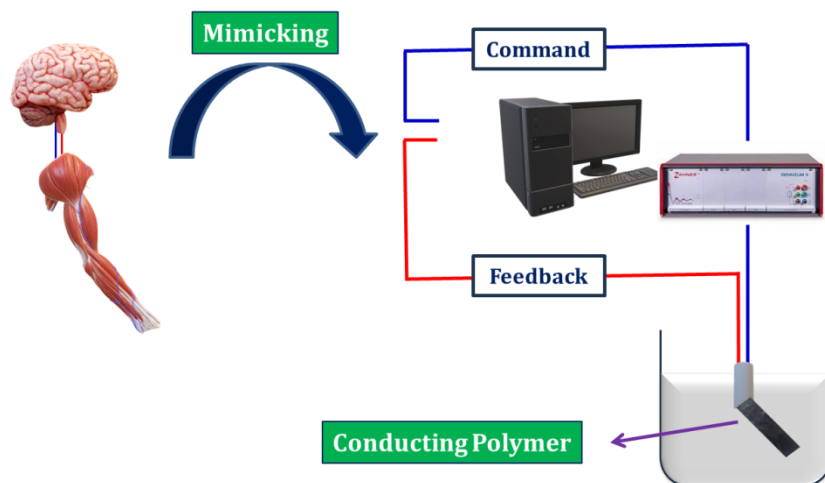


Figure 1.16 Schematic representation of biomimicking property of CPs

1.9. The present work

The last two decades have witnessed tremendous advancement in the field of CPs. Their distinctive electrical, optical, and electrochemical properties have driven extensive research to explore their potential applications in electronics, energy storage, sensors, actuators, etc. While the majority of research has traditionally focused on CPs in their dry state, their behavior as reactive gels when wet has immense potential for various applications due to their vast non-stoichiometric properties. The properties of CPs in their dry state are well understood within the scientific community, but there's a lack of comprehensive exploration and understanding of composition-dependent properties and their implications in the applications of CPs. This

thesis is dedicated to the investigation of CPs in their wet state, particularly focusing on the electrochemistry of PIN and PEDOT. The research aims to deeply explore reaction-driven biomimetic sensing applications and emphasizes the structural electrochemistry of these CPs.

While PIN and PEDOT remain widely explored CPs, commonly employed across various significant applications in the scientific realm, this thesis delves into the reactive sensing properties of PIN and PEDOT. Prior to this exploration, a comprehensive study was conducted to understand their structural electrochemistry, an area that has not been investigated by any researchers previously. This research sought to unravel the conformational changes in these CPs during electrochemical reactions and identify the various conformational states. The study employed a novel method, QV to explore the structural alterations during the Faradaic process. Upon comprehensive investigation of the structural Faradaic process of PIN and PEDOT, we are then aiming to leverage this structural electrochemistry for their potential application as a biomimetic sensor capable of sensing its working ambient. One of our primary objectives is to demonstrate that the reactive sensing nature is a general property of all CPs. Our research group has already established and explored the reactive sensing attributes in PANI and PPY.

Fabricating a multifunctional macromolecular motor that can sense the physical and chemical variables while working without any additional connectivity was one of the oldest dream of scientists and

engineers. We tried to address this challenge through developing a freestanding electrode material made of PIN and PEDOT. In order to have proper mechanical stability for the electrode material we have used PVA as a template.

The study delves into understanding the reactive sensing characteristics exhibited by the PIN/PVA film and PEDOT/PVA films. We then explored how the cooperative actuation of the macromolecular motor comprises of PIN and PEDOT polymer chain changes in response to alterations in the working environmental condition. Through voltammetry, this investigation demonstrates that the conformational changes observed during the Faradaic process directly correlate with sensing characteristics with respect to its working condition.

Initially, we started with chemically synthesized PIN powder and PEDOT powder. Since the processability of PIN powder and PEDOT powder for direct application as freestanding electrode material was less. We fabricated electroactive hybrid freestanding polymer film using PVA as a template for their potential application. The electrochemical redox reaction that underlies charge storage is also accountable for sensing applications. To delve into the CPs' ability to sense while working, we scrutinized the charge storage aspect of the PEDOT/PVA film. By computing the electrical energy utilized during both the charge and discharge processes, we explored into how the PEDOT/PVA film senses its working electrical condition.

We then fabricated a symmetrical solid-state two-electrode device using the PEDOT/PVA film. The material was studied for its

supercapacitor application and its ability to sense simultaneously its electrical and thermal working conditions Investigating the device's capacity to sense while it charges and discharges via a single connection draws a parallel with the sensing nature of biological muscles. Like the brain-muscle interface, it processes commands from the computer and relays sensing feedback through the same connections. Through our studies on the reactive sensing characteristics of CPs with respect to their working conditions.

References

- [1] M. J. Kletter, T. Woerner, A. Pron, A. G. MacDiarmid, A. J. Heeger, Y. Park, *J. Chem. Soc., Chem. Commun.* **1980**, 426b-428.
- [2] G. Marsh, *Mater. Today* **2001**, *4*, 4-6.
- [3] aC. K. Chiang, C. Fincher Jr, Y. W. Park, A. J. Heeger, H. Shirakawa, E. J. Louis, S. C. Gau, A. G. MacDiarmid, *Physical review letters* **1977**, *39*, 1098; bA. J. Heeger, A. G. MacDiarmid, in *The Physics and Chemistry of Low Dimensional Solids: Proceedings of the NATO Advanced Study Institute held at Tomar, Portugal, August 26-September 7, 1979*, Springer, **1980**, pp. 354-391; cH. Shirakawa, E. J. Louis, A. G. MacDiarmid, C. K. Chiang, A. J. Heeger, *J. Chem. Soc., Chem. Commun.* **1977**, 578-580.
- [4] Y. Cao, P. Smith, A. J. Heeger, *Polymer* **1991**, *32*, 1210-1218.
- [5] A. G. MacDiarmid, A. J. Heeger, *Synthetic Metals* **1980**, *1*, 101-118.
- [6] T. Clarke, B. McQuillan, J. Rabolt, J. Scott, G. Street, *Molecular Crystals and Liquid Crystals* **1982**, *83*, 1-16.
- [7] J. Bobacka, Z. Gao, A. Ivaska, A. Lewenstam, *Journal of Electroanalytical Chemistry* **1994**, *368*, 33-41.
- [8] S. Ghosh, V. Gueskine, M. Berggren, I. V. Zozoulenko, *The Journal of Physical Chemistry C* **2019**, *123*, 15467-15476.
- [9] aS.-J. Choi, S.-M. Park, *Journal of the electrochemical society* **2002**, *149*, E26; bF. Ziaeimoghaddam, R. Arefinia, *Prog. Org. Coat.* **2022**, *170*, 106952.
- [10] Z. Ping, H. Neugebauer, J. Theiner, A. Neckel, *J. Chem. Soc., Faraday Trans.* **1997**, *93*, 121-129.
- [11] J. Choi, S. K. Jang, F. S. Kim, *physica status solidi (a)* **2018**, *215*, 1701019.
- [12] B. J. Polk, K. Potje-Kamloth, M. Josowicz, J. Janata, *The Journal of Physical Chemistry B* **2002**, *106*, 11457-11462.

-
- [13] I. Ikemoto, M. Sakairi, T. Tsutsumi, H. Kuroda, I. Harada, M. Tasumi, H. Shirakawa, S. Ikeda, *Chem. Lett.* **1979**, *8*, 1189-1192.
- [14] A. Watanabe, M. Tanaka, J. Tanaka, *Bull. Chem. Soc. Jpn.* **1981**, *54*, 2278-2281.
- [15] M. Breitenbach, K.-H. Heckner, *Journal of Electroanalytical Chemistry and Interfacial Electrochemistry* **1973**, *43*, 267-286.
- [16] G. Tourillon, F. Garnier, *Electrochemical Society, Journal* **1983**, *130*, 2042-2044.
- [17] N. Murthy, L. Shacklette, R. Baughman, *The Journal of chemical physics* **1987**, *87*, 2346-2348.
- [18] S. Ramanavicius, A. Ramanavicius, *Nanomaterials* **2021**, *11*, 371.
- [19] J. C. Lacroix, K. I. Chane-Ching, F. Maquere, F. Maurel, *Journal of the American Chemical Society* **2006**, *128*, 7264-7276.
- [20] P. Bätz, D. Schmeisser, W. Göpel, *Physical Review B* **1991**, *43*, 9178.
- [21] A. Yussuf, M. Al-Saleh, S. Al-Enezi, G. Abraham, *International Journal of Polymer Science* **2018**, *2018*.
- [22] A. Epstein, W.-P. Lee, V. Prigodin, *Synthetic metals* **2001**, *117*, 9-13.
- [23] E. Punkka, M. Rubner, J. Hettlinger, J. Brooks, S. Hannahs, *Physical Review B* **1991**, *43*, 9076.
- [24] G. Tourillon, F. Garnier, *The Journal of Physical Chemistry* **1983**, *87*, 2289-2292.
- [25] Pooja, A. Kumar, P. Prasher, H. Mudila, *Carbon Letters* **2023**, *33*, 307-324.
- [26] A. F. Diaz, K. K. Kanazawa, G. P. Gardini, *J. Chem. Soc., Chem. Commun.* **1979**, 635-636.
- [27] T. Jarosz, P. Ledwon, *Materials* **2021**, *14*, 281.
- [28] K. A. Milakin, Z. Morávková, R. Konefał, S. Gupta, U. Acharya, Z. Walterová, P. Bober, *Polymer* **2022**, *239*, 124447.
- [29] X. Guo, J. Li, F. Wang, J. H. Zhang, J. Zhang, Y. Shi, L. Pan, *Journal of Polymer Science* **2022**, *60*, 2635-2662.
- [30] aS. K. Verma, S. Samanta, A. K. Srivastava, S. Biswas, R. M. Alsharabi, S. Rajput, *Advances in Materials Science and Engineering* **2022**, *2022*; bA. Shabeeba, L. Rajan, M. P. Sidheekha, M. S. Thayyil, Y. A. Ismail, *Journal of Energy Storage* **2022**, *55*, 105724.
- [31] L. Benny Mattam, A. Bijoy, D. Abraham Thadathil, L. George, A. Varghese, *ChemistrySelect* **2022**, *7*, e202201765.
- [32] Y. Lei, J. Xu, in *Corrosion and Protection of Marine Engineering Materials: Applications of Conducting Polymers and Their Composites*, CRC Press, **2023**, pp. 1-27.
- [33] S. Shahabuddin, R. Gaur, N. Mukherjee, P. Chandra, R. Khanam, *Materials Today: Proceedings* **2022**, *62*, 6950-6955.
-

- [34] A. F. Wibowo, J. W. Han, J. H. Kim, A. Prameswati, S. A. N. Entifar, J. Park, J. Lee, S. Kim, D. C. Lim, M.-W. Moon, *Science and Technology of Advanced Materials* **2022**, *23*, 332-340.
- [35] R. Baughman, L. Shacklette, R. Elsenbaumer, E. Plichta, C. Becht, in *Conjugated polymeric materials: Opportunities in electronics, optoelectronics, and molecular electronics*, Springer, **1990**, pp. 559-582.
- [36] J. Barisci, C. Conn, G. Wallace, *Trends in Polymer Science* **1996**, *9*, 307-311.
- [37] aH. Makki, A. Troisi, *Journal of Materials Chemistry C* **2022**, *10*, 16126-16137; bN. M. Sadiq, S. B. Aziz, M. F. Kadir, *Gels* **2022**, *8*, 153.
- [38] P. Shen, Z. Jiang, J. Viktorova, B. Pollard, A. Kumar, Z. Stachurski, L. A. Connal, *ACS Applied Nano Materials* **2023**, *6*, 986-994.
- [39] O. Folorunso, P. Olukanmi, S. Thokozani, *Materials Today Communications* **2023**, 106308.
- [40] B. Zhang, Y. Dong, J. Han, Y. Zhen, C. Hu, D. Liu, *Advanced Materials* **2023**, 2301320.
- [41] P. H. Patil, V. V. Kulkarni, S. A. Jadhav, *Journal of Composites Science* **2022**, *6*, 363.
- [42] aA. Chithrambattu, Y. A. Ismail, *Journal of Adhesion Science and Technology* **2020**, *34*, 2685-2702; bR. Rajamany, S. Prakash, Y. A. Ismail, *Plastics, Rubber and Composites* **2022**, *51*, 240-249.
- [43] Y. Xiao, Y. Wang, X. Wu, Y. Ma, *High Perform. Polym.* **2023**, *35*, 213-227.
- [44] N. A. Peppas, A. S. Hoffman, in *Biomaterials science*, Elsevier, **2020**, pp. 153-166.
- [45] Y. Yang, X. Zhao, J. Yu, X. Chen, X. Chen, C. Cui, J. Zhang, Q. Zhang, Y. Zhang, S. Wang, *ACS applied materials & interfaces* **2020**, *12*, 34161-34169.
- [46] J. Fu, *Journal of Materials Chemistry B* **2019**, *7*, 1523-1525.
- [47] A. Khandan, H. Jazayeri, M. D. Fahmy, M. Razavi, *Biomater Tissue Eng* **2017**, *4*, 143-169.
- [48] M. Mahinroosta, Z. J. Farsangi, A. Allahverdi, Z. Shakoory, *Materials Today Chemistry* **2018**, *8*, 42-55.
- [49] D. Mawad, A. Lauto, G. G. Wallace, *Polymeric hydrogels as smart biomaterials* **2016**, 19-44.
- [50] Y. Zhao, B. Liu, L. Pan, G. Yu, *Energy & Environmental Science* **2013**, *6*, 2856-2870.
- [51] L. Pan, G. Yu, D. Zhai, H. R. Lee, W. Zhao, N. Liu, H. Wang, B. C.-K. Tee, Y. Shi, Y. Cui, *Proceedings of the National Academy of Sciences* **2012**, *109*, 9287-9292.
-

-
- [52] aL. Rajan, M. P. Sidheekha, A. Shabeeba, Y. A. Ismail, *Materials Chemistry Frontiers* **2022**, *6*, 1706-1718; bB. Guo, Z. Ma, L. Pan, Y. Shi, *J. Polym. Sci., Part B: Polym. Phys.* **2019**, *57*, 1606-1621.
- [53] Y. A. Ismail, A. Shabeeba, M. P. Sidheekha, L. Rajan, *Actuators: Fundamentals, Principles, Materials and Applications* **2020**, 211-252.
- [54] M. Bansal, A. Dravid, Z. Aqrave, J. Montgomery, Z. Wu, D. Svirskis, *J. Controlled Release* **2020**, *328*, 192-209.
- [55] D. Mawad, E. Stewart, D. L. Officer, T. Romeo, P. Wagner, K. Wagner, G. G. Wallace, *Advanced Functional Materials* **2012**, *22*, 2692-2699.
- [56] aX. Han, G. Xiao, Y. Wang, X. Chen, G. Duan, Y. Wu, X. Gong, H. Wang, *Journal of Materials Chemistry A* **2020**, *8*, 23059-23095; bY. Shi, L. Peng, G. Yu, *Nanoscale* **2015**, *7*, 12796-12806.
- [57] C. Kleber, K. Lienkamp, J. Rhe, M. Asplund, *Advanced Biosystems* **2019**, *3*, 1900072.
- [58] Y. A. Ismail, S. R. Shin, K. M. Shin, S. G. Yoon, K. Shon, S. I. Kim, S. J. Kim, *Sensors and Actuators B: Chemical* **2008**, *129*, 834-840.
- [59] T. Yang, C. Xu, C. Liu, Y. Ye, Z. Sun, B. Wang, Z. Luo, *Chem. Eng. J.* **2022**, *429*, 132430.
- [60] Y. Chen, X. Fu, S. Kang, L. Wang, W. Lu, *ACS Applied Electronic Materials* **2021**, *3*, 3889-3897.
- [61] aL. M. Lira, S. I. Crdoba de Torresi, *Electrochem. Commun.* **2005**, *7*, 717-723; bS. Brahim, D. Narinesingh, A. Guiseppi-Elie, *Anal. Chim. Acta* **2001**, *448*, 27-36.
- [62] aM. P. Sidheekha, L. Rajan, Y. A. Ismail, *Materials Chemistry and Physics* **2022**, *279*, 125769; bA. Shabeeba, M. P. Sidheekha, L. Rajan, Y. A. Ismail, *RSC Advances* **2022**, *12*, 31911-31922.
- [63] C. Kleber, M. Bruns, K. Lienkamp, J. Rhe, M. Asplund, *Acta Biomaterialia* **2017**, *58*, 365-375.
- [64] L. Xiao, Y. Zhao, G. Chang, H. Yan, R. Zou, X. Zhang, S. Wang, H. He, *Anal. Chim. Acta* **2023**, *1269*, 341341.
- [65] aL. Wang, T. Xu, X. Zhang, *TrAC, Trends Anal. Chem.* **2021**, *134*, 116130; bX. Liu, X. Chen, X. Chi, Z. Feng, C. Yang, R. Gao, S. Li, C. Zhang, X. Chen, P. Huang, *Nano Energy* **2022**, *92*, 106735.
- [66] aZ. Ma, W. Shi, K. Yan, L. Pan, G. Yu, *Chemical science* **2019**, *10*, 6232-6244; bL. Li, Y. Shi, L. Pan, Y. Shi, G. Yu, *Journal of Materials Chemistry B* **2015**, *3*, 2920-2930.
- [67] M. Uz, S. K. Mallapragada, *Journal of the Indian Institute of Science* **2019**, *99*, 489-510.
- [68] aY. A. Ismail, J. G. Martnez, A. S. Al Harrasi, S. J. Kim, T. F. Otero, *Sensors and Actuators B: chemical* **2011**, *160*, 1180-1190; bY. A. Ismail, J. G. Martnez, A. S. Al Harrasi, S. J. Kim, T. F. F. Otero, in
-

- Electroactive Polymer Actuators and Devices (EAPAD) 2011, Vol. 7976, SPIE, 2011, pp. 450-461.*
- [69] Y. A. Ismail, J. Chang, S. R. Shin, R. S. Mane, S.-H. Han, S. J. Kim, *Journal of The Electrochemical Society* **2009**, *156*, A313.
- [70] aM. Moussa, M. F. El-Kady, D. Dubal, T. T. Tung, M. J. Nine, N. Mohamed, R. B. Kaner, D. Losic, *ACS Applied Energy Materials* **2019**, *3*, 923-932; bM. P. Sidheekha, A. Shabeeba, L. Rajan, M. S. Thayyil, Y. A. Ismail, *Engineered Science* **2023**, *23*, 890.
- [71] H. L. Youmans, J. B. Rush, V. H. Brown, *J. Heterocycl. Chem.* **1976**, *13*, 949-953.
- [72] G. Tourillon, F. Garnier, *Journal of Electroanalytical Chemistry and Interfacial Electrochemistry* **1982**, *135*, 173-178.
- [73] R. J. Waltman, A. Diaz, J. Bargon, *The Journal of Physical Chemistry* **1984**, *88*, 4343-4346.
- [74] G. Zotti, S. Zecchin, G. Schiavon, R. Seraglia, A. Berlin, A. Canavesi, *Chemistry of materials* **1994**, *6*, 1742-1748.
- [75] H. Talbi, E. Maarouf, B. Humbert, M. Alnot, J. Ehrhardt, J. Ghanbaja, D. Billaud, *J. Phys. Chem. Solids* **1996**, *57*, 1145-1151.
- [76] K. Phasukom, A. Sirivat, *Synthetic Metals* **2016**, *219*, 142-153.
- [77] H. Talbi, J. Ghanbaja, D. Billaud, B. Humbert, *Polymer* **1997**, *38*, 2099-2106.
- [78] W. Zhou, J. Xu, *Polymer Reviews* **2017**, *57*, 248-275.
- [79] K. M. Choi, K. H. Kim, *Journal of applied polymer science* **1992**, *44*, 751-763.
- [80] aP. S. Abthagir, K. Dhanalakshmi, R. Saraswathi, *Synthetic metals* **1998**, *93*, 1-7; bR. Lazzaroni, A. De Pryck, C. Debaisieux, J. Riga, J. Verbist, J. Bredas, J. Delhalle, J. André, *Synthetic Metals* **1987**, *21*, 189-195.
- [81] S. An, T. Abdiryim, Y. Ding, I. Nurulla, *Mater. Lett.* **2008**, *62*, 935-938.
- [82] M. Yurtsever, E. Yurtsever, *Polymer* **2002**, *43*, 6019-6025.
- [83] K. Ryu, N. Park, K. Kim, Y. Lee, Y. Park, S. Lee, C. Jeong, J. Joo, S. Chang, *Synthetic metals* **2003**, *135*, 397-398.
- [84] J. Xu, J. Hou, W. Zhou, G. Nie, S. Pu, S. Zhang, *Spectrochimica Acta Part A: Molecular and Biomolecular Spectroscopy* **2006**, *63*, 723-728.
- [85] S. Goel, *Advanced Science, Engineering and Medicine* **2012**, *4*, 438-441.
- [86] B. N. Reddy, M. Deepa, *Polymer* **2013**, *54*, 5801-5811.
- [87] M. Yahaya, *African Journal of Advances in Science and Technology Research* **2022**, *6*, 62-75.
- [88] K. Phasukom, W. Prissanaroon-Ouajai, A. Sirivat, *Sensors and Actuators B: Chemical* **2018**, *262*, 1013-1023.
-

-
- [89] K. Phasuksom, A. Sirivat, *RSC advances* **2022**, *12*, 28505-28518.
- [90] G. Nie, Y. Zhang, Q. Guo, S. Zhang, *Sensors and Actuators B: Chemical* **2009**, *139*, 592-597.
- [91] C. Zhijiang, S. Xianyou, Z. Qing, L. Yuanpei, *Journal of Materials Science* **2017**, *52*, 5417-5434.
- [92] P. Pandey, *Sensors and Actuators B: Chemical* **1999**, *54*, 210-214.
- [93] M. Osial, M. Warczak, P. Kulesza, P. Krysiński, M. Gniadek, *Journal of Electroanalytical Chemistry* **2020**, *877*, 114664.
- [94] W. Zhou, Y. Du, F. Ren, C. Wang, J. Xu, P. Yang, *Int. J. Hydrogen Energy* **2010**, *35*, 3270-3279.
- [95] W. Zhou, Y. Du, H. Zhang, J. Xu, P. Yang, *Electrochim. Acta* **2010**, *55*, 2911-2917.
- [96] C. Zhijiang, H. Chengwei, *Journal of Power Sources* **2011**, *196*, 10731-10736.
- [97] H. Mudila, P. Prasher, M. Kumar, A. Kumar, M. Zaidi, A. Kumar, *Materials for Renewable and Sustainable Energy* **2019**, *8*, 1-19.
- [98] aI. Marriam, Y. Wang, M. Tebyetekerwa, *Energy Storage Materials* **2020**, *33*, 336-359; bA. Shokry, A. Elshaer, J. El Nady, S. Ebrahim, M. Khalil, *Electrochim. Acta* **2022**, *423*, 140614.
- [99] L. Joshi, R. Prakash, *Mater. Lett.* **2011**, *65*, 3016-3019.
- [100] G. Rajasudha, H. Shankar, P. Thangadurai, N. Boukos, V. Narayanan, A. Stephen, *Ionics* **2010**, *16*, 839-848.
- [101] J. Arjomandi, H. Soleimani, M. H. Parvin, E. Azizi, *Polym. Compos.* **2019**, *40*, 496-505.
- [102] L. Joshi, A. K. Singh, R. Prakash, *Materials Chemistry and Physics* **2012**, *135*, 80-87.
- [103] K. Phasuksom, W. Prissanaroon-Ouajai, A. Sirivat, *RSC advances* **2020**, *10*, 15206-15220.
- [104] Ö. Eraldemir, B. Sari, A. Gök, H. İbrahim Ünal, *Journal of Macromolecular Science Part A--Pure and Applied Chemistry* **2008**, *45*, 205-211.
- [105] N. B. Taylan, B. Sari, H. I. Unal, *J. Polym. Sci., Part B: Polym. Phys.* **2010**, *48*, 1290-1298.
- [106] G. Ürkmez, B. Sarı, H. İ. Ünal, *Journal of Applied Polymer Science* **2011**, *121*, 1600-1609.
- [107] L. Rajan, A. Shabeeba, M. P. Sidheekhaa, Y. Ismail, *Chemistry--An Asian Journal* **2023**, e202300742.
- [108] D. Pan, Q. Zhou, S. Rong, G. Zhang, Y. Zhang, F. Liu, M. Li, D. Chang, H. Pan, *Microchimica Acta* **2016**, *183*, 361-368.
- [109] N. Ş. Aşık, R. Taş, S. Sönmezoglu, M. Can, G. Çankaya, *J. Non-Cryst. Solids* **2010**, *356*, 1848-1853.
- [110] F. Köleli, Y. Arslan, M. Düdükçü, *Synthetic metals* **2002**, *129*, 47-52.
-

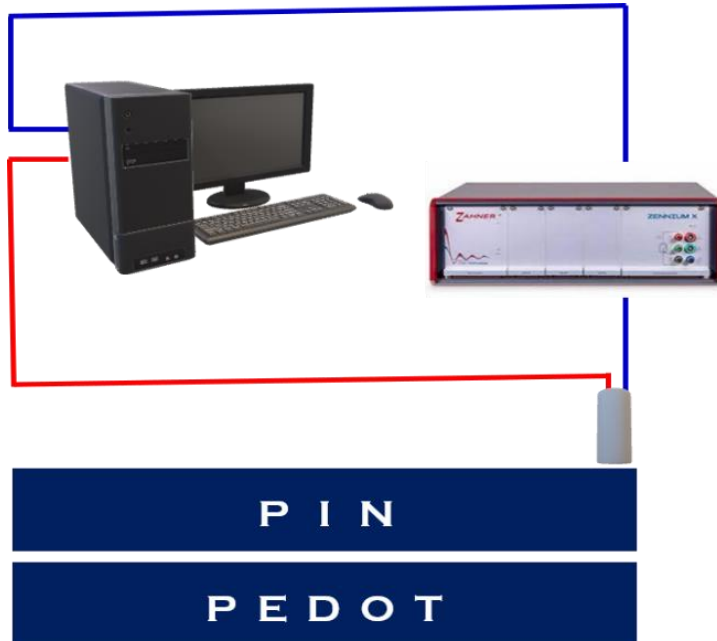
- [111] J. Arjomandi, M. Malmir, R. Holze, *Iranian Polymer Journal* **2016**, *25*, 1-13.
- [112] N. Wadatkar, S. Waghuley, *Optical and Quantum Electronics* **2022**, *54*, 596.
- [113] G. Nie, X. Han, S. Zhang, J. Xu, T. Cai, *Journal of applied polymer science* **2007**, *104*, 3129-3136.
- [114] C. Li, C. Liu, L. Shi, G. Nie, *Journal of Materials Science* **2015**, *50*, 1836-1847.
- [115] B. Gupta, A. K. Singh, A. A. Melvin, R. Prakash, *Solid state sciences* **2014**, *35*, 56-61.
- [116] G. Heywang, F. Jonas, Wiley Online Library, **1992**.
- [117] aW. Cheng, Y. Liu, Z. Tong, Y. Zhu, K. Cao, W. Chen, D. Zhao, H. Yu, *EcoMat* **2023**, *5*, e12288; bX. Han, J. Sun, Q. Li, X. He, L. Dang, Z. Liu, Z. Lei, *ACS Sustainable Chemistry & Engineering* **2023**, *11*, 2938-2948.
- [118] Q. Zhao, R. Jamal, L. Zhang, M. Wang, T. Abdiryim, *Nanoscale research letters* **2014**, *9*, 1-9.
- [119] T. Yamamoto, M. Abla, *Synthetic Metals* **1999**, *100*, 237-239.
- [120] aQ. Pei, G. Zuccarello, M. Ahlskog, O. Inganäs, *Polymer* **1994**, *35*, 1347-1351; bG. Zotti, S. Zecchin, G. Schiavon, F. Louwet, L. Groenendaal, X. Crispin, W. Osikowicz, W. Salaneck, M. Fahlman, *Macromolecules* **2003**, *36*, 3337-3344.
- [121] aN. Massonnet, Université de Grenoble **2014**; bJ. Roncali, P. Blanchard, P. Frère, *Journal of Materials Chemistry* **2005**, *15*, 1589-1610.
- [122] G. Huseynova, Y. Hyun Kim, J.-H. Lee, J. Lee, *Journal of Information Display* **2020**, *21*, 71-91.
- [123] A. Elschner, W. Lövenich, *MRS Bull.* **2011**, *36*, 794-798.
- [124] aZ. Su, Y. Jin, H. Wang, Z. Li, L. Huang, H. Wang, *ACS Applied Energy Materials* **2022**, *5*, 11915-11932; bP. S. Devi, S. N. Chanu, P. Dasgupta, B. S. Swain, B. P. Swain, *Appl. Phys. A* **2022**, *128*, 403.
- [125] M. Do, C. Park, S. Bae, J. Kim, J. H. Kim, *Org. Electron.* **2021**, *93*, 106106.
- [126] aA. L. Soares, B. M. Hryniewicz, A. E. Deller, J. Volpe, L. F. Marchesi, D. E. Souto, M. Vidotti, *ACS Applied Nano Materials* **2021**, *4*, 9945-9956; bN. Ariyasajjamongkol, K. Phasuksom, N. Paradee, A. Sirivat, *Synthetic Metals* **2023**, *297*, 117413.
- [127] aM. O. Farea, H. A. Alhadlaq, Z. M. Alaizeri, A. A. Ahmed, M. O. Sallam, M. Ahamed, *ACS omega* **2022**, *7*, 22492-22499; bL. Vigna, A. Verna, S. Marasso, M. Sangermano, P. D'Angelo, F. Pirri, M. Cocuzza, *Sensors and Actuators B: Chemical* **2021**, *345*, 130381.
- [128] B. A. Kuzubasoglu, E. Sayar, S. K. Bahadir, *IEEE Sens. J.* **2021**, *21*, 13090-13097.
-

-
- [129] aH. A. Rahman, M. Rafi, B. R. Putra, W. T. Wahyuni, *ACS omega* **2023**, *8*, 3258-3269; bT. F. Otero, J. G. Martinez, *Journal of Materials Chemistry B* **2013**, *1*, 26-38.
- [130] W. Jeong, G. Gwon, J.-H. Ha, D. Kim, K.-J. Eom, J. H. Park, S. J. Kang, B. Kwak, J.-I. Hong, S. Lee, *Biosens. Bioelectron.* **2021**, *171*, 112717.
- [131] aG. B. Tseghai, D. A. Mengistie, B. Malengier, K. A. Fante, L. Van Langenhove, *Sensors* **2020**, *20*, 1881; bI. S. Jin, J. U. Lee, J. W. Jung, *Polymers* **2021**, *13*, 945.
- [132] V. M. Udowo, M. Yan, F. Liu, E.-H. Han, *Coatings* **2023**, *13*, 944.
- [133] E. Dauzon, Y. Lin, H. Faber, E. Yengel, X. Sallenave, C. Plesse, F. Goubard, A. Amassian, T. D. Anthopoulos, *Advanced Functional Materials* **2020**, *30*, 2001251.
- [134] A. Corletto, J. G. Shapter, *Journal of Materials Chemistry C* **2021**, *9*, 14161-14174.
- [135] A. Abedi, M. Hasanzadeh, L. Tayebi, *Materials Chemistry and Physics* **2019**, *237*, 121882.
- [136] L. Zhang, X. Hu, Z. Wang, F. Sun, D. G. Dorrell, *Renewable and Sustainable Energy Reviews* **2018**, *81*, 1868-1878.
- [137] M. Winter, R. J. Brodd, *Chem. Rev.* **2004**, *104*, 4245-4270.
- [138] M. E. Şahin, F. Blaabjerg, A. Sangwongwanich, *Energies* **2022**, *15*, 674.
- [139] J. Tan, Z. Li, M. Ye, J. Shen, *ACS Applied Materials & Interfaces* **2022**, *14*, 37259-37269.
- [140] W. Hsieh, T.-L. A. Horng, H.-C. Huang, H. Teng, *Journal of Materials Chemistry A* **2015**, *3*, 16535-16543.
- [141] R. Chen, M. Yu, R. P. Sahu, I. K. Puri, I. Zhitomirsky, *Advanced Energy Materials* **2020**, *10*, 1903848.
- [142] D. P. Chatterjee, A. K. Nandi, *Journal of Materials Chemistry A* **2021**, *9*, 15880-15918.
- [143] B. Zhu, E. W. C. Chan, S. Y. Li, X. Sun, J. Travas-Sejdic, *Journal of Materials Chemistry C* **2022**, *10*, 14882-14891.
- [144] M. P. Sidheekha, G. E. Rajendran, A. Shabeeba, Y. A. Ismail, *J. Mater. Res.* **2021**, *36*, 1914-1926.
- [145] aJ. Wang, Y. Huang, Y. Gao, J. Dai, X. Sun, *Journal of Energy Storage* **2022**, *51*, 104581; bA. R. Peringath, M. A. Bayan, M. Beg, A. Jain, F. Pierini, N. Gadegaard, R. Hogg, L. Manjakkal, *Journal of Energy Storage* **2023**, *73*, 108811.
- [146] A. Thadathil, N. Edavan Chathoth, Y. A. Ismail, P. Anjukandi, P. Periyat, *The Journal of Physical Chemistry C* **2022**, *126*, 16965-16982.
- [147] T. F. Otero, *Polymer Reviews* **2013**, *53*, 311-351.
- [148] J. Arias-Pardilla, T. F. Otero, J. G. Martínez, Y. A. Ismail, *Biomimetic sensing-actuators based on conducting polymers*.
-

- [149] T. F. Otero, *Electrochim. Acta* **2021**, 368, 137576.
- [150] T. F. Otero, S. Beaumont, *Sensors and Actuators B: Chemical* **2017**, 253, 958-966.
- [151] T. Otero, J. Martinez, *Journal of Materials Chemistry B* **2016**, 4, 2069-2085.
- [152] T. Otero, J. Martinez, J. Arias-Pardilla, *Electrochim. Acta* **2012**, 84, 112-128.

Chapter 2

Materials and methods



In this chapter, we described the experimental framework and methodologies used for the examination and evaluation of our research problems. We present comprehensive information regarding the materials' composition, their synthesis and fabrication methods, the experimental setup used for the characterization and property studies, and the steps taken in the analysis of data. Our meticulous documentation of these procedures seeks to guarantee the precision and reproducibility of our research, thereby adding to the progression of scientific understanding.

2.1 Materials

All the materials and chemicals used for the studies are listed in the table given below. All the chemicals used here are analytical grade.

Table 2.1 *List of materials/chemicals used for the entire study and their manufacturer*

Materials (purity)	Manufacturer
Indole (99%)	Himedia
Anhydrous Ferric chloride (98%)	Spectrochem
Polyvinyl alcohol (99%)	Sigma Aldrich
Acetonitrile (99.5%)	Spectrochem
Cetyl trimethylammonium bromide (98.5%)	Himedia
Sodium chloride (99%)	Merck
Hydrochloric acid	Merck
Methanol (99%)	Merck
3,4-ethylenedioxythiophene (99%)	TCI
Ammonium persulfate (98.5%)	Qualigens
Lithium chloride (99%)	Qualigens
Lithium bromide (99%)	Qualigens
Lithium perchlorate (99%)	Sigma Aldrich
Lithium bis(trifluoromethanesulfonyl)imide (99%)	Sigma Aldrich
Isopropyl alcohol	Spectrochem
Conducting carbon paste	MG Chemicals
Conducting carbon cloth	Fuel Cell Earth

The indole is recrystallized from ethanol before use and all other chemicals are used as received. The double distilled water was used throughout the experiments.

2.2. Synthesis and fabrication methods

2.2.1 Synthesis of Polyindole

Conductive PIN powder was synthesized through chemical oxidative polymerization using FeCl_3 as a catalyst and NaCl as a dopant in a mixture of acetonitrile and water^[1]. In the standard procedure, 0.01 mole of indole monomer was dissolved in 50 mL of acetonitrile/water mixture (1:3), along with 0.01 mole of NaCl . The surfactant CTAB (0.01 mole) was introduced to the mixture and stirred for 2 hours. Subsequently, a solution of 0.0125 mole of FeCl_3 in 50 mL water was added to the monomer solution slowly. After 24 hours, the resulting dark green powder was filtered using Whatman 40 filter paper. The precipitate was then washed multiple times with double distilled water to remove the oxidant, followed by methanol

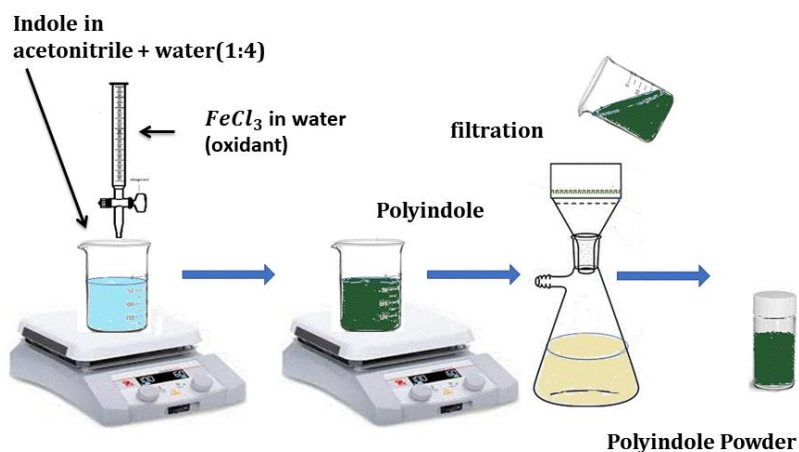


Figure 2.1. Synthesis method of PIN

to remove the oligomers and unreacted monomers. The product was left to dry for 24 hours at 50 °C in an air oven^[2].

2.2.1.1 Working electrode fabrication using PIN

All the electrochemical investigations related to PIN were conducted using the three-electrode method, where finely grounded PIN powder served as the working electrode. To prepare the working electrode, 5 mg of PIN powder and 5 mg of conducting carbon paste were dissolved in 200 μ L of isopropyl alcohol through ultrasonication. Then, 40 μ L of the solution was drop-cast onto a glassy carbon electrode (GCE) and allowed to dry^[3]. The resulting GCE with the embedded PIN and conducting carbon paste was used for all electrochemical characterizations in the context of the three-electrode method.

2.2.2 Fabrication of PIN/Polyvinyl alcohol film

PVA films were fabricated from a 2 wt. % of its solution, dissolving 5g of PVA powder in 250 mL of hot water. The resulting solution was cast onto a glass petri dish and dried at 50 °C for 24 hours, after which the film was carefully peeled off. The PIN/PVA film was fabricated through in-situ chemical polymerization of indole, utilizing NaCl as the dopant and ferric chloride as the oxidant. The PVA film was suspended in a solution containing 0.01 mole of indole and 0.01 mole of NaCl in a 50 mL mixture of acetonitrile and water (1:4, V/V) for 2 hours. 0.01 mole of CTAB was added to the mixture as the surfactant. Subsequently, a solution of 0.0125 mole of FeCl₃ in 50 mL of water was slowly added to the monomer solution

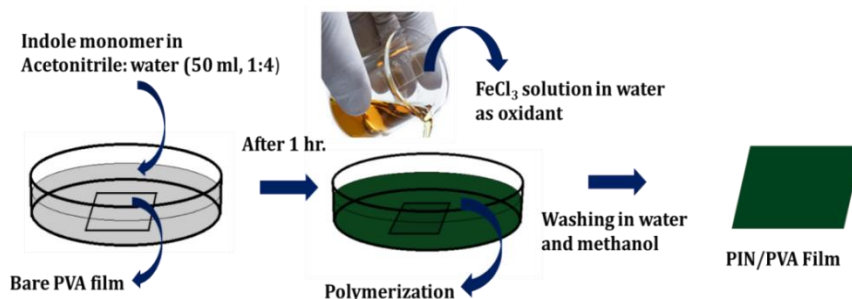


Figure 2.2 Schematic representation of fabrication of PIN/PVA hybrid film

containing the PVA film. The polymerization process was conducted at room temperature for 24 hours. The singly coated PIN/PVA hybrid film was washed with double distilled water many times to remove the oxidant, followed by washing with methanol to remove the oligomers and unreacted monomers. Finally, the hybrid film was dried at room temperature. The procedure was repeated on the singly coated film to produce a doubly coated PIN/PVA hybrid film^[4].

2.2.2.1 Working electrode preparation using PIN/Polyvinyl alcohol film

A PIN/PVA hybrid film with an area of 1 cm² is affixed to the platinum wire using the conducting carbon paste, which serves as the working electrode. The working electrode is connected to the electrochemical workstation^[5].

2.2.3 Synthesis of Poly(3, 4-ethylenedioxythiophene)

Conductive Poly(3, 4-ethylenedioxythiophene) (PEDOT) in the powder form was synthesized via chemical oxidative polymerization, using ammonium persulfate (APS) as the catalyst in acetonitrile/water mixture. In the typical procedure, the 3, 4-

ethylenedioxythiophene monomer (0.01 mole) was dissolved in 50 mL of acetonitrile/water mixture (1:3, V/V). The surfactant CTAB (0.01 mole) was added to the mixture and stirred for 2 hours. 0.0125 mole of APS solution in 50 mL of water was slowly added to the monomer solution with constant stirring. After 24 hours, the resulting dark powder was filtered using Whatman 40 filter paper. The precipitate was then washed thoroughly with double distilled water many times to remove the oxidant and later with methanol to remove the oligomers and unreacted monomers. The product was then dried for 24 hours at 50 °C in an air oven^[6].

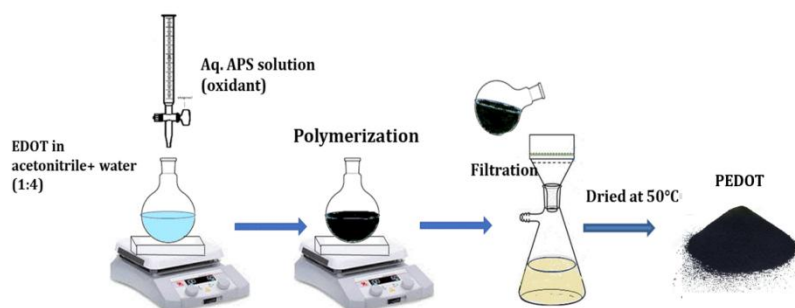


Figure 2.3 Schematic representation of synthesis of PEDOT

2.2.3.1 Working electrode fabrication using Poly(3, 4-ethylenedioxythiophene)

The PEDOT powder was employed as the working electrode by affixing it onto a glassy carbon electrode using conducting carbon paste. A mixture containing 5 mg of PEDOT powder and 5 mg of conducting carbon paste was dissolved in 200 μL of isopropyl alcohol using ultrasonication. Later, 20 μL of the solution was drop

cast onto a glassy carbon electrode (GCE) and left to dry. The resulting GCE with the embedded PEDOT can be utilized as the working electrode for all electrochemical characterizations in three-electrode methods^[7].

2.2.4 Fabrication of Poly(3, 4-ethylenedioxythiophene) /Polyvinyl alcohol film

PEDOT/PVA film was produced through in-situ chemical polymerization of EDOT using PVA film as the template and ammonium persulfate as the oxidant. The PVA film was immersed in a solution of 0.01 mole of EDOT in 50 mL of a 1:4 (V/V) mixture of acetonitrile and water for 2 hours. To the mixture, 0.01 mole of CTAB was added as the surfactant. A solution containing 0.0125 moles of APS in 50 mL of water was added slowly. The polymerization was allowed to take place at room temperature for 24 hours. The resulting singly coated PEDOT/PVA hybrid film was washed thoroughly multiple times with double distilled water to remove the oxidant and then with methanol to remove the oligomers and unreacted

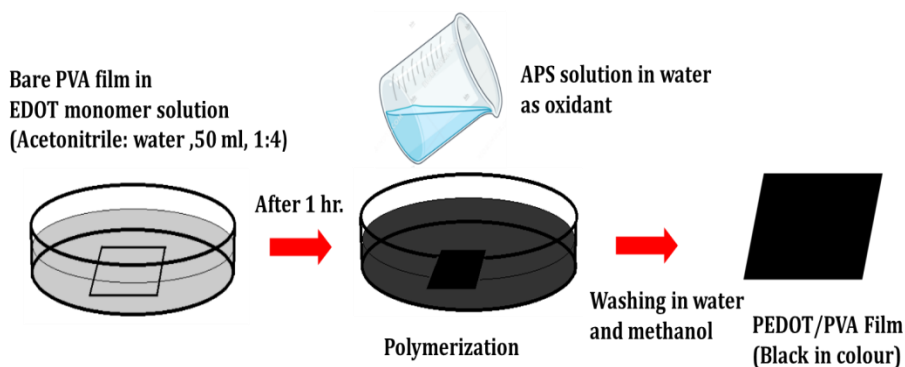


Figure 2.4 Schematic representation employed for the Fabrication method of PEDOT/PVA hybrid film

monomers. The hybrid film was then air-dried. The procedure was repeated on the singly coated film to fabricate a doubly coated PEDOT/PVA hybrid film^[8].

2.2.4.1 Working electrode fabrication using Poly(3, 4-ethylenedioxythiophene) /Polyvinyl alcohol film

PEDOT/PVA hybrid film with an area of 1 cm² is attached to the platinum wire using conducting carbon paste, which is used as the working electrode.

2.2.4.2 Fabrication of solid-state Poly(3, 4-ethylenedioxythiophene) /Polyvinyl alcohol device

A symmetric solid-state supercapacitor device was fabricated by sandwiching two PEDOT/PVA films using a separator made of filter paper/PVA/NaCl electrolyte. To prepare the electrolyte, 2 g of NaCl was mixed with 2 g of PVA in 20 mL of deionized water, and the mixture was heated up to 80 °C with continuous stirring to dissolve the PVA, resulting in a transparent solution. Subsequently, a piece of filter paper was immersed in the solution for half an hour and then left to dry. The two PEDOT/PVA films, each measuring 1 cm², were stacked together and pressed with the filter paper/PVA/NaCl separator placed in between, forming the symmetric solid-state supercapacitor device^[9].

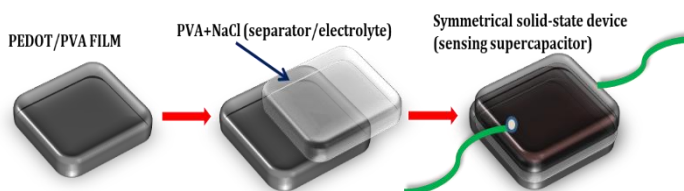


Figure 2.5 Schematic representation of fabrication of PEDOT/PVA based symmetric solid-state device

2.3 Characterization Techniques

Various characterization techniques were employed, and their details are outlined here. The Fourier transform infrared (FTIR) spectra of the powder samples were recorded using a Jasco FTIR 4100, spectrometer, Japan, covering a range of 4000 cm^{-1} to 400 cm^{-1} . The FTIR spectra of the film samples were obtained using a Jasco FTIR 4700, spectrometer Japan with attenuated total reflectance (ATR) technology having the same range. The UV-Visible spectra of the samples were recorded using the UV-Vis Jasco V-770 spectrometer, Japan. Thermo gravimetric analysis (TGA) was conducted using the PerkinElmer STA 8000 thermogravimeter, USA. The surface morphology of the film and powder polymer was studied using the ZEISS GeminiSEM 300, field emission scanning electron microscope (FE-SEM), Germany, while the transmission electron microscopic image was obtained from the JEOL/JEM 2100 high-resolution transmission electron microscope (HR-TEM), Japan with a 200 kV accelerating voltage and lattice resolution of 0.14 nm. Elemental analysis was carried out using an energy-dispersive X-ray spectrometer (EDX) equipped with EDAX octane plus with Gemini 300/EDS microscope. The mechanical properties of the bare and coated films were evaluated in dry and wet conditions utilizing the Shimadzu AG-Xplus universal testing machine (UTM), Japan, up to 10 kN force. The electrical conductivity (I-V plot) of the PIN/PVA film was analyzed using a four-probe method employing the Keithley 2450 Source meter electrometer, USA, at room temperature and the electrical conductivity of the PEDOT powder was analyzed

using a Broadband dielectric spectrometer of Novocontrol technologies, Germany, at room temperature. Lastly, all electrochemical characterizations, including cyclic voltammetry, chronopotentiometry, galvanostatic charge-discharge, and impedance spectrometry, were carried out using the Zahner Zanium PRO electrochemical workstation (galvanostat/potentiostat) controlled by the ThalesXT analysis software, Germany.

2.3.1 Fourier Transform Infrared Spectroscopy

FTIR spectroscopy is a useful tool for analyzing the chemical structure and composition of molecules. In this study, the FTIR spectra of the powder sample were recorded in the absorption range of 400 cm^{-1} to 4000 cm^{-1} . The samples were prepared by mixing with KBr, which are pelletized after finely pulverizing the mixture with a pestle in a mortar. For film samples, FTIR spectra were recorded using attenuated total reflectance (ATR) attached to the FTIR spectrometer with this requiring minimal sample preparation compared to the KBr disc method. In the infrared spectroscopic methods, infrared radiation interacts with molecular vibrations, causing the molecule to absorb quantized frequencies. This absorption, occurring in the stretching and bending vibrational frequencies of bonds, results in their characteristic absorption bands. This interaction helps identify the functional groups present in the material and information about the nature of the covalent bond. Each sample's unique combination of atoms produces a distinct infrared spectrum, acting as a molecular fingerprint. The

experimental setup of an FTIR instrument includes a light source, sample holder, interferometer, detector, and computer^[10].

2.3.2 UV-Visible Spectroscopy

UV-visible (UV-Vis) spectroscopy, a widely employed analytical method, examines the absorption and transmission of ultraviolet (UV) and visible light by molecules within a sample. In this technique, a light beam within the UV and visible range (200 to 800 nm) corresponds to the electronic transitions in molecules. Therefore it is also known as electronic spectroscopy. The spectrum obtained offers an understanding of how the molecules in the sample change their energy states. This spectroscopic method relies on the Beer-Lambert law, where absorbance (A) equals the product of the molar absorption coefficient (ϵ), the molar concentration of the substance (c), and the path length (l). This approach allows both qualitative analysis to understand the sample's structure and quantitative analysis to determine its concentration^[11]. This technique is straightforward, non-destructive, and requires minimal sample preparation, making it a favored choice for routine analysis in laboratories and research works.

Additionally, determining the band gap energy provides a method for evaluating the sample's optical absorption. The optical band energy gap can be computed using the Tauc equation 2.1.

$$(\alpha h\nu)^\gamma = A(h\nu - E_g) \quad (2.1)$$

In this context, α represents the absorption coefficient, 'A' stands for the probability transition constant (approximately 1 for amorphous materials such as CPs), $h\nu$ denotes the energy of incident photons,

and γ is a variable indicating the nature of electronic transition (where $\gamma = 2$ and $\gamma = 1/2$ represent indirect and direct allowed electronic transitions, respectively). By extrapolating the linear section of the Tauc plot, the corresponding E_g values can be obtained. The extent of delocalization and conjugation influences the energy band gap, which in turn determines whether the conducting polymer behaves as a metal, semiconductor, or insulator.

UV-Vis spectra of powder materials in this study were recorded over a wavelength of 200-800 nm using DMSO as the solvent.

2.3.3 Thermogravimetric Analysis

Thermogravimetric analysis (TGA) is a technique used to examine the weight reduction of the sample in relation to temperature changes that is thermal degradation. The thermal characteristics of the vacuum-dried samples in this study were examined in a nitrogen atmosphere, ranging from 30 °C to 800 °C, with a heating rate of 10 °C per minute.

This method reveals information about the chemical and physical processes, including phase transition, decomposition, chemisorption, physisorption, adsorption-desorption etc. The study provides insight into the thermal stability of the samples studied^[12].

2.3.4 Field Emission Scanning Electron Microscope

The Field Emission Scanning Electron Microscope (FE-SEM) serves as an advanced imaging tool extensively utilized to investigate the surface morphology and microstructure of diverse materials. Its operation relies on electron-matter interaction, where a focused electron beam scans across the sample surface, leading to the

generation of various signals such as backscattered electrons, secondary electrons, X-rays, or light. Among these, secondary electron detection is commonly employed to capture high-resolution images of the sample. FE-SEM provides exceptional spatial resolution, enabling researchers to visualize intricate details and nanoscale structures. This potent technique finds applications in various scientific and engineering domains for in-depth material analysis and characterization, delivering valuable insights into their microstructure, composition, and surface characteristics. In this present study, the morphology of both the fabricated films and the powder samples is determined at an accelerating voltage of 5 kV. Materials under examination must possess electrical conductivity; otherwise, they are coated with a thin layer of conductive material such as gold or silver using the sputtering technique^[13].

2.3.5 High Resolution Transmission Electron Microscopy

The High-Resolution Transmission Electron Microscope (HR-TEM) is utilized for the direct visualization of the atomic arrangement within the sample. It serves as a traditional technique to investigate the material's atomic-level properties^[14]. By analyzing the interaction between the sample and the electron beam, the transmitted electrons provide atomic-level images. The TEM image reveals intricate details concerning the material's internal structure, including pore volume, size, and shape, as well as the chain structure of the polymer material. TEM images of PIN/PVA film and PEDOT powder were taken in this study. In the case of PIN/PVA film, the image is captured by coating the film on a polycarbon grid. The

image was captured by dispersing PEDOT powder in methanol and coating it on a carbon-coated copper grid of 3 mm dimension. TEM elemental mapping analysis has also been carried out in the case of PEDOT powder.

2.3.6 Energy Dispersive X-ray Spectroscopy

Energy Dispersive X-ray Analysis (EDS), also known as Energy Dispersive X-ray Spectroscopy (EDXA) or X-ray Energy Dispersive Spectroscopy (XEDS), is a powerful technique applied in materials science and electron microscopy to ascertain the elemental makeup of a sample. During EDX analysis, a focused high-energy electron beam interacts with the atoms of the sample, inducing the emission of characteristic X-rays. These emitted X-rays possess distinct energies corresponding to specific elements present in the sample. The EDS detector captures and measures the energies of these X-rays, generating a spectrum that unveils the sample's elemental composition.

The intensity of the peaks in the spectrum relates to the abundance of each element, facilitating both qualitative and quantitative analysis of the sample's elemental composition. EDX is extensively employed in conjunction with scanning electron microscopy (SEM) and transmission electron microscopy (TEM) to provide valuable insights into the elemental distribution and chemical analysis of various materials, encompassing metals, minerals, ceramics, and biological specimens^[13]. In this study, the films underwent elemental analysis using EDS integrated with the SEM.

2.3.7 Universal Testing Machine

A Universal Testing Machine (UTM) is used to analyze the mechanical properties of the films. For this study, 10 kN force UTM with a crosshead speed of 5 mm/min was employed. Film samples having a dimension of 6 cm × 2 cm were selected and fixed between two mechanical gripping units of the machine, leaving a gauge length of 3 cm for mechanical loading. The samples were then stretched until they fractured. UTM is a versatile mechanical testing apparatus extensively employed in materials science and engineering to assess the mechanical characteristics of diverse materials. The UTM can apply various mechanical forces to test specimens, including tension, compression, bending, and shear. The machine comprises a load frame, which accommodates the test specimen and administers controlled force, and a load cell or transducer to accurately measure the applied load. An extensometer or displacement sensor is utilized to gauge the specimen's displacement or deformation. By monitoring the applied force and the resulting deformation, the UTM generates stress-strain curves, enabling researchers and engineers to determine crucial mechanical properties such as tensile strength, Young's modulus, percentage elongation, and ultimate strength. The Young's modulus was determined by subjecting the specimens to a constant stretching force (F). Young's modulus was calculated using the formula. 2.2.

$$\text{Young's Modulus} = \frac{\text{stress}}{\text{strain}} \quad (2.2)$$

Stress represents the force (F) in newton (N) per unit area (A) in mm², while strain denotes the change in length (ΔL) per initial length

(L₀). Following the experiment, findings were presented in the form of stress-strain graphs. UTMs are essential tools in quality control, material research, and product development across various industries, providing a comprehensive understanding of material behavior under distinct mechanical conditions^[15].

2.3.8 Electrical Conductivity Studies

In this study, two methods were used to determine the electrical conductivity of the samples. One is in the case of PIN/PVA film using the four-point probe method and the second is in the case of PEDOT powder using Broadband Dielectric Spectrometer (BDS) using a two-point probe method at room temperature and ambient pressure within the frequency range of 10⁻² Hz to 10⁷ Hz.

The four-point probe method which was used to measure the conductivity of PIN/PVA film is a widely employed method for determining the electrical conductivity of materials, particularly semiconductors and thin films. The method involves four equidistant electrical contacts (probes) that are directly in contact with the material being analyzed. A constant current is passed through the outer two probes, while the inner two probes measure the resulting voltage drop. Through the use of a Kelvin bridge, the voltage drop caused by contact resistance is eliminated, enabling precise measurement of the material's resistivity or conductivity from the I-V plot using equation 2.3.

$$\sigma = \frac{I}{V} \left(\frac{1}{t} \right) \quad (2.3)$$

Where σ represents the AC conductivity, V is the potential, I is the current, and t is the thickness of the film. In this study, the film

having 0.3 mm thickness was used. This technique offers significant benefits as it provides accurate electrical conductivity measurements, even for materials with high electrical resistivity or low sheet resistance. It finds diverse applications in the characterization of various materials for electronic devices, including integrated circuits, solar cells, and thin-film coatings^[16].

Another method employed in this study is Broadband Dielectric Spectroscopy (BDS), which is a versatile tool also used to explore how well polymeric systems conduct electricity. It studies the electrical properties of materials by measuring how they react to an electric field across a broad range of frequencies. This usually includes frequencies from 10^{-2} Hz to 10^7 Hz or even higher. BDS is valuable for understanding the electrical conduction behavior of various materials and is particularly useful in investigating polymeric systems. BDS analyzes dielectric properties like permittivity and conductivity based on frequency. This helps in studying how a material reacts to electric fields at different frequencies. The details gathered from BDS are crucial for understanding the molecular and microstructural dynamics of various materials, including polymers, glasses, and biological substances^[17].

The vacuum-dried pellet made of powder sample was placed between two parallel gold plates connected with copper electrodes. The PEDOT powder sample was compressed into a pellet using a stainless steel die with a diameter of 1.3 cm and a hydraulic press. The thickness of the samples was determined using an electronic

screw gauge. The DC electrical conductivity can be calculated by fitting the frequency-dependent conductivity data to Jonscher's power law, which is expressed as follows:

$$\sigma(\omega) = \sigma_0 + A\omega^n \quad (2.4)$$

In this context, $\sigma(\omega)$ represents the AC conductivity at frequency ω , while σ_0 signifies the DC conductivity. A stands for a constant linked to the magnitude of the AC conductivity, ω represents the angular frequency ($\omega=2\pi f$), where f is the frequency, and n indicates the frequency exponent, typically ranging from 0 to 1. This exponent provides insights into the distribution of relaxation times within the material.

2.4. Electrochemical Characterizations

Studying the basic electrochemical behavior of the various materials involved in this study is one of the most important objectives of this thesis. All the materials (films, powders, and devices) involved in this study are promising for various electrochemical applications. Therefore, the various electrochemical properties of the materials used here need to be understood in depth. The instrument used in this study is capable of CV, GCD, Chronopotentiometry, and EIS for applications such as electrochemical sensing, supercapacitors, batteries, and electrochemical polymerization. Among them, reactive sensing capability and supercapacitor studies have been conducted using the above techniques.

All the electrochemical studies were carried out in a conventional three-electrode assembly with the hybrid film or modified glassy carbon electrode (GCE) as the working electrode (WE), Ag/AgCl (3

M KCl) as the reference electrode (RE), and Pt mesh as the counter electrode (CE) or auxiliary electrode using aqueous HCl and NaCl as the electrolyte depending upon the working electrode.

The WE is fabricated by mixing the powder samples with carbon paste and coating the glassy carbon electrode. However the WE is fabricated by cutting the film samples to a certain dimension and pasting them over a Pt wire using carbon paste. Before all electrochemical analysis, the samples were allowed to equilibrate by immersed in the electrolyte for a certain period before applying the potential. The reference electrode controls the potential of the working electrode using a potentiostat. The RE has a very precise and constant electrode potential and is a non-polarized electrode.

2.4.1. Cyclic Voltammetry

CV is an electrochemical technique used to study the redox behavior of materials in a solution. During CV, a voltage waveform is applied to an electrochemical cell, causing the potential of the working electrode to vary linearly with time. The resulting current response is measured, and the process is reversed to complete one cycle. By sweeping the voltage over a range of values and observing the corresponding current, a voltammogram is obtained (current v/s potential plot), which represents the electrochemical behavior of the analyte. The rate at which we change the potential in an experiment is called the scan rate or sweep rate. When the scan rate goes up, the potential sweeps more quickly, and it takes less time to finish one cycle. CV provides valuable information about the redox properties, electron transfer kinetics, and electrochemical reactions of

materials, making it a fundamental tool for studying the electrochemistry of materials and their applications such as corrosion studies, energy storage, sensors, and actuators^[18].

CV is also used to analyze various electrochemical properties of conducting polymers. When a potential is applied, CV is useful to understand whether the reaction taking place in the conducting polymer is redox reaction / faradaic process or non-faradaic process, if it is a redox reaction, to find the redox state and calculate the redox charge consumed in each redox process^[19]. In addition, in this study, CV is used to study the reactive sensing capability of conducting polymers and to study the charge storage capacity or supercapacitor application. In this study, the areal capacitances of PEDOT/PVA film were calculated using CV using the equation 2.5^[9].

$$C_{SA} = \frac{\int_{V_1}^{V_2} IdV}{Av(V_2 - V_1)} \quad (2.5)$$

In this context, C_{SA} represents the areal-specific capacitance, and A refers to the area of the film or the active part of the device, I represent the applied current, m stands for the active mass of the material, ΔV corresponds to the potential window, and v denotes the scan rate used in the cyclic voltammetry.

The diffusion-controlled characteristic of the reaction occurring at the electrode-electrolyte interface can be verified by performing cyclic voltammetry at various scan rates, employing the Randle-Sevcik equation 2.6^[20]. This equation illustrates that the peak current of the cyclic voltammetry exhibits a linear increase with the square root of the scan rate.

$$i_p = 0.446nFAC \left(\frac{nFv}{RT} \right)^{\frac{1}{2}} \quad (2.6)$$

In this scenario, where i_p denotes the peak current (A), n represents the number of electrons, F symbolizes Faraday, A signifies the electrode surface area (cm^2), D (cm^2s^{-1}) corresponds to the diffusion coefficient, and C denotes the bulk concentration of the analyte (molcm^{-3}). In the case of a diffusion-controlled process, both the peak current i_p and the square root of the scan rate $v^{1/2}$ will exhibit a linear relationship.

2.4.2. Chronopotentiometry

Chronopotentiometry is a galvanostatic electrochemical technique used to study the kinetics and transport processes in electrochemical systems. In chronopotentiometry, a constant electric square current is applied to the electrochemical cell, and the resulting potential (voltage) response is monitored over time. By recording the potential as a function of time chronopotentiogram (potential v /s time graph) is obtained, which gives an insight into various electrochemical processes, such as electrode reactions, charge transfer kinetics, and mass transport phenomena. This technique is particularly useful for studying reaction mechanisms, electrode surface processes, and diffusion rates in electrochemical systems^[21]. After the first change in potential caused by different resistances in the solution, material, counterion, and material-solution interface when the current is first turned on, the measured potential gradually changes as the reactant concentration at the electrode surface decreases. If the current goes beyond a certain

limit, the flux needed to sustain it can't be produced by diffusion. This causes the electrode potential to rise until it matches the potential of the next available reaction, and so on. In current reversal chronopotentiometry, the applied current is then reversed. If the current switches suddenly from anodic to cathodic, the anodic product or byproduct begins to be reduced. Consequently, the potential shifts in the cathodic direction as the cathodic product concentrations increase.

In this work, chronopotentiometry is used to analyze the reactive sensing nature of the fabricated materials. The square current wave is shown in Figure 2.6 (a) and the corresponding chronopotentiogram is given in Figure 2.6 (b). The second cycle (figure 2.6 (b)) of the anodic and cathodic potential evolution of all experiments is used for the analysis^[22]. The physical or chemical variables that influence the rate of the electrode reaction affect the potential evolution of the electrode^[23]. The electrical energy (U) consumed during the redox reaction can be obtained by integrating the chronopotentiogram and using equation 2.7.

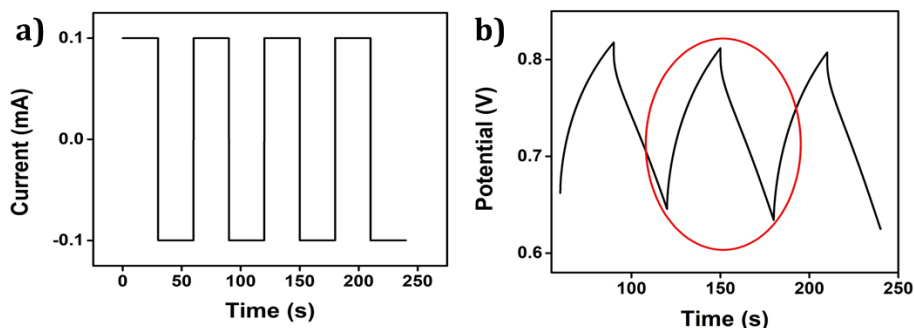


Figure 2.6 a) square current waves applied to the material. **b)** Anodic and cathodic potential evolution with respect to time (chronopotentiogram or charge-discharge)

$$U = I \int E dt \quad (2.7)$$

Where E is the potential evolved, I is the current applied.

2.4.3. Galvanostatic Charge-Discharge

Galvanostatic Charge-Discharge is an electrochemical technique used to investigate the charge and discharge behavior of supercapacitors and energy storage devices. During this process, a constant electric current is applied to the electrochemical cell, driving either the charging or discharging process. When charging, the current flows into the cell, leading to the accumulation of charge within the active material. Conversely, during discharge, the stored charge is released as electrical current flows out of the cell. By monitoring the voltage response over time, researchers can study the capacity, efficiency, and performance characteristics of the energy storage system. Galvanostatic charge-discharge experiments are crucial for understanding the energy storage capabilities of batteries and evaluating their suitability for various applications, including electric vehicles, renewable energy systems, and portable electronics. Figure 2.6 (b) also represents the charge-discharge curve of the sample.

The specific areal capacitance of the materials can be calculated from the GCD curve. The areal-specific capacitance is given as

$$C_{SA} = \frac{I \Delta t}{A \Delta V} \quad (2.8)$$

Where I denote the supplied current, Δt and A stand for the discharging time in seconds and the area of the film, respectively.

The potential window ΔV (V_2-V_1) in volts sets the range of potential within which the charge-discharge process occurs.

2.4.4. Electrochemical Impedance Spectroscopy

Electrochemical Impedance Spectroscopy (EIS) is a potent and extensively employed electrochemical technique utilized to investigate the electrical characteristics of materials and interfaces within electrochemical systems. EIS involves subjecting the system to a small sinusoidal voltage perturbation and measuring the resulting current response over a range of frequencies. EIS can be visually represented through a Nyquist plot and a Bode plot. A Nyquist plot illustrates both the imaginary and real parts of impedance measurements, where semicircular and linear segments indicate charge transfer and diffusion-controlled processes, respectively. In this study, EIS measurements of the samples were conducted at an open-circuit voltage of 10 mV across a frequency range from 0.1 Hz to 100 kHz. The findings were analyzed using an equivalent circuit model suggested by Zman software.

By analyzing the impedance data, which represents the complex ratio of the applied voltage to the measured current, researchers gain valuable insights into various electrochemical processes, including charge transfer resistance, double-layer capacitance, mass transport limitations, and interfacial phenomena. EIS is exceptionally versatile and can be applied to study diverse electrochemical systems, such as batteries, fuel cells, sensors, and corrosion protection coatings. Its capacity to offer comprehensive information in both the frequency and time domains renders it a

fundamental tool for comprehending the behavior of electrochemical systems and optimizing their performance.

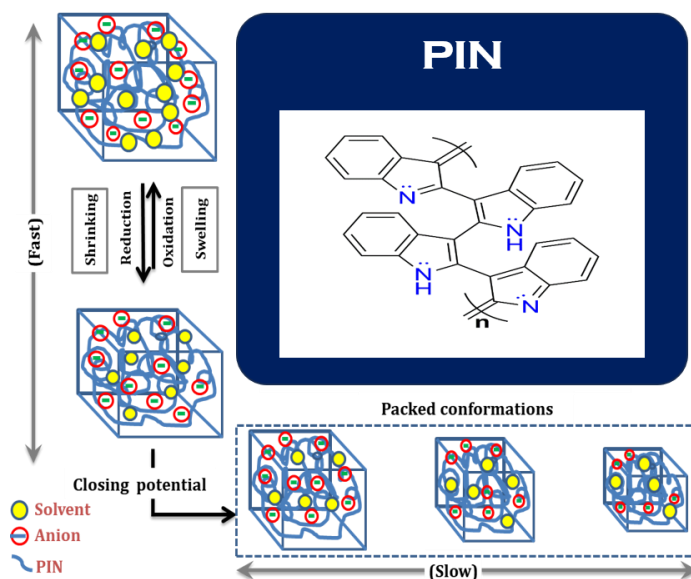
References

- [1] Ö. Eraldemir, B. Sari, A. Gök, H. İbrahim Ünal, *Journal of Macromolecular Science Part A--Pure and Applied Chemistry* **2008**, *45*, 205-211.
- [2] aO. Erol, H. I. Unal, B. Sari, *Polym. Compos.* **2010**, *31*, 471-481; bS. Anandhi, M. L. Edward, V. Jaisankar, *Materials Today: Proceedings* **2021**, *40*, S93-S101.
- [3] D. Deletioğlu, E. Hasdemir, A. O. Solak, Z. Üstündağ, R. Güzel, *Thin Solid Films* **2010**, *519*, 784-789.
- [4] L. Rajan, A. Shabeeba, M. P. Sidheekha, Y. Ismail, *Chemistry–An Asian Journal* **2023**, e202300742.
- [5] A. Shabeeba, L. Rajan, M. P. Sidheekha, M. S. Thayyil, Y. A. Ismail, *Journal of Energy Storage* **2022**, *55*, 105724.
- [6] aF. Louwet, L. Groenendaal, J. Dhaen, J. Manca, J. Van Luppen, E. Verdonck, L. Leenders, *Synthetic Metals* **2003**, *135*, 115-118; bS. V. Selvaganesh, J. Mathiyarasu, K. Phani, V. Yegnaraman, *Nanoscale Research Letters* **2007**, *2*, 546-549.
- [7] L. Rajan, M. P. Sidheekha, A. Shabeeba, S. C. Unnikrishnan, Y. A. Ismail, *Res. Chem. Intermed.* **2022**, *48*, 4313-4329.
- [8] L. Rajan, M. P. Sidheekha, A. Shabeeba, Y. A. Ismail, *Materials Chemistry Frontiers* **2022**, *6*, 1706-1718.
- [9] M. P. Sidheekha, A. Shabeeba, L. Rajan, M. S. Thayyil, Y. A. Ismail, *Engineered Science* **2023**, *23*, 890.
- [10] M. A. Mohamed, J. Jaafar, A. Ismail, M. Othman, M. Rahman, in *Membrane characterization*, Elsevier, **2017**, pp. 3-29.
- [11] G. Verma, M. Mishra, *World J. Pharm. Res* **2018**, *7*, 1170-1180.
- [12] H. Ng, N. M. Saidi, F. S. Omar, K. Ramesh, S. Ramesh, S. Bashir, *Encyclopedia of polymer science and technology* **2002**, 1-29.
- [13] M. Abd Mutalib, M. Rahman, M. Othman, A. Ismail, J. Jaafar, in *Membrane characterization*, Elsevier, **2017**, pp. 161-179.
- [14] Y. Kauffmann, A. Rečnik, W. D. Kaplan, *Mater. Charact.* **2005**, *54*, 194-205.
- [15] H. Kweon, S. Choi, Y. Kim, K. Nam, *Int. J. Mod Phys B* **2006**, *20*, 4432-4438.
- [16] V. Shaktawat, N. Jain, R. Saxena, N. Saxena, T. Sharma, *Journal of optoelectronics and advanced materials* **2007**, *9*, 2130.
- [17] F. Kremer, A. Schönhal, *Broadband dielectric spectroscopy*, Springer Science & Business Media, **2002**.

- [18] C. Costentin, J.-M. Saveant, *The Journal of Physical Chemistry C* **2015**, *119*, 12174-12182.
- [19] P. Puthongkham, B. J. Venton, *Analyst* **2020**, *145*, 1087-1102.
- [20] M. S. Ting, B. N. Narasimhan, J. Travas-Sejdic, J. Malmström, *Sensors and Actuators B: Chemical* **2021**, *343*, 130167.
- [21] Y. A. Ismail, J. G. Martínez, T. F. Otero, *Electrochim. Acta* **2014**, *123*, 501-510.
- [22] Y. A. Ismail, J. G. Martinez, T. F. Otero, *Journal of Electroanalytical Chemistry* **2014**, *719*, 47-53.
- [23] J. Martinez, T. Otero, *RSC Advances* **2014**, *4*, 29139-29145.

Chapter 3

Electrochemical characterization of polyindole with a special emphasis on its structural electrochemistry



This chapter presents an in-depth electrochemical investigation of polyindole (PIN). For the first time, we delve into the redox process of PIN with a thorough examination using voltammetry. Furthermore, we applied the concept of coulovoltammetry, which is instrumental in studying the diverse molecular structural changes induced by the electrochemical reactions of PIN. We have quantified the charge consumed during each specific structural variation and identified the corresponding potential limits. This comprehensive study sheds new light on the intricate electrochemical behavior of polyindole, offering valuable insights into its redox processes and underlying structural transformations.

3.1. Introduction

One of the principal merits of CPs lies in their capacity to respond to external stimuli, such as changes in temperature, humidity, voltage chemical surroundings, etc.^[1]. This responsiveness can be attributed to the Faradaic process, during which anions can be exchanged between the electrolyte and polymer chain resulting in the continuous composition variations of CPs (which are considered reactive gels)^{[2][3]}.

In this chapter, we explored the reactive sensing capabilities^[4] and conformational changes occurring during the electrochemical reaction of PIN. The structural changes during the Faradaic process accompanied by continuous composition variation and the associated conformational movement are also explored^[5]. In its neutral state, the σ bond of the polymer chain can undergo unrestricted rotation^[6]. However, upon oxidation, radical cations or dications are formed, impeding this free rotation and giving rise to a planar structure^[3c]. This intriguing behavior of the CP leads PIN into a molecular motor.

Here we explore a novel domain concerning the change in structure and the corresponding charge consumption during unique electrochemical reaction processes. The charge consumption during the reversible redox process and irreversible process of PIN elicit diverse structural conformations. As the polymer chain undergoes conformational movements, the macroscopic response encompasses swelling, shrinking, compaction, and relaxation of the structure, thereby generating or eliminating free volume to

accommodate the counter anion and solvent molecules during oxidation^[7]. To assess the structural variations and changes in electrochemical response, we also tried to provide a theoretical explanation^[8]. We also focused on elucidating how the voltammetric and coulometric responses play a vital role in acquiring and identifying the structural components at play^[5].

To thoroughly investigate the responsive sensing attributes of PIN in varying working conditions, a comprehensive analysis of its diverse conformational structures is essential^[9]. Additionally, exploring the potential limits of the reversible process is crucial to our examination. We aim to ascertain whether any parallel reactions, such as irreversible reduction or oxidation, take place within the system^[10].

3.2. Results and discussion

The chemically prepared PIN is thoroughly characterized by employing FTIR, UV-Vis, FE-SEM, EDX, TGA, cyclic voltammetry, and coulometric techniques. The subsequent findings are deliberated upon in the subsequent sections.

3.2.1. FTIR spectra

Figure 3.1 shows the FTIR spectra of the synthesized PIN powder where characteristic peaks observed at 3402, 1563, and 743 cm^{-1} , are attributed to N-H stretching, N-H deformation, and the benzene ring's out-of-plane deformation, respectively^[11]. Interestingly, the two peaks found around 746 cm^{-1} and 721 cm^{-1} in the indole monomer, attributed to the out-of-plane deformation of C₂-H and C₃-H bonds, were absent in the polymer. The presence of aromatic ring

stretching peaks at 1615, 1454, 1213, and 1110 cm^{-1} further supported the results^[12]. The absence of N-H vibration and benzene ring deformation indicated that nitrogen and the benzene ring did not take part in the polymerization of indole, pointing to polymerization occurring at the 2 and 3 positions. During the polymerization, CTAB acted as the surfactant, and its aliphatic chain's C-H stretching vibrations were observed at around 2920 and 2850 cm^{-1} , suggesting its incorporation into the polymer chain^[13].

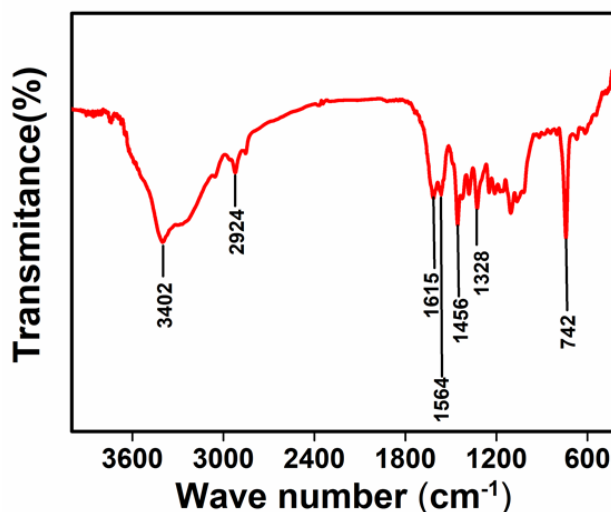


Figure 3.1 FTIR spectrum of PIN

3.2.2. UV-VIS Spectra

The UV-VIS spectra of the PIN powder dissolved in dimethyl sulfoxide (DMSO) are illustrated in Figure 3.2. The Figure reveals two prominent peaks at 269 nm and 303 nm, signifying the $\pi \rightarrow \pi^*$ transition of the polymer chain and the conjugation of the benzene ring respectively. Additionally, the peak observed at 346 nm indicates the $n \rightarrow \pi^*$ transition of the benzene ring in the PIN structure^[14]. The fourth peak is probably due to the polaron.

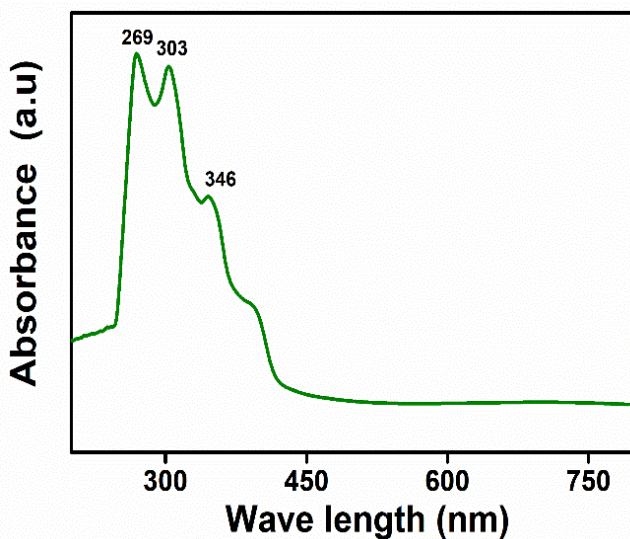


Figure 3.2 UV-VIS spectrum of PIN

3.2.3. Morphological characterization-FE-SEM

The surface morphology of the polymer powder was meticulously examined using the scanning electron microscope (Gemini SEM 300) and the elemental analysis carried out via the energy dispersive X-ray spectrum (EDX- Octane plus) as depicted in Figure 3.3, provides valuable insights. The FE-SEM images reveal a clustering of particles in the nano range, displaying irregular and agglomerated morphology shapes (Figure 3.3(a)) [15]. This irregular particle distribution reflects the amorphous nature of the polymer. Since the polymerization was carried out using the surfactant CTAB which facilitates the formation of micelles. Consequently, a repulsive force arises between the positively charged head of the CATB micelle and the positively charged PIN powder, effectively increasing the micelle's size [6b].

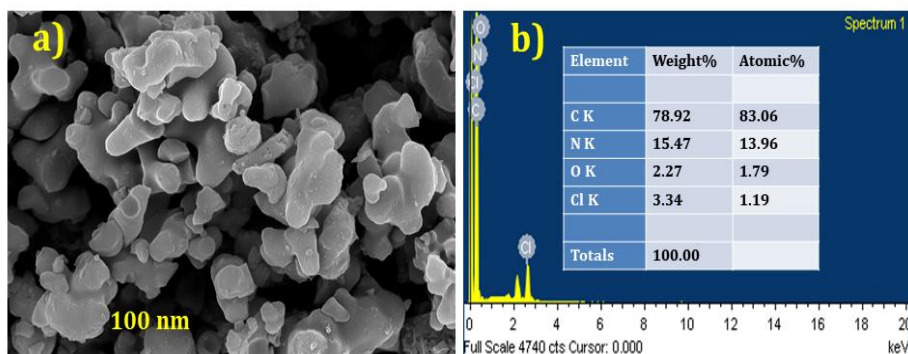


Figure 3.3 (a) FE-SEM image of PIN. **(b)** EDX data of PIN

3.2.4. Thermal characterization- TGA

The thermal stability of the PIN powder material was carefully assessed through the thermogravimetric analysis. The resulting thermograms are shown in Figure 3.4. Notably, the figure exhibits a three-step weight loss pattern, consistent with existing literature. The initial step occurring around 100 °C, involves the detachment of absorbed water molecules, and surfactants. The second step spanning temperatures between 193 °C to 304 °C, signifies the elimination of unreacted monomers and degradation of oligomers.

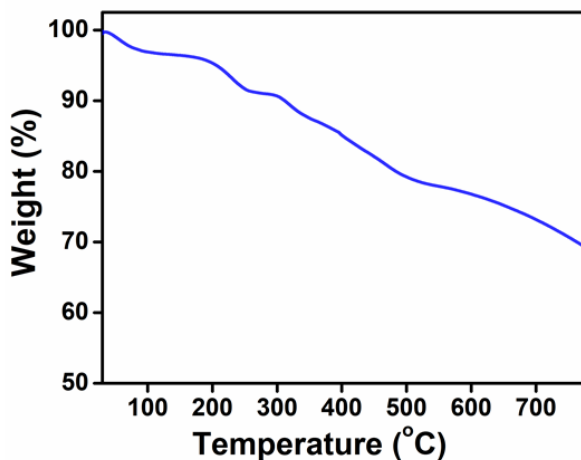


Figure 3.4 TGA curve of PIN at the rate of $10^{\circ} \text{min}^{-1}$

Lastly, the third step observed from 405 °C to 576 °C, depicts the degradation of the polymer backbone^[16].

3.2.5. Electrochemical characterization

3.2.5.1. Cyclic voltammetry

The electrochemical characteristics of the PIN were explored using voltammetric analysis. The cyclic voltammogram (CV) of the PIN was recorded using a three-electrode cell setup at room temperature. The configuration included a PIN-coated glassy carbon electrode as the working electrode, an Ag/AgCl electrode serving as the reference electrode, and a platinum wire as the counter electrode. A stable cyclic voltammogram (CV) was recorded by subjecting the polymer to multiple consecutive potential cycles and allowing the polymer reaction to reach a steady state^[17] as depicted in Figure 3.5. The potential was systematically cycled from -0.2 V to 0.75 V in a 1M HCl solution, employing a scan rate of 25 mVs⁻¹ at ambient temperature (28 ± 1 °C).

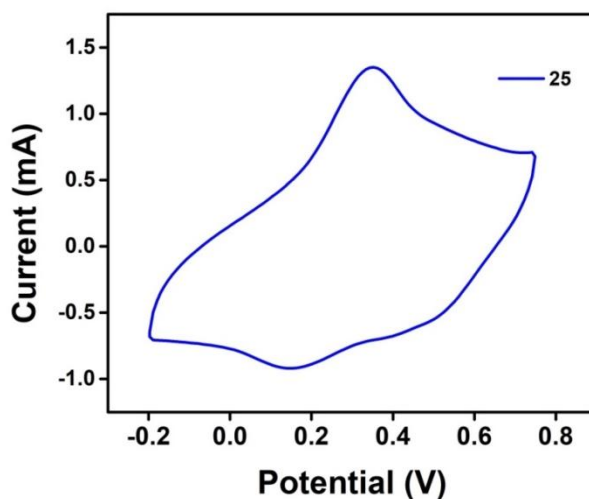


Figure 3.5 CV curve of PIN

During the electrochemical redox process, the PIN exchanges anions with the electrolyte, effectively compensating for the charge generated on the polymer backbone by its redox reaction^[18]. Simultaneously, the exchange of solvent molecules between the polymer chain and the electrolyte solution occurs to maintain the osmotic balance, this is disrupted by the intercalation of counter ions. This intriguing process induces volume variation as the counter anions and solvent molecules are inserted/expelled to/from the polymer matrix^[19]. Consequently, during oxidation, the polymer experiences swelling while reduction leads to a contraction^[20]. The PIN displayed distinctive anodic and cathodic peaks corresponding to the oxidation and reduction events, respectively.

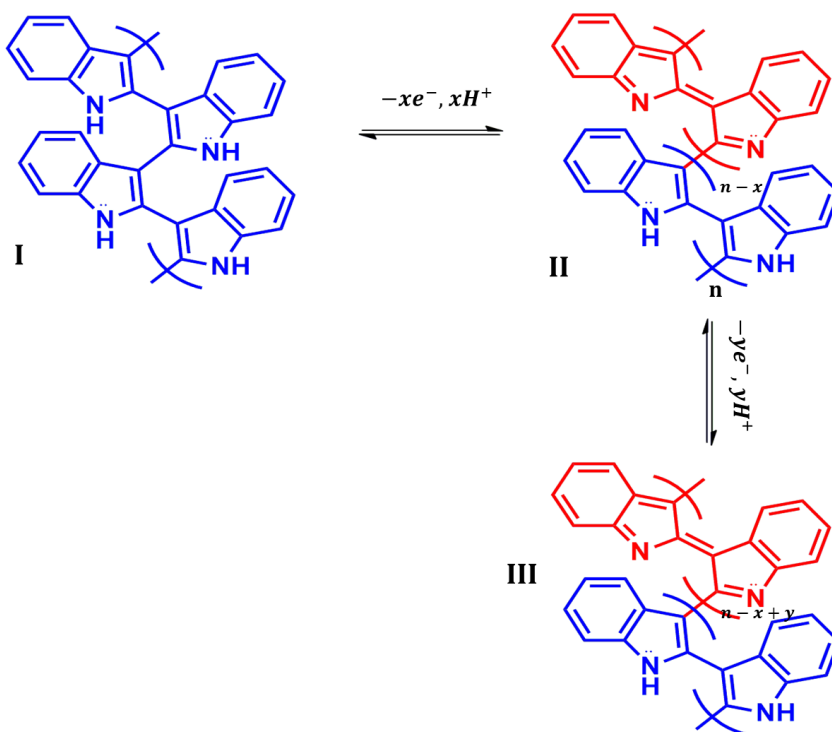
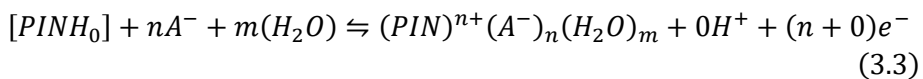
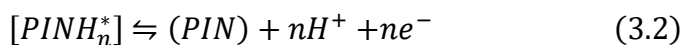
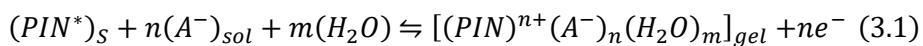


Figure 3.6 Schematic representation of PIN oxidation mechanism

The first anodic peak corresponds to the oxidation of the polymer by releasing x number of electrons and protons from x number of monomeric unit chains during the potential scan while the subsequent peak represents y number of electrons and protons from y number of monomeric units of the polymer chain^[6b]. In the second stage, a fully oxidized ($(x + y)$ units) of the polymer chain is obtained. Notably, the exchange of one electron per monomeric unit results in the creation of a radical cation that extends along these monomeric units, forming a π -conjugated structure. A comprehensive scheme is provided below (Figure 3.6).

During the reverse potential sweep, the corresponding reduction processes took place. Throughout the process, the charge balancing occurs through the counter ions, as the positive charge resulting from the oxidation of the polymer chain is compensated by the intake of counter anions into the polymer chain from the electrolyte. Moreover, exchange of solvent molecules also takes place between the polymer chain and the electrolyte to maintain osmotic pressure equilibrium caused by anion intercalation. The reversible reaction of the polymer's active center can be expressed as follows:



PIN^* denotes the polymer's active center, which is the region at the polymer/electrolyte interface where the removal of an electron results in the generation of a positive charge. The $(A^-)_{sol}$ symbolizes the monovalent anion present in the electrolyte, and H^+ represents

the proton. The oxidation of the polymer leads to the formation of the polymeric gel, as depicted in Equation 3.1. 'ne⁻' indicates a consecutive process involving the ejection of 'n' electrons from each polymeric chain. To validate the process occurring during the redox reaction of the polymer, a relationship between the variations of anodic/cathodic peak current against the scan rate was thoroughly examined.

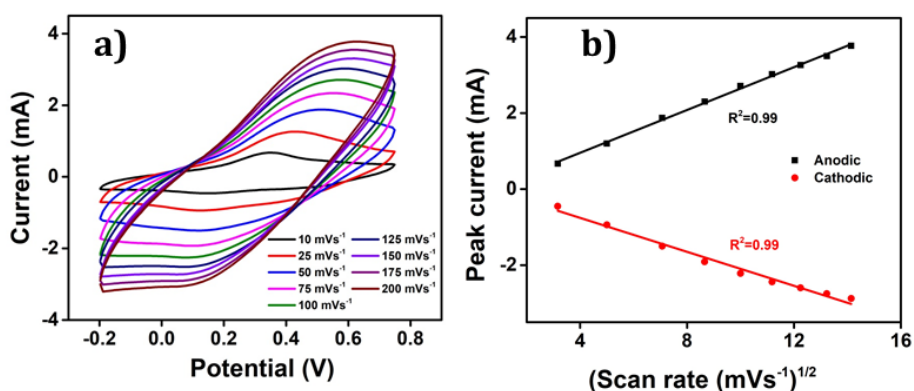


Figure 3.7 (a) CVs of PIN at different scan rates. (b) Linear fit of anodic and cathodic peak current with square root of scan rate

The CV responses of the PIN were recorded at various scan rates and the results are illustrated in Figure 3.7(a). The anodic peak current shifted towards more positive potential values, while the cathodic peak currents shifted towards more negative potential values as the scan rates increased. This observation provides conclusive evidence supporting the argument that the redox reaction becomes more resistive at higher scan rates due to the restricted entry and expulsion of counter anions through the polymer chain. Conversely, a reverse shift in potential values occurred as the scan rate was decreased, affirming that a significant conformational change took

place due to the creation or demolition of an increased quantity of free volume, allowing for the entry and expulsion of a greater number of counter ions and solvent molecules. Moreover, Figure 3.7(b) revealed a linear variation of the anodic and cathodic current peaks with the square root of the scan rates, suggesting that the process occurring at the electrode-electrolyte interface is diffusion-controlled up to 200 mVs^{-1} . The schematic representation of conformational changes occurring during the oxidation-reduction reaction of the PIN is demonstrated in Figure 3.8.

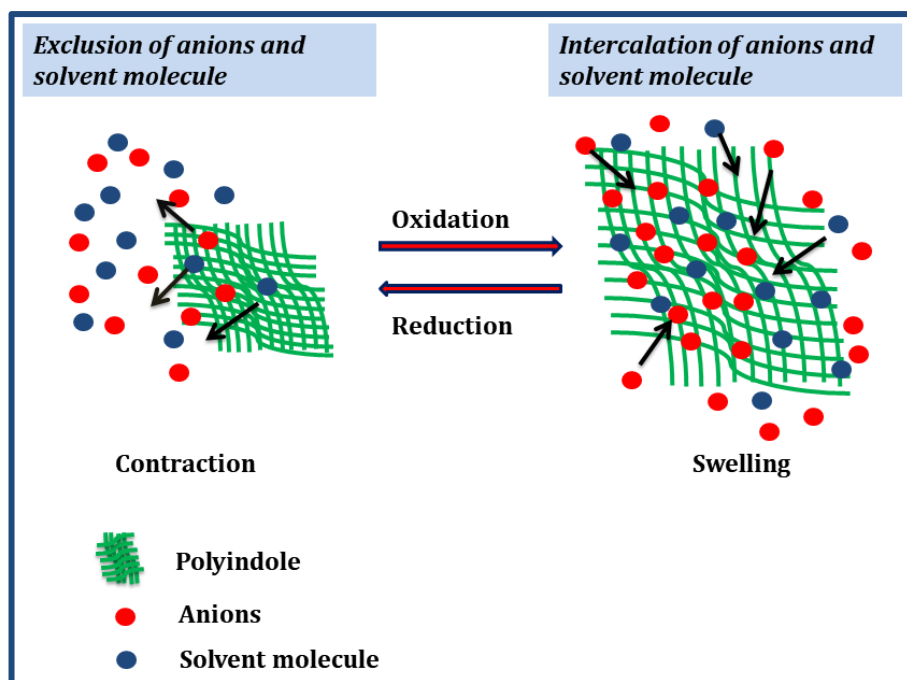


Figure 3.8 Swelling and de-swelling of PIN during oxidation and reduction

3.2.5.2. Coulovoltammogram

The coulovoltammogram, QV, is a plot of charge versus potential and was obtained by integrating the corresponding CV of PIN recorded

at a scan rate of 25 mVs^{-1} . The QV is shown in Figure 3.9. This QV curve provides valuable information about the reversible and irreversible charge consumed during the polymer electrochemical reaction 3.1 within a specified potential range. The figure shows a closed loop of QV, where the oxidation charge equals the reduction charge, indicating that only a reversible reaction is involved. The positive increment of charge represents the reversible oxidation, while the negative increment represents the reversible reduction of the polymer material. The minima of the QV curve are set at zero, and the difference between the maxima and minima of the closed loop gives the total reversible charge consumed during the process. In some cases, a parallel irreversible process may occur (section 3.2.2.4) due to hydrogen evolution, which is represented as an open part to the left side of the closed loop in the QV.

In the closed loop of the QV curve (shown in Figure 3.9), four distinct slope variations (dQ/dE) can be observed, revealing fundamental

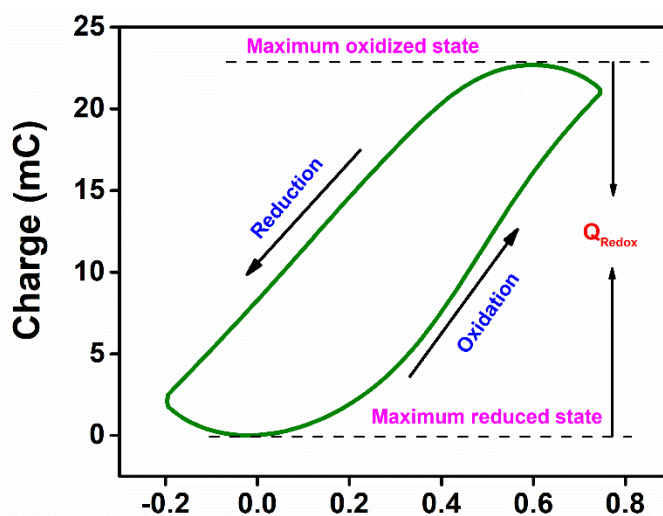


Figure 3.9 QV of PIN

structural conformational changes in the polymer chain^[21]. These variations include reduction-shrinking, reduction-compaction, oxidation-relaxation, and oxidation-swelling, which are typical characteristics of CPs. Any alteration in the QV slope indicates a corresponding modification in the PIN reaction (3.1) attributed to changes in the polymer chain's structure. Specifically, the cathodic potential sweep leads to the reduction of the polymer, involving two structural processes: reduction-shrinking and reduction-compaction. The charge consumed during these processes, along with the associated energy, can be precisely quantified from the QV.

3.2.5.3. Structural faradaic process in PIN

The exceptional electrochemical behavior of CPs has revealed their ability to mimic the reactions, composition variations, and properties of intercellular matrices (ICM) of biological systems establishing the fact that the CPs can be considered as electroactive reactive gels capable of mimicking some of the biological functions^[22].

In this study, we explored the generation of structural changes in the PIN chains induced by the electrochemical reaction of PIN. These reactions prompt conformational changes within the polymer chain, leading to macroscopic swelling, shrinking, compaction, and relaxation, thereby creating or eliminating free volume to accommodate or expel counter anions and solvent molecules. To understand the molecular and macroscopic conformational changes, we employed the electrochemically stimulated conformational relaxation (ESCR) model, which allows for the analysis and

quantitative assessment of the structural electrochemical responses exhibited by CPs^[23].

According to the ESCR model, of the CPs during oxidation (reaction 3.1), the material undergoes swelling and forms a dense gel as counter anions and solvent molecules are inserted into the polymer chain. In contrast, during electrochemical reduction of the polymer, electrons are inserted, while anions and solvent molecules are expelled simultaneously. The reduction process involves the counter anions pushing the polymer chain to create a path towards the solution (backward reaction of reaction 3.1). As reduction progresses, the polymer chain compacts, resulting in a densely packed conformational structure at higher cathodic potentials or when reduced for an extended time (Figure 3.10). Hence, at the same reduction rate, the reaction goes on from a fast reduction-shrinking state to slow reduction-compaction state. This compacted polymer structure can only be oxidized when additional energy (relaxation energy) is supplied to relax the conformation of the polymer chain, thereby creating free volume to accommodate anions and solvent molecules (reaction 3.1).

The relaxation of the compacted conformation is a slow step or rate-determining step. At the initial stage, a considerable amount of relaxation energy is required to initiate the structural relaxation from the reduced-compacted state.

Once the structure is relaxed, swelling ensues rapidly, facilitated by the fast diffusion of counter anions through the swelling polymer chain from the electrolyte. The unique electrochemical reactions

involving oxidation-reduction reactions drive the structural movements of the polymer chains.

Though, this model may seem complex, for the first time we applied this model to PIN. To thoroughly explore the structural electrochemistry of PIN, using CVs and QVs for the first time. The primary objective of this study was to identify, differentiate, and quantify the components involved in the PIN electrochemical reactions. Each polymer chain can be oxidized and reduced by ejecting and inserting n electrons, respectively, through consecutive n steps, with one electron in each step. The reaction progresses through n consecutive conformational states of the polymeric chain, akin to molecular motors driving the conformational movements of

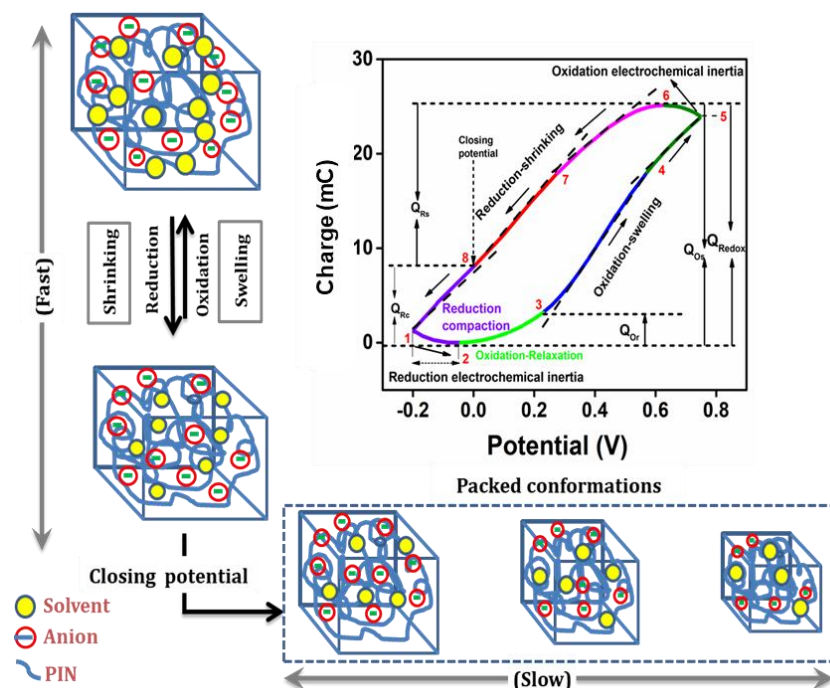


Figure 3.10 Different structural processes during the electrochemical reaction from QV in 1 M HCl at 25 mV s^{-1}

the polymer chain. The polymer chain undergoes relaxation and swelling during oxidation, and shrinking, closing, and compacting during reduction. Figure 3.10 gives in-depth information about these conformational changes.

The QV obtained at a scan rate of 25 mVs^{-1} in 1M HCl at room temperature is illustrated in Figure 3.10. The QV reveals the structural changes that occur during the distinctive electrochemical reaction (faradaic process), there are six slope variations observed in the case of PIN during the reaction, signifying the structural processes involved. Among these, four processes are evident: reduction-shrinking (comprising two stages), reduction-compactation, oxidation-relaxation, and oxidation swelling (comprising two stages).

The rapid reduction process initiates from the highest oxidation point (point 6, QV maximum) in the QV curve, exhibiting the steepest slope (Q/E). During this reduction, anions and water molecules are expelled, and protons are inserted (point 7), leading to a sudden shrinking of the polymer chain (points 6 to 8). The kinetics of counter-anion diffusion into the electrolyte solution plays a significant role in this reduction shrinking, indicating a kinetic control process. As the cathodic potential increases beyond point 8, the rate of reduction shrinking decreases, indicated by the lower slope of the curve at that point. This slow reduction process occurs due to the slow diffusion of the counter anion into the solution, as the distance between the polymer chains and the average diameter of the counter anions becomes almost equal during the reduction.

The closure of the gel structure occurs at point 8, potential at point 8 is known as closing potential (E_c). However, the reduction does not halt beyond the closing potential. The conformational movement is observed as anions push the chains, creating a path to diffuse towards the solution. Beyond the closing potential, a kinetic control reaction takes place due to the slow conformational movement of the polymer chain, resulting in a more packed conformation (compaction) of the polymer chain, known as reduction-compaction. This slow rate reduction continues until the QV minimum (point 2), from where the anodic potential limit starts (0.0059 V). Thus, the polymer reduction is not completed at the cathodic potential limit; it is partially oxidized at -0.2 V, and the reduction continues. Therefore, points 1 to 2 in the figure are referred to as oxidation electrochemical inertia.

The PIN oxidation commences from the QV minimum. The PIN compact structure gradually relaxes, creating free volume to accommodate anions and solvent molecules during oxidation. Points 2 to 3 in the figure depict the oxidation-relaxation of the polymer. At point 3, a significant increase in the anodic slope is observed, representing the fast oxidation-swelling process of the polymer, comprising two steps. The first step involves the insertion of anions and solvent molecules from the solution, as shown by the curve from 3 to 4, followed by the ejection of protons, represented by 4 to 5. The fast oxidation-swelling is also driven by the diffusion of counter anions from the solution to the polymer chain, a kinetic control process. The polymer oxidation is not completed at the anodic

potential limit of 0.75 V (point 5 in Figure 3.10), but it is fully oxidized at the beginning of the cathodic potential limit, QV maximum. This phenomenon is known as oxidation electrochemical inertia. The charge consumed during each structural process was determined from the QV.

The sum of the charge from QV maximum to the closing potential (termed as fast reduction shrinking charge, Q_{RS}) and from the closing potential to QV minimum (Reduction compaction charge, Q_{RC}) provides the total reduction charge. The total oxidation charge is obtained by adding the oxidation-relaxation charge (from 2 to 3, Q_{Or}), fast oxidation-swelling charge (from 3 to 5, Q_{Os}), and the charge corresponding to oxidation electrochemical inertia (from 5 to 6, Q_{Oei}).

$$Q_{Red} = Q_{RS} + Q_{RC} \quad (3.4)$$

$$Q_{Ox} = Q_{Or} + Q_{Os} + Q_{ei} \quad (3.5)$$

The charge consumed during each structural process and the corresponding potential ranges are given in Table 3.1. From the table it can be found that, for the reversible faradaic process of the polymer, $Q_{Ox} = Q_{Red}$.

Table 3.1 Structural Faradaic process in PIN, potential ranges and the consumed electrical charges

Structural process	Oxidation (Q_{Ox})			Reduction (Q_{Red})	
	Relaxation (Q_{Or})	Swelling (Q_{Os})	OEI (Q_{Oei})	Shrinking (Q_{RS})	Compaction (Q_{RC})

Potential range (V)	-0.051 to 0.233	0.233 to 0.745	0.745 to 0.621	0.621 to 0.004	0.004 to -0.051
Charge (mC)	3.32	20.46	1.34	16.96	8.2
Total charge (mC)	25.12				-25.12
	$Q_{Ox} = Q_{Or} + Q_{Os} + Q_{Oei}$			$Q_{Red} = Q_{Rs} + Q_{Rc}$	

3.2.5.4. Influence of cathodic potential limit on voltammetric and coulometric responses

Steady-state voltammograms were recorded for various cathodic potential limits while maintaining a constant anodic potential of 0.75 V. The voltammograms were recorded at a scan rate of 25 mVs⁻¹ in 1 M HCl aqueous solution using Ag/AgCl as the reference electrode. The results are presented in Figure 3.11(a) our major observations are given below.

- It is observed that a low current flows beyond the cathodic potential of -0.2 V.
- The reduction current persists at the start of the anodic potential sweep, indicating that the PIN reduction is not completed at this point. We wanted to determine at which cathodic potential limit the reduction process concludes.

- As the cathodic potential limits increase to more negative values, the oxidation peak current increases, suggesting deeper reductions in the film are achieved until that specific limit. We identified the optimal potential range for the reversible redox reaction of PIN.
- Beyond -0.75 V, the reduction current increases, indicating the presence of a new reduction process.
- From this study, we determined the cathodic potential limit at which the film reduction reaches completion.
- Established the potential range for the reversible oxidation/reduction of PIN.
- Identified the nature of the structural process, and quantitatively distinguish between different reversible and irreversible reactions involved.

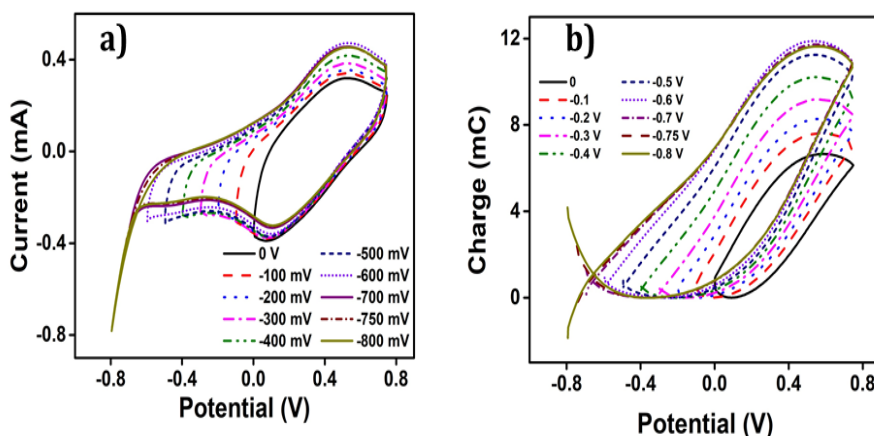


Figure 3.11 (a) CVs obtained for PIN in 1 M HCl at 25 mV s^{-1} from different cathodic potential limits. (b) QVs were obtained by integration of the CVs

- By increasing the cathodic potential limit, a more reduced and compact state was achieved. Additionally, the charge consumed during the reduction process and energy required for the initial relaxation of the packed structure during oxidation were calculated.

Detection of irreversible processes involved

It is clear from Figure 3.11(b), that a closed QV loop is obtained for potentials up to -0.2 V, indicating that at these potentials, the polymer undergoes a reversible redox process. This is confirmed by the obtained oxidation and redox charges, which are quantitatively equal. The difference between the maximum and minimum values of the closed loop in the QV gives the total charge consumed during the reversible redox process (Q_{redox}), which exhibits an increase with the increase in the cathodic potential limit. That is, we concluded that only reversible processes can occur for potentials up to -0.2 V.

Beyond -0.2 V, the QV exhibits two distinct regions: a closed loop representing the reversible process and an open part extending beyond the loop representing an irreversible process parallel to the reversible reduction of the PIN chain. The difference between the starting and ending points of the open section in the QV response indicates the charge consumed during the irreversible reduction, which commences from -0.3 V. Meanwhile, the reversible redox charge consumed (closed loop of the QV) increases as the cathodic potential limit increases from -0.3 V to -0.6 V, suggesting that the polymer reduction continues up to -0.6 V, beyond which an irreversible process takes place.

Reversible charge and shift of the material composition

The total reduction charge (Q_{red}) during each QV cycle, beyond -0.2 V is given in equation 3.6.

$$Q_{Red} = Q_{Redox} + Q_{Irr} \quad (3.6)$$

The charge associated with the redox process (Q_{Redox}) and the irreversible processes (Q_{Irr}) are clearly visible in QV displayed in Figure 3.11(b). Furthermore, this enables precise identification of the cathodic threshold limit of the involved reaction, which initiates at -0.3 V, suggesting the onset of the irreversible reaction.

Figure 3.12(a) displays the variation in charge during the oxidation/reduction reaction at different cathodic potential limits. It is evident from the figure that within the range of 0 V to -0.2 V, the oxidation and reduction charges overlap for the potential limits up to -0.2 V, suggesting only reversible processes take place up to -0.2 V. Beyond -0.2 V, two distinct charge components, corresponding to reversible and irreversible processes, namely Q_{Redox} and Q_{Irr} became apparent. From -0.3 V to -0.6 V, the redox charge shows a linear increase, while beyond -0.6 V, it decreases until -0.8 V it is clearly observed from Figure 3.12(a) that the second oxidation peak is shifted towards higher potentials, indicating an incomplete oxidation of the polymer chain beyond -0.6 V. Additionally, the charge consumed during the parallel irreversible process increases as the cathodic potential limit increases. Figure 3.12(b) represents the irreversible reduction charge associated with the irreversible reduction reaction. The charges consumed during different cathodic potential limits are given in Table 3.2.

Table 3.2 Charges consumed during different cathodic potential limit

Cathodic limit	Q_{redox} (mC)	Q_{irr} (mC)	Q_{total} (mC)
0	6.65		6.65
-0.1	7.60		7.60
-0.2	8.27		8.27
-0.3	9.18	0.16	9.34
-0.4	10.21	0.2	10.41
-0.5	11.24	0.3	11.54
-0.6	11.88	0.4	12.28
-0.7	11.73	1.14	12.87
-0.75	11.66	2.95	14.61
-0.8	11.66	6.04	17.70

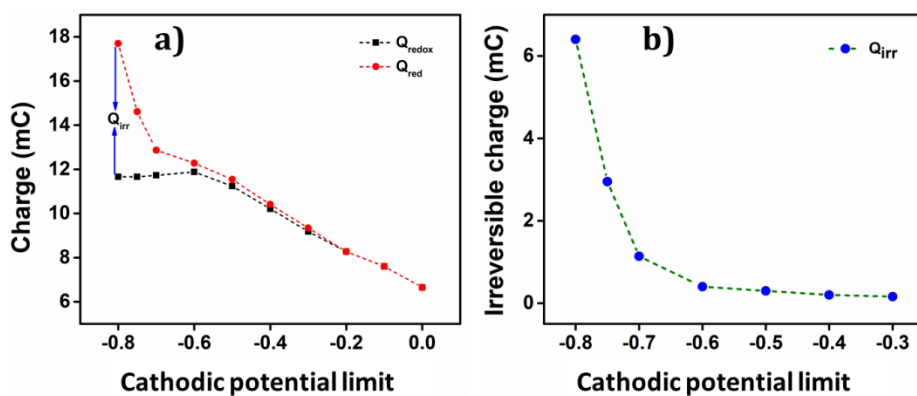


Figure 3.12 (a) Charge consumed in the oxidation and reduction of PIN and (b) irreversible reduction charge obtained for different cathodic potential limit

3.2.5.5 The influence of anodic potential limit on voltammetric and coulometric response

The closed QV loop spanning from 0 V to -0.2 V exemplifies the reversible structural changes of PIN during the distinctive electrochemical process (Figure 3.11). Subsequently, a constant cathodic potential of -0.2 V was selected to investigate the impact of the anodic potential limit on the voltammetric responses and structural changes (including reversible and irreversible processes, as well as consumed charges) of PIN.

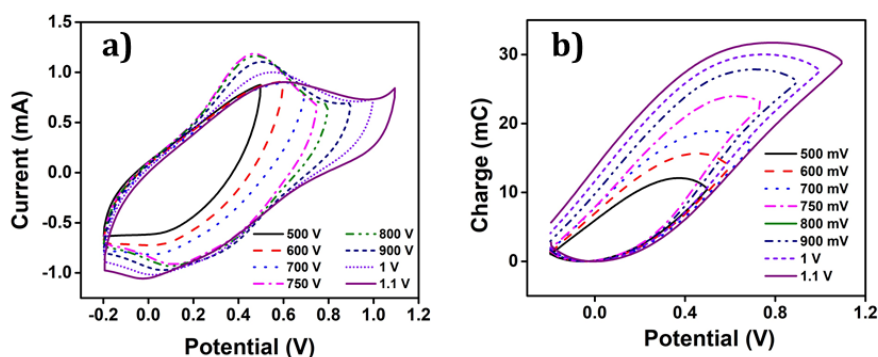


Figure 3.13 (a) CVs obtained for PIN in 1 M HCl at 25 mV s^{-1} from different anodic potential limits. (b) QVs obtained by integration of the CVs from (a)

Figure 3.13(a) illustrates the stationary voltammograms obtained after five consecutive potential cycles for each of the anodic potential limits studied. The corresponding QV responses were obtained by integrating the voltammograms presented in Figure 3.13(b). Closed QV loops were obtained, indicating that only reversible reactions can take place in the polymer chain. Conversely, anodic potential limits exceeding 0.75 V show larger oxidation

charges compared to reduction charges, resulting in open QV loops, suggesting new irreversible oxidation reactions is taking place in the PIN chain. The total charge consumed during this irreversible oxidation process ($Q_{I_{\text{rox}}}$) is determined from the difference between the charges at the beginning and end of the open QV loops (Figure 3.13(b)). The reversible charge is then obtained by subtracting $Q_{I_{\text{rox}}}$ from the total charge Q_{total} (the difference between QV maxima and minima). Figure 3.14 displays the distinct charge consumption during various processes for different anodic potential limits.

$$Q_{\text{Red}} = Q_{\text{Total}} + Q_{I_{\text{rox}}} \quad (3.7)$$

The studied potential limits reveal the same four structural processes discussed earlier: reduction-shrinking, reduction-compaction, oxidation-relaxation, and oxidation-swelling.

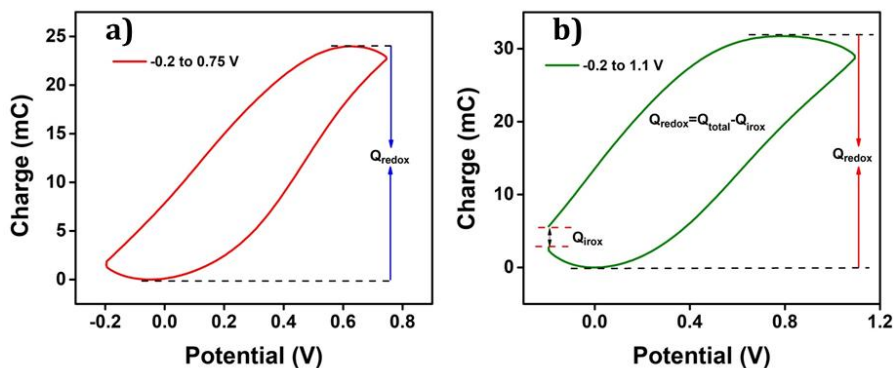


Figure 3.14 QV obtained in 1M HCl at the scan rate 25 mVs^{-1} **(a)** at the anodic potential limit 0.75 V and **(b)** at the anodic potential limit 1.1 V

Figure 3.15(a) illustrates the charge variation during the oxidation/reduction reaction for different anodic potential limits studied. For the potential range corresponding to 0.5 V to 0.75 V, the overlap of oxidation and reduction charges is observed. Beyond 0.75

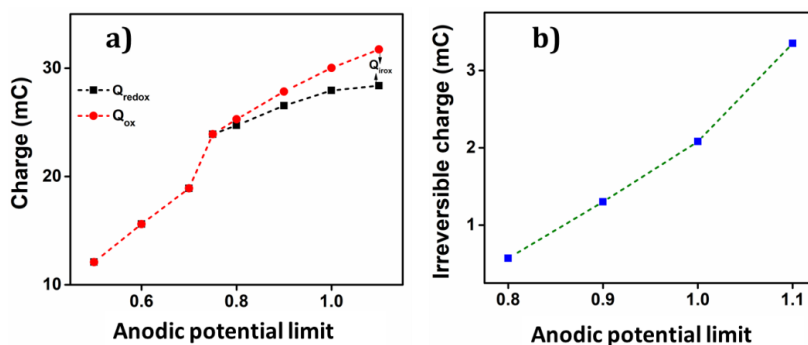


Figure 3.15 (a) Charge consumed in the oxidation and reduction of PIN and **(b)** irreversible reduction charge obtained for different anodic potential limits

V, two distinct charge components, reversible and irreversible, are clearly visible. Figure 3.15(b) indicates that the irreversible charge also increases as the anodic potential limit increases. The charge consumed during different anodic potential limits is given in Table 3.3.

Table 3.3 Charge consumed during different anodic potential limit

Anodic limit	Q_{Redox} (mC)	Q_{iox} (mC)	Q_{total} (mC)
0.5	12.09		12.09
0.6	15.60		15.60
0.7	18.90		18.90
0.75	23.90		23.90
0.8	25.28	0.57	24.71
0.9	27.84	1.3	26.54
1	30.02	2.08	27.94
1.1	31.73	3.35	28.38

3.3. Conclusion

An electroactive PIN in powder form was synthesized chemically by using anhydrous FeCl_3 as the oxidant, resulting in agglomerated granular morphology. The synthesized polymer is characterized using FTIR, UV-Vis, FE-SEM, EDX and TGA analysis. The electrochemical properties of PIN are explored through CV, chronopotentiometry, and QV.

The CV of PIN displays a well-defined couple of oxidation and corresponding reduction peaks. The potential window of the PIN during CV is optimized using QV, which is essential and the effect of cathodic and anodic potential limits on the charge consumption of the polymer is also explored using QV. A closed QV loop is observed within the potential range of -0.2 V to 0.75 V, indicating that only the reversible redox process occurs within this specific potential window in an aqueous 1M HCl solution.

The different structural variations during the unique electrochemical reaction (conformational process): reduction-shrinking, reduction-compactation, oxidation-relaxation and oxidation-swelling are demonstrated using QV analysis. Each structural processes are indicated by the slope of the graph obtained by plotting the consumed electrical charge against potential (QV) and the corresponding charges during these conformational variations were also calculated. By doing so, we have aimed to present a comprehensive and insightful account of the structural electrochemistry of the PIN and the potential applications of this intriguing material. At potentials beyond -0.2 V, an irreversible

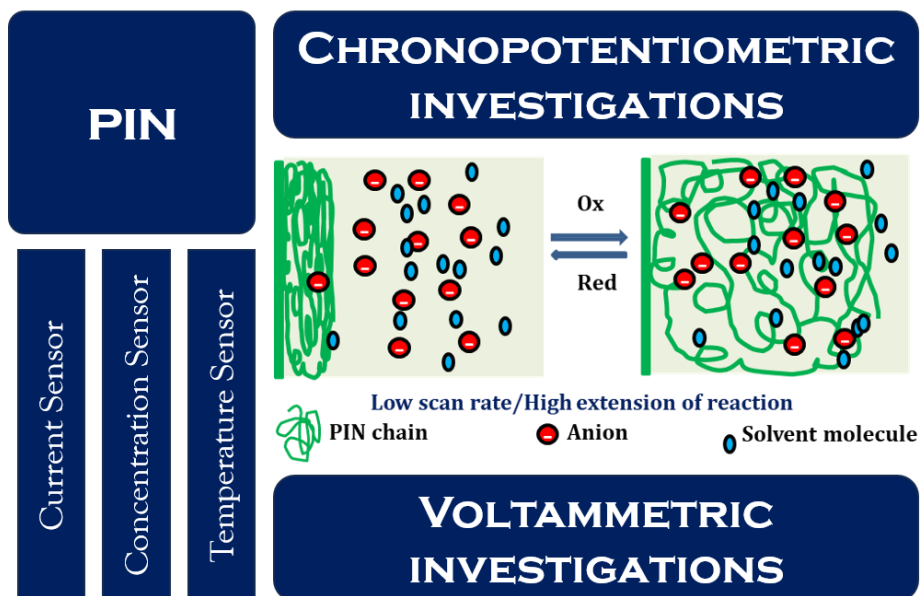
reduction (hydrogen evolution) is observed parallel to the reversible processes, while beyond 0.75 V, a parallel irreversible oxidation process takes place (oxygen evolution and polymeric over oxidation). The charges consumed during both the reversible and irreversible processes are also accurately calculated using QV. Thus, we are able to provide a first-time report on the structural electrochemistry of PIN.

References

- [1] aT. F. Otero, J. M. Sansiñena, *Bioelectrochem. Bioenerg.* **1995**, *38*, 411-414; bT. F. Otero, M. T. Cortés, *Advanced Materials* **2003**, *15*, 279-282; cY. A. Ismail, J. G. Martínez, T. F. Otero, *Electrochim. Acta* **2014**, *123*, 501-510.
- [2] T. F. Otero, in *Modern Aspects of Electrochemistry*, Springer, **1999**, pp. 307-434.
- [3] aJ. G. Martinez, T. F. Otero, E. W. Jager, *Langmuir* **2014**, *30*, 3894-3904; bY. A. Ismail, J. G. Martínez, A. S. Al Harrasi, S. J. Kim, T. F. Otero, *Sensors and Actuators B: chemical* **2011**, *160*, 1180-1190; cA. Thadathil, H. Pradeep, D. Joshy, Y. A. Ismail, P. Periyat, *Materials Advances* **2022**, *3*, 2990-3022.
- [4] L. Rajan, M. P. Sidheekha, A. Shabeeba, S. C. Unnikrishnan, Y. A. Ismail, *Res. Chem. Intermed.* **2022**, *48*, 4313-4329.
- [5] T. F. Otero, M. Alfaro, V. Martinez, M. A. Perez, J. G. Martinez, *Advanced Functional Materials* **2013**, *23*, 3929-3940.
- [6] aT. Anjitha, T. Anilkumar, G. Mathew, M. T. Ramesan, *Polym. Compos.* **2019**, *40*, 2802-2811; bL. Rajan, M. P. Sidheekha, A. Shabeeba, Y. A. Ismail, *Materials Chemistry Frontiers* **2022**, *6*, 1706-1718.
- [7] aA. Shabeeba, L. Rajan, M. P. Sidheekha, M. S. Thayyil, Y. A. Ismail, *Journal of Energy Storage* **2022**, *55*, 105724; bY. A. Ismail, S. R. Shin, K. M. Shin, S. G. Yoon, K. Shon, S. I. Kim, S. J. Kim, *Sensors and Actuators B: Chemical* **2008**, *129*, 834-840; cH. Grande, T. F. Otero, *Electrochim. Acta* **1999**, *44*, 1893-1900.
- [8] aT. F. Otero, I. Boyano, *The Journal of Physical Chemistry B* **2003**, *107*, 6730-6738; bT. F. Otero, J. G. Martinez, *Advanced Functional Materials* **2014**, *24*, 1259-1264.
- [9] T. F. Otero, *Journal of Materials Chemistry B* **2013**, *1*, 3754-3767.

- [10] T. F. Otero, J. G. Martinez, *Progress in Polymer Science* **2015**, *44*, 62-78.
- [11] aM. Ramesan, *Polym. Compos.* **2012**, *33*, 2169-2176; bD. Devadathan, R. Raveendran, *International Journal of Chemical Engineering and Applications* **2014**, *5*, 240.
- [12] S. An, T. Abdiryim, Y. Ding, I. Nurulla, *Mater. Lett.* **2008**, *62*, 935-938.
- [13] K. N. Handore, S. V. Bhavsar, N. Pande, P. K. Chhattise, S. B. Sharma, S. Dallavalle, V. Gaikwad, K. C. Mohite, V. V. Chabukswar, *Polymer-Plastics Technology and Engineering* **2014**, *53*, 734-741.
- [14] aN. Wadatar, S. Waghuley, *Egyptian Journal of Basic and Applied Sciences* **2015**, *2*, 19-24; bD. Bhagat, G. Dhokane, *Mater. Lett.* **2014**, *136*, 251-253.
- [15] aM. Elango, M. Deepa, R. Subramanian, A. M. Musthafa, *J. Alloys Compd.* **2017**, *696*, 391-401; bB. Gupta, D. S. Chauhan, R. Prakash, *Materials Chemistry and Physics* **2010**, *120*, 625-630.
- [16] aP. S. Abthagir, R. Saraswathi, *Thermochim. Acta* **2004**, *424*, 25-35; bS. Sankar, A. A. Naik, T. Anilkumar, M. Ramesan, *Journal of Applied Polymer Science* **2020**, *137*, 49145.
- [17] E. Azizi, J. Arjomandi, A. Salimi, J. Y. Lee, *Polymer* **2020**, *195*, 122429.
- [18] aA. Shabeeba, Y. A. Ismail, *Mater. Res. Bull.* **2022**, *152*, 111817; bA. Shabeeba, M. P. Sidheekha, L. Rajan, Y. A. Ismail, *RSC Advances* **2022**, *12*, 31911-31922; cJ. G. Martinez, T. F. Otero, E. W. H. Jager, *Langmuir* **2014**, *30*, 3894-3904; dT. F. Otero, H. Grande, J. Rodríguez, *Journal of Electroanalytical Chemistry* **1995**, *394*, 211-216.
- [19] T. F. Otero, J. G. Martinez, *Journal of Materials Chemistry B* **2013**, *1*, 26-38.
- [20] S. Sharma, P. Joshi, S. Mehtab, M. G. H. Zaidi, K. Singhal, T. I. Siddiqi, *Journal of Analysis and Testing* **2020**, *4*, 13-22.
- [21] T. F. Otero, J. G. Martinez, M. Fuchiwaki, L. Valero, *Advanced Functional Materials* **2014**, *24*, 1265-1274.
- [22] T. F. Otero, J. G. Martinez, *Advanced Functional Materials* **2013**, *23*, 404-416.
- [23] T. F. Otero, *Electrochim. Acta* **2016**, *212*, 440-457.

Polyindole as Biomimetic sensors of electrical, chemical, and thermal working environment



Different structural Faradaic processes occurring in PIN are studied in detail. We applied the concept of structural electrochemistry of PIN for its potential application as a biomimetic sensor of working conditions. The biomimetic reactive sensing nature of PIN is presented for the first time through its chronopotentiometric and voltammetric responses recorded from aqueous solutions of HCl. The electrical energy and the redox charge consumed during the reaction are proved as the sensing parameters. The results suggest that the PIN can act as a biomimetic macro molecular sensor of working conditions as biological muscles do.

4.1. Introduction

Biomimicking is a fascinating approach that draws inspiration from nature to solve complex problems and provide innovative solutions. By studying nature's brilliant adaptations, scientists, engineers, and designers seek to replicate these adaptations to human-made technologies, products, and systems helping us to create a balanced connection between our innovations and the environment. Mimicking one of the fascinating biological phenomena, i.e., brain-muscle interfacing remains a great challenge to the scientific community^[1]. The working of biological muscles is based on the electrical signals generated in the brain; sending the same to the muscles through the motor neuron, liberating Ca^{2+} ions inside the cell and initiating the reaction-driven conformational movements of the actin-myosin-ATP (muscular contraction)^[2]. Any muscle is an electro-chemo-mechanical organ working by cooperative actuation of the constitutive macromolecular motors (actin-myosin proteins)^[3]. While actuation, biological muscles are capable of sensing their surrounding condition (temperature, pressure, muscle potential, and chemical potential in the body), and transmitting back this sensing information to the brain through the sensing neuron^[4]. The school of these processes is based on the reactive nature of the biological system. The scientific community is in search of a reactive material model constituted by macromolecular motors that can mimic this simultaneous actuation and sensing abilities using the same connectivity: actuation orders and sensing signals present, simultaneously in the same two connecting wires^[5].

Every chain of a CP acts as a macromolecular motor during electrochemical reactions mimicking the sensing ability of the biological muscle and its feedback communication back to the brain^[4]. The cooperative actuation of the CP chains during the oxidation/reduction reactions in liquid electrolytes promotes the generation/destruction of free volume required for the incorporation/expulsion of balancing counter ions and solvent, required for osmotic balance: the reactions drive reversible structural changes (relaxation, swelling, shrinking and contraction). The reaction is driven by electrical signals (potential, and/or current) sent to the material. The electrical responses during reactions (consumed charge, consumed energy, and potential evolution) are different for different working (chemical, thermal, electrical) conditions^[6]. The signal, the order, and the sensing responses are embedded simultaneously within only two connecting wires.

Among the CPs, the remarkable biomimetic simultaneous reactive sensing abilities of polypyrrole and polyaniline have been effectively demonstrated recently^[7]. A theoretical description of the reactive sensing nature of the CPs towards their working variables and the variation of consumed electrical energy and the electrical charge by changing the working ambient were suggested by the same group^[8]. Since the reactions of CPs take place outside the equilibrium conditions, any perturbation such as a change in working variables on the reaction rate will shift the consumed electrical energy and the electrical charge that can easily be sensed by the CPs^[9]. We are

trying to establish that, the principle suggested by Otero (Any physical or chemical variables (current, active site concentration, electrolyte concentration, mechanical stress, and temperature) that disturb the electrochemical reaction rate should modify the reaction overpotential (electrical energy) to self-adapt to the newly imposed energetic requirements) is true for all the CPs.

This self-sensing property of CPs other than polypyrrole has not yet been explored in detail. A few studies on the reactive sensing nature of polyanilines and their composites have been reported by Ismail et al., recently^[10]. In this work, we are presenting the evidence for our claim that all CPs can act as biomimetic multistep macromolecular sensors of the working conditions by taking, for the first time, PIN and its electrochemical reaction as the model material and process, respectively, for mimicking the related biological process occurring in natural muscles. In this work, we have proved that a chemically synthesized PIN can act as a multi-step macromolecular sensor of the electrical, chemical, and thermal working conditions.

4.2. Results and discussions

Chronopotentiometry and cyclic voltammetry were used to examine the sensing behavior of the PIN.

4.2.1. Reactive sensing ability of PIN towards the working electrical, chemical, and thermal ambient; chronopotentiometry

The biomimetic reactive sensing ability of PIN towards its working ambient is studied by using chronopotentiometry. The constant reaction rate of the PIN, the constant shift of the PIN polymer

composition, and the evolution of the material potential were controlled by the flow of constant current, anodic or cathodic passed through the polymer. This was analyzed by recording the chronopotentiometric responses. The physical or chemical variables influencing the rate of the electrode reaction affected the potential evolution of the PIN chain. The PIN was subjected to constant current waves (square current) to check whether the material could sense the electrical, chemical, and thermal working conditions (current, electrolyte concentration, and temperature). Before obtaining the chrono-potentiometric responses, the material was stabilized by recording 20 consecutive cycles of voltammograms. The consecutive square current gives the chronopotentiometric responses by applying a constant charge. The potential evolution of the material during the reaction changes by changing the studied variables.

4.2.1.1. Sensing of electrical working condition- current sensor

In order to evaluate its electrical working condition, different anodic and cathodic currents ranging from ± 0.05 mA to ± 1 mA were applied to the PIN at a constant charge of 6 mC, by varying the time of the current flow in 1 M HCl. The results are depicted in Figure 4.1. The electrical energy consumed during the redox process was calculated using the equation

$$U = I \int E dt \quad (4.1)$$

From Figure 4.1, it can be observed that the potential evolved during the redox process was increased with an increase in the anodic

current. The potential shifted to larger negative values with an increase in the cathodic current. The electrical energy consumed during the reaction was found to be the sensing parameter which varied linearly with the applied anodic and cathodic currents (Figure 4.1(c)). This suggests that the material is capable of sensing the applied current during these reactions^[11].

4.2.1.2. Sensing chemical working condition-concentration sensor

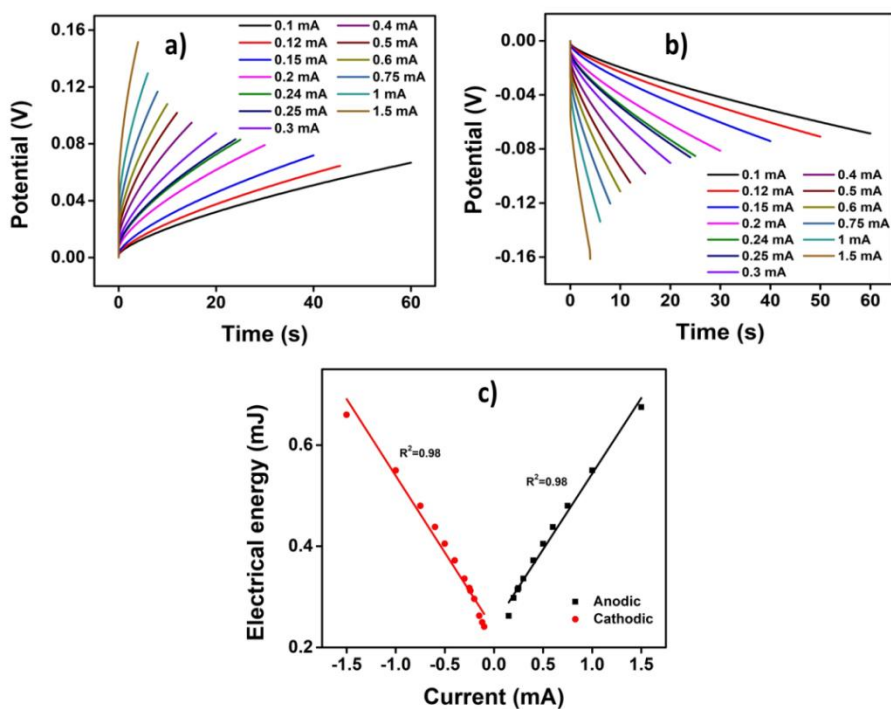


Figure 4.1 Chronopotentiograms obtained when different constant (a) anodic and (b) cathodic currents were applied to PIN by passing a constant charge of 3 mC in 1 M HCl solution (c) Electrical energy consumed by the PIN as a function of applied current

In order to study the sensing ability of PIN towards the chemical working condition, the chronopotentiometric responses of PIN in HCl electrolytes of various concentrations (from 0.01 M to 1 M) were recorded. The results are shown in Figure 4.2. The experiment involved applying a constant charge of 6 mC at room temperature by maintaining a constant anodic and cathodic current of 0.05 mA and -0.05 mA, respectively, for 60 s. The potential evolution during the polymer reaction was found to vary with the concentration of the electrolytes. At higher electrolyte concentrations the available

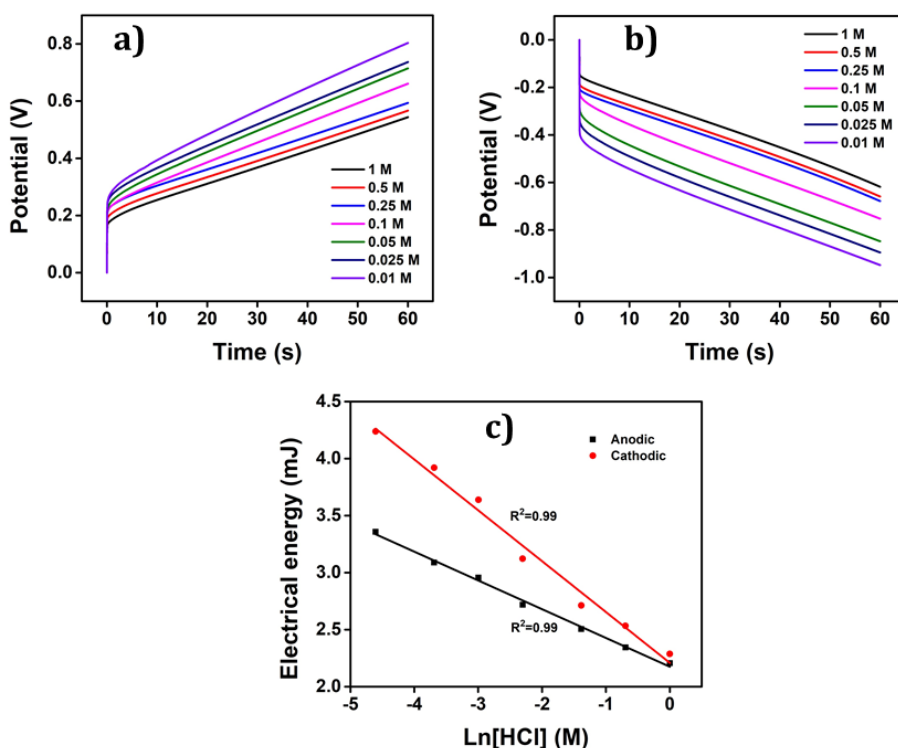


Figure 4.2 Chronopotentiogram obtained from different concentrations of HCl when (a) 0.05 mA and (b) -0.05 mA of current were applied to the PIN for the 60 s. (c) Electrical energy (U) consumed by the PIN

chemical energy is large. Therefore, the reaction rate for the anodic and cathodic processes increases as the concentration increases. Resulting in the potential evolution at lower values for higher concentrations of the electrolyte^[12].

It is observed that the consumed electrical energy during the reaction has a linear relationship with the logarithmic function of concentration as shown in Figure 4.2(c). That is the material can sense any changes in the concentration of electrolytes.

4.2.1.3. Sensing of thermal working condition- temperature sensor

The temperature sensing ability of the PIN was examined by applying +0.1 mA and -0.1 mA current for anodic and cathodic processes respectively for 60 s (maintaining a constant charge of 6 mC) in 1 M HCl for different temperatures as depicted in Figure 4.3. The Arrhenius concept was used to explain the observed results. As the temperature increases, the available thermal energy also increases, which results in fast conformational movement of the polymer chain and a high diffusion coefficient. The reaction as shown in equation 4.1 occurs to the same extent by applying a constant current for constant time (i.e., constant charge), but at a lower potential evolution, consuming lower energy as the temperature increases^[13].

That is for the anodic process, the potential evolution goes to lower values as the temperature increases, while for the cathodic process, potential evolution goes to lower negative values with increasing temperature. The consumed electrical energy has a linear

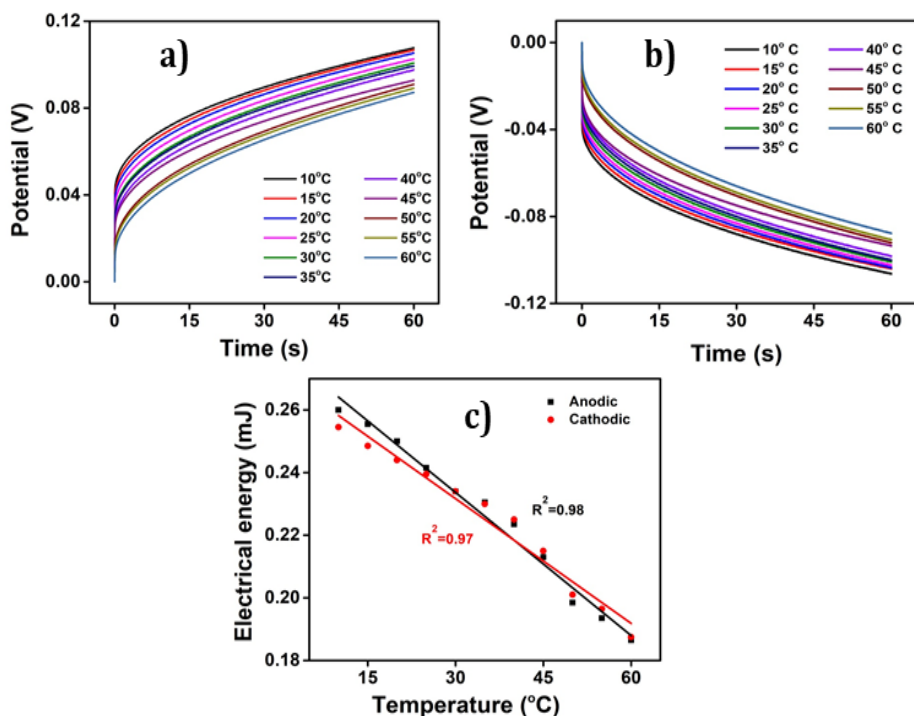


Figure 4.3 Chronopotentiogram obtained from different experimental temperatures when (a) +0.1 mA and (b) -0.1 mA of current were applied to the PIN for the 60 s. (c) The variation of electrical energy (U) consumed during the anodic and cathodic process

dependence on temperature, which was fitted with theoretical equation 4.8^[14]. This suggests that the PIN has the ability to sense the working temperature as biological muscles do.

Theoretical description

The reactive sensing capability of PIN originated through the redox reactions. Nernst equation gives the potential of PIN at equilibrium condition which is expressed as

$$E = E_0 - \frac{RT}{nF} \ln \frac{[A^-][PINH_0]}{(H^+)[(PIN)^{n+}(A^-)_n(H_2O)_m]} \quad (4.2)$$

Where, E is the potential evolved, E_0 is the standard electrode potential, R is the universal gas constant ($R=8.314 \text{ J mol}^{-1} \text{ K}^{-1}$), F is the Faraday constant ($F=96500 \text{ C mol}^{-1}$), $[A^-]$ is the anion concentration, $[PIN^*]$ is the concentration of the polymer active center, and $[(PIN)^{n+}(A^-)_n(H_2O)_m]$ is the concentration of oxidized polymer center of PIN. The equation (4.2) gives the relationship between the potential and the concentration of the electroactive species^[15]. Classical potentiometric sensors work under equilibrium conditions and Le Chatelier's principle is applied, according to which, when any physical or chemical variables disturb the chemical equilibrium, the system will try to nullify that disturbance by shifting the equilibrium and attaining a new equilibrium condition. The electrochemical redox reaction of the PIN (and all other CPs) occurs outside the equilibrium condition and therefore the system does not obey the Le Chatelier principle. Otero et al., reformulated Le Chatelier's principle for such a system as any chemical or physical variable that disturbs the rate of chemical reaction will shift the reaction energy to fit the newly imposed energetic conditions. Therefore, under such situations, any variable that can induce a change in reaction working energetic condition will be sensed by the material potential.

The rate of reaction of PIN can be expressed as

$$r = k[PINH_0]^a[A^-]^b[H^+]^c \quad (4.3)$$

where, r is the rate of reaction, k is the kinetic constant, and a , and b are the reaction orders of the polymer active center and the anion/electrolyte concentration respectively. The flow of constant current

through PIN gives the relationship between the current and the rate of reaction, which can be written as:

$$r = \frac{q}{FV} = \frac{it}{FV} \leftrightarrow i = \frac{rFV}{t} \quad (4.4)$$

where, q is the charge, i is current, t is the time of current flow, F is the Faraday constant and V is the volume of the active centers of PIN. The relation between the rate constant and the potential evolution during the redox process was obtained from the Butler-Volmer equation of electrochemical kinetics.

$$i_a = FV k_{\alpha} [PINH_0]^a [A^-]^b [H^+]^c \quad (4.5)$$

$$i_a = FV k_{\alpha 0} [PINH_0]^a [A^-]^b [H^+]^c \exp\left(\frac{(1-a)nF(E - E_0)}{RT}\right) \quad (4.6)$$

Here we get the evolved potential during the reaction as the functions of concentration of the electrolyte, applied current, and/or temperature. The equation for evolved potential can be obtained as,

$$E_a = E_0 + \frac{RT}{(1-a)nF} \left(\ln\left(\frac{i_a}{FV}\right) - b \ln[A^-] - a \ln[PINH_0] - cpH - \ln k_{\alpha 0} \right) \quad (4.7)$$

Equations 4.6 and 4.7 lay the foundation of the idea of the sensing property of the PIN during its anodic process. A similar equation can be obtained for the cathodic process. The anodic oxidation occurs through n consecutive steps, so the general equation can be written as;

$$E_n(t) = E_0 + i_a Z + (n-1)\Delta E + \frac{RT}{(1-a)F} \left\{ \ln\left(\frac{i_a}{FV}\right) - b \ln[A^-] - a \ln\left([PINH_0]_{initial} - cpH - \frac{i_a t}{FV}\right) - \ln k_{\alpha 0} \right\} \quad (4.8)$$

Equations 4.6, 4.7, and 4.8 are similar equations for the evolution of electrical energy during the electrochemical reaction of PIN caused by changes in its environmental variables: applied current, electrolyte concentration, and temperature. The consumed electrical energy during the reaction thus can sense the surrounding variables. This equation suggests that PIN can act as a sensor of working ambient as there exists a linear relationship between the consumed electrical energy with applied current, log concentration, and temperature.

4.2.2. Reaction-driven sensing characteristics of PIN: A voltammetric investigation

The sensing ability of the PIN to its working environment was also explored using voltammetric analysis. Stationary cyclic voltammogram of PIN at different environmental working variables (electrical, chemical, and thermal) was recorded. Here we prove that, consumed electrical charge is a sensing parameter. The electrical redox charge consumed during the reaction was obtained by integrating the CV. The total redox charge and the relation between the different working energetic conditions were from the QV and its relation with the working energetic condition is established.

4.2.2.1. Sensing electrical working condition

To study the sensing behavior of PIN towards the electrical working condition (i.e., scan rate), the PIN was submitted to stable voltammetric responses between -0.2 mV to 0.75 mV for different scan rates in 1 M HCl at room temperature^[15]. The results are shown

in Figure 4.4(a). It can be observed that, the anodic and cathodic peak currents increase by increasing the scan rates. The reversible redox charge during the reaction at different scan rates were obtained by integrating the voltammograms and the resulting QV is shown in Figure 4.4(b). From Figure 4.4(c), it can be observed that the redox charge decreases by increasing the scan rate as the time consumed for the reaction is large to lower the scan rates. The

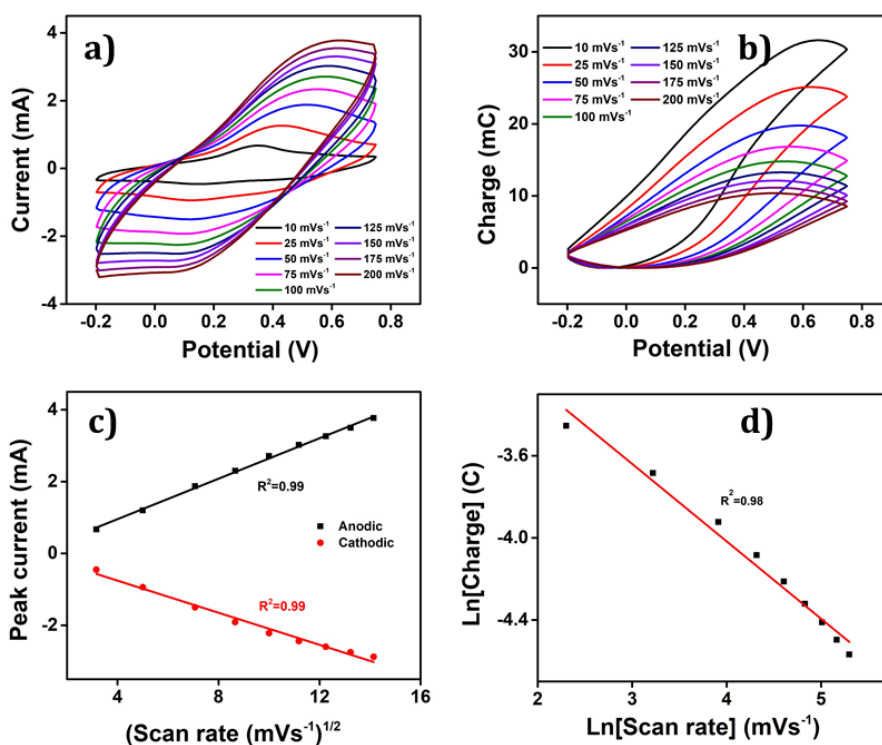


Figure 4.4 (a) CVs obtained from different scan rates in forward (5 mVs^{-1} to 200 mVs^{-1}) in 1 M HCl at room temperature within the potential window of -0.2 V to 0.75 V . (b) Corresponding coulo voltammogram obtained by integrating the CVs obtained in (a). (c) Linear fit of anodic and cathodic peak current with the square root of scan rate. (d) Logarithmic relation of redox charge consumed during the reaction of PIN obtained from the QV with the scan rate

logarithmic dependence of the scan rates and the consumed redox charge during the reaction is shown in Figure 4.4(d). The results corroborate the theoretical equation 4.16 and prove that the PIN can sense the electrical working condition by using consumed redox charge as the sensing parameter.

For lower scan rates, the reaction takes a longer time, resulting in a significant intercalation and de-intercalation of counter anions. This extended process leads to a deeper redox reaction (higher extension of reaction), increased polymer chain conformational movement,

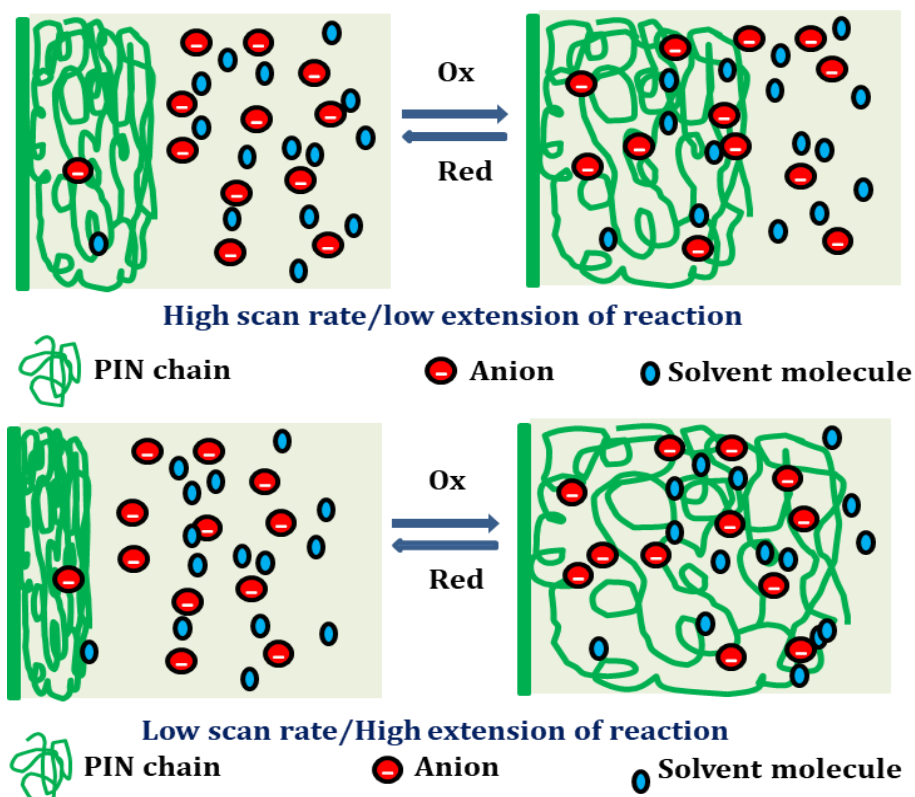


Figure 4.5 Schematic representation of the extension of reaction at lower and higher scan rates

and structural changes, which in turn cause higher charge consumption during the reaction (Figure 4.5).

Conversely, at higher scan rates, the charge consumed during the reaction is low because of the lower extension^[15]. Consequently, the consumed redox charge is regarded as the sensing parameter.

Theoretical interpretation

The rate equation can be presented in terms of the concentration of the active polymeric center because, during the reaction, the volume of the active center keeps on changing continuously and the rate equation 4.3 can be rewritten as the rate per unit mass.

$$\bar{r} = \frac{r}{m} = \frac{k}{m} [Cl^-]^\alpha [PINH_0]^\beta [H^+]^\gamma \quad (4.9)$$

Equation 4.9 can be rearranged as;

$$[PINH_0] = \frac{Q}{VzF} = \frac{q\rho}{mzF} \quad (4.10)$$

where, V is the volume of the active center in L and ρ is the density in gL^{-1} . The influence of the scan rate on the reaction extension was quantified as a function of the consumed redox charge.

The variation of concentration of the polymer active center has a direct relation with consumed oxidation or reduction charge (equation 4.10).

The variation of the concentration of the active center $[PINH_0]$ per unit time defines the rate of reaction.

The time of reaction can be obtained from potential and the scan rate (v), ($\partial t = \partial E/v$). The decrease in the concentration of the polymer active center is equal to the number of moles of electron

(number of Faraday) released from the polymer chain which is equal to the formation rate of the polarons.

$$r = -\frac{\partial[PINH_0]}{\partial t} = \frac{\partial\left(\frac{q\rho}{F}\right)}{\partial t} = \frac{v\rho}{F} \frac{\partial q}{\partial E} \quad (4.11)$$

The reaction rate can also be expressed as;

$$\frac{v\rho}{F} \frac{\partial q}{\partial E} = k[Cl^-]^\alpha [PINH_0]^\beta [H^+]^\gamma = k[Cl^-]^\alpha \left(\frac{q\rho}{F}\right)^\beta [H^+]^\gamma \quad (4.12)$$

The equations can be rearranged as;

$$\frac{1}{q^\beta} \frac{\partial q}{\partial E} = \frac{k[Cl^-]^\alpha [H^+]^\gamma F^{1-\beta}}{\rho^{1-\beta}} \frac{1}{v} \quad (4.13)$$

The left side of equation 4.13 is integrated between 0 and maximum charge consumed during redox reaction (q_R).

The right side is integrated between E_0 (potential at charge is zero) and E_R (potential at q_R).

$$\int_0^{q_R} \frac{1}{q^\beta} \partial q = \int_{E_0}^{E_R} \frac{k[Cl^-]^\alpha [H^+]^\gamma F^{1-\beta}}{\rho^{1-\beta}} \frac{1}{v} \partial E \quad (4.14)$$

$$q_R^{1-\beta} = \frac{(1-\beta)k[Cl^-]^\alpha [H^+]^\gamma F^{1-\beta} \Delta E}{\rho^{1-\beta}} \frac{1}{v} \quad (4.15)$$

The consumed redox charge during the reaction defines the reaction extension. Equation (4.15) gives the relation between the consumed redox charge during the reaction and the scan rate.

The extension of reaction or the redox charge consumed during the reaction decreases with increases in the scan rate while keeping all other working variables such as electrolyte concentration (chemical), working temperature (thermal), atmospheric pressure, and the potential window constant.

From equation 4.15 all the constant terms can be combined and considered as another constant h' . A straight-line equation was obtained by taking the logarithm of both sides of the equation 4.15.

$$\ln q_r = x - y \ln v \quad (4.16)$$

The logarithmic relation gives the slope (y ; sensitivity) and the intercept (x) of the straight line which can be defined as;

$$x = \frac{\ln h'}{1 - \beta} \quad (4.17)$$

$$y = \frac{1}{1 - \beta} \quad (4.18)$$

Equation 4.15 can be considered as the sensing equation to quantify the relation between the reaction extension and the scan rate.

4.2.2.2. Sensing of chemical working conditions-concentration sensor

To analyze the sensing nature of PIN towards the chemical working environment through voltammetry, stable voltammetric responses at different concentrations of aqueous HCl were recorded by keeping all other working variables (electrical and thermal) constant. Figure 4.6(a) shows the CVs obtained at different electrolyte concentrations at the scan rate of 25 mVs⁻¹ at room temperature. It can be seen that the anodic and cathodic current peaks increase with increasing concentration.

The QVs were obtained by integrating the corresponding CVs are shown in Figure 4.6(b). The charge consumed during the reaction was found to increase by increasing the concentration of the electrolyte.

The polymer chain was fully oxidized at higher concentrations in the same potential window because, the available chemical energy is large for higher concentrations. The large free volume generated by this complete oxidation drives the intercalation of the counter anions and water molecules from the electrolyte to the polymer matrix. At lower concentrations, the available chemical energy is low, and partial oxidation of the polymer chain takes place which generates a low amount of free volume to enter/expel the counter anions and solvent molecules during the oxidation and reduction

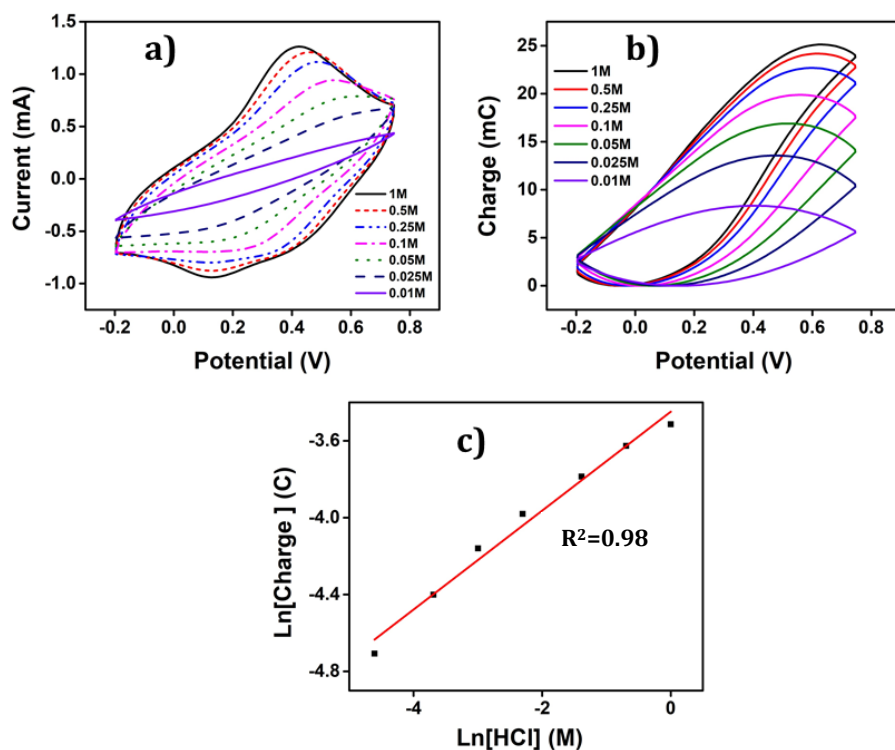


Figure 4.6 (a) CVs obtained in different concentrations of aqueous solution of HCl between -0.2 V and 0.75 V at a scan rate of 25 mVs^{-1} . (b) QV obtained by integrating the voltammograms obtained in (a). (c) logarithmic relation of the charge consumed during the redox reaction of PIN with the electrolyte concentration of aqueous HCl

working condition using consumed electrical charge as the sensing parameter.

Theoretical interpretation

The average rate of reaction presented in equation 4.9 can be rearranged as,

$$\frac{qv}{F\Delta E} = \frac{k}{m} [Cl^-]^\alpha [PINH_0]^\beta [H^+]^\gamma = \frac{k}{m} [Cl^-]^\alpha [H^+]^\gamma \left(\frac{q}{F}\right)^\beta \quad (4.19)$$

This gives a relationship between the consumed redox charge and the concentration variation of the polymer active center is obtained as equation 4.20 by rearranging equation 4.9. Further rearranging equation 4.19 we get,

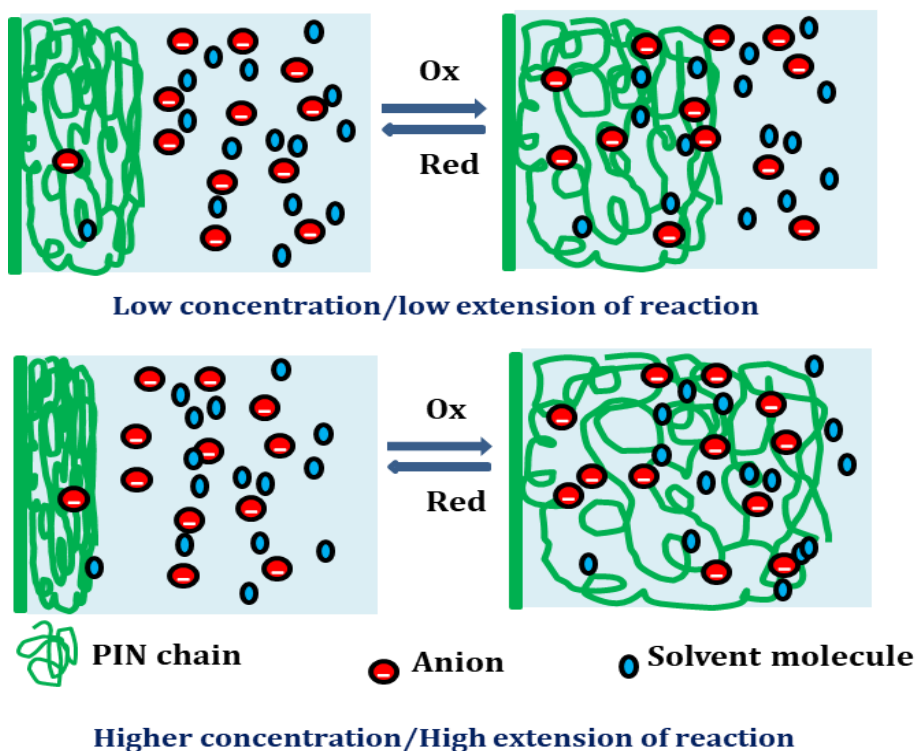


Figure 4.7 Schematic representation of extension of reaction at lower and higher concentrations of electrolyte

$$q^{1-\beta} = \frac{k\Delta EF^{1-\beta}}{\underbrace{\nu}_{k'}} [Cl^-]^\alpha [H^+]^\gamma \quad (4.20)$$

The constant terms in equation 4.20 are considered as a new constant, k' . The deprotonation process in each step of the reaction is the same. Therefore, $[H^+]^\gamma$ can be considered as constant and the logarithmic relation is obtained between the redox charge consumed during the reaction and the concentration of the electrolyte. Thus,

$$\ln(q) = a + b \ln[Cl^-] \quad (4.21)$$

where a is the intercept and b is the slope of the line. Equation 4.21 gives a linear relationship between the redox charge and the concentration of electrolyte. That is the material can act as a sensor of chemical surroundings. The experimental result (Fig. 4.5(c)) is fitted with the theoretical Equation (4.21).

$$a = \frac{\ln k' + \gamma \ln H^+}{1 - \beta} \quad (4.22)$$

$$b = \frac{\alpha}{1 - \beta} \quad (4.23)$$

The sensing characteristics arise due to the conformational movements of the PIN chain. That means PIN can act as a macromolecular sensing motor as the consumed electrical charge during the electrochemical reaction has a logarithmic dependence on electrolyte concentration.

4.2.2.3. Sensing thermal working condition-Temperature sensor

The temperature sensing ability of PIN was explored by recording stable voltammograms for different working temperatures (ranging

from 20 °C to 55 °C) at the scan rate 25 mVs⁻¹ in 1 M HCl. The results are shown in Figure 4.8(a) and it is observed from the figure that the anodic and cathodic peaks of the voltammogram increase with increasing temperature.

The consumed redox charge during the reaction was obtained from the QV at different temperatures and the results are presented in Figure 4.8(b). All QVs have a closed loop. The redox charge consumed during the reaction increases as the experimental temperature increases while all other experimental variables are constant.

The semi-logarithmic relationship between the consumed redox charge and the inverse of temperature is shown in Figure 4.8(c). The figure indicates that the PIN can sense the working temperature. The experimental result corroborates with the theoretical equation as suggested in equation 4.30.

A partial conformational relaxation occurs when the reaction takes place under the demand of low available thermal energy, i.e., when working at low temperature.

The extension of reaction is low at lower temperatures. When the temperature is low a small amount of volume is generated to lodge the counter anions and solvent molecules from the electrolyte into the polymer chain which consumes a lower oxidation charge. Therefore,

The polymer undergoes partial oxidation/reduction at lower temperatures. Faster and larger conformational relaxation occurs by

increasing the temperature because the available thermal energy is large, which creates/destroys a large amount of free volume to insert/ eject anions and solvent molecules leading to larger charge consumption during the reaction^[17].

As the temperature increases the reaction extension also increases while keeping all other experimental variables constant. As shown in Figure 4.9. at higher temperatures, the polymer experiences

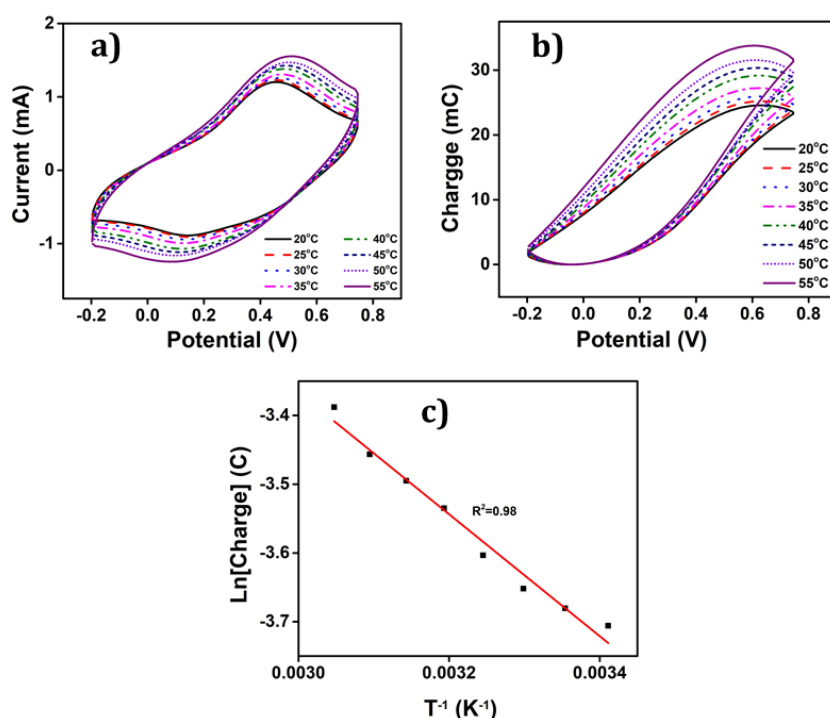


Figure 4.8 (a) CVs obtained from experimental temperatures in (20° C to 55° C) in 1 M HCl at 25 mVs⁻¹ between -0.2 to 0.75 V. (b) Corresponding QV obtained by integrating the CVs (a). (c) Semi-logarithmic relation of redox charge consumed during the reaction of PIN obtained from the QV with the inverse of temperature in Kelvin scale

deeper oxidation/reduction so that larger charges are consumed at higher temperatures.

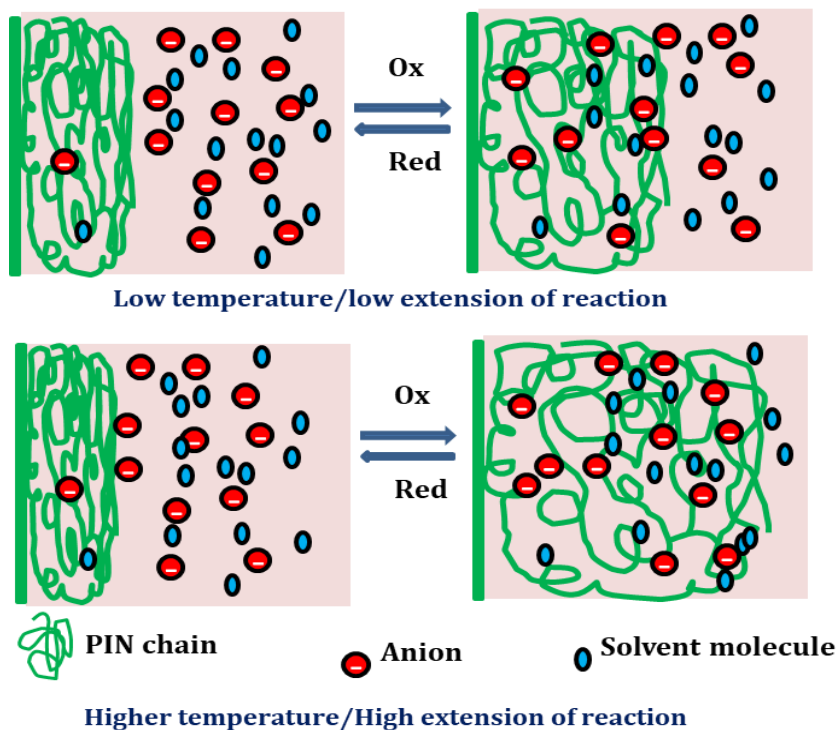


Figure 4.9 Schematic representation of the extension of reaction at lower and higher working temperatures

Theoretical interpretation

Our observation proves that reversible reaction 3.1 can sense the working thermal condition. The redox charge consumed during the reaction is the sensing parameter. The charge is quantified to prove the sensing principle of the PIN. The relation between the redox charge and the thermal working condition was derived by considering the empirical kinetics of PV oxidation.

The relation between the rate constant and working temperature was given by the Arrhenius equation,

$$k = Ae^{\frac{-E_a}{RT}} \quad (4.24)$$

where, A is the pre-exponential factor, E_a is the energy of activation, R is the universal gas constant ($\text{J mol}^{-1} \text{K}^{-1}$) and T is the absolute temperature (K). According to theoretical approach, each polymer chain of PIN having the same chain length, exchanges the same number of electrons with the electrolyte during the redox process. Therefore, the same number of polymeric gel active centers per chain is produced during the oxidation and the same positive charges are developed on each polymer chain. During the redox process, n electrons are exchanged through n consecutive steps by each polymer chain which involves one electron transfer per step. Consecutive n steps require first, second, third, etc. up to nth ionization potential to take out each electron during the reaction which implies the energy required to remove each electron from the chain is not the same. The total energy required for the n consecutive steps is given by the activation energy of the redox reaction.

Equation 4.10 shows the variation in concentration of the polymeric active center which can be considered in terms of the redox charge consumed during the process:

$$-\Delta[\text{PINH}_0] = \frac{Q}{mzF} = \frac{q}{zF} \quad (4.25)$$

where, Q is the charge consumed during the reaction, q is the charge per unit mass, and z is the counter anion valency/the valence of the polymeric active center (in this reaction Cl^- is the counter anion, so the valency is 1) and F is the Faraday constant. The specific concentration of the active center defines the specific rate of

reaction (a partial derivative of the concentration of the active center per unit time) as:

$$r = \frac{\partial[PINH_0]}{\partial t} = \frac{\partial(q)}{\partial t} = \frac{1}{F} \frac{\partial q}{\partial t} \quad (4.26)$$

The charge obtained from the QV response with respect to the time required to complete a potential window ($\Delta E/v$) gives the average specific rate of reaction as;

$$\bar{r} = \frac{\Delta[PINH_0]}{\Delta t} = \frac{q}{Ft} = \frac{qv}{F\Delta E} \quad (4.27)$$

In order to obtain the relation between the redox charge consumed per unit mass during the redox process and the working temperature, the equations (4.23), (4.24), (4.25), and (4.27) are rearranged to get

$$\frac{qv}{F\Delta E} = \frac{Ae^{\frac{E_a}{RT}}}{m} [Cl^-]^\alpha [PINH_0]^\beta [H^+]^\gamma = \frac{Ae^{\frac{E_a}{RT}}}{m} [Cl^-]^\alpha [H^+]^\gamma \left(\frac{q}{F}\right)^\beta \quad (4.28)$$

By modifying the equation (4.28) we get;

$$q^{1-\beta} = \frac{A\Delta EF^{1-\beta} [Cl^-]^\alpha [H^+]^\gamma}{\underbrace{vm}_{h'}} e^{\frac{E_a}{RT}} \quad (4.27)$$

A new constant ' h' ' is introduced to combine all the constants. A semi-logarithmic relation is obtained between specific redox charge and the inverse of working temperature.

$$(q) = a + b \frac{1}{T} \quad (4.30)$$

The intercept and the slope are given as:

$$a = \frac{\ln h'}{1 - \beta} \quad (4.31)$$

$$b = \frac{E_a}{(1 - \beta)R} \quad (4.32)$$

Equation 4.30 is considered as the sensing equation of PIN as the consumed charge is considered as the sensing parameter and therefore, PIN can function as a sensor of working temperature. The observed experimental results are fitted to the theoretical equation, as in Figure 4.8(c). The slope of Figure 4.8(c) shows the sensitivity of PIN towards the working temperature. The average reaction energy at various temperatures consumed during the reaction at constant electrical, chemical, and mechanical conditions was calculated from the consumed redox charge using the equation:

$$U = E \times Q \quad (4.33)$$

The reaction energy is higher for higher temperatures due to higher charge consumption. This implies that, the material reaction consumes lower energy at higher temperatures as muscle reaction consumes lower energy by increasing the temperature.

4.3. Conclusions

PIN was synthesized through in-situ chemical polymerization using FeCl_3 as an oxidant and was characterized electrochemically using cyclic voltammetry and chronopotentiometry in aqueous HCl solution of different concentrations, at different applied currents, and at different working temperatures for their application as sensors of electrical, chemical, and thermal working ambient respectively.

The working electrodes were fabricated using PIN powder on glassy carbon electrodes.

From chronopotentiometry, the consumed electrical energy during the reaction was calculated and proved to function as the sensing parameter. Electrical energy varies linearly with the applied electric current and working temperature. The consumed electrical energy had a semi-logarithmic dependence with the concentration of the electrolytes. The slope of the linear plot defines the sensitivity of the PIN. This experimental result was fitted with the theoretical equation. The consumed redox charge was obtained from QVs which varied as a logarithmic function of working electrical and chemical ambient and has a semi-logarithmic relation to the inverse of temperature.

According to the electrochemical reaction kinetics, the change in applied current (electrical working condition), the concentration of electrolyte (chemical working ambient) and working temperature (thermal working condition) disturb the rate of the electrochemical reaction that was sensed by the material potential evolution in terms of the consumed electrical energy and the redox charge as the sensing parameters. From the obtained result, it is concluded that the PIN can act as reactive sensors of working electrical, chemical, and thermal ambient. Biological muscles work according to instructions given by the brain. That instruction is transmitted via the signal neuron to the muscle sarcomeres and their conformational movement takes place. While working, these muscles sense their working condition and transmit that information to the brain via sensory neurons. Our results here proved that PIN is a material capable of mimicking this biological

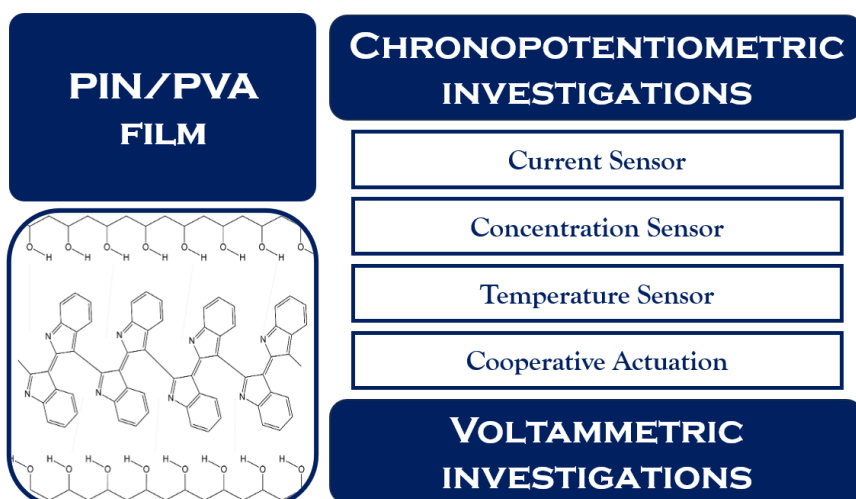
property. CPs that show this property, including PIN, have conformational movement according to instructions from the computer, sense the working condition, and report the information to the computer. For that, they use only two connecting wires like biological muscles.

Reference

- [1] T. F. Otero, M. Alfaro, V. Martinez, M. A. Perez, J. G. Martinez, *Adv. Funct. Mater.* **2013**, *23*, 3929-3940.
- [2] M. H. Doran, M. J. Rynkiewicz, D. Rasicci, S. M. Bodt, M. E. Barry, E. Bullitt, C. M. Yengo, J. R. Moore, W. Lehman, *J. Gen. Physiol.* **2023**, *155*, e202213267.
- [3] F. García-Córdova, L. Valero, Y. A. Ismail, T. F. Otero, *J. Mater. Chem. B* **2011**, *21*, 17265-17272.
- [4] T. F. Otero, *J. Mater. Chem. A* **2009**, *19*, 681-689.
- [5] aT. F. Otero, J. G. Martinez, *J. Mater. Chem. B* **2013**, *1*, 26-38; bT. Otero, J. Martinez, *J. Mater. Chem. B* **2016**, *4*, 2069-2085.
- [6] L. Rajan, A. Shabeeba, M. P. Sidheekhaa, Y. Ismail, *Chem. Asian J.* **2023**, e202300742.
- [7] aL. Rajan, M. P. Sidheekha, A. Shabeeba, Y. A. Ismail, *Mater. Chem. Front.* **2022**, *6*, 1706-1718; bM. P. Sidheekha, A. Shabeeba, L. Rajan, M. S. Thayyil, Y. A. Ismail, *Eng. sci.* **2023**, *23*, 890; cF. García-Córdova, L. Valero, Y. A. Ismail, T. F. Otero, *J. Mater. Chem.* **2011**, *21*, 17265-17272; dY. A. Ismail, J. G. Martinez, T. F. Otero, *J. Electroanal. Chem.* **2014**, *719*, 47-53.
- [8] aL. Valero, T. F. Otero, J. G. Martínez, *ChemPhysChem* **2014**, *15*, 293-301; bT. Otero, H. Grande, J. Rodriguez, *J. Electroanal. Chem.* **1995**, *394*, 211-216; cT. Otero, M. Broschart, *J. Appl. Electrochem.* **2006**, *36*, 205-214.
- [9] A. Shabeeba, Y. A. Ismail, *Mater. Res. Bull.* **2022**, *152*, 111817.
- [10] aY. A. Ismail, J. G. Martínez, T. F. Otero, *Electrochim. Acta* **2014**, *123*, 501-510; bA.-I. Bitá, G. Stan, M. Niculescu, I. Ciuca, E. Vasile, I. Antoniac, *J Adhes Sci Technol* **2016**, *30*, 1968-1983; cY. A. Ismail, F. Mohammad, A. Ahmad, *Journal of Macromolecular Science, Part A* **2011**, *48*, 952-961.
- [11] L. Rajan, A. Shabeeba, M. P. Sidheekhaa, Y. Ismail, *Chemistry–An Asian Journal* **2023**, e202300742.
- [12] M. P. Sidheekha, A. Shabeeba, L. Rajan, M. S. Thayyil, Y. A. Ismail, *Engineered Science* **2023**, *23*, 890.

- [13] A. Shabeeba, M. P. Sidheekha, L. Rajan, Y. A. Ismail, *RSC advances* **2022**, *12*, 31911-31922.
- [14] Y. A. Ismail, J. G. Martínez, A. S. Al Harrasi, S. J. Kim, T. F. Otero, *Sensors and Actuators B: Chemical* **2011**, *160*, 1180-1190.
- [15] T. F. Otero, H. Grande, J. Rodríguez, *Journal of Electroanalytical Chemistry* **1995**, *394*, 211-216.
- [16] T. F. Otero, S. Beaumont, *Sensors and Actuators B: Chemical* **2018**, *263*, 493-501.
- [17] T. F. Otero, S. Beaumont, *Electrochim. Acta* **2017**, *257*, 403-411.

Cooperative actuation of polyindole/polyvinyl alcohol hybrid film and their applicability as a free-standing electrode material for self-sensing working ambient



Based on the previous results on the electrochemical properties of PIN we have fabricated a freestanding electrode material using PIN. For the first time, an electroactive flexible polyindole/polyvinyl alcohol (PIN/PVA) hybrid film is fabricated which could function as a freestanding electrode material. Its biomimetic reactive sensing behavior was explored using chronopotentiometry and coullovoltammetry. For the first time we have explored the cooperative actuation of PIN using this hybrid film providing further insight into the reversible conformational movement of the PIN chain and their role in simultaneously sensing in their working ambient.

5.1. Introduction

The ability of PIN to sense the variations in working energetic conditions was explored in the previous chapter. To design a free-standing electrode for sensing the working electrical, chemical, and thermal variables, a mechanically robust material based on PIN capable of functioning effectively both in the wet and dry state is needed^[1]. It exhibits potential for fabricating devices and can function effectively both when dry and when immersed in solution. Poor processability, poor solubility, poor mechanical strength, and poor cyclic stability of PIN powder limit their practical application^[2]. One of Our main objectives is to fabricate a novel macromolecular motor based on CPs for biomimetic reactive sensing applications^[3]. To fulfil this objective, a flexible, mechanically stable free-standing material capable of imbibing electrolytes is essential^[4]. Hence, this chapter is dedicated to an exploration of the sensing abilities of an electroactive, free-standing hybrid material based on PIN. In order to fabricate this hybrid material, which possesses both conductivity, mechanical resilience, and biocompatibility, we used a polyvinyl alcohol (PVA) hydrogel film as a template to fabricate an electroactive PIN/PVA hybrid film^[5].

PVA stands as an insulating hydrogel with substantial mechanical strength even when immersed in moisture^[6]. This water-soluble synthetic organic polymer is derived from the hydrolysis of polyvinyl acetate, a process that boosts the PVA's degradability^[7]. It is a biocompatible and non-toxic thermoplastic, making it suitable for biological applications^[8]. The above-mentioned characteristics

of PVA make it adaptable for a diverse range of applications, encompassing areas like textile encasement^[9], 3D printing^[10], binder^[11], drug delivery^[12], anti-corrosion agent^[13], etc.

In order to fabricate the PIN/PVA hybrid film, an in situ chemical oxidative polymerization method was employed^[14]. The film's ability to sense the changes in its surroundings has been explored using chronopotentiometry and cyclic voltammetry^[15].

Here we have also introduced a new concept, cooperative actuation of the PIN/PVA films during the electrochemical reaction of the polymer^[16]. The polymer's oxidation/reduction reaction triggers a reversible change in the conformation of the polymer chain, leading to relaxation and compaction of the polymer chain as anions and solvent molecules exchange with the electrolyte^[17]. This reversible conformational movement is termed cooperative actuation, similar to how muscle sarcomeres respond to cerebral directives^[18]. However, unlike natural muscle sarcomeres, PIN/PVA film experiences an irreversible cooperative actuation^[19]. Therefore the PIN chain in the PIN/PVA film can be considered a macromolecular machine, in which a molecular-level reversible conformational movement occurs. The charge consumed during these structural changes/ cooperative actuation is influenced by external working energetic conditions. As such, variations in working conditions can be sensed by the film through the redox charge^[15b, 20].

Here, we are providing evidence to support our claim that PIN/PVA film has the potential to function as biomimetic, multi-step macromolecular sensors, capable of responding to various working

conditions. We have chosen PIN as our model material and its electrochemical reaction as the representative process to mimic the parallel biological processes observed in natural muscles. The findings from our research on PIN suggest the possibility of constructing new multifunctional devices comprised of several actuators and sensors working simultaneously driven by the same electrochemical reaction and requires only two connecting wires.

5.2. Results and discussion

The fabrication method of PIN/PVA film is discussed in Chapter 2.

The doubly coated PIN/PVA film is used for entire studies.

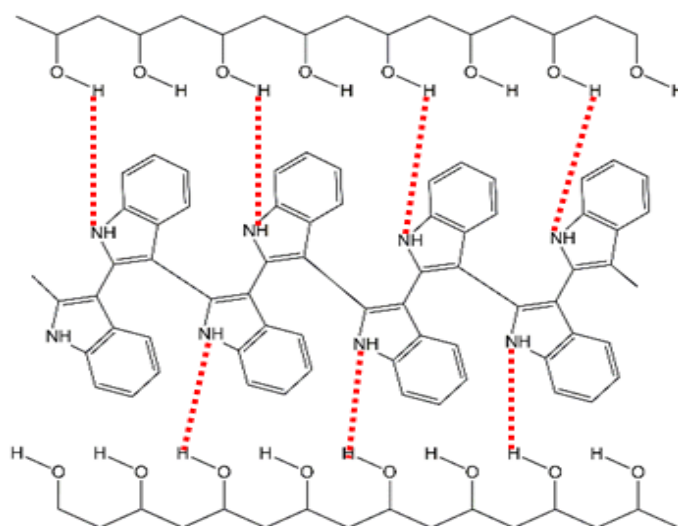


Figure 5.1 Schematic representation of H-bonding in PIN/PVA hybrid film

5.2.1. FTIR-ATR spectra

The reflective FTIR spectrum of the film was recorded using an FTIR spectrometer. Figure 5.2 shows the FTIR spectra of PIN/PVA hybrid film and bare PVA film. The characteristic peaks from the FTIR

spectrum confirmed the polymerization of Indole on PVA film^[1a, 5b]. The characteristic peaks at 730 cm^{-1} , 1552 cm^{-1} , and 3212 cm^{-1} correspond to out-of-plane deformation of the benzene ring, N-H deformation, and N-H stretching respectively^[21]. The OH stretching peak of the PVA was shifted from 3258 cm^{-1} to 3214 cm^{-1} due to the presence of a hydrogen bond between the NH and OH groups of the PIN and PVA respectively (Figure 5.1). The peaks appeared around 1611 , 1425 , 1210 , and 1110 cm^{-1} are due to the stretching of the aromatic ring. The NH vibration and the deformation of the benzene ring confirmed the polymerization took place at the 2 and 3 positions of the Indole monomer^[22].

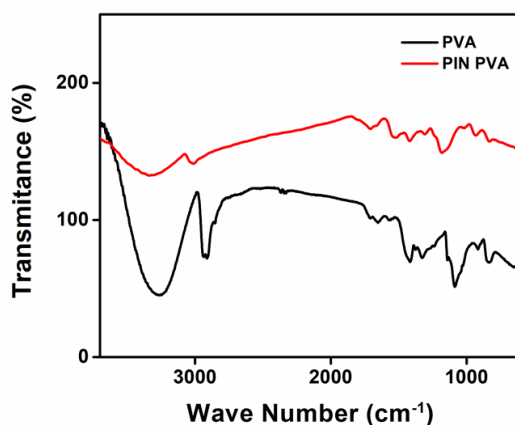


Figure 5.2 FTIR spectrum of PIN and PIN/PVA film

5.2.2. Thermogravimetric analysis

Thermograms of the films are presented in Figure 5.3. It can be seen from the figure that a three-step weight loss was observed in the PIN/PVA hybrid film, the first step represents the loss of water molecules. The second stage of weight loss corresponding to the removal of low molecular weight oligomers was observed between

190 °C to 305 °C. The polymer chain degradation occurs between the temperature ranges of 4400 °C to 575 °C^[23]. It can be seen from the figure that the bare PVA film undergoes two-step weight loss has occurred. The first step indicates the elimination of water from 70 °C to 135 °C. The second step between 235 °C to 518 °C indicates the polymer backbone degradation^[24]. The PIN/PVA film has an improved thermal stability.

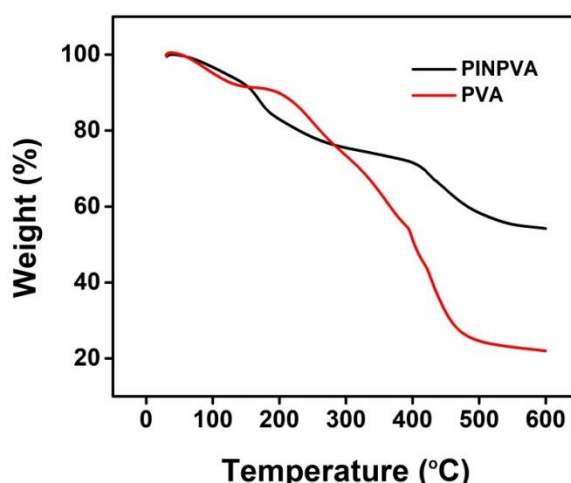


Figure 5.3 Thermograms of PVA and PIN/PVA films

5.2.3. FE-SEM and elemental analysis

FE-SEM images of the films are shown in Figure 5.4. An agglomerated globular structure with a nanometer dimension of the PIN grown on the bare PVA film is observed. The irregular arrangements of the particle show the amorphous nature of the polymer^[25]. From the figure, it can be observed that the hybrid film has sufficient porosity on the surface that encourages the intercalation of the ions along with the solvent molecule into the polymer matrix thus enhancing the electrochemical reaction during

cycling^[26]. Figures 5.4c and 5.4d show the elemental analysis data from the EDX analysis^[27]. The enhancement of the weight percentage of chloride ions from 0% to 2.18% in PIN/PVA film confirms the chloride doping during oxidative polymerization. The bare PVA contains 0% of chloride ion.

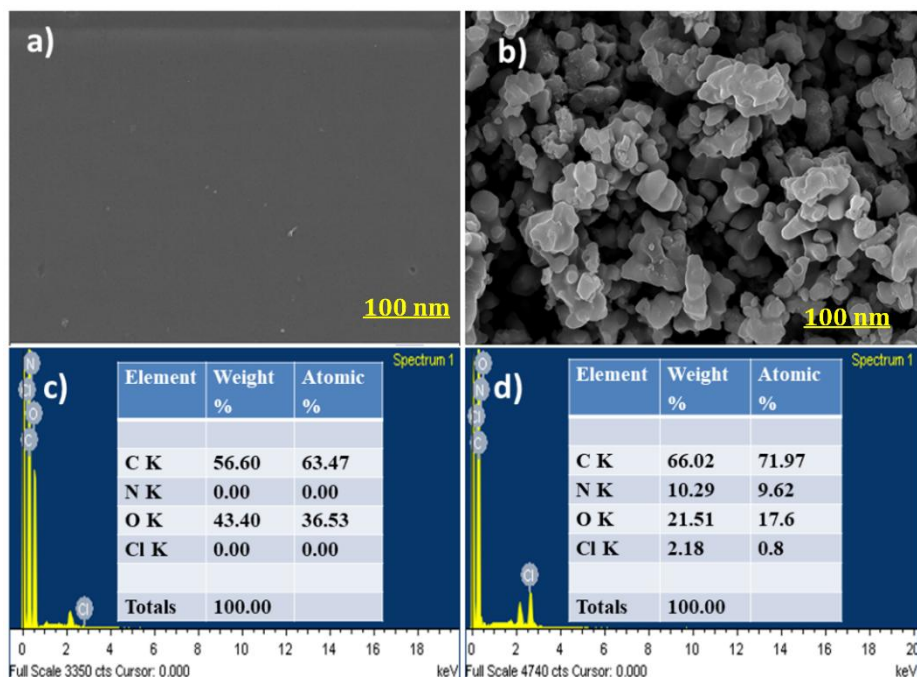


Figure 5.4 FE-SEM images of **a)** PVA film **b)** PIN/PVA film and EDX of **c)** PVA film **d)** PIN/PVA film

5.2.4. High-resolution transmission electron microscopy (HRTEM)

The high-resolution transmission electron microscopy (HRTEM) depiction of the PIN/PVA film, as presented in Figure 5.5, aligns with the granular attributes of the PIN observed in the FE-SEM image. The nano-structures and the granular characteristics of the PIN chains become evident in HR-TEM. The resultant morphology of the

PIN/PVA film is vital for electrode material as the ions from the electrolyte can easily diffuse through the active material to increase the active site responsible for the Faradaic reaction^[28].

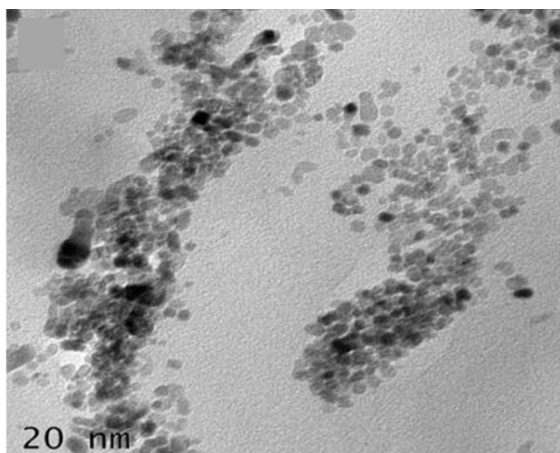


Figure 5.5 HRTEM image of PIN/PVA film

5.2.5. Mechanical characterization-UTM analysis

The mechanical properties of the bare and coated films were studied in dry and wet conditions using a universal testing machine. The Young's modulus, tensile strength, and percentage elongation were calculated by subjecting the samples to a stationary stretching force^[1a]. The mechanical properties of the films were studied from tensile stress-strain analysis. The value of Young's modulus, tensile strength and percentage elongation at break of bare PVA film and of PIN/PVA film in dry as well as wet states were compared and the results are presented in Figure 5.6 and Table. 5.1. It can be observed from the figure that the tensile strength and Young's modulus of the PIN/PVA film are much greater than bare PVA film in the dry state as well as in the wet condition of the films, which is attributed to the

strong hydrogen bonding interaction between PVA and the PIN^[2, 29]. This is consistent with our observation from the FTIR spectra.

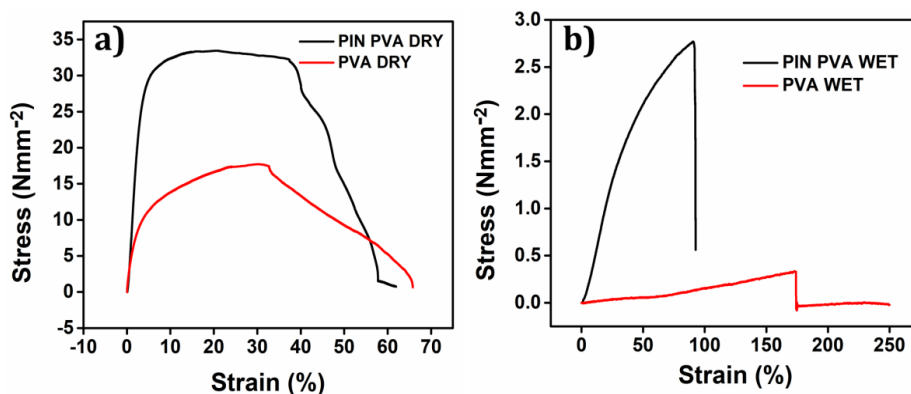


Figure 5.6 Stress-strain curve of the films **(a)** in the dry state. **(b)** In wet state

Table 5.1 The Mechanical properties of the bare PVA and PIN/PVA film in dry and wet state

Properties	Bare PVA film (dry state)	PIN/PVA hybrid film (dry state)	Bare PVA film (wet state)	PIN/PVA hybrid film (wet state)
Tensile strength(N/mm ²)	17.7154	33.4499	0.3353	2.7702
Young's modulus(N/mm ²)	0.5855	1.6065	0.00194	0.0306
% Elongation	30.2522	20.8216	172.844	90.5883

5.2.6. Electrical Conductivity

The electrical conductivities of the bare PVA and PIN/PVA hybrid films were measured using a four-point probe method at room temperature. The I-V plots are shown in Figure 5.7. The electrical conductivity(σ) was calculated from the I-V plot using the equation 2.3.

The calculated electrical conductivity of the PIN/PVA film is found to be $5.076 \times 10^{-5} \text{ S cm}^{-1}$. This electrical conductivity of PIN/PVA film is in the semi-conductor range, which is good enough for its electrochemical characterization^[14a].

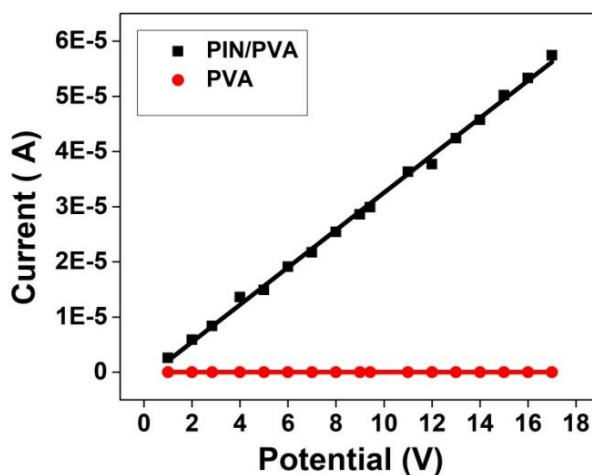


Figure 5.7 I-V characteristic of bare PVA film and PIN/PVA hybrid film

5.2.7. Electrochemical characterization

5.2.7.1. Cyclic voltammetry

The electrochemical characteristics of the PIN/PVA hybrid film were explored using voltammetric analysis. The CV of the film was recorded using a three-electrode cell setup at room temperature.

The PIN/PVA film-coated Pt wire was used as the working electrode, an Ag/AgCl electrode served as the reference electrode, and another Pt wire as the counter electrode. A stable CV was recorded by subjecting the film to multiple consecutive potential cycles and allowing the polymer reaction to reach a steady state as depicted in Figure 5.8. The potential was cycled from 0 V to 0.6 V in a 1 M HCl solution, employing a scan rate of 25 mVs⁻¹ at room temperature.

The CV of the PIN/PVA hybrid film shows two anodic and corresponding cathodic peaks in 1 M HCl^[25, 30]. The chemistry behind the generation of these couple of anodic and cathodic peaks is explained detail in Chapter 3. The schematic representation of the redox reaction of the PIN is shown in Figure 3.6^[31]. The positive charge and osmotic pressure developed during the oxidation were balanced by the intercalation of counter anions and solvent molecules from the electrolyte. A significant conformational movement has occurred during oxidation. The coiled, compacted structure of the polymer is converted to a planar, relaxed structure, which creates a large volume to accommodate the anions and solvent molecules. Therefore, the film swells during oxidation. The reverse process is found to occur during reduction, resulting in the shrinking of the film^[3b].

A stationary QV of the film was obtained by integrating the voltammetric response, and the resulting QV is shown in Figure 5.8(b). The difference between the QV maxima and minima (charge origin) gives the total redox charge consumed during the whole process^[32]. The consumed oxidation charge is indicated by the

positive charge increment (forward reaction in 3.1) and the negative charge increment indicates the reduction charge (backward reaction of reaction 3.1). The closed loop of the QV represents the total redox charge consumed during the process where the oxidation charge is equal to the reduction charge. A parallel irreversible reaction was also found to take place as a result of hydrogen evolution at the interface of film and Pt electrode; an irreversible charge was consumed during this reaction which was represented by the small open part left side to the closed loop^[3b].

The CV of the film recorded for different scan rates up to 200 mVs^{-1} and the results are shown in Figure 5.9(a). The anodic and cathodic peak current was plotted against the square root of the scan rate: the linear dependence confirms that the redox process occurring in the film is diffusion-controlled up to 200 mVs^{-1} . The redox process is more resistive at higher scan rates and the charge consumed during the entry/expulsion of the counter anion decreases by increasing the scan rates as can be observed in Figure 5.9(b). The redox reaction of the PIN/PVA film can be considered as taking place outside the

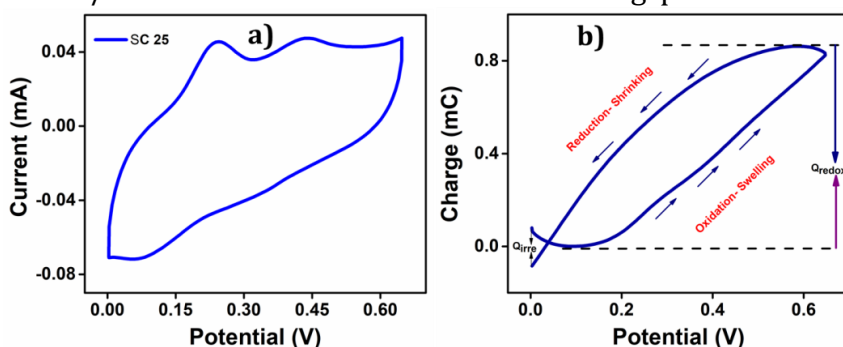


Figure 5.8 a) CV obtained from PIN/PVA film in 1 M HCl against Ag/AgCl electrode at the scan rate of 25 mVs^{-1} at room temperature. **b)** Corresponding QV

equilibrium because the electronic energy level of the polymer chain within the film is changing continuously along with the continuous variation of polymer composition with varying potential.

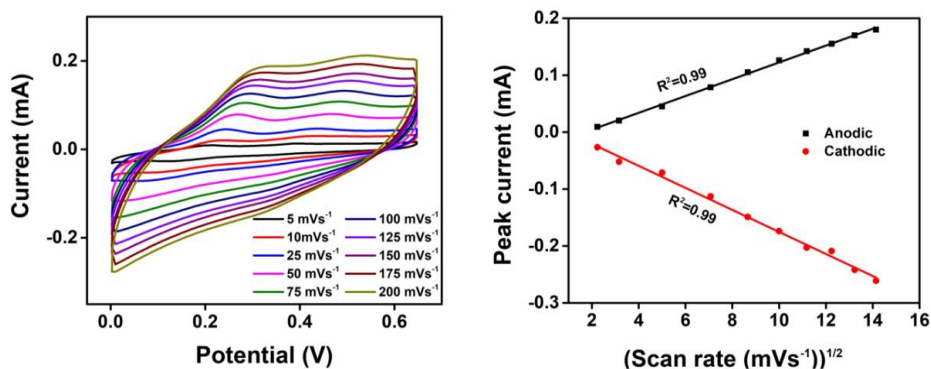


Figure 5.9 a) CVs obtained at different scan rates in 1 M HCl, at room temperature **b)** Relation of anodic and cathodic peak currents with the square root of scan rates

5.2.7.2. Reaction-driven sensing characteristics of PIN/PVA hybrid film: Chronopotentiometric study

The chronopotentiogram of PIN/PVA is generated by the continuous application of square current waves either anodic or cathodic to the film. Through this method, a continuous shift in the potential evolution from the film is occurred. This is due to the polymer reaction rate, equation 3.1, and the polymer composition could be influenced by the applied current and charge. Any change in the working ambient of the film influences the rate of polymer reaction and the film's potential evolution^[33].

5.2.7.2.1. Sensing electrical working conditions: Current Sensor

For current sensing, different anodic and cathodic currents ranging from ± 0.05 mA to ± 1 mA were applied to the PIN/PVA film at a

constant charge of 3 mC, by varying the time of current flow in 1 M HCl.

The anodic and cathodic responses are given in Figure 5.10(a) and Figure 5.10(b) respectively. It is observed from the figures that, the potential increases to a more positive value as the anodic current increases, and goes to a large negative value with the increase of the cathodic current. The consumption of electrical energy during the redox reaction is calculated using the equation, $U = I \int Edt$ ^[34]. The calculated electrical energy was plotted against the applied current

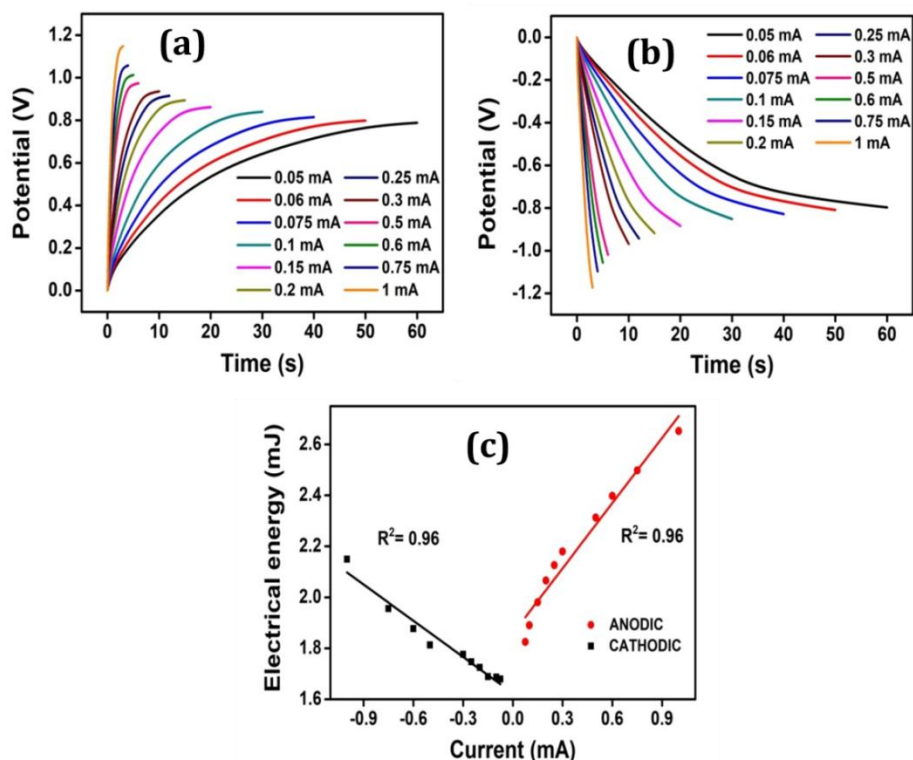


Figure 5.10 Chronopotentiograms obtained when different constant (a) anodic and (b) cathodic currents were applied to PIN/PVA hybrid film by passing a constant charge of 3mC in 1 M HCl solution (c) Electrical energy consumed by the film as a function of applied current (R^2 is the correlation factor)

and the results are shown in Figure 5.10(c). From Otero's principle, any physical or chemical variables (here electric current) disturbing the reaction rate of the CP reaction can be sensed by the material through the electrical energy consumed during the reaction [35]. The linear dependence of electrical energy with applied electric current confirms that the PIN/PVA film can sense the applied driving current during the redox reaction as electrical energy can act as the sensing parameter.

5.2.7.2.2. Sensing chemical working conditions- Concentration sensing

For concentration sensing, the CP responses were obtained by subjecting a constant current of 0.05 mA and -0.05 mA for anodic and cathodic processes respectively for 60 seconds in different electrolyte concentrations at room temperature. The results are shown in Figure 5.11. The rate of the reaction was increased by increasing the concentration while all other working variables were constant. At constant charge, the reaction is less resistive by increasing the concentration. This results lower potential evolution. From Figure 5.11(c), it can be seen that the consumed electrical energy during the reaction has a semi-logarithmic dependence on electrolyte concentration. Hence the PIN/PVA film is found to sense the chemical working condition. The slope of the calibration curve represents the sensitivity towards the chemical working ambient, which is -0.00106 and -0.00019 mJ M⁻¹ for anodic and cathodic processes, respectively.

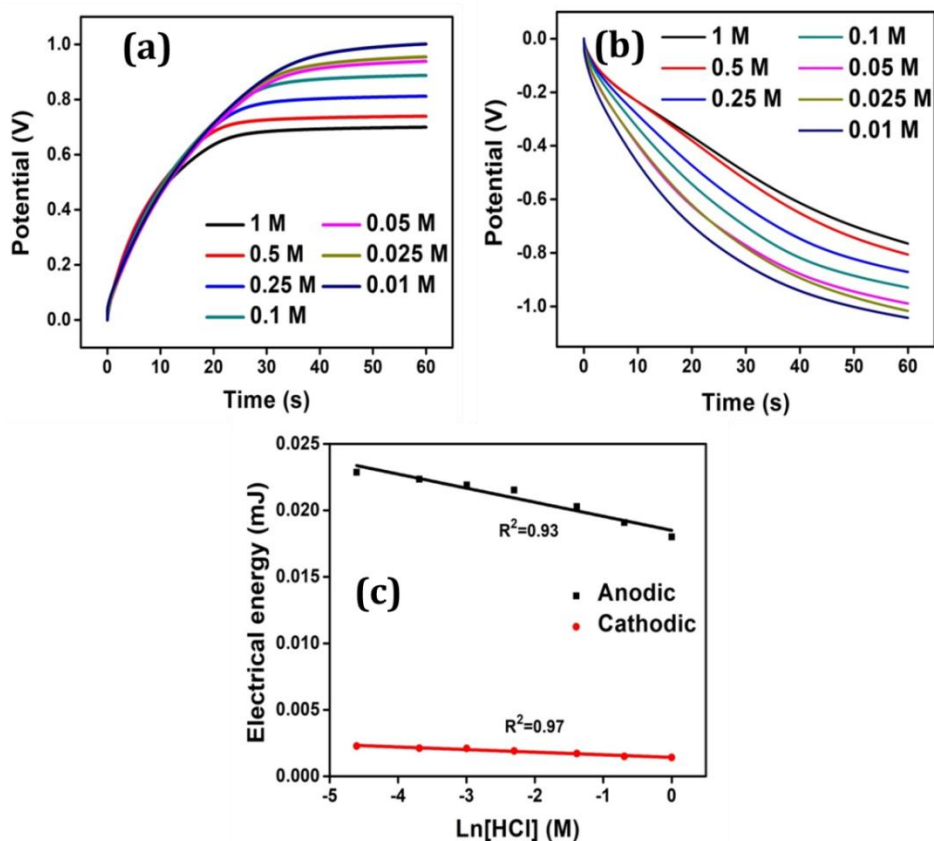


Figure 5.11 Chronopotentiogram obtained from different concentrations of HCl when (a) 0.05 mA and (b) -0.05 mA of current were applied to the PIN/PVA hybrid film for 60 s. (c) The electrical energy consumed by the film during the reaction is a semi-logarithmic function of electrolyte concentration at room temperature

5.2.7.2.3. Sensing thermal working condition-Temperature sensing

In order to check the sensing ability of the PIN/PVA film towards working temperature, a constant square current wave was applied to the material at a constant charge of 3 mC for different working temperatures. A constant chronopotentiogram was recorded after

20 consecutive potential cycles. The chronopotentiometric response of the third square current wave was recorded for different temperatures. The temperature sensing was studied by submitting +0.1 mA and -0.1 mA for anodic and cathodic processes respectively for 60 s in 1 M HCl. The process was repeated for different temperatures. The results are shown in Figure 5.12. According to the Arrhenius concept, the temperature will influence reaction 3.2: as the temperature increases the conformational movement of the

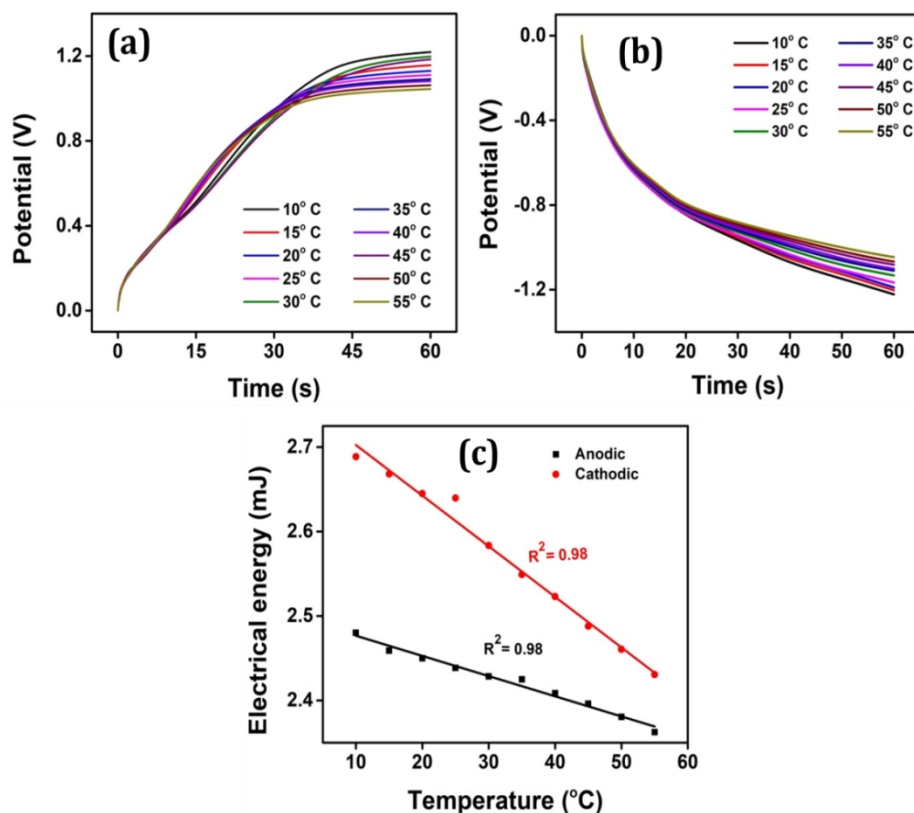


Figure 5.12 Chronopotentiogram obtained from different experimental temperatures when (a) +0.1 mA and (b) -0.1 mA of current were applied to the PIN/PVA hybrid film for 60 s. (c) The variation of electrical energy consumed during anodic and cathodic processes with temperature

polymer chain will be faster and the diffusion coefficient will be high. Reaction 3.2 occurs to the same extension by applying the constant charge, the reaction consumes lower energy by increasing the temperature. Therefore lower potential evolution is observed by increasing the temperature. It can be observed from Figure 5.12(a) that for the anodic process the potential evolution shifts towards lower values by increasing the temperature while for the cathodic process, the potential evolution shifts to a lower negative value by increasing the temperature as shown in Figure 5.12(b). Figure 5.12(c) shows the linear dependence of the electrical energy with the temperature which was fitted with the theoretical equation for the evolved potential outside the equilibrium as proposed by Otero et al.,^[36](Equation 4.8).

Equation 4.8 gives the general equation for the electrical energy consumed during the redox reaction. The linear relationship between the consumed electrical energy and the temperature confirms that the PIN/PVA film can respond to or sense the working temperature while keeping all other variables are constant.

In this study, the applied current follows a linear dependence with the electrical energy consumed during the reaction while keeping electrolyte concentration and the working temperature constant. Similarly, the log of electrolyte concentration follows a linear dependence on electrical energy consumed during the redox reaction while keeping the current and working temperature constant. The temperature also follows a linear relation with the electrical energy consumed during the reaction when the electrolyte

concentration and applied current are constant. The sensing signal can be visualized as transferring it to the computer like the neuron impulse from the haptic muscle of a cold-blooded animal. Therefore the PIN/PVA film can act as a biomimetic macro molecular motor to sense the working environment: electrical, chemical, and thermal conditions without any other additional connectivity.

5.2.7.3. Cooperative actuation induced working ambient sensing ability of PIN/PVA film: Voltammetric study

The macromolecular motor constituted by the PIN/PVA film generates/destroys free volume to accommodate/expel the counter anions from/to the electrolyte respectively during the cooperative actuation. This is similar to sarcomere working under the cooperative actuation (conformational relaxation) of the electro-chemo mechanical protein: actin-myosin of the biological muscles. The anions and solvent molecules penetrate the polymer matrix during oxidation and the reverse process occurs during reduction generating volume variation reversibly. The free volume generated by the conformational relaxation during the cooperative actuation can accommodate anions and solvent molecules from the electrolyte^[16]. The coiled compacted structure of the CP relaxes by uncoiling during the diffusion of the anions and solvent molecule from the solution: the conformation of the polymer is changed. The reverse process occurs during reduction: the compacted structure is reformed^[37]. At the reduction compaction stage, the polymer chains get pushed by the anions during the diffusion into the solution: volume variation is observed during the process. This

conformational relaxation-compactation during the redox process is known as cooperative actuation^[38]. The conformational movement or the structural change of the macromolecular machine (polymer active center) can be influenced by the electrical energetic condition of the polymer active center^[39]. The working ambient such as electrical, chemical and thermal working conditions can influence the cooperative actuation and the material can respond to or sense these working conditions. The charge/energy consumed during the reaction can be measured and they can act as the sensing parameters of the working ambient^[40].

The above process is similar to the mimicking of biological muscle characteristics. The conformational change (cooperative actuation) in the natural muscles takes place by the command of the brain^[41]. The electrochemical cooperative actuation of the protein-constituted sarcomere is the driving force of the working of muscles (actin-myosin)^[42]. Our material composed of PIN chains is a macromolecular machine that can mimic this biological property during their unique electrochemical reaction. The only difference between the biological muscles and our material system is that the cooperative actuation of the muscle induced by the electrical signals from the brain is an irreversible process whereas our system undergoes reversibly. Therefore the reactive sensing characteristics of PIN/PVA films can be explained through their cooperative actuations as detailed below.

5.2.7.3.1. Cooperative actuation of PIN/PVA film senses the electrical working condition

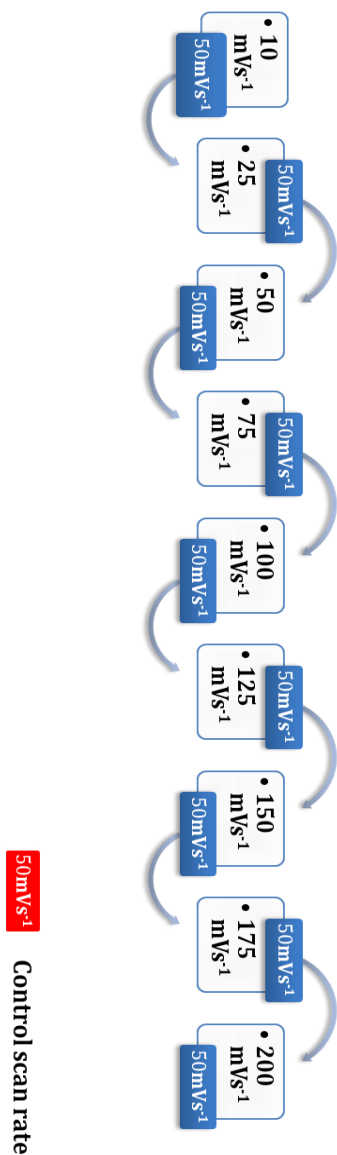


Figure 5.13 *Experimental procedure adopted for the study of cooperative actuation of PIN/PVA film at different electrical working conditions (scan rate)*

In order to study the influence of electrical working conditions on the electrochemical reaction of the polymer active center, the voltammetric responses at different scan rates were examined. The conformational movement i.e., cooperative actuation of the polymer chain during the electrochemical reaction by changing the scan rate was examined while keeping all other variables constant. The following consecutive steps were used to study the influence of scan rates on the conformational movement of the polymer chain [43].

After attaining a stable voltammetric response, the PIN/PVA film was submitted to three consecutive potential sweeps between 0 V to 0.6 V at the scan rate of 10 mVs^{-1} in 1 M HCl at room temperature. Then submitted to another three consecutive cycles within the same

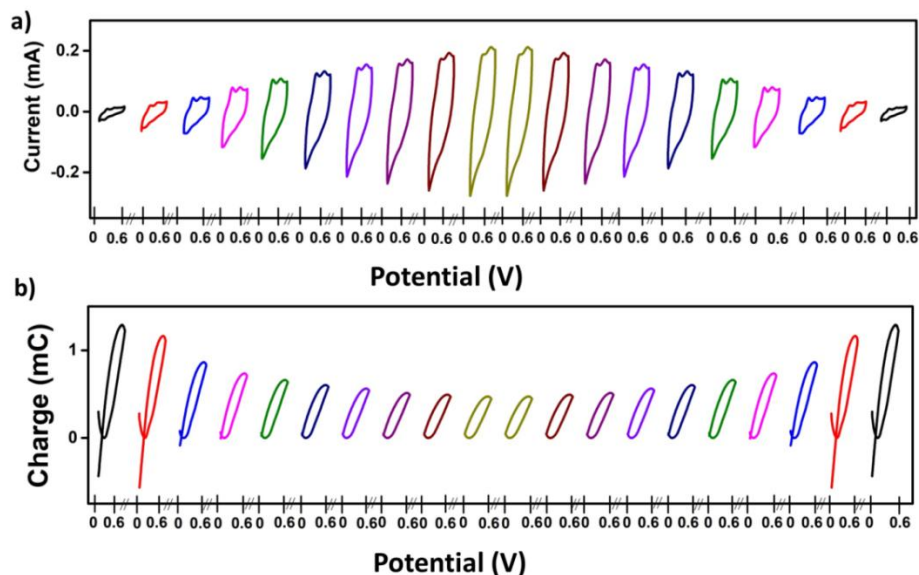


Figure 5.14 (a) CVs obtained from different experimental scan rates in increasing (5 mVs^{-1} to 200 mVs^{-1}) and decreasing (200 mVs^{-1} to 5 mVs^{-1}) scan rate direction between 0 V to 0.6 V in 1 M HCl at room temperature. (b) Corresponding QVs

potential sweep at a control scan rate of 50 mVs^{-1} to get a stable voltammetric response. The whole experiment was repeated for different scan rates, first for increasing and then for decreasing order, that is from 10 mVs^{-1} to 200 mVs^{-1} then from 200 mVs^{-1} to 10 mVs^{-1} (10, 25, 50, 75, 100, 125, 150, 175, 200, 200, 175, 150, 125, 100, 75, 50, 25, and 10) as shown in Figure 5.13. In between two consecutive switching, the material is submitted to the control scan rate, and the voltammetric responses are recorded.

Figure 5.14(a) shows the stable voltammetric response from the PIN/PVA film for experimental scan rates. The anodic and cathodic currents were found to increase with the increase of scan rates. The corresponding stationary coulouvoltammograms obtained from each studied scan rate are shown in 5.14(b). From the figure, it is clear

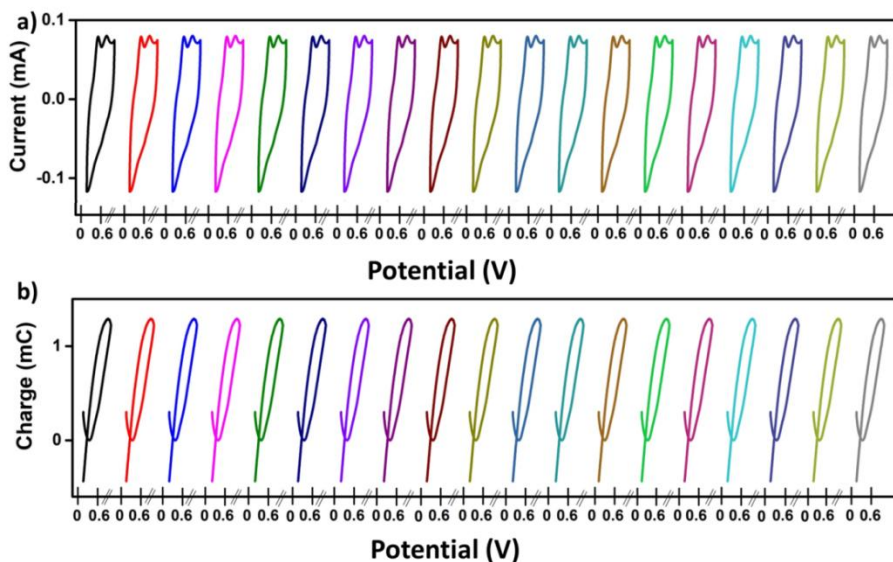


Figure 5.15 a) CVs obtained in a control scan rate (50 mVs^{-1}) in 1 M HCl between 0 and 0.6 V at room temperature. **b)** Corresponding QVs

that the redox charge consumed during the reaction decreases with an increase in scan rates. The closed loop of the QV for every scan rate shows that the oxidation and reduction charges are equal. The electroactivity of the film remains unchanged, which was observed from the 'control' voltammetric response recorded in between two consecutive scan rates at a scan rate of 50 mVs^{-1} . The results are shown in Figure 5.15(a).

The stationary coul voltammetric responses were obtained from the 'control' CVs as shown in Figure 5.15(b). The overlapping QV responses confirm that the same charge is consumed for each control scan rate. Thus the experimental results confirm that the conformational movements of the macromolecular motors of PIN/PVA film are reversible, i.e., the cooperative actuation of the film is reversible. The logarithmic relation (straight line) between the consumed redox charge and the scan rate indicates that the PIN/PVA film can sense the scan rate as a function of the

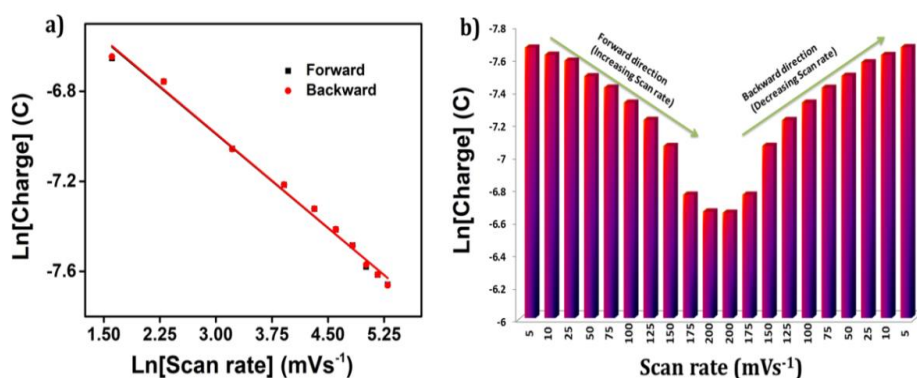


Figure 5.16 (a) Logarithmic relation of redox charge consumed during the reaction of PIN/PVA film by increasing (forward) and decreasing (backward) the scan rates. **(b)** Bar diagram of corresponding consumed redox charge during the process

consumed redox charge shown in Figure 5.16(a) and the consumed redox charge variation during forward and backward process also shown as a bar diagram in Figure 5.15(b).

The experimental result in Figure 5.16a was aligned with the theoretical equation (Equation 4.16). The sensitivity of the film towards electrical working conditions is indicated by the slope, on the curve. At lower scan rates, a larger conformational change in the polymer chain is observed. This is due to the extended time required for the oxidation/reduction of the polymer chain. This results in the generation/removal of a substantial volume within the film to accommodate/expel the counter anions and solvent molecules

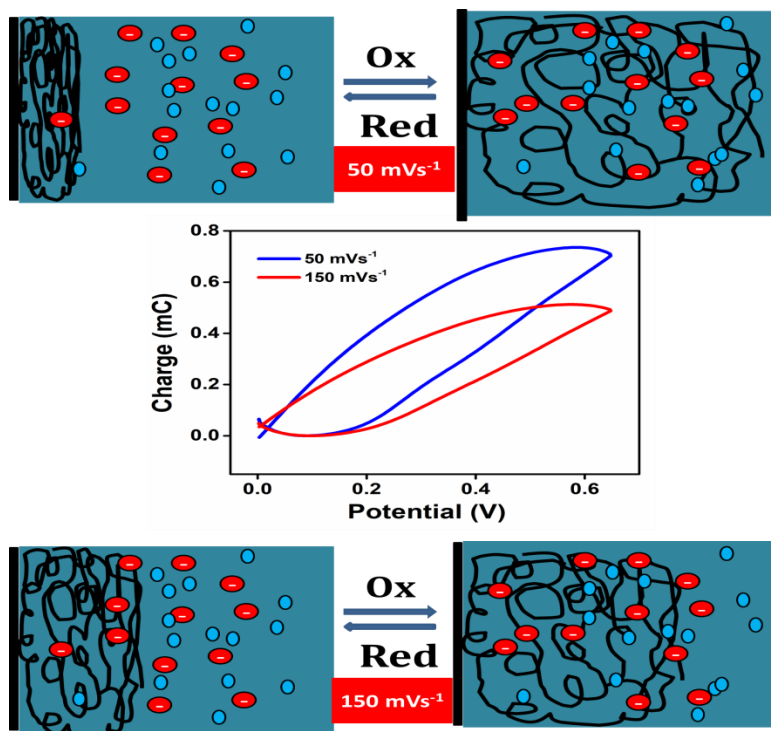


Figure 5.17 Schematic representation of the reaction extension based on cooperative actuation of the PIN/PVA hybrid film and corresponding QVs

respectively. Thus the charge consumed during the reaction is higher for lower scan rates^[43].

These findings suggest that the conformational changes prompted by the polymer reactions machine result in shorter displacements (reduced reaction extension/less redox charge utilization) in comparison to the faster muscular motions (higher scan rate) as depicted in Figure 5.17. The illustration indicates that for 150 mVs⁻¹, the reaction extension/charge consumption was lower, while for 50 mVs⁻¹, it was higher. In the case of muscles, signals are transmitted to the brain via sensory neurons, and the conformational shifts occur through the guidance of brain instructions conveyed by the same connecting neurons ^[44].

5.2.7.3.2. Cooperative actuation of PIN/PVA film senses chemical working condition

In order to further verify the sensing capability of PIN with respect to chemical working conditions the co-operative actuation characteristics of PIN/PVA film obtained through controlled voltammetric responses driven by the electrolyte concentration was studied^[17a]. For this purpose, the PIN/PVA film was placed in a cell containing the electrolyte after attaining a stable stationary voltammetric response. After subjecting the PIN/PVA film to several consecutive potential sweeps to attain a stable voltammetric response the electrode was transferred again, to the control solution (0.1 M HCl), and cycled again to attain a stable voltammetric response. The whole process was repeated for different electrolyte concentrations first from lower to higher concentration and then

higher to lower concentration. That is, from 0.01 M to 1 M and then from 1 M to 0.01 M (0.01, 0.025, 0.05, 0.1, 0.25, 0.5, 1, 1, 0.5, 0.25, 0.1, 0.05, 0.025, and 0.01).

The resulting voltammetric responses are shown in Figure 5.18(a). It can be seen that the anodic and cathodic peak currents increase with increasing concentrations, and then decrease with decreasing the electrolyte concentration. Figure 5.19(a) shows the voltammetric responses of PIN/PVA film in the control solution (0.1 M HCl), recorded in between two consecutive electrolyte concentrations. The results confirm that the PIN/PVA film has maintained its electroactivity throughout the experiment.

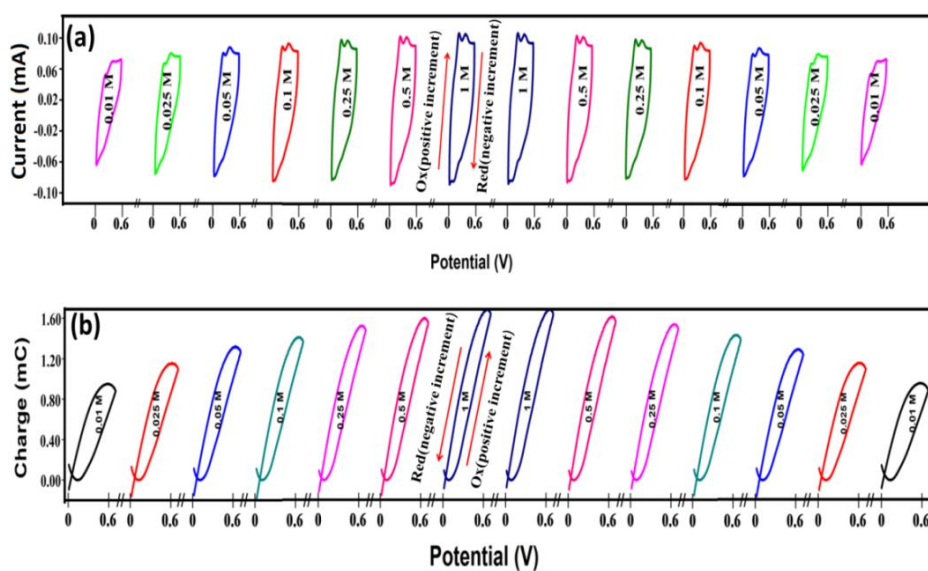


Figure 5.18 (a) CVs obtained in different concentrations of aqueous solution of HCl for increasing and decreasing the concentration at a scan rate of 25 mVs^{-1} . **(b)** Corresponding QVs

The corresponding QV responses are shown in Fig. 5.18(b). Always the QV minima is considered as the charge origin. The reversible

charge consumed during the reaction is a function of the electrolyte concentration. The QV loop contains the anodic and cathodic parts. As discussed earlier, the redox reaction of the polymer results the conformational movement of the film due to the entry and expulsion of the counter anions and solvent molecules to and from the electrolyte for the charge compensation and osmotic pressure balance^[39].

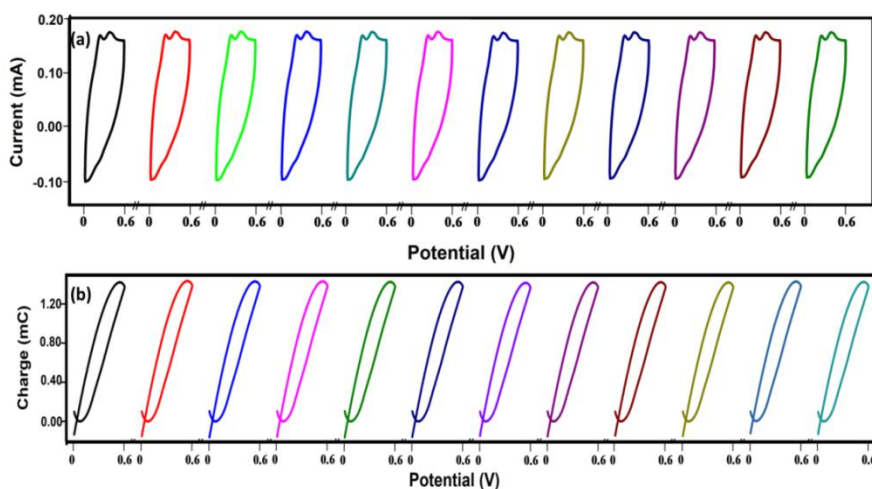


Figure 5.19 (a) CVs obtained from the control solution of HCl (0.1 M) between 0 V and 0.6 V at a scan rate of 25 mVs^{-1} . (b) corresponding QVs

The QV obtained from the voltammogram of the control solution is shown in Figure 5.19(b), which indicates that the electroactivity of the film was stable. The charge consumed by the reversible reaction increases with an increase in the electrolyte concentration and vice versa as evidenced from Figure 5.21.

The polymer chain was partially oxidized in the same potential window as the available chemical energy was low at lower

concentrations. The conformational movement of the polymer chain was driven by the variation in chemical energy (change in electrolyte concentration), which can drive the generation of free volume to bring the counterion and the solvent molecules from the electrolyte (Figure 5.20)^[45]. At lower concentrations, the amount of free volume is low; the number of counter ions and the solvent molecules entering/leaving the polymer chain is also less while keeping other variables constant. The amount of free volume increases by increasing the concentration, and hence the amount of counter ion and solvent molecules that entered into the film also increases as concentration increases^[44]. The charge consumption during this reversible process changes proportionally with the concentration of the electrolyte (Figure 5.21), which corroborates equation 4.21.

At the same temperature (thermal), pressure (mechanical), potential sweep, and scan rate (electrical energetic condition), the reversible charge increases with a rise in the concentration of the electrolyte, which results in an extreme oxidation/reduction state of the film associated with the rising of free volume, redox charge and the counter ions which exchanged during the redox process. This directs the conformational movements and structural changes (swelling or de-swelling) of the reacting polymeric gel: the cooperative actuation^[46]. These physical and chemical changes are the functions of chemical energy so that the charge becomes the sensing parameter of the changing variables. Thus, the reacting polymer gel can mimic the biological functions driven by these chemical

reactions involving conformational and structural changes and can sense the working conditions similar to biological muscles^[47].

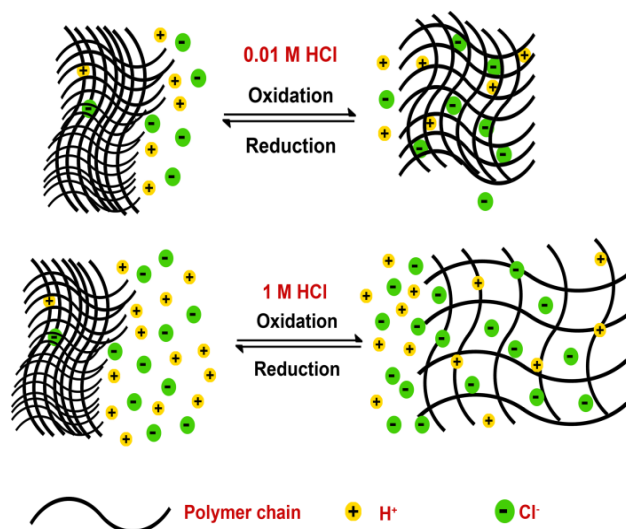


Figure 5.20 A schematic representation of the extension of reaction of PIN/PVA hybrid film in 0.01 M HCl and 1 M HCl

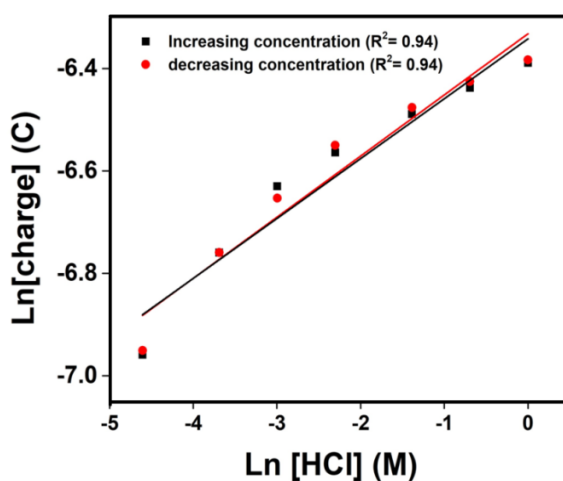


Figure 5.21 Logarithmic relation of the charge consumed during the redox reaction of PIN/PVA hybrid film with the electrolyte concentration of aqueous HCl

We argue that these types of materials can sense the available chemical energy as a function of charge which can be regarded as the sensing parameter. This is the fundamental theory of sensing motors; the reacting polymer gel material that can sense working variables simultaneously while actuating through the conformational and structural changes induced by a change in concentration. Thus PIN/PVA films can function as sensing motors.

5.2.7.3.3. Cooperative actuation of PIN/PVA film senses the thermal working condition

The available thermal energy is low at lower temperatures. Therefore, smaller conformational movement occurs at lower temperatures. Therefore, the lower amount of counter anions and solvent molecules penetrate the polymer matrix which consumes a low amount of oxidation charge. The large conformational movement of the chain due to the rising temperature leads to the creation of free volume. Therefore, a large amount of counter anions and solvent molecules are interchanged between the electrolytes that consume a higher reaction charge. The large conformational movement and relaxation of the chain by varying the temperature at constant electrical, chemical, and mechanical conditions can influence the electrical charge consumed during the reaction.

The reaction 3.2 shifts to the maximum oxidation/reduction state as temperature increases. Hence the number of solvent molecules and the counter anions lodged to the free volume increases which leads to large conformational movement of the polymer chain. Therefore, the extension of reaction is large at higher temperatures^[17b]. The

consumed charge changes as a function of available thermal energy. Therefore, the reaction charge can be considered as the sensing parameter of the thermal working condition.

The temperature-influenced cooperative actuation of the PIN/PVA film was studied using a voltammetric response. For this study, the stable voltammetric response was recorded by submitting consecutive 30 potential cycles at a scan rate of 25 mVs^{-1} in an aqueous 1 M HCl solution at room temperature. Then the cell temperature was changed to a 'control' temperature of $30 \text{ }^\circ\text{C}$ and cycled again to attain a stable voltammetric response. The whole process was repeated for different working temperatures first from lower to higher temperatures and then higher to lower

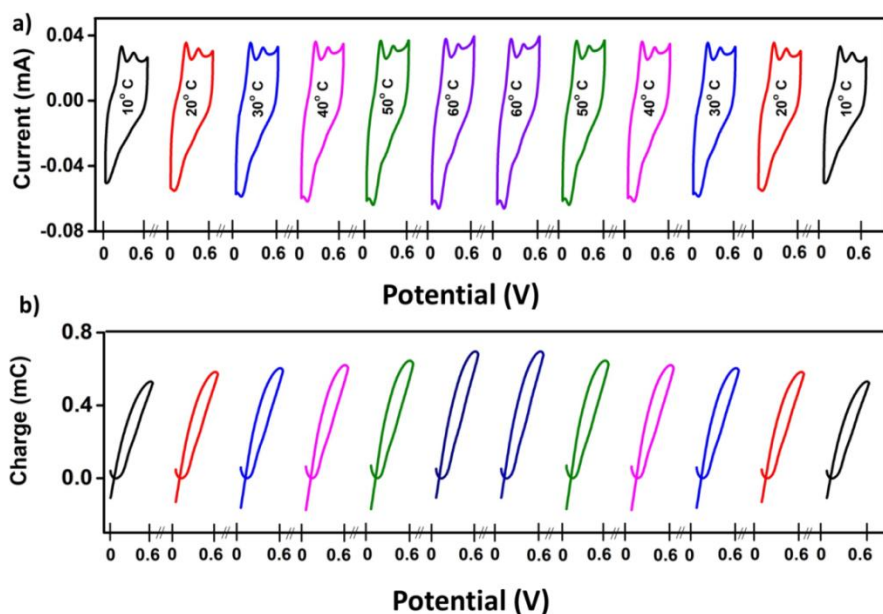


Figure 5.22 (a) CVs obtained from increasing ($10 \text{ }^\circ\text{C}$ to $60 \text{ }^\circ\text{C}$) and decreasing ($60 \text{ }^\circ\text{C}$ to $10 \text{ }^\circ\text{C}$) the temperature in 1 M HCl at 25 mVs^{-1}
(b) Corresponding QVs

temperatures, i.e., from 10 °C to 60 °C and then from 60 °C to 10 °C with an increment of 10 °C.

The resulting voltammetric response is shown in Figure 5.22(a). It can be seen from the figure that the anodic and cathodic peak currents increase with increasing temperature and decrease with decreasing temperature. The corresponding QVs are shown in Figure 5.22(b). The redox charge consumed during the reaction is calculated from corresponding QVs.

From Figure 5.22(b), it is clear that the reversible redox charge consumed by the film increases with increasing working temperatures. The redox charge decreases with decreasing temperature. The semi-logarithmic dependence of consumed redox charge with the inverse of temperature confirms that the PIN/PVA film can sense the working temperature. The consumed redox charge is the sensing parameter (Figure 5.23(a)). The theoretical equation 4.30 corroborates the experimental result obtained in Figure 5.23(a).

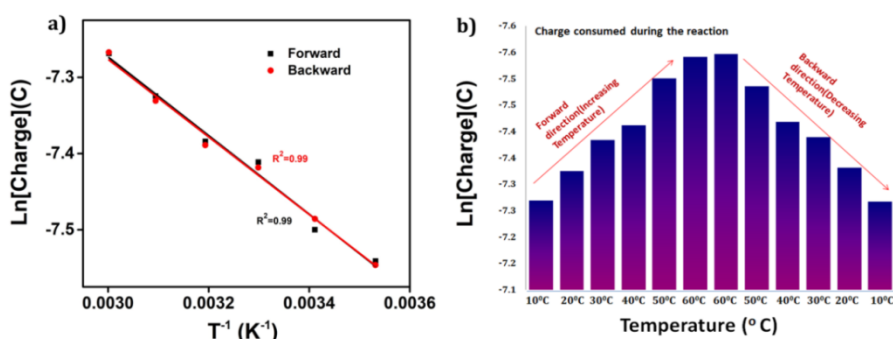


Figure 5.23 (a) Semi logarithmic relation of redox charge consumed during the reaction of PIN/PVA hybrid film by increasing (forward) and decreasing (backward) the temperature **(b)** Bar diagram of redox charge consumed during the reaction

Figure 5.24 shows a schematic representation of the conformational movement of the polymer chain by varying the temperature. Experimentally, we have proved that a large structural relaxation has occurred as increasing the temperature. Therefore a large number of ions and solvent molecules can enter the polymer matrix. This results higher charge consumption by increasing the temperature, i.e., the extension of reaction is large for higher temperatures.

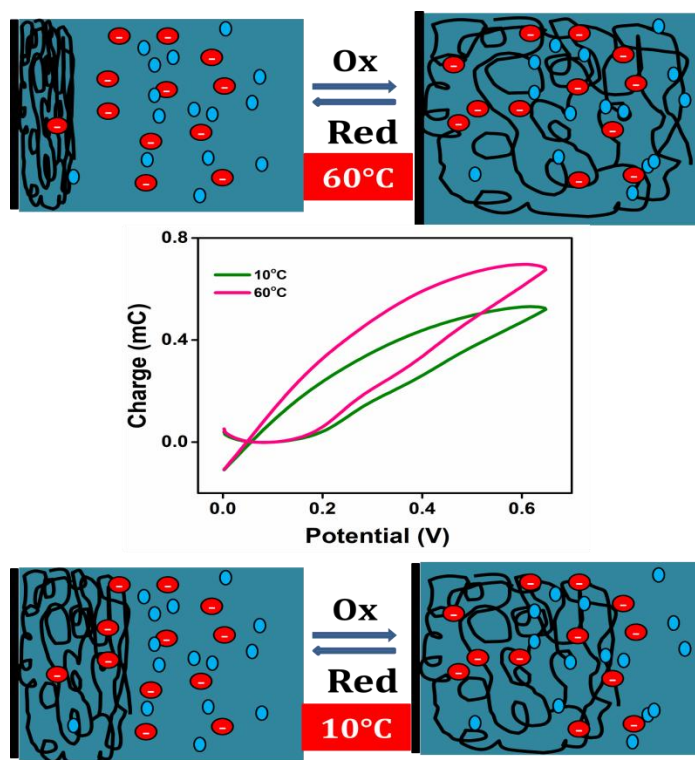


Figure 5.24 Schematic representation of the extension of reaction of the PIN/PVA film at 60 °C and 10 °C and corresponding QV responses

The CVs obtained from the control temperature are shown in Figure 5.25(a). The corresponding QV responses are shown in Figure 5.25(b). It can be observed from the figure that the electro-activity

of the film remains constant during the whole experiment. There is no major structural change or chemical memory effect to influence the electro-activity of the film. The result proves that the extension of reaction is the same for the same temperature irrespective of the direction of the experiment, i.e., the conformational movement of the polymer chain is reversible during the polymer reaction.

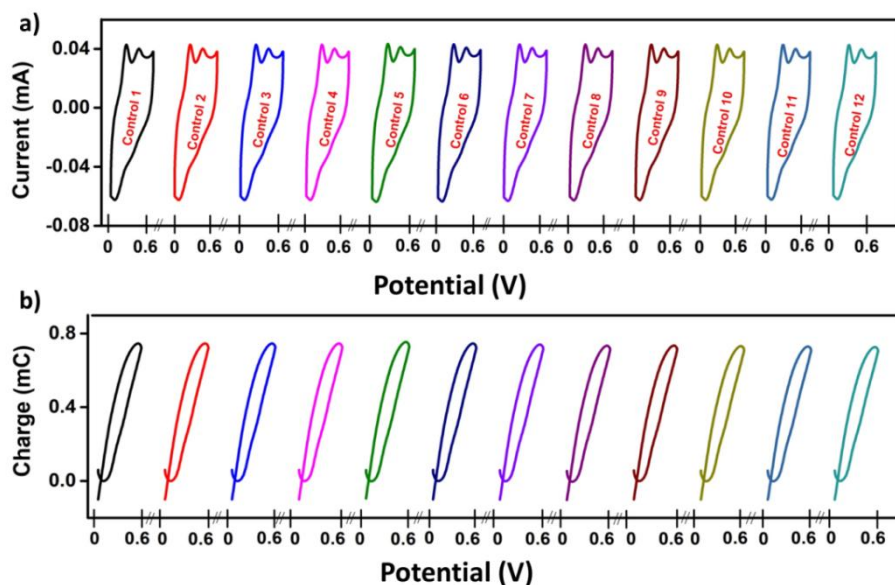


Figure 5.25 (a) CV obtained in a control temperature ($30\text{ }^{\circ}\text{C}$) in 1 M HCl at 25 mVs^{-1} . (b) Corresponding QV responses

5.3. Conclusion

A flexible film hybrid PIN/PVA was fabricated by in situ polymerization with indole using PVA film as a template. The PIN on the film imparted the electro activity, allowing it to function as a sensing motor. The film was thoroughly characterized using CV, QV and chronopotentiometry in HCl solutions to study its electrochemical properties with a special emphasis on its

biomimetic sensing characteristics. The extension of reaction was identified from the charge consumed during the reaction which was calculated from the QV.

Based on the chronopotentiometric responses, it was concluded that the electrical energy consumed during the redox reaction could sense changes in the applied current, electrolyte concentration, and working temperature. The electrical energy has a linear relationship with the applied current and temperature, while it exhibits a semi-logarithmic relationship with the electrolyte concentration. When the electrochemical redox reaction occurred at a constant reaction rate, the experimental results for the PIN/PVA hybrid film are well aligned with the theoretical equation. Thus, these results confirm that the PIN/PVA film can sense the reactive energetic working condition as biological muscles do. The electrochemical reaction of the PIN/PVA film results the formation of a dense gel constituted by the macromolecular polymer chain, ions and water. This dense gel is similar to those components of the muscle cells. Thus we proved that the PIN/PVA film can mimic the biological functions of these muscle cells.

The cooperative actuation of the PIN/PVA film during the reaction and the influence of the working energetic conditions on this cooperative actuation was also explored. The QV is employed to assess the extension/charge consumption during the film's conformational movements. The logarithmic relationship of the consumed charge with the scan rate and the electrolyte concentration and the semi-logarithmic relationship with the

inverse of temperature confirm that the film can act as a sensor of its working energetic conditions. This corroborates the theoretical equations. The consumed charge is the sensing parameter. This cooperative actuation of PIN/PVA film is similar to the muscle sarcomere actuation while changing the environmental variables.

The biological muscles sense their working energetic conditions while working by the command of the brain. The commanding signals are transferred to the muscles through the neurons as electric signals. The feedback-sensing signals from the muscles will transfer to the brain through the sensory neurons. These two connecting neurons are required for this brain-muscle communication. Similarly for PIN/PVA film, only two connecting wires are required for this communication. The results proved that the PIN/PVA film can act as macromolecular sensing motors while working without any additional connectivities similar to the biological muscles sensing their surrounding environment while working. These results on PIN/PVA film further support our argument that the reactive sensing characteristics are a general property of all CPs.

References

- [1] aM. Ramesan, T. Anjitha, K. Parvathi, T. Anilkumar, G. Mathew, *Adv. Polym. Tech.* **2018**, *37*, 3639-3649; bP. Jayakrishnan, M. Ramesan, *Journal of Inorganic and Organometallic Polymers and Materials* **2017**, *27*, 323-333.
- [2] A. Sebastian, R. Gopika, R. Anju, M. Verma, M. Ramesan, *Phys. Scr.* **2023**, *98*, 065911.
- [3] aA. Shabeeba, L. Rajan, M. P. Sidheekha, M. S. Thayyil, Y. A. Ismail, *Journal of Energy Storage* **2022**, *55*, 105724; bL. Rajan, M. P. Sidheekha, A. Shabeeba, Y. A. Ismail, *Materials Chemistry Frontiers* **2022**, *6*, 1706-1718.

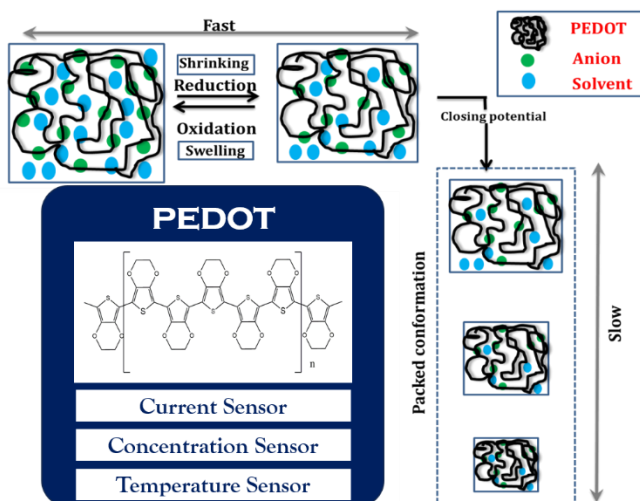
-
- [4] aM. P. Sidheekha, A. Shabeeba, L. Rajan, M. S. Thayyil, Y. A. Ismail, *Engineered Science* **2023**, *23*, 890; bR. B. Choudhary, S. Ansari, B. Purty, *Journal of Energy Storage* **2020**, *29*, 101302.
- [5] aE. Dhandapani, R. Vasudevan, R. Ramesh, N. Duraisamy, *Surfaces and Interfaces* **2023**, 103194; bG. Dhokane, D. Bhagat, *RESEARCH JOURNEY* **2019**, 109.
- [6] aL. W. Chan, J. S. Hao, P. W. S. Heng, *Chem. Pharm. Bull.* **1999**, *47*, 1412-1416; bK. Chan, H. Senin, I. Naimah, in *AIP Conference Proceedings, Vol. 1136*, American Institute of Physics, **2009**, pp. 366-369.
- [7] aH. Abral, A. Atmajaya, M. Mahardika, F. Hafizulhaq, D. Handayani, S. Sapuan, R. Ilyas, *Journal of Materials Research and Technology* **2020**, *9*, 2477-2486; bN. Jain, V. K. Singh, S. Chauhan, *Journal of the Mechanical Behavior of Materials* **2017**, *26*, 213-222; cZ. Guohua, L. Ya, F. Cuilan, Z. Min, Z. Caiqiong, C. Zongdao, *Polym. Degrad. Stab.* **2006**, *91*, 703-711.
- [8] aM. Liong, H. Shao, J. B. Haun, H. Lee, R. Weissleder, *Advanced materials* **2010**, *22*, 5168-5172; bS. M. Mahdi, M. A. Habeeb, *Polym. Bull.* **2023**, 1-20; cM. I. Baker, S. P. Walsh, Z. Schwartz, B. D. Boyan, *Journal of Biomedical Materials Research Part B: Applied Biomaterials* **2012**, *100*, 1451-1457; dE. A. Kamoun, S. A. Loutfy, Y. Hussein, E.-R. S. Kenawy, *Int. J. Biol. Macromol.* **2021**, *187*, 755-768.
- [9] M. Jiang, X. Song, G. Ye, J. Xu, *Compos. Sci. Technol.* **2008**, *68*, 2231-2237.
- [10] aA. Goyanes, P. R. Martinez, A. Buanz, A. W. Basit, S. Gaisford, *Int. J. Pharm.* **2015**, *494*, 657-663; bA. Goyanes, M. Kobayashi, R. Martínez-Pacheco, S. Gaisford, A. W. Basit, *Int. J. Pharm.* **2016**, *514*, 290-295; cF. Liu, W. Li, H. Liu, T. Yuan, Y. Yang, W. Zhou, Y. Hu, Z. Yang, *Macromolecular Bioscience* **2021**, *21*, 2000398.
- [11] aB.-H. Park, J.-H. Choi, *Electrochim. Acta* **2010**, *55*, 2888-2893; bZ. Liu, S. Han, C. Xu, Y. Luo, N. Peng, C. Qin, M. Zhou, W. Wang, L. Chen, S. Okada, *RSC advances* **2016**, *6*, 68371-68378; cJ. Song, M. Zhou, R. Yi, T. Xu, M. L. Gordin, D. Tang, Z. Yu, M. Regula, D. Wang, *Advanced functional materials* **2014**, *24*, 5904-5910.
- [12] aH. Shagholani, S. M. Ghoreishi, M. Mousazadeh, *Int. J. Biol. Macromol.* **2015**, *78*, 130-136; bM. Nadeem, M. Ahmad, M. S. Akhtar, A. Shaari, S. Riaz, S. Naseem, M. Masood, M. Saeed, *PloS one* **2016**, *11*, e0158084; cG. Rivera-Hernandez, M. Antunes-Ricardo, P. Martínez-Morales, M. L. Sanchez, *Int. J. Pharm.* **2021**, *600*, 120478.
- [13] C. Verma, M. Quraishi, *Corrosion Engineering, Science and Technology* **2022**, *57*, 796-812.
- [14] aH. Mudila, P. Prasher, M. Kumar, A. Kumar, M. Zaidi, A. Kumar, *Materials for Renewable and Sustainable Energy* **2019**, *8*, 1-19; bG.
-

- Konwar, S. Deka, D. Mahanta, *Journal of Energy Storage* **2023**, *62*, 106847.
- [15] aL. Rajan, M. P. Sidheekha, A. Shabeeba, S. C. Unnikrishnan, Y. A. Ismail, *Res. Chem. Intermed.* **2022**, *48*, 4313-4329; bA. Shabeeba, M. P. Sidheekha, L. Rajan, Y. A. Ismail, *RSC advances* **2022**, *12*, 31911-31922.
- [16] aM. Fuchiwaki, J. G. Martinez, T. F. Otero, *Advanced Functional Materials* **2015**, *25*, 1535-1541; bT. F. Otero, S. Beaumont, *Sensors and Actuators B: Chemical* **2017**, *253*, 958-966.
- [17] aT. F. Otero, S. Beaumont, *Sensors and Actuators B: Chemical* **2018**, *263*, 493-501; bT. F. Otero, S. Beaumont, *Electrochim. Acta* **2017**, *257*, 403-411.
- [18] aJ. DEL R. MILLÁN, P. W. Ferrez, F. Galán, E. Lew, R. Chavarriaga, *International Journal of Pattern Recognition and Artificial Intelligence* **2008**, *22*, 959-972; bA. Bruschi, D. M. Donati, P. Choong, E. Lucarelli, G. Wallace, *Advanced healthcare materials* **2021**, *10*, 2100041.
- [19] S. Lee, M. Park, K. Lee, J. Lee, *ACM Transactions On Graphics (TOG)* **2019**, *38*, 1-13.
- [20] T. F. Otero, J. G. Martinez, *Progress in Polymer Science* **2015**, *44*, 62-78.
- [21] K. N. Handore, S. V. Bhavsar, N. Pande, P. K. Chhattise, S. B. Sharma, S. Dallavalle, V. Gaikwad, K. C. Mohite, V. V. Chabukswar, *Polymer-Plastics Technology and Engineering* **2014**, *53*, 734-741.
- [22] T. Anjitha, T. Anilkumar, G. Mathew, M. Ramesan, *Polym. Compos.* **2019**, *40*, 2802-2811.
- [23] A. Thadathil, J. Kavil, G. R. Kovummal, C. P. Jijil, P. Periyat, *ACS omega* **2022**, *7*, 11473-11490.
- [24] A. Thadathil, Y. A. Ismail, P. Periyat, *RSC advances* **2021**, *11*, 35828-35841.
- [25] A. Thadathil, N. Edavan Chathoth, Y. A. Ismail, P. Anjukandi, P. Periyat, *The Journal of Physical Chemistry C* **2022**, *126*, 16965-16982.
- [26] M. Elango, M. Deepa, R. Subramanian, A. Mohamed Musthafa, *Polymer-Plastics Technology and Engineering* **2018**, *57*, 1440-1451.
- [27] S. Sankar, A. A. Naik, T. Anilkumar, M. Ramesan, *Journal of Applied Polymer Science* **2020**, *137*, 49145.
- [28] aV. Q. Trung, D. N. Huyen, in *Journal of Physics: Conference Series*, Vol. 187, IOP Publishing, **2009**, p. 012058; bSunaryono, M. F. Hidayat, M. N. Kholifah, A. Taufiq, Aripriharta, N. Mufti, M. Diantoro, S. Soontaranon, Darminto, *Journal of Inorganic and Organometallic Polymers and Materials* **2020**, *30*, 4278-4288.
- [29] S. Awad, *Int. Polym. Proc.* **2021**, *36*, 137-143.
-

-
- [30] C. Zhijiang, H. Chengwei, *Journal of Power Sources* **2011**, *196*, 10731-10736.
- [31] A. Thadathil, H. Pradeep, D. Joshy, Y. A. Ismail, P. Periyat, *Materials Advances* **2022**, *3*, 2990-3022.
- [32] T. F. Otero, *Polymer Reviews* **2013**, *53*, 311-351.
- [33] aY. A. Ismail, J. G. Martínez, A. S. Al Harrasi, S. J. Kim, T. F. Otero, *Sens. Actuators B Chem.* **2011**, *160*, 1180-1190; bY. A. Ismail, J. G. Martínez, T. F. Otero, *Electrochim. Acta* **2014**, *123*, 501-510.
- [34] Y. A. Ismail, J. G. Martínez, A. S. Al Harrasi, S. J. Kim, T. F. Otero, *Sensors and Actuators B: chemical* **2011**, *160*, 1180-1190.
- [35] aY. A. Ismail, J. G. Martinez, T. F. Otero, *Journal of Electroanalytical Chemistry* **2014**, *719*, 47-53; bY. A. Ismail, J. G. Martínez, T. F. Otero, *Electrochim. Acta* **2014**, *123*, 501-510.
- [36] Y. A. Ismail, S. R. Shin, K. M. Shin, S. G. Yoon, K. Shon, S. I. Kim, S. J. Kim, *Sensors and Actuators B: Chemical* **2008**, *129*, 834-840.
- [37] M. Fuchiwaki, J. G. Martinez, T. F. Otero, *Electrochim. Acta* **2016**, *195*, 9-18.
- [38] T. F. Otero, *International Journal of Smart and Nano Materials* **2017**, *8*, 125-143.
- [39] M. Beregoi, S. Beaumont, S. I. Jinga, T. F. Otero, I. Enculescu, *Smart Mater. Struct.* **2022**, *31*, 105012.
- [40] T. F. Otero, *The Chemical Record* **2018**, *18*, 788-806.
- [41] M. E. M. Mashat, G. Li, D. Zhang, *Scientific reports* **2017**, *7*, 11001.
- [42] aC. Poggesi, C. Tesi, R. Stehle, *Pflügers Archiv* **2005**, *449*, 505-517; bB. C. W. Tanner, T. L. Daniel, M. Regnier, *PLoS computational biology* **2007**, *3*, e115.
- [43] T. F. Otero, S. Beaumont, *Electrochim. Acta* **2017**, *258*, 1293-1303.
- [44] T. F. Otero, *Electrochim. Acta* **2021**, *368*, 137576.
- [45] A. Shabeeba, Y. A. Ismail, *Mater. Res. Bull.* **2022**, *152*, 111817.
- [46] S. Beaumont, T. F. Otero, *Smart Mater. Struct.* **2018**, *27*, 074001.
- [47] T. F. Otero, *Advanced Intelligent Systems* **2022**, *4*, 2100058.
-

Chapter 6

Electrochemical characterization of Poly(3,4-ethylene dioxythiophene) with a special emphasis on its structural electrochemistry and biomimetic sensing characteristics



We conducted an in-depth electrochemical investigation of PEDOT, focusing on understanding its structural electrochemistry during the faradaic process, a topic that has not been previously explored extensively. Using coullovoltammetry, we examined various conformational states of PEDOT and their corresponding charge consumption, providing new insights into its electrochemical behavior. This comprehensive coullovoltammetric study allowed us to explore PEDOT's unique electrochemical characteristics and reactions in detail for the first time. Additionally, we analyzed PEDOT's reactive sensing capabilities in its environmental condition, proving its simultaneous and biomimetic self-sensing properties.

6.1. Introduction

CPs can mimic the reactive sensing properties of biological muscles. So they can be used as a model material to study some of the biological functions such as self-sensing properties of muscles and brain-muscle feedback communication. The muscles can sense their working conditions and inform the brain through neurons. The same muscles work according to the instructions of the brain. These instructions and sensing signals are transferred simultaneously through the same two connecting neurons. We argue that CP can mimic this simultaneous communication that takes place between the brain and muscle.

The biomimetic reactive sensing nature of polypyrrole has been studied extensively. Polyaniline and its derivatives have also been studied by our group. We have also proved for the first time the reactive sensing capability of PIN (previous chapter)

In this chapter, we explore the reactive sensing characteristics of another major CP, PEDOT. Through this work, we aim to demonstrate that the reactive sensing ability is a common property of all CPs. PEDOT boasts numerous advantages, including ease of synthesis, high electrical conductivity, lightweight, and precise control over its electrochemical performance^[1]. These outstanding properties have led to its versatile applications in various fields, such as actuators^[2], sensors^[3], supercapacitors^[4], batteries^[5], tissue engineering^[6], and electrocatalysis^[7]. Unfortunately, an in-depth electrochemical analysis of PEDOT focusing on understanding its structural electrochemistry and its biomimetic reactive sensing

capabilities has not been carried out by the scientific community yet. That means detailed studies need to be carried out on the structural faradaic processes of PEDOT. The objective of this chapter is to understand the electrochemical reaction-induced structural variation of PEDOT and its biomimetic sensing characteristics.

6.2. Results and discussion

6.2.1. FTIR spectra

The FTIR spectrum of PEDOT is shown in Figure 6.1. Specifically, the peaks at 1514 cm^{-1} and 1323 cm^{-1} correspond to the symmetric stretching mode of the C=C bond and the inter-ring stretching mode of the C-C bond, respectively^[8]. The bending vibrations of C-O-C bonds in the ethylenedioxy groups in PEDOT appeared at 1045 cm^{-1} , 1088 cm^{-1} , 1138 cm^{-1} , and 1188 cm^{-1} . Additionally, the bands at

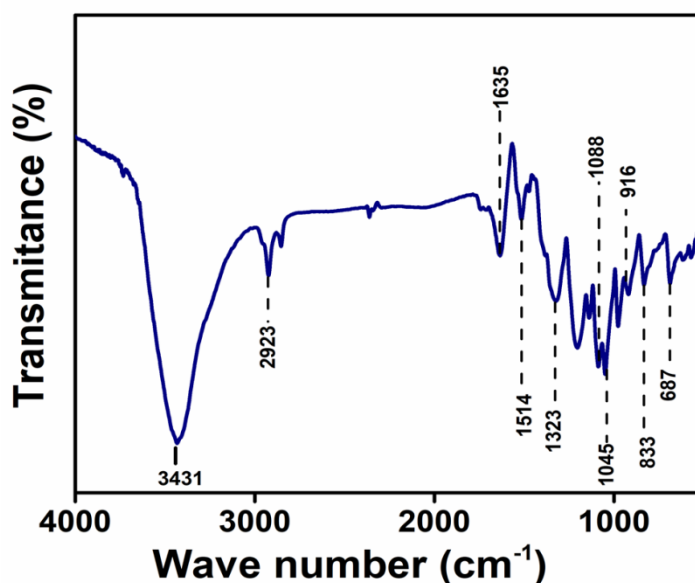


Figure 6.1 FTIR spectrum of PEDOT

972 cm^{-1} , 916 cm^{-1} , 833 cm^{-1} , and 687 cm^{-1} are attributed to the

stretching vibrations of C-S-C bonds in the thiophene ring. Moreover, the bands at 3431 cm^{-1} and 2923 cm^{-1} are indicative of the C-H and C-O stretching within the ring, respectively. These characteristic bands serve as robust evidence confirming the successful polymerization and formation of PEDOT^[9].

6.2.2. TGA

The thermogram of PEDOT is shown in Figure 6.2. The figure shows that the PEDOT undergoes a three-stage weight loss. The initial stage corresponds to the expulsion of the absorbed water molecule and occurs up to $130\text{ }^{\circ}\text{C}$. The subsequent step, spanning $155\text{ }^{\circ}\text{C}$ to $290\text{ }^{\circ}\text{C}$, is associated with the removal of low molecular weight oligomers and dopant ions^[10]. Polymer chain degradation becomes evident at $330\text{ }^{\circ}\text{C}$ ^[11].

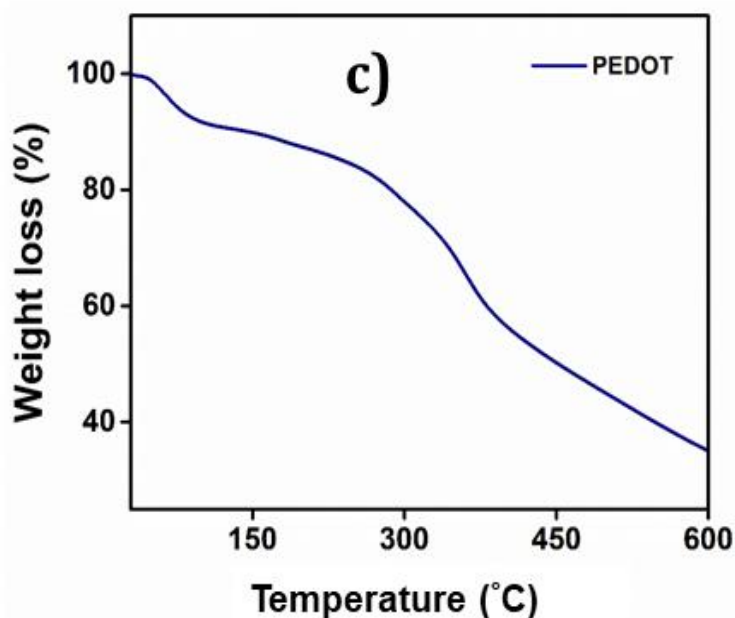


Figure 6.2 Thermogram of PEDOT

6.2.3. FE-SEM

The FE-SEM image of PEDOT is shown in Figure 6.3. The SEM images show an agglomerated granular morphology for PEDOT. A zoomed-in image at 100 nm magnification shows larger granular particles that are perfectly interconnected and clustered. Moreover, the surface exhibits sufficient porosity, allowing for the intercalation/diffusion of anions and solvent molecules^[12]. The image also indicates that the PEDOT particles exhibit heterogeneity in size.

The elemental analysis of the PEDOT was also carried out. The results are shown in Figure 6.3(c). The presence of carbon, nitrogen, and sulfur is confirmed.

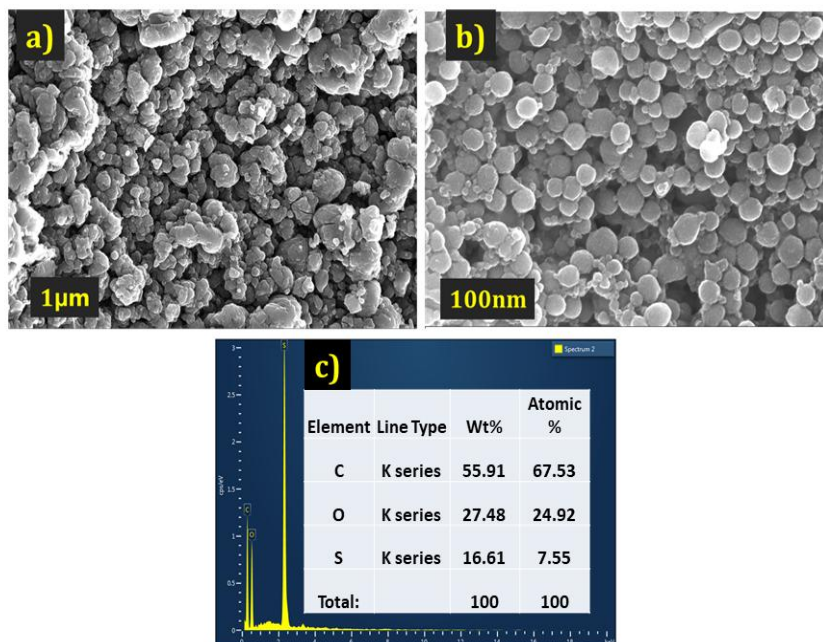


Figure 6.3. The FE-SEM image of PEDOT **a)** at 1 μm. **b)** at 100 nm **c)** EDX data of the PEDOT

6.2.4. HR-TEM

The HR-TEM image and elemental mapping of PEDOT are shown in Figure 6.4. The agglomerated granular morphology obtained from FE-SEM images is further confirmed by the HR-TEM image (Figure 6.4a). The elemental mapping EDS analysis gives the distribution of the elements on the surface of the polymer (Figure 6.4b -6.4e) and entails the presence of sulfur^[13]

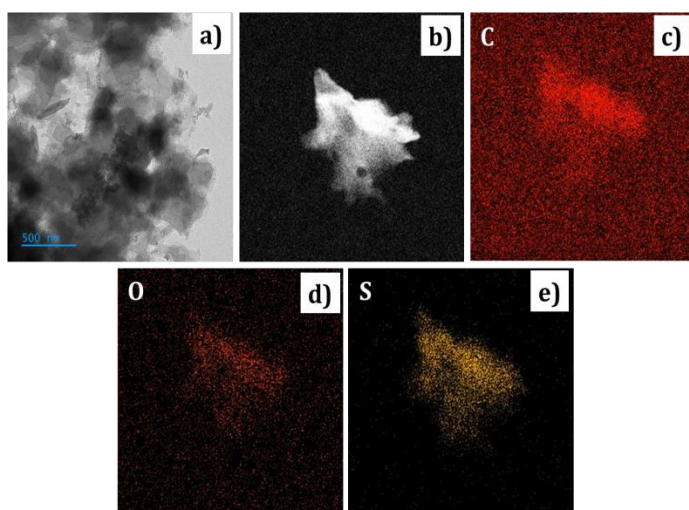


Figure 6.4. *a) HR-TEM image of PEDOT b) secondary electron image in EDS elemental mapping of PEDOT c) Carbon in PEDOT d) Oxygen in PEDOT e) Sulphur in PEDOT and APS dopant*

6.2.5. Electrical Conductivity

The electrical conductivity of the PEDOT and PEDOT-carbon paste mixture was determined through a two-point probe method using a Broadband dielectric spectrometer. The samples were pelletized and sandwiched between a couple of parallel gold-plated electrodes in the frequency range of 10^{-2} to 10^7 Hz at room temperature and

ambient pressure. The results are shown in Figure 6.5. It is obtained that PEDOT has electrical conductivities of $6 \times 10^{-3} \text{ Scm}^{-1}$.

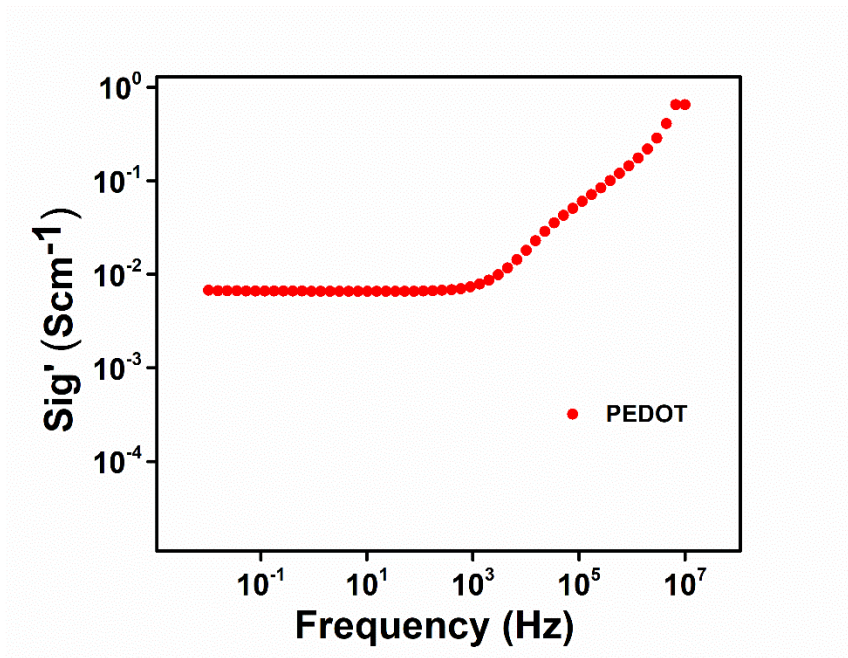


Figure 6.5. Log-log plot of the frequency dependence of the AC conductivity data of the PEDOT

6.2.6. Electrochemical characterization

6.2.6.1. Voltammetric analysis

A detailed investigation into the electrochemical behavior of PEDOT was carried out through voltammetric analysis. The cyclic voltammogram was recorded in a three-electrode cell configuration at room temperature. PEDOT pasted on a glassy carbon electrode served as the working electrode, while the reference electrode was an Ag/AgCl (3M) electrode, and the counter electrode was a platinum wire^[14]. The potential was cycled between -0.6 V and 0.8 V in 1 M aqueous NaCl solution,

at a scan rate of 25 mVs^{-1} . The repeated potential cycles resulted in a stable cyclic voltammogram as shown in Figure 6.6^[15].

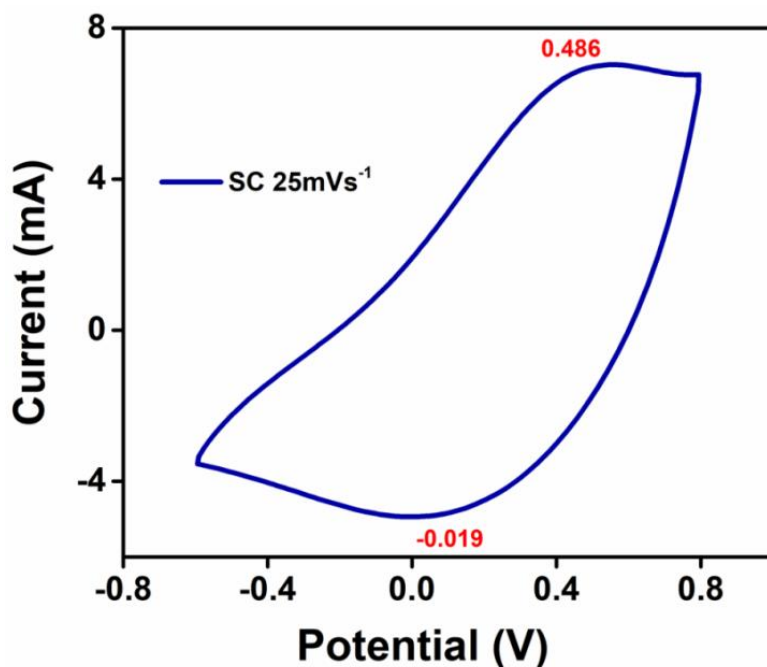
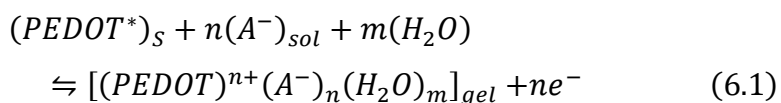


Figure 6.6 CV plot of PEDOT

The oxidation of the polymer chain by extraction of one electron per active centre results in a reorganization of the double bonds along several monomeric units with a generation of a positive charge (in fact a radical cation or polaron). For charge balance, this charge is effectively compensated by the incorporation of a monovalent counterion (anion) from the electrolyte^[16]. Furthermore, solvent molecules are interchanged between the polymer and the electrolyte to maintain equilibrium amidst anion intercalation-induced osmotic pressure^[15b, 17]. The reaction goes on by extraction of

consecutive electrons from each polymeric chain as the potential increases to promote conformational movements of the polymeric chains (macromolecular electrochemical motors) with the generation of free volume required to incorporate balancing counter ions and solvent molecules. The reversible reaction of the polymer's active centres can be precisely described as:



The active center referred to as "PEDOT*", is the key player responsible for generating a positive charge at the interface of the electrode and the electrolyte when the first electron is removed from the polymer chain. The monovalent anion present in the electrolyte is represented as "(A⁻)_{sol}." Upon oxidation, the cooperative actuation of the polymeric motors promotes the incorporation of counterions and solvent molecules. The polymer swells and forms a polymeric gel, as depicted in Reaction 6.1^[18]. This volume variation is a large reaction-driven structural change. The term "ne⁻" indicates that up to "n" electrons are expelled from each polymeric chain through n consecutive steps. The polymer reduction drives reverse processes: the expulsion of counterions and solvent molecules and contraction of the polymeric chain.

To confirm that, the full volume of PEDOT involved during the redox reaction, the relationship between the anodic/cathodic peak current and the scan rate was examined, and the results

are shown in Figure 6.7(a). This figure shows that, as the scan rates increase, the anodic peaks shift towards more positive values, while the cathodic peaks shift towards more negative values, providing solid evidence that the redox reaction becomes more resistant at higher scan rates due to the constrained entry/expulsion of counter ions through the full polymer volume. Conversely, a reversed trend is observed when the scan rate is reduced; confirming that the conformational movements of the polymeric chains are significantly impacted due to the generation/destruction of a larger quantity of free volume, which is essential to accommodate the increased number of counter ions and solvent molecules. Figure 6.7(b) shows a linear relationship between the anodic and cathodic peak currents with the square root of the scan rate, implying that the process at the electrode-electrolyte interface is under diffusion control up to 200 mV⁻¹.

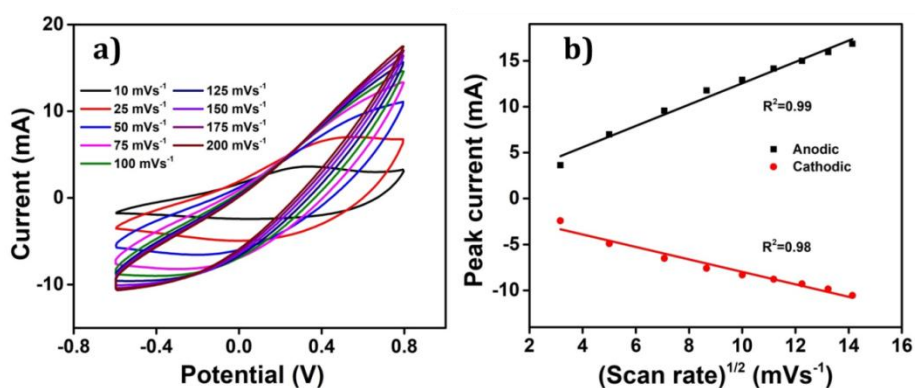


Figure 6.7 a) (a) CVs of PEDOT at different scan rates. (b) Linear fit of anodic and cathodic peak currents with the square root of scan rate

6.2.6.2. Coulovoltammogram

The QV of PEDOT corresponding to the CV recorded at a scan rate of 25 mVs^{-1} is shown in Figure 6.8. The charge consumed during the reaction is calculated from the QV. The closed loop of the QV indicates a full reversible reaction, equation 6.1, (the oxidation charge equals the reduction charge), and the absence of any other parallel irreversible reaction in the studied potential range. The difference between the highest and lowest points of this closed loop gives the total redox charge consumed during the reaction: the oxidation charge perfectly matches the reduction charge^[19].

This QV presents a great asymmetry between the evolution of the oxidation charge and that of the reduction charge. This means that by integration a great asymmetry will be obtained

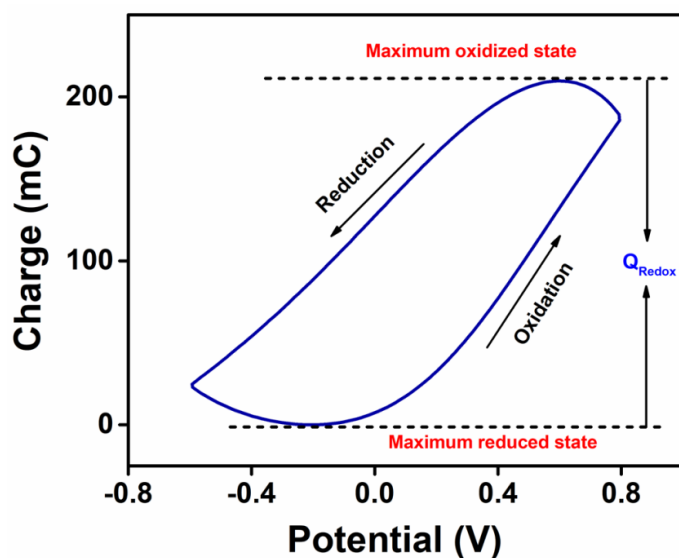


Figure 6.8 QV of PEDOT

between the concomitant consumed energies. This fact linked to the actuation of electro-chemo-mechanical macromolecular motors is being explored as a model to understand why and how Mother Nature has developed asymmetric biological functions based on electro-chemo-mechanical proteins: muscles only work by contraction or ionic channels only allow one-way ionic flow: the most efficient from an energetic point of view^[20].

6.2.7. Structural Faradaic Processes in PEDOT

Figure 6.9 presents the QV, obtained by integrating the CV recorded in a 1 M NaCl solution at room temperature at a scan rate of 25 mVs⁻¹, showing the structural variations of PEDOT material during the Faradaic processes^[18]. The closed QV loop displays four distinct basic slope variations, shedding light on the structural changes of PEDOT induced by the reaction-driven conformational movements of the polymeric chains, including reduction-shrinking (from point 5 to point 6), reduction-compaction (from point 6 to 2), oxidation-relaxation (from point 2 to 3), and oxidation-swelling (from point 3 to 5), which can be characteristic of all CPs^[17].

The closed QV of PEDOT exhibits four distinct slope variations like polypyrrole^[19a, 21]. These four slope variations correspond to the structural changes occurring during the redox process: starting from a swollen oxidized PEDOT material, 1) identified as fast reduction-shrinking leading to closing the polymer structure at a particular potential when the average intrachain

distances equals the diameter of the counter ions, 2) slow subsequent reduction compaction, 3) slow oxidation relaxation^[22] during which channels open through the compacted structure and 4) fast oxidation swelling.

All of these structural processes are controlled by the reaction kinetics under conformational kinetic control (compaction and relaxation) or counter ion diffusion control (Figure 6.7(a)) swelling and shrinking. The oxidation process in the PEDOT commences from the QV minimum. As electrons are extracted from the polymer chain, a positive charge is generated, initiating the relaxation of the reduced-compacted polymer

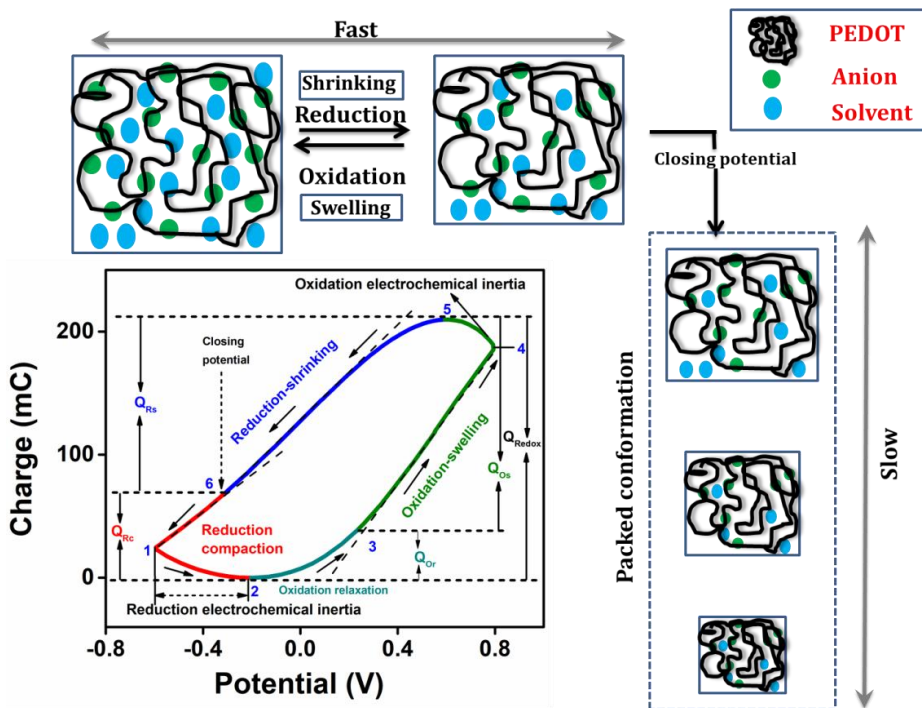


Figure 6.9 Different structural processes during the electrochemical reaction from QV in 1 M NaCl at 25 mV s⁻¹

chains to create sufficient free volume for accommodating anions and solvent molecules.

Prior to relaxation, the polymer chain adopts a compact structure. The portion of the curve in Figure 6.9, starting from point 2 to point 3, corresponds to the structural change known as oxidation-relaxation. Following the relaxation, the polymer undergoes fast oxidation-swelling, which starts from point 3 on the QV curve. The significant anodic slope observed from point 3 to point 4 on the QV curve indicates the occurrence of the oxidation-swelling process, governed by the kinetics. The rate at which anions diffuse from the solution to the polymer chain plays a crucial role in this process. It is worth noting that the anodic potential limit at point 4 in Figure 6.9 (0.8 V) does not mark the boundary of the oxidation process. Instead, the process continues beyond this anodic potential limit at the beginning of the cathodic potential sweep, up to the QV maximum. This fact is known as oxidation electrochemical inertia (OEI).

The reduction process of the polymer commences from the QV maximum, which is also where the oxidation process ends. The rate of this reduction-shrinking process is determined by the diffusion of anions and solvent molecules from the film to the solution. As a result, the reduction-shrinking is classified as a fast kinetic control process. The polymer material experiences shrinking during reduction until it reaches the closing potential (point 6 on the QV curve in Figure 6.9). Upon reaching the closing potential, the rate of shrinking decreases despite the

higher cathodic potential due to the fact that the counter ions must push apart those polymeric chains (still this is a soft and wet material allowing movements of the polymeric chains) closing its way towards the solution: this fact consumes energy and time. At the closing potential, the distance between adjacent polymer chains almost equals the hydrated anion diameter. Consequently, the rate of diffusion reduces, and the anions push against the polymer chain, leading to a more compact conformation known as reduction-compaction. The reduction-compaction process initiates from the closing potential and continues until the QV minimum is reached. Notably, the reduction of PEDOT is not completed at the cathodic potential limit. From points 1 to 2 in Figure 6.9, a slow reduction persists for the partially oxidized polymer chain (at -0.6 V), which is referred to as reduction electrochemical inertia. The closed QV loop indicates that the PEDOT reaction at this specific potential limit is reversible. In a reversible redox process, the charge consumed during oxidation is equivalent to the charge consumed during reduction. Therefore, the total redox charge and the charge for each structural process can be determined from the QV. The overall oxidation charge (Q_{Ox}) is calculated by adding the charge from oxidation-relaxation (Q_{Or}) and the charge from oxidation-swelling, which includes the oxidation electrochemical inertia (Q_{Oei}). Conversely, the reduction charge is the sum of the fast reduction-shrinking charge (Q_{Rs}) and the reduction-compaction charge (Q_{Rc}).

The total charge consumed in each structural process is listed in Table 6.1.

Table 6.1 Structural faradic processes in PEDOT, potential ranges, and corresponding electrical charges

<i>Structura l process</i>	<i>Oxidation(Q_{Ox})</i>			<i>Reduction(Q_{Red})</i>	
	<i>Relaxatio n (Q_{Or})</i>	<i>Swellin g (Q_{Os})</i>	<i>OEI Q_{Oei}</i>	<i>Shrinkin g (Q_{Rs})</i>	<i>Compactio n (Q_{Rc})</i>
<i>Potential range (V)</i>	-0.213 to 0.234	0.234 to 0.793	0.79 to 3 to 0.58 2	0.582 to -0.313	-0.313 to -0.213
<i>Charge (mC)</i>	38.87	146.79	23.9 6	-141.18	-68.44
<i>Total Charge (mC)</i>	209.62			-209.62	
	$Q_{Ox} = Q_{Or} + Q_{Os} + Q_{Oei}$			$Q_{Red} = Q_{Rs} + Q_{Rc}$	

6.2.7.1. Influence of cathodic potential limit on voltammetric and coul voltammetric responses

Figure 6.10(a) shows the CVs recorded at various cathodic potential limits while maintaining a constant anodic potential limit of 0.8 V against the Ag/AgCl reference electrode at a scan rate of 25 mVs⁻¹ in 1 M NaCl solution. Corresponding QVs for different cathodic potential limits are presented in Figure 6.10(b).

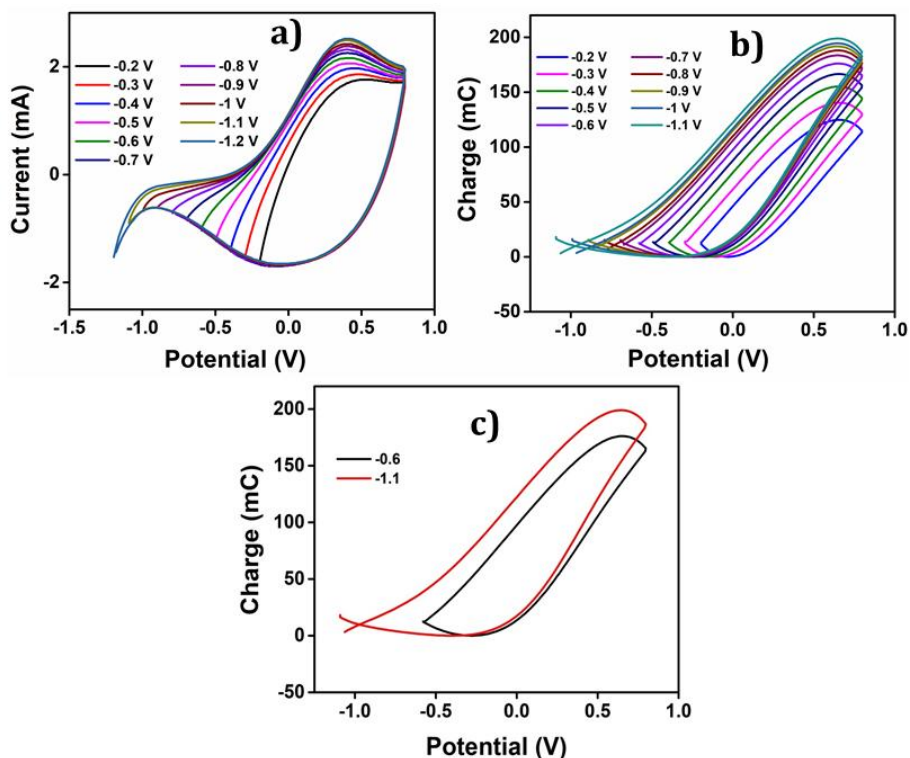


Figure 6.10 (a) Stationary CVs obtained for PEDOT in 1 M NaCl at a scan rate of 25 mV s^{-1} from different cathodic potential limits. (b) Corresponding QVs. (c) QVs obtained at the cathodic potential limits of -0.6 V and -1.1 V

The steady-state voltammetric response is obtained after performing three consecutive cycles. The findings from the studies are summarized below:

- In the cathodic region, there is a continuation of the reduction process beyond -0.5 V , as evidenced by the presence of a low current. The specific cathodic potential limits at which the reduction process concludes need to be determined.
- With an increase in the cathodic potential limit, the oxidation current peak shows a noticeable rise, indicating a deeper

reduction of PEDOT. The potential limit for the reversible redox process of the PEDOT electrode must be identified.

- Beyond -0.7 V, there is a notable increase in the reduction current, suggesting the occurrence of a new reduction process. The nature of this reduction process needs to be investigated to determine whether it is reversible or irreversible.

To uncover all the valuable insights gathered from the CVs, QVs are explored. QVs reveal the nature of the process-induced structural variations and the corresponding charge consumption throughout the reaction. Major observations and their interpretations are:

- As evidenced by the CV results, the low cathodic current flow beyond -0.2 V which is attributed to the slow reduction-compactation of PEDOT.
- A closed loop is observed in the QV curves recorded for different cathodic limits from -0.2 V to -0.6 V, which confirms the presence of only reversible reduction process in these studied cathodic limits. Thus, we have optimized the maximum potential window as -0.6 V to 0.8 V, where the oxidation charge is equal to the reduction charge.
- Beyond -0.6 V, the QV curve displays two distinct segments: the closed loop representing the reversible reduction process and an open part signifying the parallel irreversible reduction caused by hydrogen evolution during the reaction.
- The total reversible redox charge consumed during the reaction is determined from the difference between the QV maximum and QV minimum points.

- Similarly, the charge consumed during the irreversible reduction process (Q_{Irr}) is calculated by finding the difference between the starting and ending points of the open section in the QV curve.
- Consequently, the overall charge consumed during the two reactions is computed as $Q_{\text{Red}} = Q_{\text{Redox}} + Q_{\text{Irr}}$.

Figure 6.10(c) illustrates the QVs obtained at -0.6 V and -1.1 V, to distinguish the reversible and irreversible QVs.

The charge consumed during each cathodic potential limit is calculated and listed in Table 6.2

Table 6.2 *Charge consumed at various cathodic potential limits*

Cathodic limit (V)	Q_{redox} (mC)	Q_{irr} (mC)	$Q_{\text{reduction}}$ (mC)
-0.2	124.76		124.76
-0.3	140.43		140.43
-0.4	155.18		155.18
-0.5	166.57		166.57
-0.6	176.08		176.08
-0.7	183.57	4.34	187.91
-0.8	188.04	7.7	195.74
-0.9	191.75	8.28	200.03
-1	194.47	12.59	207.06

Figure 6.11(a) illustrates the charge consumption during the cathodic potential limit. Remarkably, the reduction-compaction process persists beyond the maximum reduction potential of -0.6 V.

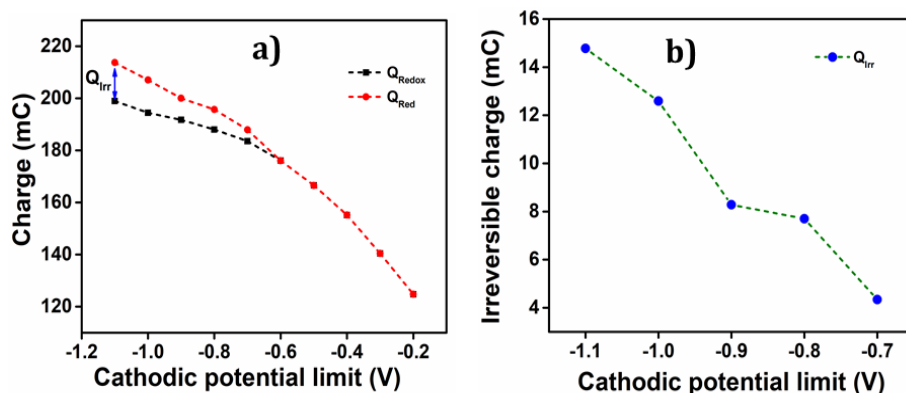


Figure 6.11 (a) Charge consumed in the oxidation and reduction of PEDOT as a function of the cathodic potential limit and (b) irreversible reduction charge obtained for different cathodic potential limits

As depicted in Figure 6.11(a), from -0.2 V to -0.6 V, an overlap of oxidation and reduction charges is observed, clearly indicating only reversible redox reaction, equation 6.1 occurring within this range. The charge variations exhibit a linear relationship with the cathodic potential limit during this reversible process. However, after reaching -0.6 V, the charge profile shows two separate components, namely Q_{Redox} and Q_{Irr} . Notably, the rising compacted structure beyond 0.8 V gives a slower reduction and disrupts the linearity, leading to a reduction in charge up to the potential limit of -1.1 V. Furthermore, the parallel irreversible charge consumption increases as the cathodic potential limit increases. Figure 6.11(b) showcases the variation of this irreversible charge with the cathodic potential limit.

6.2.7.2. Influence of anodic potential limit on voltammetric and QV responses

From the impact of various cathodic potential limits on both the CV and QV responses closed loops were obtained within the potential domain of -0.2 V to -0.6 V, signifying the occurrence of the reversible redox polymeric equation 6.1. at the polymer active center. Consequently, we maintain a constant cathodic potential limit of -0.6 V to investigate the influence of the anodic potential limits on the electrode process of PEDOT. Figure 6.12(a) showcases the stable CVs recorded up to different anodic potential limits after three consecutive cycles, along with its corresponding QVs (Figure 6.12(b)). The confirmed findings are given below.

- Up to 0.8 V, a closed loop consisting of only a reversible process is observed. Beyond 0.8 V, the anodic potential exhibits a higher oxidation charge than the reduction charge, indicating the presence of parallel irreversible oxidation reactions during the process.
- The irreversible charge consumed during the reaction is determined by calculating the difference between the starting and ending points of the open loop. Consequently, the reversible charge (Q_{Redox}) consumed is derived by subtracting the irreversible oxidation charge (Q_{Irox}) from the total charge Q_{Total} (the difference between QV maxima and QV minima),

$$Q_{\text{Redox}} = Q_{\text{Total}} - Q_{\text{Irox}}$$

The parallel irreversible oxidation occurring during the reaction which means the overlap with the polymeric redox process is

attributed to the liberation of oxygen from the electrode, leading to over-oxidation.

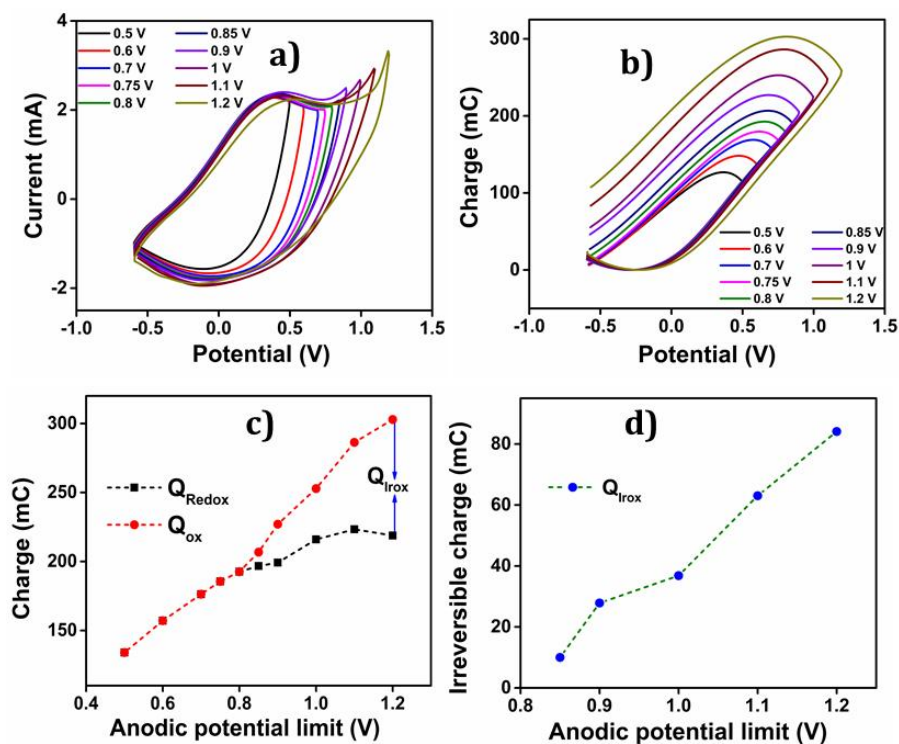


Figure 6.12 (a) CVs obtained for PEDOT in 1 M NaCl at a scan rate of 25 mV s⁻¹ from different anodic potential limits. (b) Corresponding QVs (c) Charge consumed in the oxidation and reduction of PEDOT and (d) irreversible oxidation charge obtained for different anodic potential limits

Figure 6.12(c) illustrates the charge variation during the oxidation-reduction process at different anodic potential limits. It is evident from the figure that the oxidation charge and reduction charge show an overlap up to 0.8 V. Beyond 0.8 V, two distinct components of charges are observed; one for reversible and the other for irreversible processes.

The Q_{Ox} is greater than Q_{Redox} due to the irreversible oxygen evolution and PEDOT over-oxidation, initiated at a potential of 0.85 V and extending up to 1.2 V. The charge consumed during each anodic potential limit is calculated and is given in Table 6.3.

Table 6.3 *Charge consumed at each anodic potential limits*

Anodic limit (V)	Q_{redox} (mC)	Q_{Irox} (mC)	Q_{total} (mC)
0.5	126.85		126.85
0.6	148.28		148.28
0.7	168.95		168.95
0.75	179.63		179.63
0.8	192.62		192.62
0.85	206.75	10	196.75
0.9	227.04	27.85	199.19
1	252.83	36.82	216.01
1.1	286.35	63.02	223.33
1.2	302.91	84.1	218.81

The graph in Figure 6.12(d) depicts the change in irreversible oxidation charge for various anodic potential limits. It is evident

from the figure that as the anodic potential increases, the irreversible oxidation charge also increases.

Based on the discussions in the preceding sections, the potential range for the reversible redox process of the PEDOT in an aqueous NaCl electrolyte takes place between -0.6 V and 0.8 V. Thus, we have avoided the possibility of any hydrogen or oxygen evolution by fixing the anodic and cathodic potential limit. Another important point related to figures 6.11(a) and 6.12(c) is that the polymeric oxidation/reduction goes on beyond those limits as an increase of the redox charge was observed.

6.2.8. Sensing ability of PEDOT electrode material towards the working electrical, chemical, and thermal ambient using voltammetric study

Voltammetry was employed to validate the ability of PEDOT to sense its surrounding working conditions. The study delved into the influence of electrical, chemical, and thermal variables on charge consumption during its electrochemical reaction^[23]. The extent of the redox process was ascertained by calculating the redox charge consumed throughout the process.

When the reaction reaches a high degree, it generates a substantial free volume that accommodates counter anions and solvent molecules, thus leading to more profound oxidation and greater charge consumption during the process^[24].

The amount of charge consumed in this process was calculated using the QV ^[25]. The reversible redox charge consumed during

the reaction serves as a sensing parameter, providing quantitative predictions about the working environment.

6.2.8.1. Sensing electrical working condition

To evaluate the polymer's sensing ability towards different electrical conditions, the influence of scan rate on the reversible electrochemical reaction was investigated at room temperature. 1 M aqueous NaCl solution used as the electrolyte. The redox charge consumed during the process was then calculated from the corresponding QV. Throughout the experiment, other environmental factors like temperature and chemical composition are kept constant for accurate observations.

The corresponding voltammetric response at different scan rates is presented in Figure 6.7(a). It can be seen that as scan rate increases there is an increase in both anodic and cathodic peak currents. Figure 6.13(a) shows corresponding QVs. The reversible charge consumed during the reaction at different scan rates was obtained from this QV response. From the figure, it can be observed that there is a decrease in redox charge as the scan rate increases. The double logarithmic correlation between scan rates and consumed redox charge, as depicted in Figure 6.13(b) validates the facts that the PEDOT can sense its electrical working conditions, with consumed redox charge as the sensing parameter. The sensitivity was found to be $-0.5653 \text{ C (mVs}^{-1})^{-1}$. Decreasing the scan rates results in a prolonged reaction time, this, in turn, leads to an exchange of a larger

number of anions and solvent molecules. This increases the extension of the reaction and results in a higher consumption of redox charge at lower scan rates. Conversely, at higher scan rates, the exchange of anions and solvent molecules is decreased. This is because of the reduction in the reaction for higher scan rates, causing a smaller extension of the reaction and consequently lower redox charge consumption. Figure 6.14 illustrates the schematic representation of this reaction extension at different scan rates.

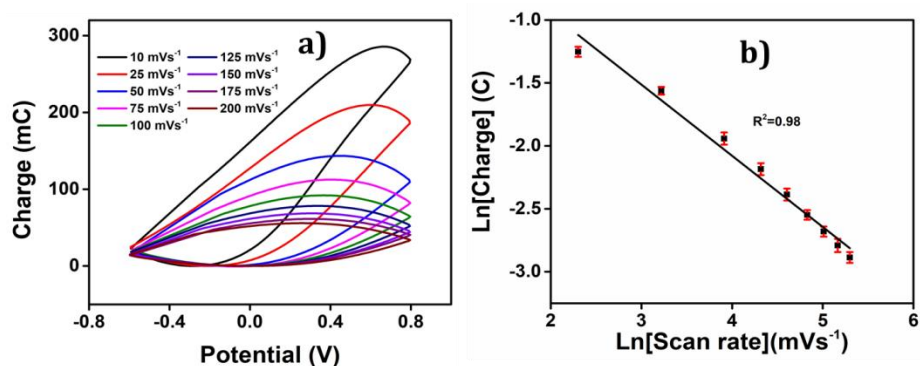


Figure 6.13 (a) QVs obtained by integrating the corresponding CVs from 6.7(a). (b) Double logarithmic relation of redox charge consumed during the reaction of PEDOT with the scan rate

6.2.8.1.1. Theoretical description

Through the observation of the reversible equation 6.1, we have successfully showcased the capability of PEDOT to sense the changes in electrical conditions. The consumed redox charge is the sensing parameter. To establish the relationship between the redox charge and the scan rate, a thorough investigation of the PEDOT oxidation kinetics was conducted, representing the forward reaction of equation 6.1.

$$R = k[Cl^-]^\alpha [PEDOT]_0^\beta \quad (6.2)$$

where R is the reaction rate. The specific reaction rate can be denoted as "r" and the rate constant as "k." The concentration of the counter anions, Cl^- , and the concentration of the active centre is represented as $[PEDOT]_0$. The reaction orders corresponding to the concentrations of the counter ion and polymer gel's active centre are denoted as " α " and " β ,"

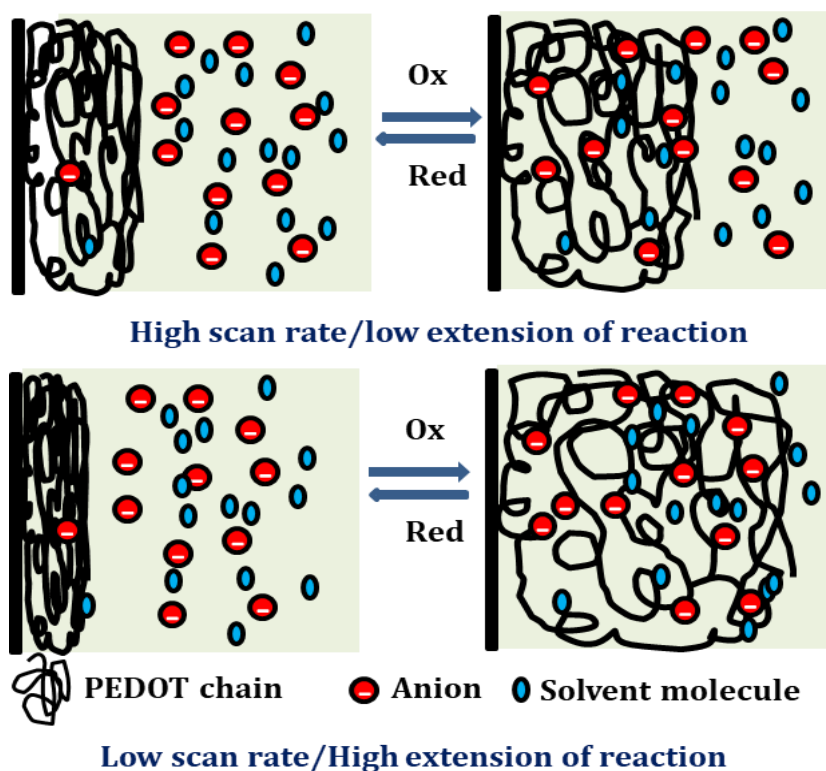


Figure 6.14 Schematic representation of extension of reaction at different scan rates respectively. As the volume of the active centre undergoes continuous changes during the reaction, the rate equation can be expressed in terms of the concentration of the active centre

per unit of dry polymeric mass (specific concentration). In other words, the rate equation can be reformulated as the rate per unit mass.

$$r = \frac{R}{m} = \frac{k}{m} [Cl^-]^\alpha [PEDOT]_0^\beta \quad (6.3)$$

where, r is the specific reaction rate. Equation 6.1 demonstrates the variation in the concentration of the active centre, which can be assessed from the redox charge consumed during the reaction.

$$-\Delta [PEDOT]_0 = \frac{Q}{mzF} = \frac{q}{zF} \quad (6.4)$$

The specific reaction rate is defined as the partial derivative of the specific concentration of the active centre per unit of time, which is determined from the specific charge, denoted as q . The charge consumed during the reaction is denoted by Q , and z represents the valence of the counter anion or the valence of the polymeric active centre (in this instance, Cl^- possesses a valence of 1). F , the Faraday constant, stands for the Faraday constant.

$$r = \frac{\partial [PEDOT]_0}{\partial t} = \frac{\partial (q)}{\partial t} = \frac{1}{F} \frac{\partial q}{\partial t} \quad (6.5)$$

The mean specific reaction rate \bar{r} can be ascertained by examining the QV response and computing the duration required to complete a potential window ($\Delta E/v$).

$$\bar{r} = \frac{\Delta [PEDOT]_0}{\Delta t} = \frac{q}{Ft} = \frac{qv}{F\Delta E} \quad (6.6)$$

Equation (6.4) can be rearranged as;

$$[\text{PEDOT}]_0 = \frac{Q}{VzF} = \frac{q\rho}{mzF} \quad (6.7)$$

The function of the consumed redox charge was employed to assess the impact of scan rate on the reaction extension, where V represents the volume of the active centres in litre, and ρ is the density in grams per liter. The consumed oxidation or reduction charge, as given by equation 6.7, determines the change in concentration of the polymer active centre. The rate of reaction is defined by the rate of change of the concentration of the active centre $[\text{PEDOT}]$ per unit time, which can be calculated using the potential, scan rate (v), and time ($\partial t = \partial E/v$). The formation rate of polarons is equivalent to the reduction in the concentration of the polymer active centre per unit time, which also corresponds to the number of moles of electrons (number of Faraday) released from the polymer chain.

$$R = -\frac{\partial[\text{PEDOT}]_0}{\partial t} = \frac{\partial\left(\frac{q\rho}{F}\right)}{\partial t} = \frac{v\rho}{F} \frac{\partial q}{\partial E} \quad (6.8)$$

The reaction rate also can be expressed as;

$$\frac{v\rho}{F} \frac{\partial q}{\partial E} = k[\text{Cl}^-]^\alpha [\text{PEDOT}]_0^\beta = k[\text{Cl}^-]^\alpha \left(\frac{q\rho}{F}\right)^\beta \quad (6.9)$$

The equations can be rearranged as;

$$\frac{1}{q^\beta} \frac{\partial q}{\partial E} = \frac{k[\text{Cl}^-]^\alpha F^{1-\beta}}{\rho^{1-\beta}} \frac{1}{v} \quad (6.10)$$

Integration of the left side can be performed for the reversible QV charge employed during the reaction, ranging from the minimum QV charge (charge = 0) to the maximum charge (q_R).

Conversely, the right side can be integrated from the potential when the charge is zero (E_0) to the potential at the maximum charge (E_R).

$$\int_0^{q_R} \frac{1}{q^\beta} \partial q = \int_{E_0}^{E_R} \frac{k[Cl^-]^\alpha F^{1-\beta}}{\rho^{1-\beta}} \frac{1}{v} \partial E \quad (6.11)$$

$$q_R^{1-\beta} = \frac{(1-\beta)k[Cl^-]^\alpha F^{1-\beta} \Delta E}{\underbrace{\rho^{1-\beta}}_{h'}} \frac{1}{v} \quad (6.12)$$

The degree of a reaction is established by the quantity of redox charge expended throughout the process. Equation 6.12 establishes a relationship between the consumed charge and the scan rate. When all other factors like electrolyte concentration, working temperature, atmospheric pressure, and potential window remain constant, the extension of reaction or the consumed redox charge decreases as the scan rate increases. The constant terms in equation 6.12 can be combined and represented as a new constant, denoted by 'h'. By taking the logarithm of both sides of equation 6.12, a linear equation can be derived as.

$$\ln q_r = x - y \ln v \quad (6.13)$$

The double logarithmic relation provides the slope (y , indicating sensitivity) and the intersection point (referred to as x) of the linear equation, which can be described as follows:

$$x = \frac{\ln h'}{1-\beta} \quad (6.14)$$

$$y = \frac{1}{1-\beta} \quad (6.15)$$

The sensing equation 6.13 establishes a relationship between the reaction extension and the scan rate, allowing for the assessment of changes in the electrical condition (scan rate) and its impact on the conformational movement of the polymer chain. This observation highlights the biomimetic nature of the PEDOT.

Through the utilization of the theoretical equation 6.13, a fitting analysis was performed on the experimental results as shown in Figure 6.13(b). The sensing equation 6.13 provides support for the significant conformational changes occurring in the polymer chain at lower scan rates. These changes arise due to the extended time available for the oxidation/reduction of the polymeric chains, leading to the creation/destruction of a substantial amount of free volume to accommodate/expel the counter anions, respectively. Consequently, a decrease in scan rates results in a notable increase in the redox charges.

The findings from the experiment indicate that the structural variations of the PEDOT chain during reactions result in reduced motion, shorter extension, and lower redox charge consumption at rising scan rates.

6.2.8.2. Chemical working condition sensing-concentration sensor

To explore PEDOT's ability to sense its chemical environment, under constant electrical and thermal conditions, stable voltammetric responses were recorded for different electrolyte concentrations (different chemical energies). The results are depicted in Figure 6.15(a). The figure shows that the CV

obtained at a scan rate of 25 mVs^{-1} shows an increase in both anodic and cathodic peak currents as the electrolyte concentration increases (higher chemical energy), followed by a decrease in both anodic and cathodic peak currents when the concentration of the aqueous electrolyte decreases.

The corresponding QV is shown in Figure 6.15(b), revealing that the redox charge consumed during the reaction increases with higher electrolyte concentration. At higher concentrations, the polymer chain undergoes deeper oxidation within the potential window consuming a higher charge. A large amount of available chemical energy drives the intercalation of more counter anions and solvent molecules into the polymer matrix (higher extension of reaction).

On the other hand, at lower concentrations, partial oxidation occurs, resulting in a smaller amount of free volume for the counter anions and solvent molecules to enter or exit during oxidation and reduction, respectively (smaller extension of reaction). Figure 6.16 shows the schematic representation of the extension of the reaction and conformational movement during the reaction at different concentrations of the electrolyte. Figure 6.15(c) shows a double logarithmic relationship between the electrolyte concentration and the consumed redox charge, demonstrating the capability of the PEDOT reaction to sense, simultaneously, its chemical working condition, and the sensitivity being $0.1209 \text{ Cmole}^{-1}$ (slope of the curve).

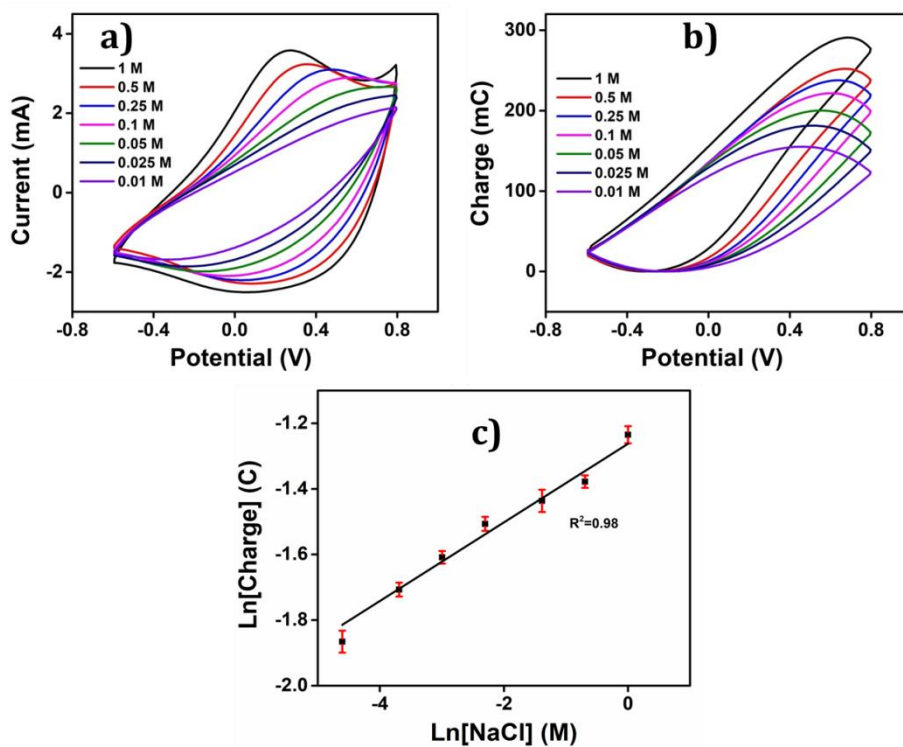


Figure 6.15 (a) CVs obtained in different concentrations of aqueous solution of NaCl at a scan rate of 25 mVs^{-1} . (b) Corresponding QVs (c) Double logarithmic relation of the charge consumed during the redox reaction of PEDOT with the electrolyte concentration of aqueous NaCl

Consequently, the polymeric gel responds to or senses the chemical ambient by undergoing larger conformational movements and structural changes, as higher chemical energy is available and the consumed charge is the sensing parameter. Therefore, the PEDOT can mimic the reactive sensing properties of biological muscles.

6.2.8.2.1. Theoretical interpretation

Equation 6.3 can be rearranged to get an alternative expression for representing the average reaction rate.

$$\frac{qv}{F\Delta E} = \frac{k}{m} [Cl^-]^\alpha [PEDOT_0]^\beta = \frac{k}{m} [Cl^-]^\alpha \left(\frac{q}{F}\right)^\beta \quad (6.15)$$

Rearranging the above equation we get equation 6.16, which establishes the relationship between the changes in concentration of the electrolyte and the redox charge consumed during the reaction.

$$q^{1-\beta} = \underbrace{\frac{k\Delta EF^{1-\beta}}{v}}_{k'} [Cl^-]^\alpha \quad (6.16)$$

The constants in equation 6.16 are consolidated into a new constant, represented as 'k'. Upon taking the logarithm of equation 6.16, a logarithmic correlation emerges, relating the

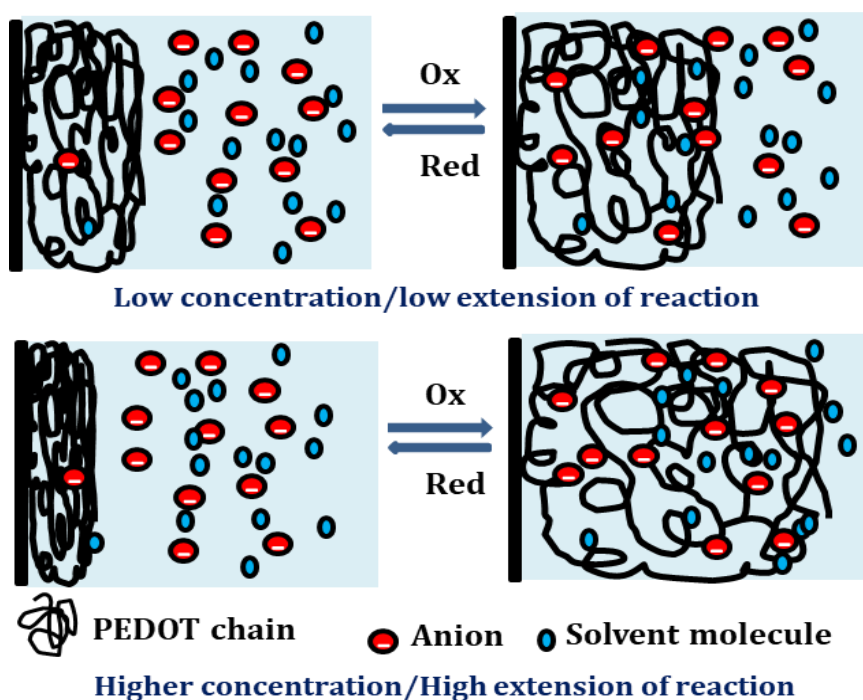


Figure 6.16 Schematic representation of extension of reaction at different concentrations of NaCl

consumed redox charge during the reaction (under constant pressure, temperature, potential sweep, and scan rate) to the electrolyte concentration.

$$\ln(q) = a + b \ln[Cl^-] \quad (6.17)$$

Equation 6.17 portrays a direct relationship between the redox charge and the electrolyte concentration, with the parameter "a" signifying the intercept, and the slope of the line designated as "b".

$$a = \frac{\ln k'}{1 - \beta} \quad (6.18)$$

$$b = \frac{\alpha}{1 - \beta} \quad (6.19)$$

The experimental results in Figure 6.15(c) fit the theoretical equation 6.17. PEDOT's sensing ability is rooted in the reaction-driven conformational movements of its polymeric chain. This is similar to the conformational movement of the sarcomere with the change in concentration of the ATP in the biological muscles. The biological muscles inform about the fatigue state (chemical condition) to the brain and sense the working environment during above mentioned conformational movement. Thus we suggest that PEDOT can mimic this property of biological muscles through its electrochemical reaction.

6.2.8.3. Sensing Thermal working condition-Temperature sensor

The thermal working condition sensing characteristics of PEDOT were explored using voltammetric experiments. After

the stable voltammetric response, the CVs were recorded for different working temperatures ranging from 20 °C to 50 °C at a scan rate of 25 mVs⁻¹. The results are provided in Figure 6.17(a). From the figure, it is observed that, as the temperature rises (i.e. the thermal energy increases), both the anodic and cathodic peak currents in the voltammogram increase.

The concomitant QVs are depicted in Figure 6.17(b). All QVs exhibited a distinctive closed loop indicating that only the reversible redox reaction of the polymer material takes place.

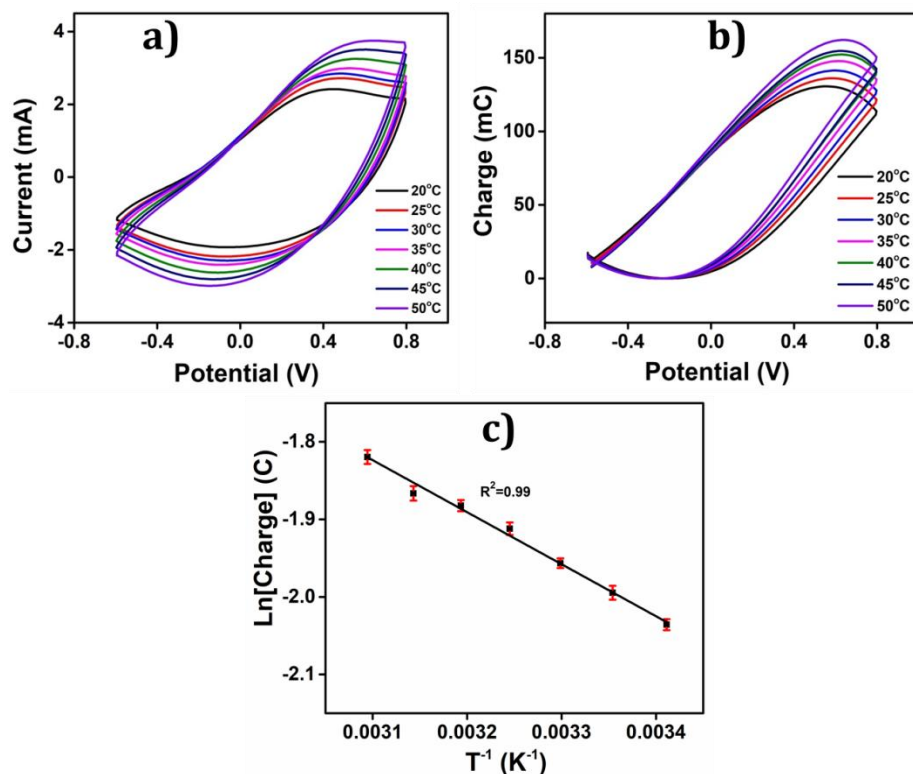


Figure 6.17 (a) CVs obtained from experimental temperatures (20° C to 55° C) in 1 M NaCl at 25 mVs⁻¹, (b) Corresponding QVs (c) calibration curve showing the Semi logarithmic relation of redox charge consumed with the inverse of temperature

The redox charge consumed during the reaction increases with increasing experimental temperature. This results in an increase in the reaction extension under constant chemical, physical, and mechanical energetic conditions.

Figure 6.17(c) shows the semi-logarithmic relationship between the consumed redox charge and temperature possesses the ability to sense the working temperature. Proved that the PEDOT can act as a temperature sensor. The results strongly validate the proposed theoretical equation 6.23.

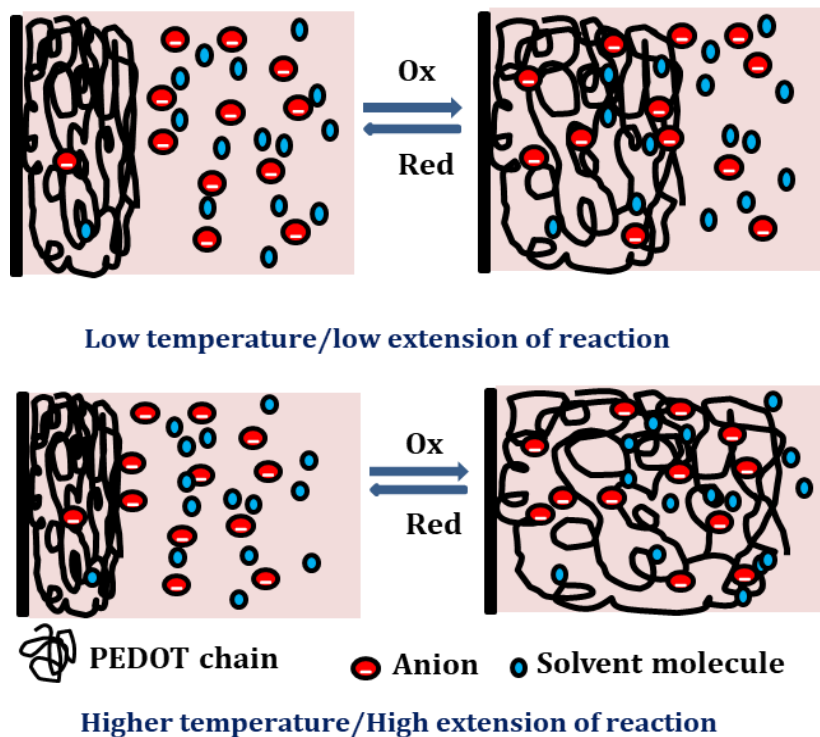


Figure 6.18 Schematic representation of extension of reaction at different working temperatures

At lower temperatures, where thermal energy is less, the reaction experiences only partial conformational relaxation,

leading to a smaller extension of the reaction. This is due to the limited generation of free volume for the insertion of counter anions and solvent molecules into the polymer chain, resulting in a low consumption of oxidation charge. Conversely, elevating the temperature provides more thermal energy, resulting in faster and more extensive conformational relaxation. This generates a larger free volume, enabling the insertion and ejection of anions and solvent molecules, leading to increased charge consumption during the reaction. Consequently, under constant chemical, electrical, and mechanical conditions, the reaction extension is large at higher temperatures. Higher temperatures drive the polymer chain to undergo a more profound oxidation/reduction state, yielding a larger redox charge. Figure 6.18 shows the schematic representation of the extension of the reaction at different working temperatures.

6.2.8.3.1. Theoretical interpretation

The relation between the rate constant and the working temperature is expressed using the Arrhenius equation, as follows:

$$k = Ae^{\frac{-E_a}{RT}} \quad (6.20)$$

The redox process involves a series of 'n' consecutive steps, with each polymer chain exchanging one electron per step. However, the energy required to remove each electron from the chain varies, depending on the ionization potential. The total energy needed for all n steps is defined as the activation energy of the redox reaction, where A represents the pre-exponential factor, E_a is the activation

energy, R is the universal gas constant (J mol⁻¹ K⁻¹), and T is the temperature (K)

In order to establish a relation between the redox charge consumed per unit mass in the PEDOT redox process and the working temperature, we rearranged equations 6.3, 6.4, 6.6, and 6.20 leading to the following equation:

$$\frac{qv}{F\Delta E} = \frac{Ae^{\frac{-E_a}{RT}}}{m} [Cl^-]^\alpha [PEDOT]_0^\beta = \frac{Ae^{\frac{-E_a}{RT}}}{m} [Cl^-]^\alpha \left(\frac{q}{F}\right)^\beta \quad (6.21)$$

By modifying the equation 6.21 we get;

$$q^{1-\beta} = \frac{A\Delta EF^{1-\beta} [Cl^-]^\alpha e^{\frac{E_a}{RT}}}{\underbrace{vm}_{h'}} \quad (6.22)$$

To account for all the constants associated with the ionic exchange during oxidation/reduction, a new constant 'h' is introduced. This gives rise to a semi-logarithmic correlation between the specific redox charge acquired and the working temperature.

$$\ln(q) = a + b\frac{1}{T} \quad (6.23)$$

Equation 6.23 is a linear equation (y = mx + C) that offers valuable insights into the direct relationship between the redox charge and the working temperature. The intercept and slope values are given as:

$$a = \frac{\ln h'}{1 - \beta} \quad (6.24)$$

$$b = \frac{E_a}{(1 - \beta)R} \quad (6.25)$$

Equation 6.23 is the sensing equation, offering insights into the polymer chain's conformational movements triggered by the reaction at different temperatures. The semi-logarithmic relation between the redox charge and the working temperature indicates that the charge acts as the sensing parameter. The PEDOT can effectively sense the available thermal energy (working temperature) with a sensitivity (slope of the curve) of $-671.1401 \text{ C (T}^{-1}\text{)}^{-1}$ while keeping all the other working variables constant.

The experimental findings are juxtaposed with the theoretical equation, as shown in Figure 6.17(c). Figure 6.17(c) illustrates that the PEDOT responds to or senses the changes in working temperature. The mean energy utilized during the reaction, while electrical, chemical, and mechanical conditions remain constant, was calculated from the redox charge consumed, as depicted in the subsequent equation:

$$U = E \times Q \quad (6.26)$$

Elevating the temperature results in greater charge consumption and, consequently, higher reaction energy leading to a larger reaction extension. This suggests that the polymer reaction demands less energy at higher temperatures. This mechanism explains how the biological muscle of a cold-blooded organism senses the surrounding temperature and conveys this information to the brain through variations in reaction energy at various working temperatures.

6.2.9. Reaction-driven sensing characteristics of PEDOT towards the working ambient (electrical, chemical, and thermal): Chronopotentiometric investigation

PEDOT's reactive sensing capabilities were further verified using chronopotentiometry. Through this method, the rate of reaction, (equation 6.1) and the composition of the polymer material (polymer/counter ion ratio) could be controlled through the flowing current and the charge consumed at any time, leading to a continuous shift in the material's potential. Any physical or chemical changes in the reaction ambient that influence the reaction rate would consequently impact the material's potential evolution^[23, 26]. Thus, the PEDOT can sense the changes in its environment that affect the reaction rate. The PEDOT was subjected to a sequence of square current waves to record the chronopotentiogram. The extent of the reaction was controlled by adjusting the time of the current flow and the amount of redox charge consumed. Before recording the chronopotentiogram, the material was stabilized by potential cycling, and data was collected from 20 consecutive voltammetric cycles. The chronopotentiograms were measured between the same initial and final oxidation states, providing valuable insights into the material's response to changes in its surrounding conditions.

6.2.9.1. Sensing electrical working conditions: Current Sensor

Diverse currents ranging from ± 0.125 mA to ± 1.5 mA were applied consuming a constant anodic and cathodic charge of 6 mC. The

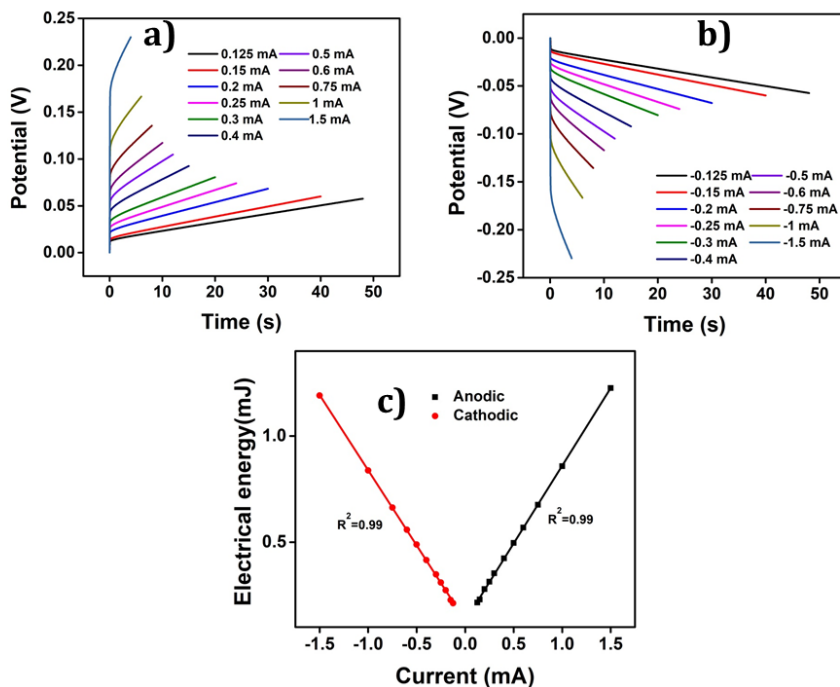


Figure 6.19 Chronopotentiograms obtained when different constant (a) anodic and (b) cathodic currents were applied to PEDOT by passing a constant charge of 6 mC in 1 M NaCl solution (c) Electrical energy consumed by the as a function of applied current (R^2 is the correlation factor)

resulting chronopotentiometric responses are depicted in Figure 6.19.

The consumed electrical energy ($U=I\int Edt$) is obtained by the integration of those chronopotentiograms. From Figure 6.19(c), it was observed that the potential evolved during the redox process increased with an increase in anodic current, while a more negative potential evolved with the increased cathodic current^[27]. The electrical energy consumed during the reaction served as the sensing parameter, being a linear function of both anodic and

cathodic currents. This implies that the material senses the applied current.

6.2.9.2. Sensing chemical working conditions: Concentration Sensor

In order to study the concentration-sensing nature of PEDOT, the chronopotentiometric responses of PEDOT were recorded for varying concentrations of NaCl electrolyte (ranging from 0.01 M to 1 M) at room temperature. A constant charge of 6 mC with a constant anodic current of 0.1 mA during oxidation and a cathodic current of -0.1 mA during reduction (both applied for 60 seconds) was applied. The results are shown in Figure 6.20.

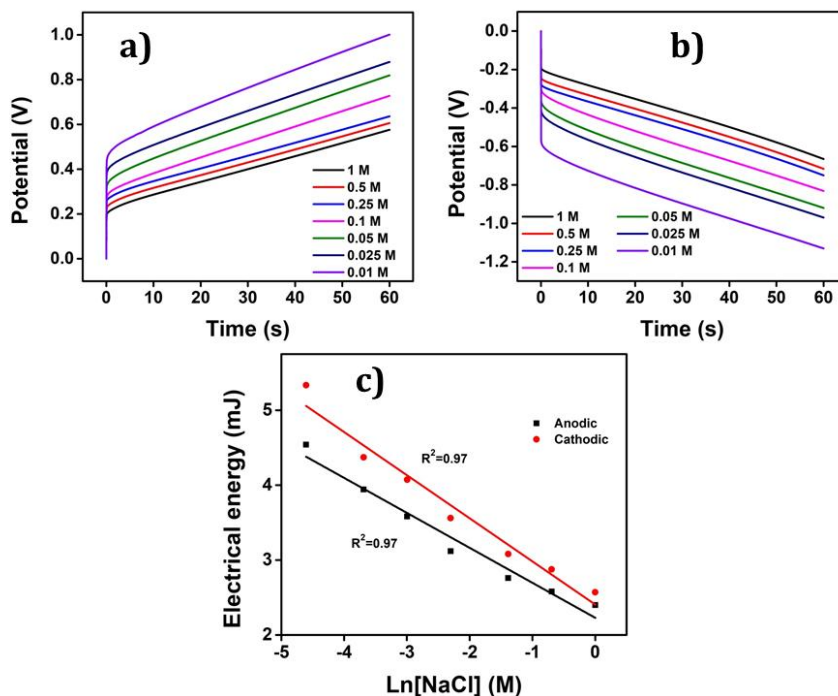


Figure 6.20 Chronopotentiogram obtained from different concentrations of NaCl when **(a)** 0.1 mA and **(b)** -0.1 mA of current were applied to the PEDOT for 60 s. **(c)** Electrical energy consumed by during the reaction as a logarithmic function of electrolyte concentration

Higher concentrations of the electrolyte lead to enhanced reaction rates and lower reaction resistance under constant current for both the anodic and cathodic processes, resulting in a lower potential difference as shown in Figures 6.20(a) and 6.20(b). Conversely, at lower concentrations of the electrolyte, the reaction experiences higher resistance leading to an increase in the potential difference. The semi-logarithmic relation between the concentration and the consumed electrical energy as shown in Figure 6.20(c) confirms that the PEDOT can sense the chemical working condition. The electrical energy consumed during the reaction is considered as the sensing parameter. The oxidation and reduction reactions involving macromolecular motors are asymmetric from an energetic point of view, consuming different energies.

6.2.9.3. Sensing thermal working conditions: Temperature Sensor

The experiment involved the application of consecutive square current waves with a constant charge at various temperatures and the recording of the chronopotentiogram. The PEDOT was submitted to +0.1 mA for anodic and -0.1 mA for cathodic processes for 60 seconds in 1 M NaCl aqueous solution at different temperatures (15 °C to 60 °C). Results are depicted in Figures 6.21(a) and 6.21(b). By integrating the chronopotentiogram, the electrical energy consumed during the reaction was determined, revealing a linear relation with the temperature as shown in Figure 6.21(c). From Figure 6.21(c), it is clear that the consumed electrical energy decreases with the increasing temperature. This is because the available thermal energy is large for higher temperatures.

Therefore, the reaction energy increases by increasing the temperature.

Again, it can be seen that the oxidation and reduction energies are asymmetric. This correlation was further analyzed using a theoretical equation for the evolved potential outside the equilibrium condition, as derived by Otero et al., (Equation 6.33).

The obtained results were elucidated using the Arrhenius concept, which proposes that, with increasing temperature, the polymer chain undergoes more rapid conformational movements, leading to a higher diffusion coefficient^[28]. Consequently, Reaction 6.1 takes place to the same extent under a constant current (constant charge) and time, but at higher temperatures, the available thermal energy is large, resulting in lower energy consumption. It means that in order to get the same reaction extension, every time the conformational movements of the macromolecular motors uses a higher fraction of the available thermal energy when the ambient temperature rises requiring a lower consumption of electrical energy, this fact provides a quantitative approach to the behavior of coldblooded animals: they use thermal energy from the ambient during biological functions based on macromolecular electrochemical motors (muscles, brain functions, and ionic channels in neurons).

The findings show that, during the anodic process, the potential evolution tends to decrease with increasing temperature, whereas, for the cathodic process, the potential evolution becomes less

negative as the temperature increases. This result indicates that PEDOT exhibits temperature-sensing capability.

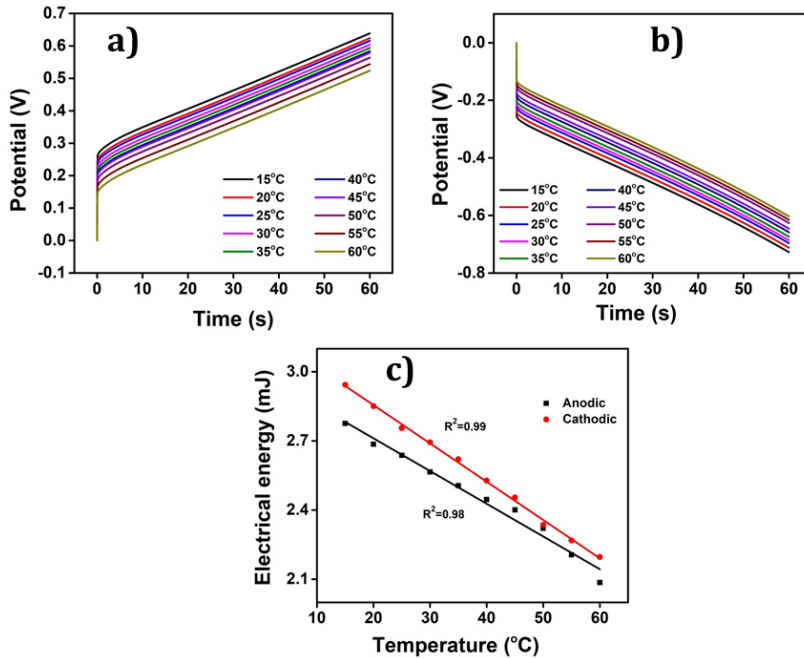


Figure 6.21 Chronopotentiogram obtained from different experimental temperatures when **(a)** +0.1 mA and **(b)** -0.1 mA of current were applied to the PEDOT for 60 s. **(c)** The variation of electrical energy consumed during anodic and cathodic processes with temperature

Theoretical Investigation

Considering the electrochemical reaction (equation 6.1) the Nernst equation employed to represent the potential of the PEDOT electrode under equilibrium conditions is given by^[29]

$$E = E_0 - \frac{RT}{nF} \ln \frac{[A^-][PEDOT^*]}{[(PEDOT)^{n+}(A^-)_n(H_2O)_m]} \quad (6.27)$$

Where E is the evolved potential, E₀ is the standard electrode potential, R is the universal gas constant, and F is the Faraday

constant. The anion concentration is given by $[A^-]$, the concentration of the active polymer centre is represented as $[PEDOT^*]$, and the concentration of the oxidized polymer centre of PEDOT is $[(PEDOT^*)^{n+}(A^-)_n(H_2O)_m]$. The electrochemical redox reaction of PEDOT and other CPs operates outside the equilibrium conditions. Otero et al., have introduced a new interpretation of the Le Chatelier principle for such systems, suggesting that changes in the reaction rate prompt a shift in reaction energy to accommodate the new energetic demands. Consequently, variations in the working energetic conditions of the reaction can be sensed by the material's potential.

The rate of the reaction of the PEDOT can be expressed as:

$$r = k[PEDOT^*]^a[A^-]^b \quad (6.28)$$

The specific reaction rate is denoted by the variable "r", and the kinetic coefficient is represented by "k", "a" and "b" are the reaction orders related to the active polymeric centres and the anion/electrolyte concentration, respectively. When a steady current is applied to the PEDOT electrode material, a correlation between the current and the reaction rate can be established.

$$r = \frac{q}{FV} = \frac{it}{FV} \leftrightarrow i = \frac{rFV}{t} \quad (6.29)$$

The quantities q (charge), i (current), t (time of current flow), F (Faraday's constant), and V (volume of the PEDOT polymer) are interconnected. The Butler-Volmer equation related to electrochemical kinetics is employed to establish the

correlation between the rate constant and the potential evolution for both the anodic and cathodic processes.

$$i_a = FV k_{\alpha} [PEDOT^*]^a [A^-]^b \quad (6.30)$$

$$i_a = FV k_{\alpha 0} [PEDOT^*]^a [A^-]^b \exp\left(\frac{(1-a)nF(E - E_0)}{RT}\right) \quad (6.31)$$

In this context, the potential generated during the reaction relies on various factors, including the electrolyte concentration, applied current, and/or temperature. It is possible to derive an equation to articulate the interrelationship between these factors and the resulting evolved potential.

$$E_a = E_0 + \frac{RT}{(1-a)nF} \left(\ln\left(\frac{i_a}{FV}\right) - b \ln[A^-] - a \ln[PEDOT^*] - \ln k_{\alpha 0} \right) \quad (6.32)$$

Equations 6.31 and 6.32 elucidate the sensor-like behaviour of the PEDOT during the anodic process. A similar equation can be derived for the cathodic process. The material undergoes n consecutive steps during the oxidation process, allowing for the formulation of a comprehensive equation.

$$E_n(t) = E_0 + i_a Z + (n-1)\Delta E + \frac{RT}{(1-a)F} \left\{ \ln\left(\frac{i_a}{FV}\right) - b \ln[A^-] - a \ln\left([PEDOT^*]_{initial} - \frac{i_a t}{FV}\right) - \ln k_{\alpha 0} \right\} \quad (6.33)$$

Equations 6.31, 6.32, and 6.33 give the relation between the electrical energy consumed by the reaction of the material as a function of the experimental variables, such as applied current, electrolyte concentration, and temperature. Here we have proved its reactive sensing ability towards the working

conditions. Thus, the PEDOT demonstrates its potential as an electrochemical sensor, capable of sensing changes in its electrical, chemical and thermal working conditions.

6.3. Conclusion

A chemically synthesized PEDOT was characterized using FTIR, UV-Vis, FE-SEM, HR-TM, EDX, and TGA analysis. The polymer was thoroughly characterized to understand its electrochemical behaviour using cyclic voltammetry (CV), chronopotentiometry, and coullovoltammetry (QV). Further, its structural electrochemistry and biomimetic sensing characteristics with respect to its working energetic conditions were thoroughly explored for the first time.

The CV of PEDOT displays well-defined oxidation and reduction peaks. Using QV we have examined the potential limits of fully reversible faradaic process. A closed QV loop was observed within the potential range of -0.6 V to 0.8 V, indicating that only the reversible redox process occurs within this specific potential window in an aqueous NaCl electrolyte. Thus the potential window for the PEDOT electrochemical reaction was optimized.

The various structural processes i.e., conformational changes such as reduction-shrinking, reduction-compaction, oxidation-relaxation and finally oxidation-swelling during the electrochemical reaction of PEDOT were studied using QV. The slope of the QV provided information regarding different conformational processes and the corresponding charges

consumed during its electrochemical reaction. By doing so, we have aimed to present a comprehensive and insightful account of the structural electrochemistry of the PEDOT and the potential applications of this intriguing material. At potentials beyond -0.6 V, the reversible processes overlap with irreversible reduction as a result of hydrogen evolution, while beyond 0.8 V, a parallel irreversible oxidation process took place due to oxygen evolution and polymer over oxidation. The charges consumed during both the reversible and irreversible processes are accurately calculated using QV, enabling a comprehensive characterization of the electrochemical behaviour of PEDOT.

The sensing behaviour of PEDOT to the working conditions such as electrical, chemical, and thermal conditions was also explored. The material's sensing capabilities were assessed through CV/QV and chronopotentiometry. The evolution of the material potential under the flow of a constant current, (chronopotentiogram), is different, that responds to and senses changes in any of the working parameters: chemical energy (electrolyte concentration), thermal energy (temperature), or imposed electrical conditions. The electrical energy consumed during the reaction obtained from the chronopotentiometric responses is the sensing parameter: the consumed energy decreases linearly with rising temperatures, increases linearly when the imposed current rises, and decreases as a semi-logarithmic function of the rising electrolyte concentrations.

Those experimental results were theoretically described. Whatever the used experimental methodology the oxidation energy and the reduction energy are asymmetric. Those facts indicate a possible reason for the existence of asymmetric biological functions based on the electro-chemo-mechanical actuation of proteins: muscles only work by contraction. Nature has selected and improved the most efficient, energetically, of the two (forward and reverse) reactions.

The responsive sensing ability was also confirmed through the use of voltammetric techniques: CV and QV. The charge consumed by the reaction under different working conditions (electrical or scan rate, electrolyte concentration, and working temperature) followed a logarithmic relationship with the scan rate, or with the electrolyte concentration, and a semi-logarithmic relationship with the inverse temperature. Those facts were described theoretically and validated that the PEDOT-based electrode can sense changes in the working variables, including electrical, chemical, and thermal conditions, using the charge as a sensing parameter.

Whatever the electrochemical methodology used to check those sensing abilities of the reaction, both the signal, the actuating electrical order (potential sweep or constant current), and the sensing response (consumed charge, potential evolution, or consumed electrical energy) are included simultaneously in the only two connecting wires. This unparalleled fact from nowadays technologies replicates

natural muscles, where the actuating signal (brain order) and the sensing signals are sent back during muscular actuation to inform brains about the mechanical, chemical, or thermal working conditions (neuronal signals) which only require two neurons: motor neuron and sensing neuron. Thus our results on PEDOT have further proved that the simultaneous sensing characteristics of CPs are the general property and they can behave as biomimetic sensing motors.

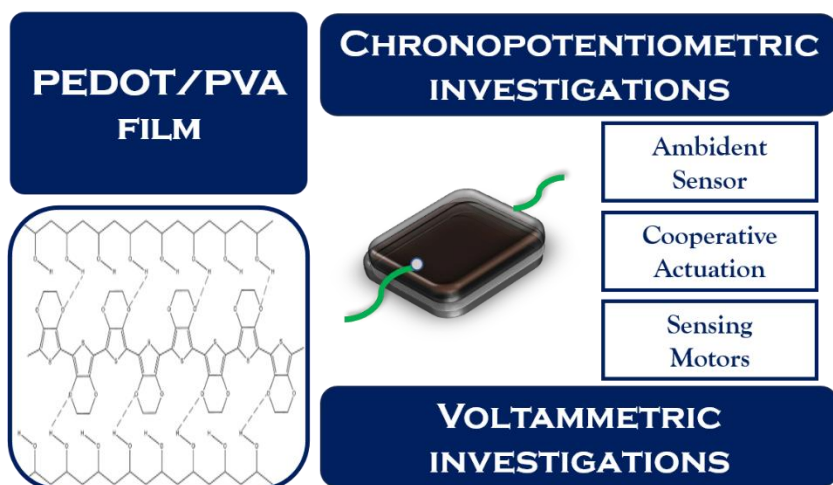
References

- [1] aX. Zhang, J.-S. Lee, G. S. Lee, D.-K. Cha, M. J. Kim, D. J. Yang, S. K. Manohar, *Macromolecules* **2006**, *39*, 470-472; bS. Panigrahy, B. Kandasubramanian, *Eur. Polym. J.* **2020**, *132*, 109726; cN. Paradee, A. Sirivat, *Polym. Int.* **2014**, *63*, 106-113.
- [2] aF. Hu, Y. Xue, J. Xu, B. Lu, *Front. Robot. AI* **2019**, *6*, 114; bH. Okuzaki, H. Suzuki, T. Ito, *Synth. Met.* **2009**, *159*, 2233-2236; cY. Li, R. Tanigawa, H. Okuzaki, *Smart Mater. Struct.* **2014**, *23*, 074010; dH. Okuzaki, S. Takagi, F. Hishiki, R. Tanigawa, *Sens. Actuators B Chem.* **2014**, *194*, 59-63; eS.-S. Kim, J.-H. Jeon, C.-D. Kee, I.-K. Oh, *Smart Mater. Struct.* **2013**, *22*, 085026.
- [3] aZ. Xu, J. Song, B. Liu, S. Lv, F. Gao, X. Luo, P. Wang, *Sens. Actuators B Chem.* **2021**, *348*, 130674; bM. Clevenger, H. Kim, H. W. Song, K. No, S. Lee, *Sci. Adv.* **2021**, *7*, eabj8958; cY. Yang, G. Zhao, X. Cheng, H. Deng, Q. Fu, *ACS Appl. Mater. Interfaces* **2021**, *13*, 14599-14611; dB. A. Kuzubasoglu, E. Sayar, S. K. Bahadir, *IEEE Sens. J.* **2021**, *21*, 13090-13097; eZ. Liu, L. Wu, J. Qian, J. Peng, R. Liu, Y. Xu, X. Shi, C. Qi, S. Ye, *J. Electron. Mater.* **2021**, *50*, 2356-2364.
- [4] aT. Xu, D. Yang, S. Zhang, T. Zhao, M. Zhang, Z.-Z. Yu, *Carbon* **2021**, *171*, 201-210; bF. Niu, X. Han, H. Sun, Q. Li, X. He, Z. Liu, J. Sun, Z. Lei, *ACS Sustain. Chem. Eng.* **2021**, *9*, 4146-4156; cJ. Song, W. Li, K. Song, C. Qin, X. Chen, Y. Sui, Y. Ye, *J. Colloid Interface Sci.* **2021**, *602*, 251-260; dK. S. Ryu, Y.-G. Lee, Y.-S. Hong, Y. J. Park, X. Wu, K. M. Kim, M. G. Kang, N.-G. Park, S. H. Chang, *Electrochim. Acta* **2004**, *50*, 843-847.
- [5] aT. J. Simons, M. Salsamendi, P. C. Howlett, M. Forsyth, D. R. MacFarlane, C. Pozo-Gonzalo, *ChemElectroChem* **2015**, *2*, 2071-2078; bH. Hareendrakrishnakumar, R. Chulliyote, M. G. Joseph, *Ionics* **2021**, *27*, 1087-1099; cC. V. Amanchukwu, M. Gauthier, T. P.

- Batcho, C. Symister, Y. Shao-Horn, J. M. D'Arcy, P. T. Hammond, *J. Phys. Chem. Lett.* **2016**, *7*, 3770-3775.
- [6] aA. G. Guex, J. L. Puetzer, A. Armgarth, E. Littmann, E. Stavrinidou, E. P. Giannelis, G. G. Malliaras, M. M. Stevens, *Acta Biomater.* **2017**, *62*, 91-101; bD. N. Heo, S.-J. Lee, R. Timsina, X. Qiu, N. J. Castro, L. G. Zhang, *Mater. Sci. Eng. C* **2019**, *99*, 582-590; cA. Abedi, M. Hasanzadeh, L. Tayebi, *Mater. Chem. Phys.* **2019**, *237*, 121882.
- [7] aH. Liu, D. Zhao, M. Dai, X. Zhu, F. Qu, A. Umar, X. Wu, *J. Chem. Eng.* **2022**, *428*, 131183; bM. Zhang, W. Yuan, B. Yao, C. Li, G. Shi, *ACS Appl. Mater. Interfaces* **2014**, *6*, 3587-3593.
- [8] M. Reyes-Reyes, I. Cruz-Cruz, R. López-Sandoval, *J. Phys. Chem. C* **2010**, *114*, 20220-20224.
- [9] C. Kvarnström, H. Neugebauer, S. Blomquist, H. Ahonen, J. Kankare, A. Ivaska, N. Sariciftci, *Synth. Met.* **1999**, *101*, 66.
- [10] I. Ivanko, J. Pánek, J. Svoboda, A. Zhigunov, E. Tomšík, *Journal of Materials Chemistry C* **2019**, *7*, 7013-7019.
- [11] M. R. Moraes, A. C. Alves, F. Toptan, M. S. Martins, E. M. Vieira, A. J. Paleo, A. P. Souto, W. L. Santos, M. F. Esteves, A. Zille, *J. Matr Chem A* **2017**, *5*, 3807-3822.
- [12] K. Manivannan, M. Sivakumar, C.-C. Cheng, C.-H. Lu, J.-K. Chen, *Sens. Actuators B Chem.* **2019**, *301*, 127002.
- [13] J. Liu, B. Wei, J. D. Sloppy, L. Ouyang, C. Ni, D. C. Martin, *ACS Macro Lett.* **2015**, *4*, 897-900.
- [14] N. A. B. Ismail, F. Abd-Wahab, W. W. A. W. Salim, in *2018 IEEE-EMBS Conference on Biomedical Engineering and Sciences (IECBES)*, IEEE, **2018**, pp. 330-335.
- [15] aA. R. Hillman, S. J. Daisley, S. Bruckenstein, *Electrochem. Commun.* **2007**, *9*, 1316-1322; bT. F. Otero, J. G. Martinez, K. Hosaka, H. Okuzaki, *J. Electroanal. Chem.* **2011**, *657*, 23-27.
- [16] J. Arias-Pardilla, P. A. Giménez-Gómez, A. de la Pena, J. L. Segura, T. F. Otero, *J. Mater. Chem. B* **2012**, *22*, 4944-4952.
- [17] T. F. Otero, M. Alfaro, V. Martinez, M. A. Perez, J. G. Martinez, *Adv. Funct. Mater.* **2013**, *23*, 3929-3940.
- [18] T. F. Otero, M. Caballero Romero, *Polym. Int.* **2010**, *59*, 329-336.
- [19] aT. F. Otero, J. G. Martinez, M. Fuchiwaki, L. Valero, *Adv. Funct. Mater.* **2014**, *24*, 1265-1274; bJ. G. Martinez, T. F. Otero, E. W. Jager, *Langmuir.* **2014**, *30*, 3894-3904.
- [20] T. F. Otero, *RSC Adv.* **2021**, *11*, 21489-21506.
- [21] T. F. Otero, J. G. Martinez, *Adv. Funct. Mater.* **2014**, *24*, 1259-1264.
- [22] T. F. Otero, H.-J. Grande, J. Rodríguez, *J. Phys. Chem. B* **1997**, *101*, 3688-3697.
- [23] Y. A. Ismail, J. G. Martínez, A. S. Al Harrasi, S. J. Kim, T. F. Otero, *Sens. Actuators B Chem.* **2011**, *160*, 1180-1190.
-

- [24] T. F. Otero, S. Beaumont, *Sens. Actuators B Chem.* **2018**, 263, 493-501.
- [25] T. F. Otero, S. Beaumont, *Sens. Actuators B Chem.* **2017**, 253, 958-966.
- [26] Y. A. Ismail, J. G. Martínez, T. F. Otero, *Electrochim. Acta* **2014**, 123, 501-510.
- [27] T. Otero, M. Cortes, *Sens. Actuators B Chem.* **2003**, 96, 152-156.
- [28] T. F. Otero, J. J. Sanchez, J. G. Martinez, *J. Phys. Chem. B* **2012**, 116, 5279-5290.
- [29] Y. A. Ismail, J. G. Martinez, T. F. Otero, *J. Electroanal. Chem.* **2014**, 719, 47-53.

Cooperative actuation of PEDOT/PVA hybrid film and its applicability as a biomimetic sensing macromolecular motor



Here we present the electrochemical reactions of PEDOT/PVA hybrid films which can act as a mechanically stable flexible freestanding electrode material to explore and quantify the ability of those reactions of polymer chains (macromolecular motors) to sense during the reaction, its working chemical, electrical, or thermal conditions. The origin of its simultaneous sensing signal was analyzed and, translated to similar parallel biological functions. A sensing supercapacitor was designed. The charge storage capacity and the simultaneous sensing property during the discharging of the PEDOT/PVA film and an integrated solid-state device also were explored.

7.1. Introduction

Life is chemistry, in fact, electro-bio-chemistry. But nowadays chemical kinetic models cannot provide any quantitative description of brain functions, proprioception, or even basic muscular sensing-actuation. The question is what must we look at in order to understand and quantify basic elements from life functions? At the moment most of the approaches are through physical elements as neuronal networks^[1]. A basic biological function as muscular action is originated by an electric pulse triggering chemical reactions in the muscle cell involving macromolecular motors, i.e., actin and myosin, ions (ATP, Ca²⁺), and water exchange with the surroundings^[2]. From that point of view, any artificial material constituted by reactive polymeric chains responding to electric pulses by changing conformations with exchange, during reactions, of ions and water molecules with its surroundings could be considered as a basic material model system to understand those biological ones. Their reactions could be used to explore and quantify any of its reactive biomimetic functions or its multifunctionality that can replicate some of the similar functions during the actuation of biological organs.

The biomimetic reactive sensing property and the detailed exploration of PEDOT's structural changes of PEDOT have been explored in the previous chapter. However, an in-depth exploration of the PEDOT's electrochemical nature and structural changes during its electrochemical reactions has remained unexplored^[3]. We have proved that the PEDOT have the ability to sense and respond

to changes in its distinctive electrochemical reaction's electrical, chemical, and thermal conditions^[4]. The potential uses of this powder material have been restricted due to its inferior mechanical properties^[5]. Thus, in this present work, we have employed a PVA hydrogel film as a template to fabricate a mechanically stable flexible PEDOT/PVA hybrid film. This has been carried out via in-situ chemical polymerizations in aqueous medium. This has resulted in a highly, flexible PEDOT/PVA film having commendable mechanical stability^[6]. The biocompatible and non-toxic nature of the PVA film complements the PEDOT, making it suitable for biological applications^[7]. The optimal technique for fabricating such kind of material has been discussed in the previous chapter (Chapter 5)^[8]. Here we present the PEDOT-PVA hybrid film as a model reactive material capable of emulating the functionalities of the reactive elements in biological organs: macromolecular electro-chemical motors, ions, and solvent. The electrical energy consumed during its electrochemical reaction senses at any reaction time any variation in the electrical (current), chemical (electrolyte concentration), or thermal (temperature) conditions^[9]. The sensing magnitude is the potential evolution of the reacting material during actuation. The sensing equations were attained. Both magnitudes, the current driving the reaction, and the sensing signals (the potential evolution) are embedded simultaneously in the only two connecting wires, mimicking brain-motor neuron-muscle-sensory neuron connections. If translated to parallel biological functions the results point to a quantitative description of muscular tiredness: the same

reaction amplitude requires higher energies under lower concentrations of one of the reactants, i.e., ATP. The consumed reaction energy decreases when the reaction temperature increases for the same reaction amplitude, indicating the parallel saved energy by cold-blooded animal organs. If the reaction energy of the macromolecular motors adjusts instantaneously to any energetic (thermal, electrical, chemical, or mechanical) condition each of those components should act on the concomitant sensing ionic channels (chemical, thermal, piezo) of the dendrites from the sensory neurons to generate the quantitative information required to inform the brain.

Additionally, the cooperative actuation of the film and how the changes in working electrical, chemical, and thermal energetic conditions affect the cooperative actuation of the film were also explored for the first time. The electrochemical reaction of PEDOT chain in PEDOT/PVA hybrid film, which occurs in a series of 'n' consecutive steps, is responsible for this cooperative actuation i.e., the reversible conformational changes of the polymer chain. As a result, the film can act as a multistep macromolecular sensor for diverse working conditions^[10].

The charge storage ability of the film was also investigated. The electrochemical reaction that accounts for the film's sensing ability towards its working conditions was used to explore its charge storage capability. This interesting feature of the film emphasizes a new technological domain for the design of an integrated device that can simultaneously perform both charge storage and sensing of

working energetic conditions without requiring additional connectivity. Accordingly, we explored the ability of PEDOT/PVA film to store the energy while simultaneously working as a sensor of its working energetic condition. Thus, we have fabricated a sensing supercapacitor capable of sensing the electrical energetic condition using the same two connecting wires. An integrated solid-state device is fabricated to demonstrate the simultaneous sensing and charge-discharge ability of the PEDOT/PVA film. Additionally, the device's capability to sense both electrical and thermal conditions was also investigated without any additional connectivities.

7.2. Results and Discussions

7.2.1. FTIR-ATR spectra

The FTIR-ATR spectra of the PVA and PEDOT/PVA films are shown in Figure 7.1. Spectra show the characteristic peaks of PEDOT at 1687 cm^{-1} , 1401 cm^{-1} , and 1583 cm^{-1} , corresponding to S-H stretching and asymmetric stretching of C=C in the thiophene ring. Additionally, absorption peaks at 972 cm^{-1} and 827 cm^{-1} are

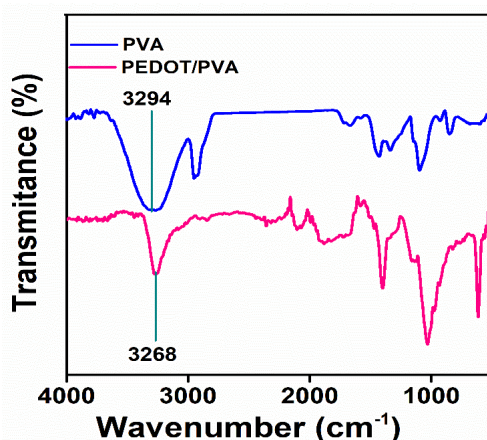


Figure 7.1 FTIR-ATR spectra of PVA and PEDOT/PVA hybrid films

associated with the vibration of the C–S bond in the thiophene ring. The OH absorption peak of PVA underwent a red shift from 3294 cm^{-1} to 3268 cm^{-1} , indicating hydrogen bonding between the PEDOT and PVA chains^[11].

7.2.2. FE-SEM and EDX analysis

The surface morphology of the films was studied using FE-SEM, shown in Figure 7.2 (a) and (b). The PEDOT grown on the surface of the PVA film as an agglomerated granular morphology. An uneven, clustered structure of the PEDOT adhered to the PVA film indicates the polymer's amorphous nature. The effective dispersion of PEDOT on the PVA film may be due to the repulsive forces generated between the micelles formed by the CTAB surfactant during polymerization and the positively charged PEDOT chains. The agglomerated granules are interlinked smoothly and exhibit

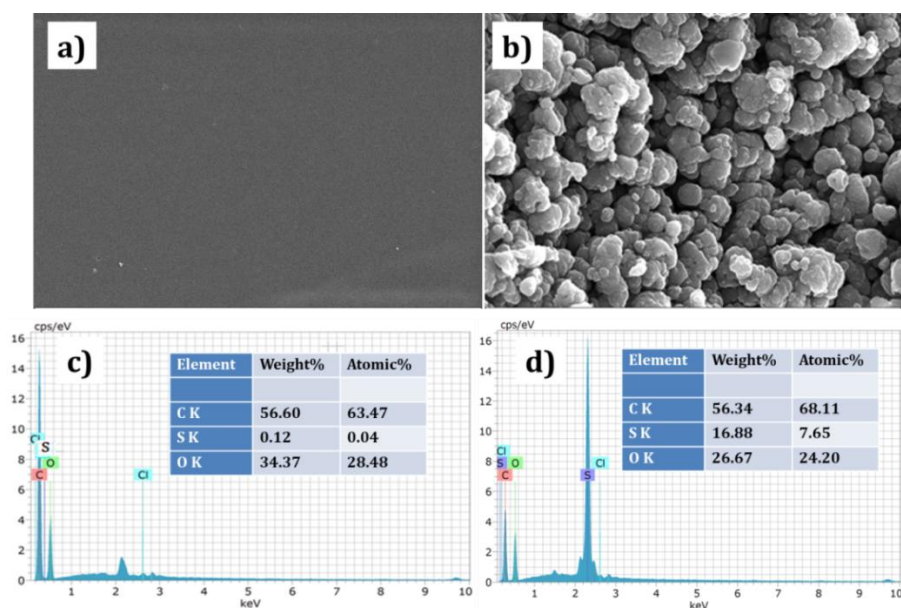


Figure 7.2 FE-SEM images of **a)** PVA **b)** PEDOT/PVA and EDX of **c)** PVA **d)** PEDOT/PVA

sufficient porosity to facilitate the exchange of anions and solvent molecules between the film and the electrolyte^[12].

Figure 7.2 (c) and (d) show the results of the EDX elemental analysis. The enhancement of the percentage of sulfur content in PEDOT/PVA film confirms the presence of PEDOT in the PVA film.

7.2.3. TGA analysis

Figure 7.3 shows the thermograms of the films. In the case of the PEDOT/PVA film, a three-stage weight loss is observed. The first stage of weight loss, up to 140 °C, corresponds to the expulsion of water molecules. The second stage of weight loss is observed up to 280 °C which is due to the removal of low molecular weight oligomers and dopant ions. Polymer chain degradation starts at 320 °C. Conversely, the bare PVA film exhibits a two-stage weight reduction as depicted in the figure. The initial stage encompasses the elimination of water between 75 °C and 130 °C. Degradation of the polymer backbone is observed from 358 °C^[13].

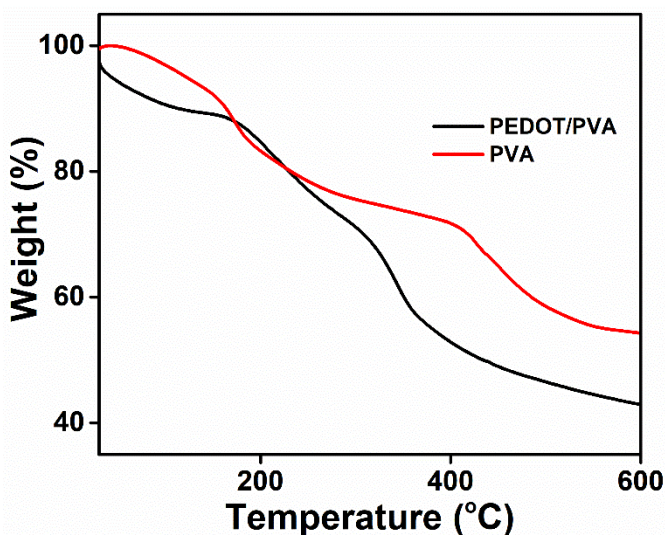


Figure 7.3 TGA of PVA and PEDOT/PVA films

7.2.4. Mechanical characterization- UTM analysis

The mechanical properties of the bare PVA and PEDOT/PVA films were studied in dry and wet conditions using a universal testing machine. The properties such as Young's modulus, tensile strength, and percentage elongation at break were investigated by applying a stationary stretching force to the samples. The stress-strain curves of the films in both wet and dry conditions are shown in Figure 7.4 and the measured parameters are given in Table 7.1. From the figure and table, it is clear that the tensile strength and Young's modulus of the PEDOT/PVA film are larger than that of the bare PVA film both in dry and wet conditions, owing to the robust hydrogen bonding interaction between PVA and PEDOT^[12].

Table 7.1 *The Mechanical properties of the bare PVA and PEDOT/PVA film in dry and wet state*

Properties	Bare PVA film (dry state)	PEDOT/PVA hybrid film (dry state)	Bare PVA film (wet state)	PEDOT/PVA hybrid film (wet state)
Tensile strength(N/mm ²)	15.7157	19.6550	0.3294	1.8851
Young's modulus(N/mm ²)	0.1064	0.1899	0.0009	0.0076
% Elongation	147.6640	103.4906	348.2376	245.6067

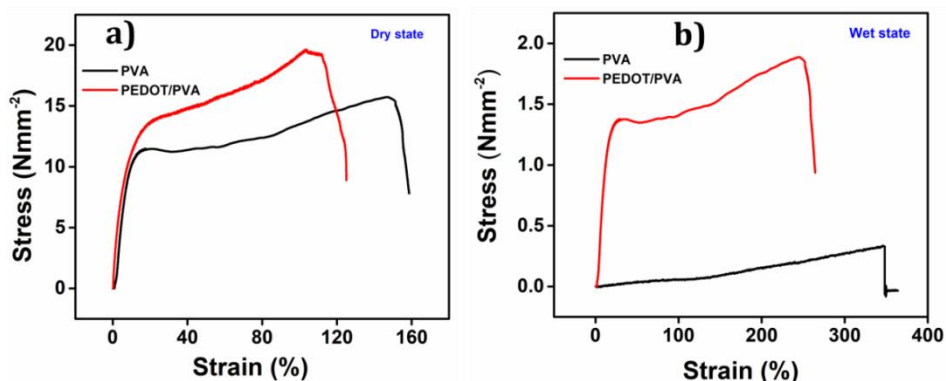


Figure 7.4 Stress-strain relation curve of the films (a) in dry state (b) In wet state

7.2.5. Electrochemical characterization

7.2.5.1. Voltammetric analysis

The CV of the PEDOT/PVA film was recorded using a three-electrode cell setup at room temperature. The PEDOT/PVA film fixed on the Pt wire is used as the working electrode. An Ag/AgCl electrode and a platinum wire were used as the reference electrode and counter electrode respectively^[14]. The potential was cycled between -0.6 V and 0.845 V in 1 M NaCl aqueous solution at a scan rate of 25 mVs^{-1} .

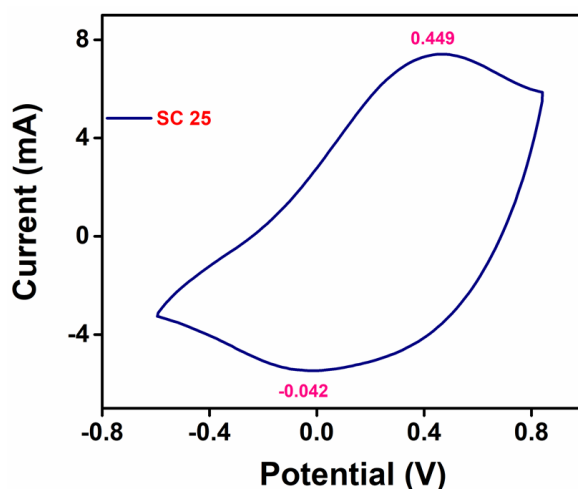


Figure 7.5 CV of PEDOT/PVA film

The stationary CV recorded after 10 consecutive potential cycles is shown in Figure 7.5^[15].

The oxidation of the polymer chain due to the extraction of one electron per step generates positive charges (polarons) on the PEDOT chains changing the redistribution of double bonds along the polymer chain and promoting reaction-driven conformational movements. Here each polymer chain acts as a macromolecular electrochemical motor^[16]. The cooperative actuation of the macromolecular motors generates the required free volume through interchain channels for the entrance of the counter ions $(Cl^-)_{sol}$ ^[17]. This is required to keep the material charge balanced at any reaction time. The rising concentration of anions breaks the osmotic balance between the film and the electrolyte: solvent molecules (H_2O) penetrate from the solution balancing the osmotic pressure arising from the anion insertion^[18]. The polymer film swells during oxidation and becomes a dense gel. The swelling process is very fast, and only takes a few seconds, in contrast to the time required (hours to days) for the commodity polymers to swell and/or dissolve in good solvents. Here the full process is accelerated by the fast reaction-driven conformational movements of the polymeric motors. The extraction of 'n' electron takes place through 'n' consecutive steps during the oxidation, represented by the term 'ne' in reaction 6.1.

The material composition, i.e., chemical macromolecular motors, ions, and water, and the involved events, i.e., reaction-driven actuation of the macromolecular motors, ionic flow through ionic

channels and osmotic balance, replicate both, the composition and consecutive events taking place in functional cells (muscle contraction, ionic channel actuation, and so on) to originate biological functions. In this way, the reactive PEDOT/PVA film can be considered as a material model of the functional biological reactions and properties. Here we are interested in exploring the multi-sensing properties of the reaction involving macromolecular motors as a reactant, trying to explore the replication of parallel multi-sensing properties of biological organs during actuation and some other characteristics of biological functions.

Reverse processes occur during the polymeric reduction: electrons are injected into the polymer chains the polymer shrinks by cooperative actuation of the macromolecular motors originating the expulsion of counter ions and solvent. Thus the reaction-driven cooperative actuation of the macromolecular motors gives macroscopic structural change starting from the most packed conformational structure of an ideal neutral polymer (high polymer-polymer interactions) initiating a structural relaxation and swelling to an open structure of the oxidized material. Reverse structural changes occur during reduction.

The reaction mechanism requires the entrance of counter ions from the solution inside the polymer film through the ionic channels generated by the reaction-driven conformational movements of the chains. The fundamental question is which the rate-limiting process is: the ion migration-diffusion through the channel or the conformational movements required to open those ionic channels?

The material was submitted to consecutive potential cycles at different scan rates. Figure 7.6(a) shows the attained stationary voltammetric responses. The fast shift of the anodic and cathodic maxima toward higher anodic and cathodic potentials corroborates the presence of some rate-limiting step inducing higher reaction resistances at higher scan rates. Taking the current at the anodic or cathodic maxima (or at the end of the anodic sweep for the higher scan rates) Figure 7.6(b) discloses that both anodic and cathodic peak currents follow a linear relationship with the square root of the scan rates. This indicates that up to 200 mVs^{-1} , oxidation/reduction reactions occur under diffusion kinetic control of the counter ions through the opening of intrachain ion channels.

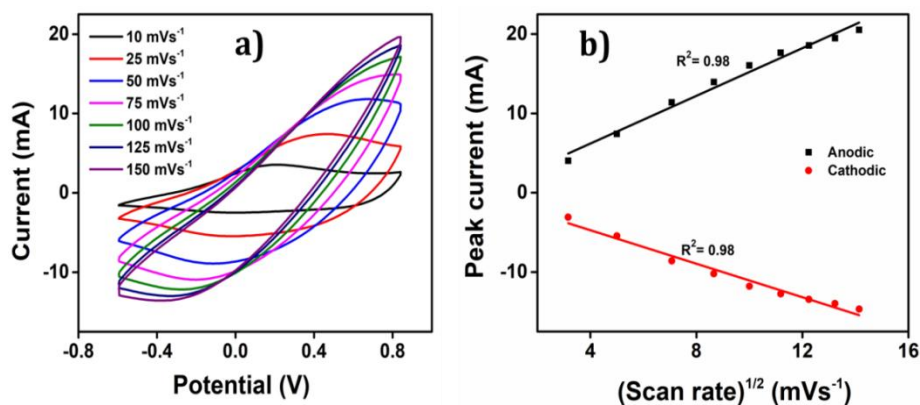


Figure 7.6 (a) CVs of PEDOT/PVA film at different scan rates. **(b)** Linear fit of anodic and cathodic peak currents with the square root of scan rates

7.2.5.2. Coulovoltammogram

The QV obtained from the corresponding CV is shown in Figure 7.7. The QV represents the evolution of the charge consumed by the concomitant reaction (oxidation, positive charge shift, or reduction,

negative charge shift) with the applied potential. The closed loop indicates that the charge consumed by the polymer oxidation reaction equals the charge consumed by the reduction reaction without the presence of any other parallel reaction in the studied potential range. The reversible redox charge consumed during the reaction determines the extension of the reaction^[19].

The great asymmetry (shape of slope variations) of the QV oxidation v/s reduction responses in Figure 7.7 indicates the presence of deep reaction-induced structural changes and slope variations. This allows the identification of some of those structural processes taking place in the polymer film as the reduction-shrinking, reduction-compaction, oxidation-relaxation, and oxidation-expansion^[16b]. The reverse reaction-driven volume variation replicates muscle contraction/relaxation, but in natural muscles, the asymmetry between actuation and relaxation is still greater requiring the actuation (contraction) of a second (antagonist) muscle to relax the muscle contracted earlier.

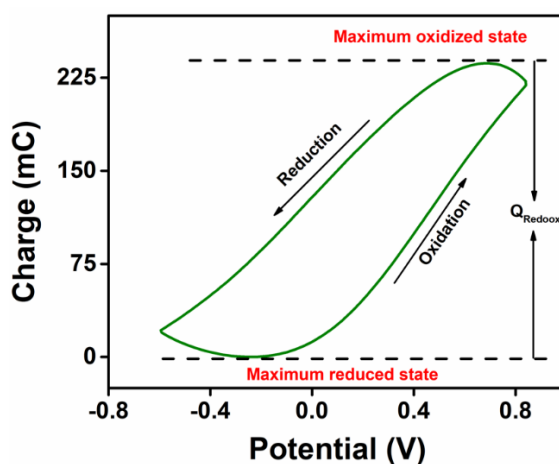


Figure 7.7 Coullovoltammogram of PEDOT/PVA

7.2.5.3. Sensing capability of PEDOT/PVA film electrode towards the working ambient using chronopotentiometry

The ability of the PEDOT/PVA film to sense its working energetic conditions was studied through chronopotentiometric analysis. By applying consecutive anodic and cathodic square current waves, the reaction rate and the shift of the polymer material composition polymer/counterion were monitored by following the potential evolution during the reaction. Any physical or chemical variable affecting the reaction rate has a strong influence on this potential therefore the material can respond to or sense, those variables, being the potential evolution as the sensing parameter [20].

Before recording the chronopotentiogram the film was stabilized by subjecting it to 20 consecutive potential cycles and consecutive square current waves were applied to the PEDOT/PVA film. The film was submitted to a constant reaction extension, imposed by the time of each constant current flow to apply a constant charge, from the same initial reduced state to the same final oxidized state.

7.2.5.3.1. Sensing of electrical working condition-current sensor

The electrical working condition sensing characteristics of the PEDOT/PVA film were studied by applying different constant currents ranging from ± 0.1 mA to ± 1.5 mA at a constant charge of 6 mC. The normalized chronopotentiometric responses are shown in Figure 7.8. The electric energy consumed during the reaction was calculated using the equation $U = I \int E dt$. The consumed electrical energy changes linearly as a function of

both, the anodic and the cathodic currents as shown in Figure 7.8(c): the consumed energy senses the applied current. For any electrochemical reaction, the consumed electrical energy at any time of the electrode reaction describes the reaction energy inside the material at that time. Thus figure 7.8(c) indicates that at any reaction time, the reaction involving macromolecular motors (artificial or natural) senses the electrical energetic conditions, being the origin of the concomitant sensing signal, the material potential here or the actuation of the concomitant ionic channel to send information to the brain in natural

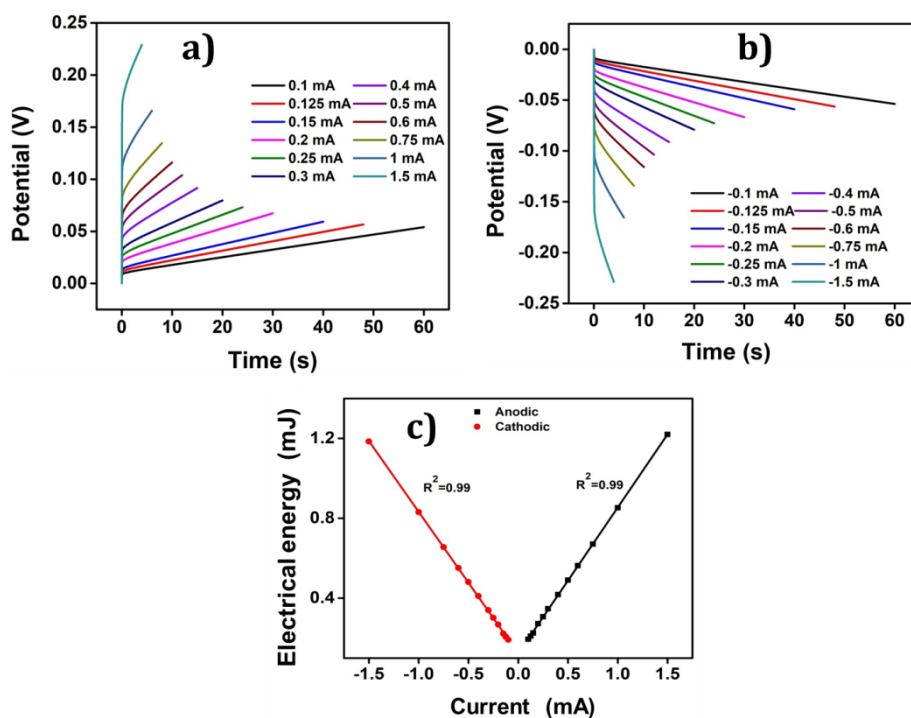


Figure 7.8 Chronopotentiograms obtained when different constant (a) anodic and (b) cathodic currents were applied to PEDOT/PVA hybrid film by passing a constant charge of 6mC in 1M NaCl solution (c) Electrical energy consumed by the film as a function of applied current (R^2 is the correlation factor)

muscles. This hypothesis for natural muscles, if corroborated should clarify an important aspect of the organs/brain communication. The Nobel Prize in Medicine 2021 was awarded to Professors Julius and Patapoutain for their discovery of the ionic channels acting as thermal and mechanical transducers in nerves generating the ionic pulses informing the brain^[21]. The unsolved point is where the energy required for their actuation comes from. If translated to internal organs figure 7.8(c) should give the response: from the reaction energy involving macromolecular motors in the actuating cell, i.e., muscle cells.

7.2.5.3.2. Sensing of chemical working condition - concentration sensor

Figures 7.9(a) and 7.9(b) show the normalized and stationary chronopotentiometric responses of the PEDOT/PVA film for different NaCl concentrations, (ranging from 0.01 M to 1 M). A constant charge of 6 mC is maintained by the flow of a constant anodic current of 0.1 mA and a constant cathodic current of -0.1 mA for 60 seconds at room temperature. Constant currents mean constant Faradaic reaction rates. The material oxidizes during the anodic current flow and reduces during the cathodic current flow attaining a stationary state after the application of two to three consecutive square current waves.

The electrical energy consumed during the reaction is the sensing parameter that follows a semi-logarithmic dependence of concentration as shown in Figure 7.9(c). As for most of the reactions

involving artificial macromolecular motors as reactants [22], the oxidation and reduction reactions are symmetrical from the charge consumption point of view. The oxidation and reduction reactions consume the same charge (6 mC here) but are asymmetrical from the point of view of the energetic consumption. From Figure 7.9(c) it can be seen that the polymeric reduction consumes higher energy, whatever may be the experimental concentration be. Those experimental asymmetries are due to the asymmetry of the concomitant reaction-driven conformational movements of the macromolecular motors (relaxation-swelling vs shrinking-

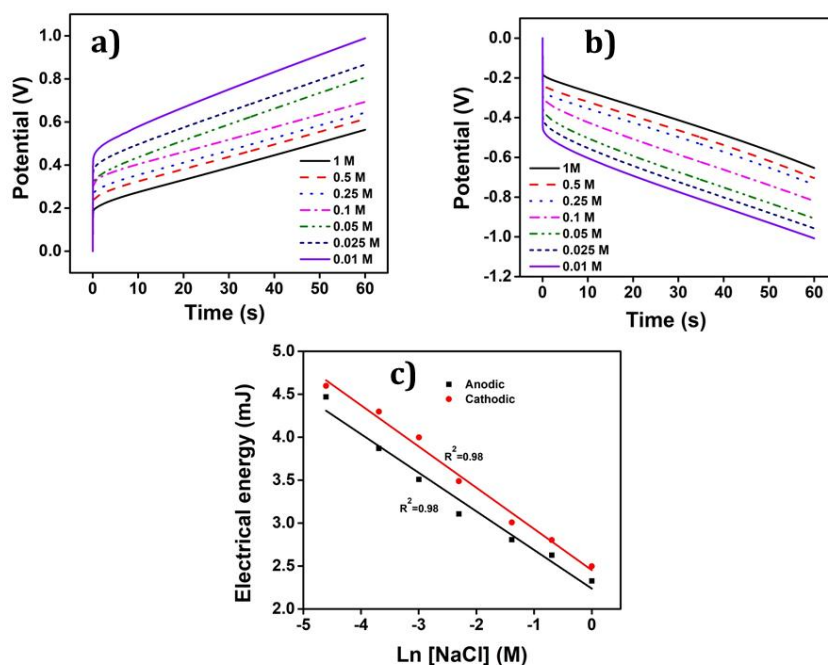


Figure 7.9 Chronopotentiogram obtained from different concentrations of aq. NaCl when **(a)** 0.1 mA and **(b)** -0.1 mA of current were applied to the PEDOT/PVA film for 60 s. **(c)** Electrical energy consumed during the reaction as a logarithmic function of electrolyte concentration

compaction). If translated this concept to similar biological systems suggests why biological functions based on reactions driving macromolecular protein motors (muscles, ionic channels, and so on) only work by contraction or allow only unidirectional ionic flow. Among the two possibilities of any initial reaction (forward and backward) involving macromolecular motors. Mother Nature has selected and improved the most efficient from an energetic point of view..

For a constant reaction extension (same consumed charge) the required energy decreases when the reactant concentrations increase: the energy consumed for the same reaction extension involving the cooperative actuation of macromolecular motors decreases when the chemical energy (concentration or chemical potential) of the reaction ambient increases. This fact could indicate the way to get a quantitative description of muscle tiredness after working for a long period of time (low ATP concentration in the muscle cells).

Again the reaction energy includes, at any reaction time, quantitative information about the working chemical conditions providing this quantitative information to the evolution of the material potential. If translated to biological organs this quantitative information should act on the concomitant ion channel of the sensing neuron dendrite to generate the ionic signal informing the brain about those chemical conditions (such as muscle tiredness). The origin of those sensing (chemical, thermal, and mechanical) signals is still unknown as mentioned above.

7.2.5.3.3. Sensing of thermal working condition-temperature sensor

Following a similar procedure the PEDOT/PVA electrode was submitted to consecutive square current waves of +0.1 mA (anodic) and -0.1 mA (cathodic) currents for 60 seconds each, in 1 M NaCl aqueous solutions at different temperatures ranging from 15 °C to 60 °C. Figures 7.10(a) and 7.10(b) show the stationary and normalized anodic and cathodic chronopotentiometric responses. Figure 7.10(c) shows that the electrical energy consumed by each reaction is a linear function of the experimental temperature. Figure 7.10(c) indicates that decreasing energies are consumed to perform the same reaction extension as the thermal energy of the reactor increases. In this case, this is the expected Arrhenius effect for any chemical reaction improved by the fact that rising thermal energies support faster conformational movements of the polymeric electrochemical motors (the polymer chains) with the concomitant faster free volume generation/destruction and faster entrance/expulsion of counterions and solvent molecules required for charge and osmotic balances. This is translated to natural muscles of ectotherm animals. Figure 7.10(c) may indicate a possible way for the quantification percentage of the chemical energy saved to perform the same activity of any animal organ at higher body temperatures. Also, it can explain that having normal activity at a low body temperature should consume very fast any stored energy source, becoming noncompatible with life: hibernation is the biological solution to save energy and life.

Any way the reaction energy responds, or senses, at any time any thermal change of the reaction providing this information to the evolution of the material potential. If this property of the reactions involving the actuation of macromolecular motors can be translated to biological functions, the thermal component of the functional reaction energy should act on the ion channels from the sensing neuron generating the nerve pulse and translating to the brain this quantitative information.

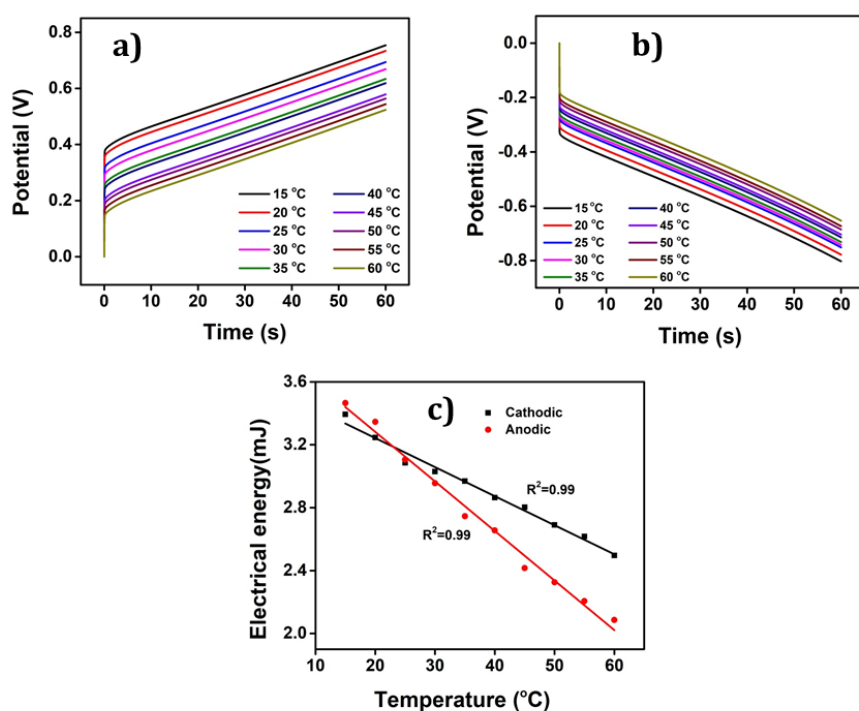


Figure 7.10 Chronopotentiogram obtained from different experimental temperatures when **(a)** +0.1 mA and **(b)** -0.1 mA of current were applied to the PEDOT/PVA film for 60 s. **(c)** The variation of electrical energy consumed during anodic and cathodic processes with temperature

As a result of these electrochemical reactions the PEDOT/PVA film becomes a dense gel constituted by macromolecular electrochemical motors ions and water. This dense gel mimics the basic components of those cells whose reactions originate biological functions. The PEDOT/PVA film was used here as a model reactive material for the parallel exploration and quantification of biological functions.

7.2.5.4. Cooperative actuation induced sensing ability of PEDOT/PVA film towards the working electrical, chemical, and thermal ambient using voltammetric study.

The concept of cooperative actuation is explained in detail in Chapter 5. The origin of these sensing capabilities of all these CP materials is the cooperative actuation. This concept is proved in the preceding section. The cooperative actuation of the PEDOT/PVA film is similar to the cooperative actuation of the muscle sarcomere. The command from the brain controls the conformational movement taking place in the natural muscles^[23]. The biological muscles work under the driving force of electrochemical reaction-induced cooperative actuation of the protein-constituted sarcomere^[24]. The PEDOT/PVA film is a macromolecular motor that can mimic this biological property during its electrochemical reaction. From the energetic point of view, it is clear that the cooperative actuation of the muscle sarcomere is irreversible whereas the PEDOT/PVA film undergoes reversibly.

The surrounding working energetic condition of both biological and artificial muscles has an influence on this conformational movement and consumed charge during the reaction. Therefore, the

PEDOT/PVA can respond to or sense working energetic conditions through their cooperative actuation.

7.2.5.4.1. Cooperative actuation of PEDOT/PVA film senses the electrical working condition

To explore how electrical working conditions influence the electrochemical reaction of the polymer's active center, we have analyzed the voltammetric response for different scan rates while keeping electrolyte concentration and temperature constant. The conformational movement at different electrical working energetic conditions is examined here. The following

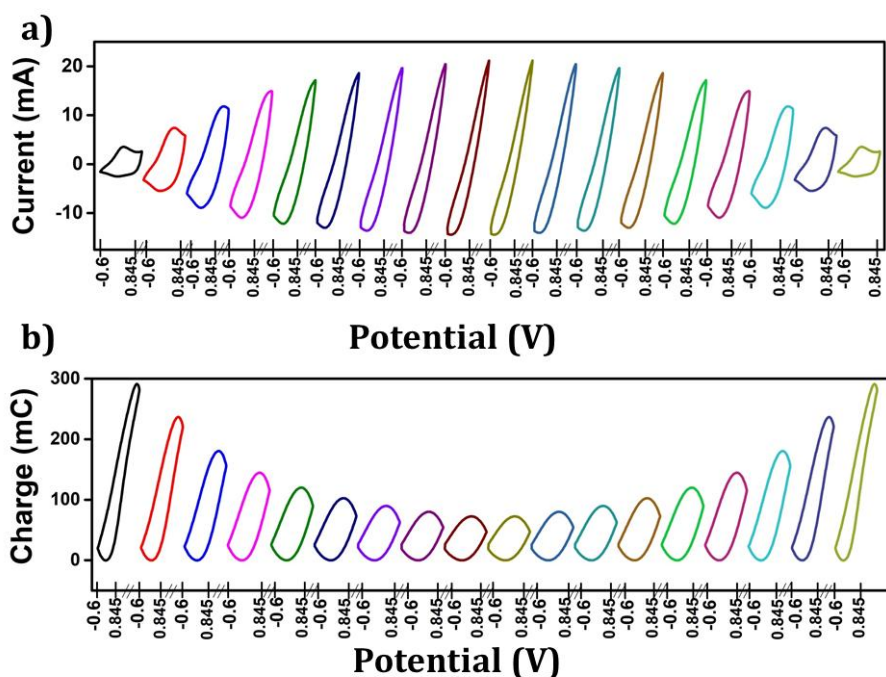


Figure 7.11 (a) CVs obtained from PEDOT/PVA film at different experimental scan rates in increasing (5 mVs^{-1} to 200 mVs^{-1}) and decreasing (200 mVs^{-1} to 5 mVs^{-1}) scan rate in 1M NaCl at room temperature. (b) Corresponding QVs

consecutive steps were employed to study the influence of electrical working conditions^[25].

The stable voltammetric responses were recorded, for the PEDOT/PVA film between the potential window of om -0.6 V to 0.845 V, at a scan rate of 10 mVs⁻¹, in 1 M NaCl solution at room temperature. Subsequently, the film was subjected to another set of three consecutive cycles under the same potential window at a control scan rate of 50 mVs⁻¹, in order to attain a stable voltammetric response (Figure 7.12(a)). This entire procedure was then repeated for various scan rates, first for increasing and then for decreasing order that is, from 10 mVs⁻¹ to 200 mVs⁻¹ then from 200 mVs⁻¹ to 10 mVs⁻¹ (10, 25, 50, 75, 100,

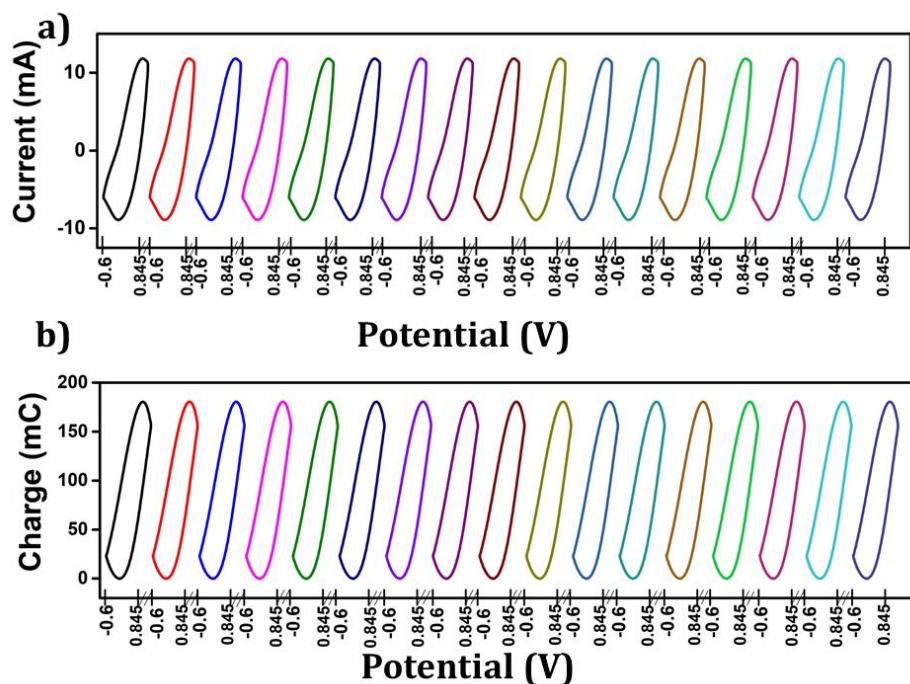


Figure 7.12 a) CVs obtained from PEDOT/PVA film in a control scan rate (50 mVs⁻¹) in 1M NaCl at room temperature. **b)** Corresponding QVs

125, 150, 175, 200, 200, 175, 150, 125, 100, 75, 50, 25, and 10). The resulting CVs are shown in Figure 7.11(a).

From Figure 7.11(a) it is clear that, as the scan rate increases, both anodic and cathodic peak current increases. The corresponding QVs are shown in Figure 7.11(b). The figure clearly shows that the redox charge consumed during the reaction decreases as scan rates increase. This is attributed to the fact that at lower scan rates, a significant conformational change in the polymer chain is observed. This is due to the extended time required for the oxidation/reduction of the polymer chain. This results in the generation/removal of a substantial volume within the film to accommodate/expel the counter anions and solvent molecules respectively. Thus the charge consumed during the reaction is higher for lower scan rates.

The film's electroactivity remains constant, as evidenced by the 'control' voltammetric response obtained at 50 mVs^{-1} between two consecutive scan rates, as shown in Figure 7.12(a). The stationary QVs corresponding to the 'control' voltammetric response are shown in Figure 7.12(b). The overlapping QV responses confirm that the same charge is consumed for each control scan rate. Thus the experimental results confirm that the conformational movements of the macromolecular motors of PEDOT/PVA film are reversible, i.e., the cooperative actuation of the film is reversible.

The logarithmic relation (displayed as a straight line) between the consumed redox charge and the scan rate, as shown in

Figure 7.13, suggests that the PEDOT/PVA film can sense the electrical working condition. The consumed redox charge is the sensing parameter. The experimental results corroborate with the theoretical equation 6.21.

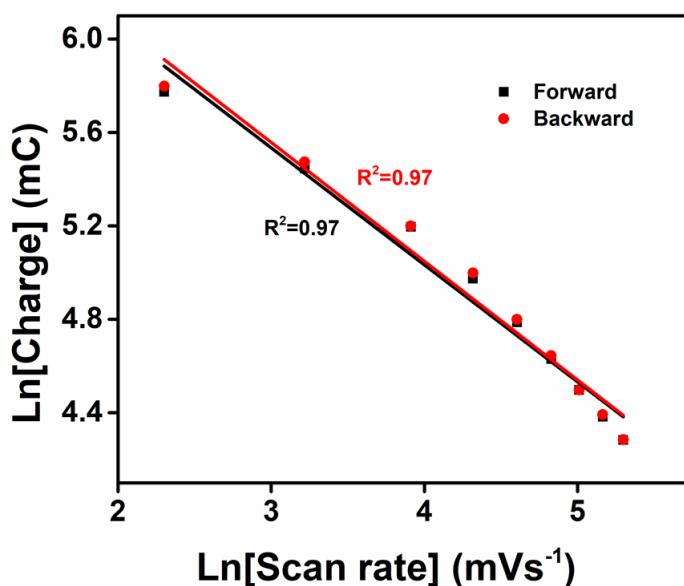


Figure 7.13 Logarithmic relation of redox charge consumed during the forward and backward reaction of PEDOT/PVA film obtained from the coullovoltammogram with the scan rate

The results suggested that the conformational changes induced by the electrochemical reaction of the PEDOT/PVA film lead to less conformational movements (reduced reaction extension/less redox charge usage) for higher scan rates analogous to the smaller conformational movement of the sarcomere under faster muscular motion.

The conformational changes in the film at different scan rates are shown in Figure 7.14. It can be seen from the figure that the

reaction extension/charge consumed during the reaction is smaller at 200 mVs^{-1} and larger at 10 mVs^{-1} .

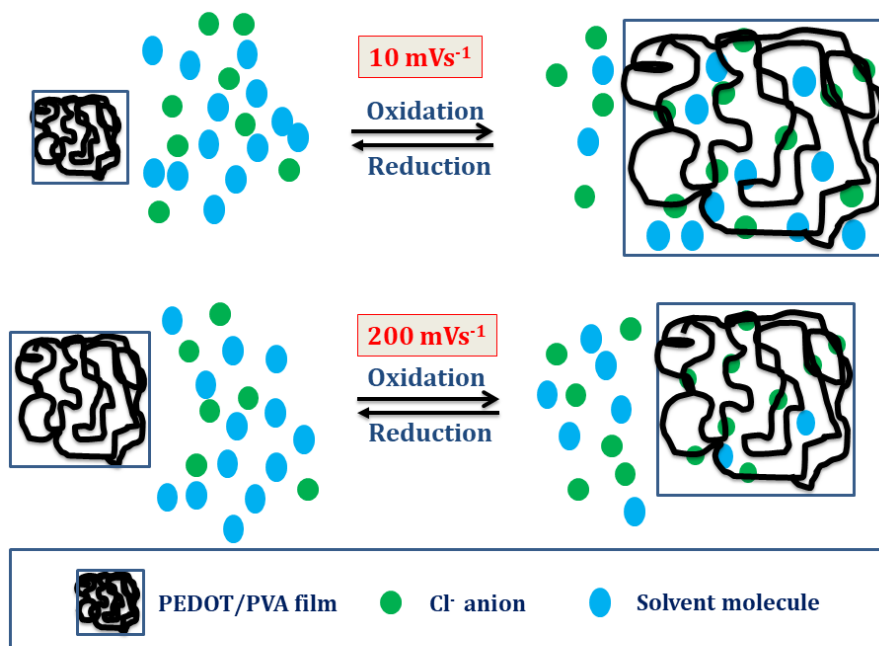


Figure 7.14 Schematic representation of the redox reaction extension based on the cooperative actuation of the PEDOT/PVA film at 10 mVs^{-1} and at 200 mVs^{-1} .

7.2.5.4.2. Cooperative actuation of PEDOT/PVA film senses the chemical working condition

To further verify the sensing capability of PEDOT/PVA film with respect to its chemical working conditions, the cooperative actuation characteristics of the film obtained through controlled voltammetric responses driven by the electrolyte concentration were studied^[26]. For this purpose, the film was placed in a cell containing the electrolyte after attaining a stable stationary voltammetric response. After subjecting the film to several

consecutive potential sweeps to attain a stable voltammetric response the film was transferred again, to the control solution (0.1 M NaCl), and cycled again to attain a stable voltammetric response. The whole process was repeated for different electrolyte concentrations first from lower to higher concentration and then higher to lower concentration. That is, from 0.01 M to 1 M and then from 1 M to 0.01 M (0.01, 0.025, 0.05, 0.1, 0.25, 0.5, 1, 1, 0.5, 0.25, 0.1, 0.05, 0.025, and 0.01).

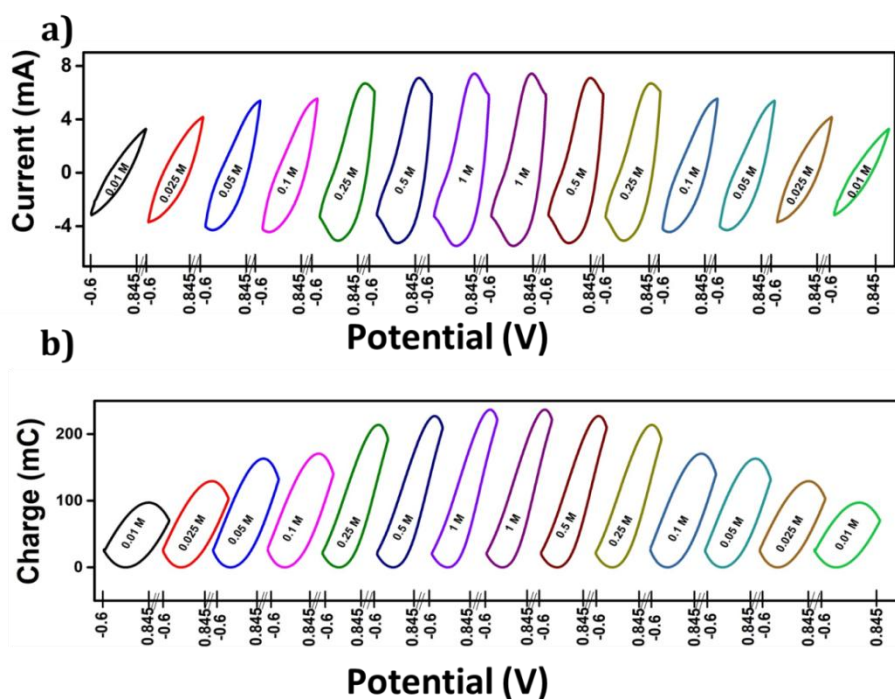


Figure 7.15 (a) CVs obtained in different electrolyte concentrations of NaCl at a scan rate of 25 mVs^{-1} . **(b)** corresponding QV

Figure 7.15(a) shows the stable voltammetric responses of the PEDOT/PVA film for varying concentrations. From the figure, it can be seen that an increase in anodic and cathodic peak

currents as concentrations increase, followed by a decrease in peak currents as the concentration decreases.

The corresponding QVs are shown in Figure 7.15(b). The closed loop in the QV indicates that the charges associated with oxidation and reduction are balanced, signifying a reversible redox process in the film under experimental conditions. The extension of reversible charge consumed during the reaction changes based on the electrolyte concentration changes. The conformational changes, involving relaxation and compaction, are triggered by the entry and exit of anions and solvent ions to and from the film, ensuring osmotic pressure equilibrium and driving the conformational movement^[26]. The figure also reveals that the extension of the reaction is the same for the same concentration irrespective of the direction of varying the concentration.

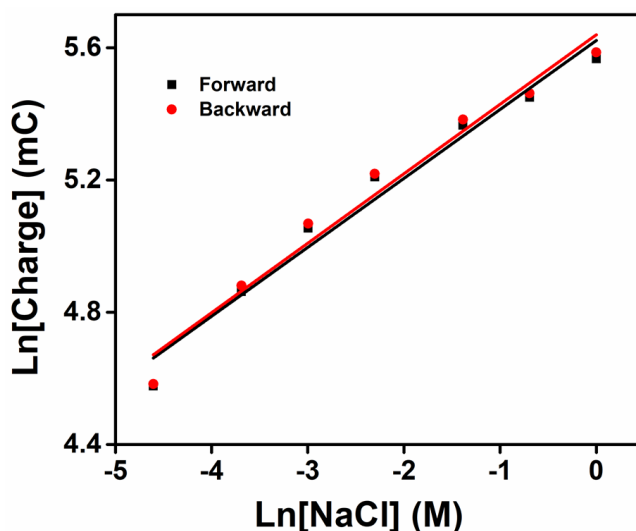


Figure 7.16 *Logarithmic relation of the charge consumed during the redox reaction of PEDOT/PVA hybrid film with the electrolyte concentration of aqueous NaCl*

The logarithmic relation between the consumed charge and the concentration of the electrolyte is shown in Figure 7.16. It can be seen that the consumed redox charge increases with increasing the concentration which corroborates equation 6.26.

The voltammetric responses of the PEDOT/PVA film in the control solution (0.1 M NaCl) were recorded between two successive electrolyte concentrations. The results are shown in Figure 7.17(a). The overlapping CVs show that the conformational movement is reversible throughout the reaction.

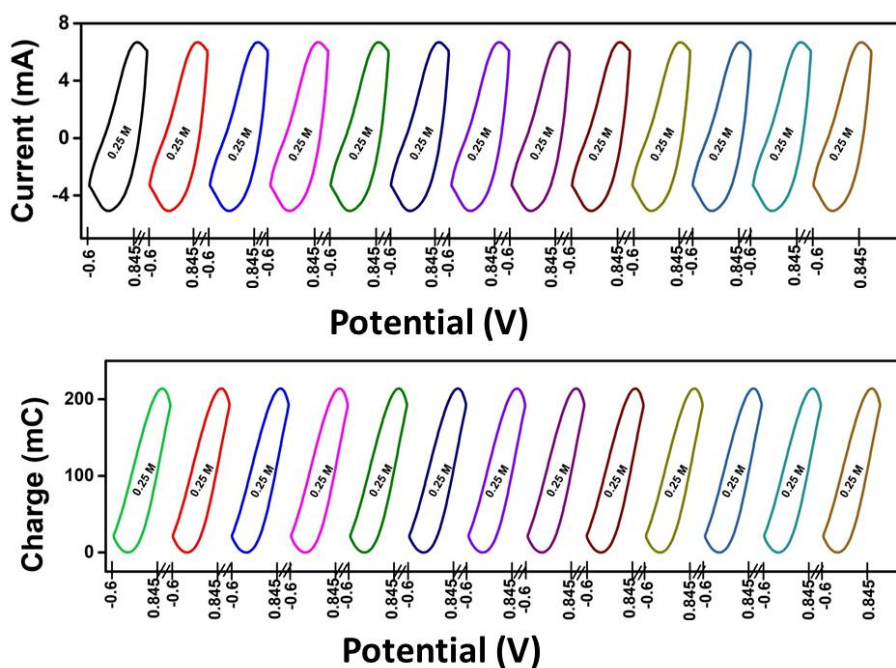


Figure 7.17 (a) CVs obtained in a control solution of NaCl (0.1 M) at a scan rate of 25 mVs^{-1} . **(b)** Corresponding QVs

The corresponding QV obtained from the CVs recorded from the control solution is shown in Figure 7.17(b). The overlapping QV can be seen from the figure which confirms that the extension of reaction is the same for all control concentrations. That means the conformational movement of the film driven by the change in chemical working conditions is reversible.

The schematic representation of the extension of the reaction by varying the concentration is shown in Figure 7.18. The figure also reveals the extension of the reaction is higher for higher concentrations and the conformational movement is reversible throughout the reaction.

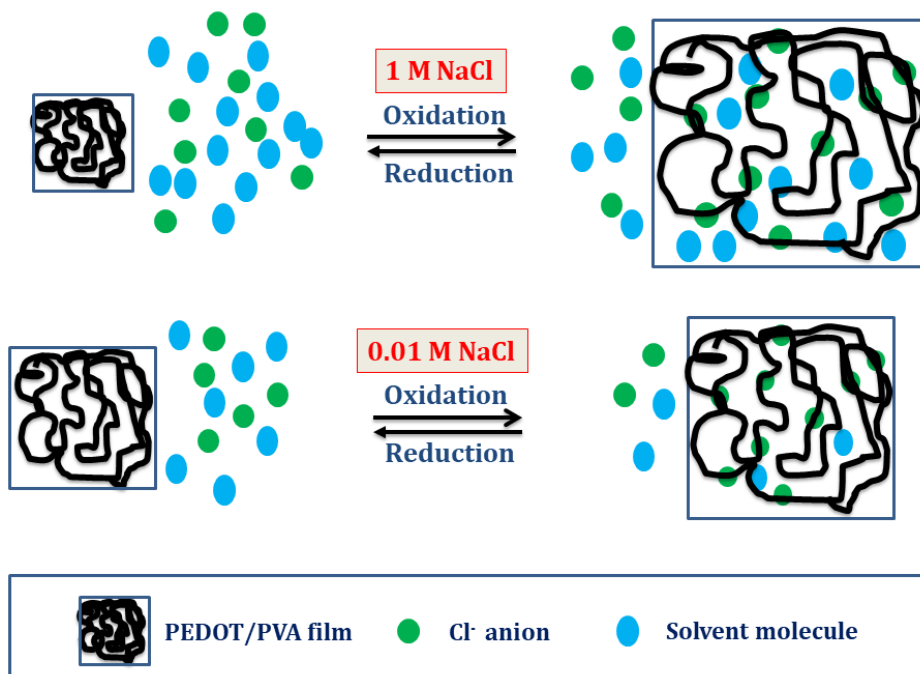


Figure 7.18 Schematic representation of the redox reaction extension based on the cooperative actuation of the PEDOT/PVA film in 0.01 M NaCl and in 1 M NaCl

These results from PEDOT/PVA film reveal that the film can mimic the biological processes, i.e., the cooperative actuation of the muscle sarcomere with the variation in ATP concentration in the muscles.

7.2.5.4.3. Cooperative actuation of PEDOT/PVA film senses the thermal working condition

To explore the cooperative actuation of the films in response to temperature changes, control voltammetric responses were recorded. This was done to explore the PEDOT/PVA film's ability to sense the changes in working temperature. In this study, a stable voltammetric response was recorded by subjecting the film to 30

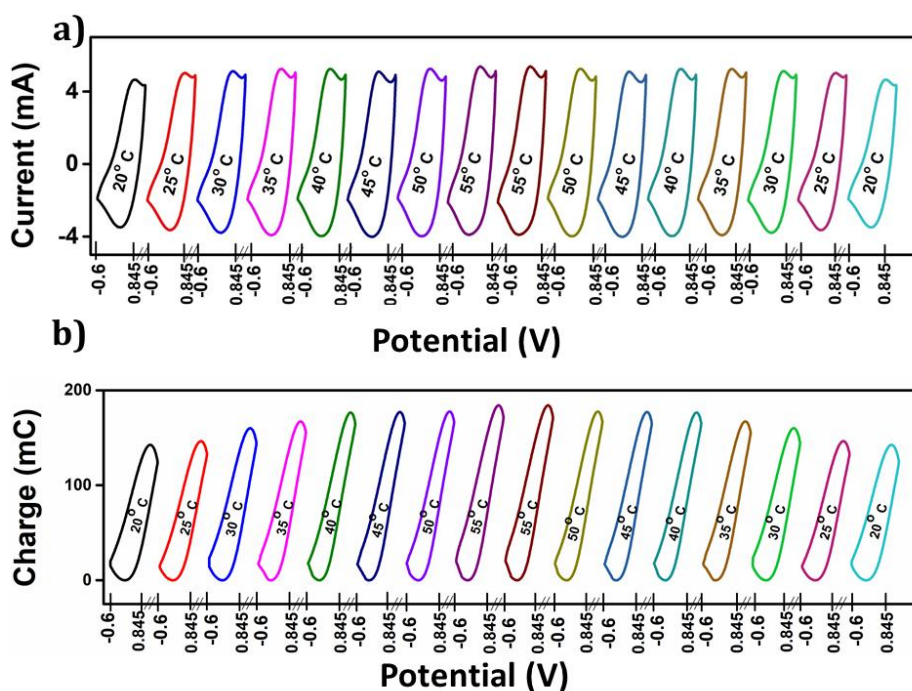


Figure 7.19 (a) CVs obtained from PEDOT/PVA film for increasing and decreasing the temperatures in 1M NaCl at 25 mVs^{-1} . **(b)** Corresponding QV obtained

consecutive potential cycles at a scan rate of 25 mVs^{-1} in an aqueous solution of 1 M NaCl at room temperature. Subsequently, the temperature was switched to a predetermined 'control' temperature of 30°C , and the same film was cycled at the same scan rate to obtain a stable voltammetric response. The entire process was then repeated for various temperatures increasing from lower to higher temperatures, and then in higher to lower temperatures, i.e, from 20°C to 55°C then from 55°C to 20°C with an increment of 5°C .

Figure 7.19(a) shows the stationary voltammetric response of the PEDOT/PVA film at different working temperatures. It is noticeable

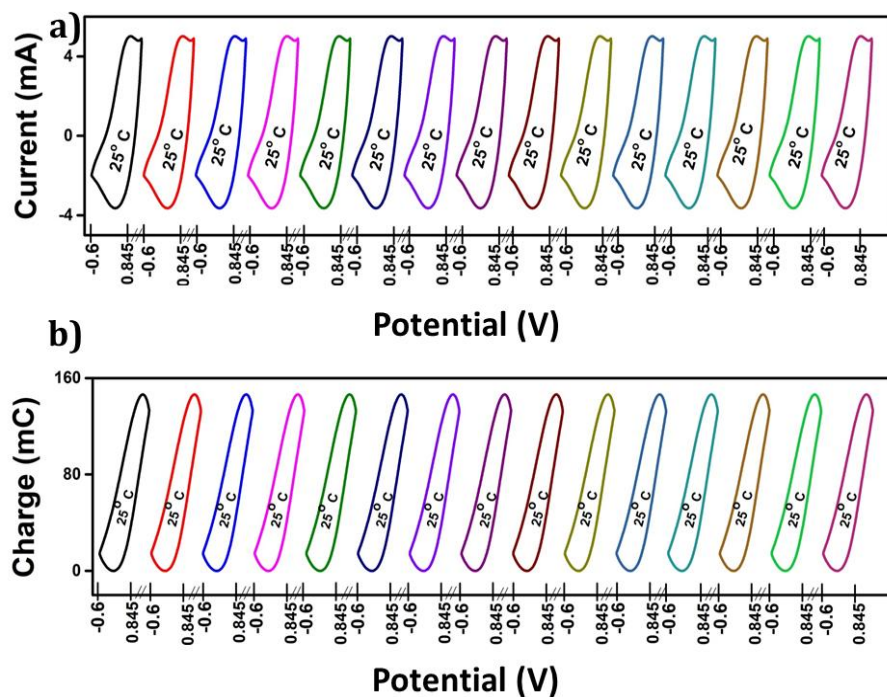


Figure 7.20 (a) CVs obtained in a control temperature (30°C) in 1 M NaCl at 25 mVs^{-1} . **(b)** Corresponding QV responses

that the anodic and cathodic peak currents increase as the temperature increases, and decrease with decreasing temperatures. The corresponding QV is shown in Figure 7.19(b).

Figure 7.19(b) reveals that the film's reversible redox charge consumption during the reaction increases as the working temperature increases. Conversely, the redox charge decreases when the temperature is decreased. The figure also pointed out that the charge consumed during the reaction is the same for the same temperature irrespective of the direction of the experiment. That means the extension of reaction is the same for the same temperature. The results confirm that the conformational movements during the reaction are perfectly reversible.

Figure 7.20(a) shows the CVs obtained from the control temperature. The resulting overlapping CVs pointed out that the

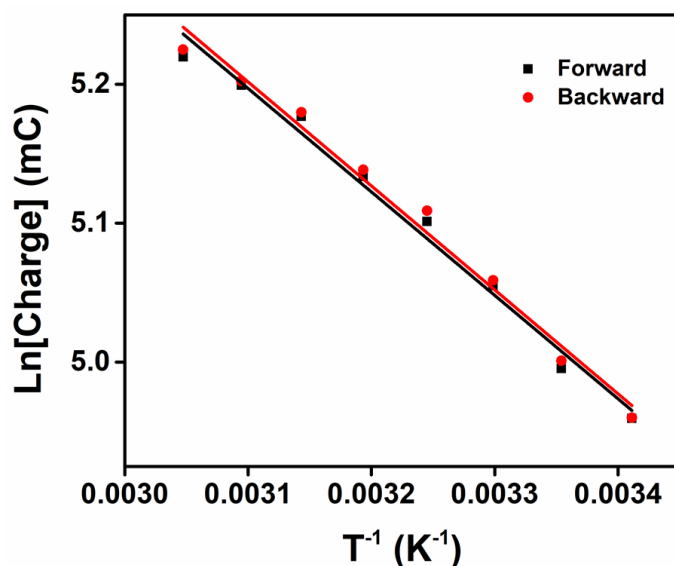


Figure 7.21 *Semi-logarithmic relation of redox charge consumed during the forward and backward reaction of PEDOT/PVA film obtained from the QV with the inverse of temperature.*

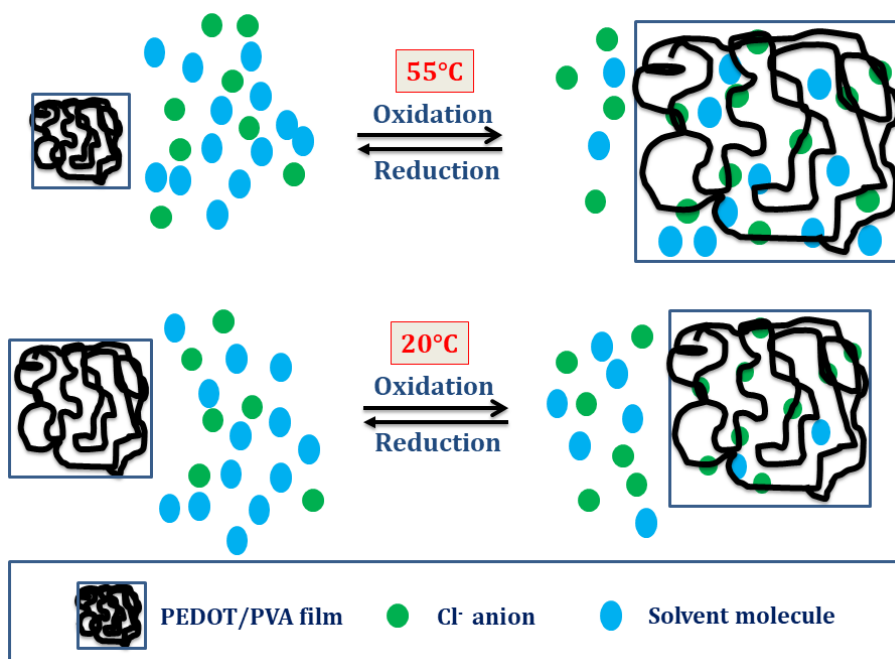
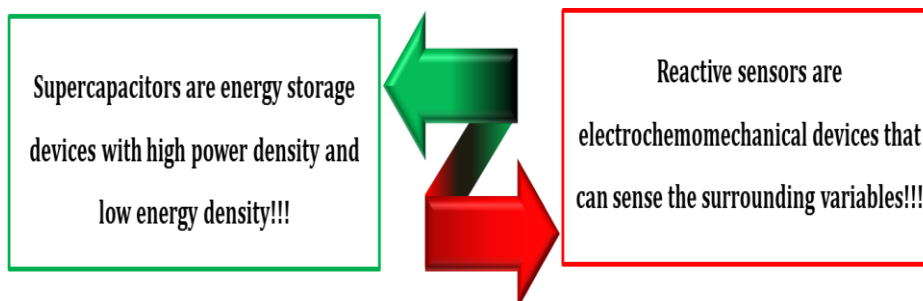


Figure 7.22 Schematic representation of the extension of redox reaction based on cooperative actuation of the PEDOT/PVA film at 55° C and 20° C

film's electroactivity remains constant throughout the experiment. The corresponding QVs as shown in Figure 7.20(b) confirm that, the absence of any significant chemical memory effects that impact the film's conformational movement and the electroactivity of the film. The semi-logarithmic relation between the consumed redox charge and the inverse of temperature is shown in Figure 7.21. The linear dependence corroborates the equation 6.32. Thus the results confirm that the film can sense the working temperature using consumed charge as the sensing parameter. The results also reveal that the change in working temperature influences the reversible conformational movements of the film.

The schematic representation of the extension of the reaction and conformation changes during the reaction at different temperatures are shown in Figure 7.22. When the temperatures increase, there is a significant structural relaxation. Consequently, a large number of ions can diffuse to the polymer matrix as counter ions, accompanied by a larger number of solvent molecules. This leads to higher charge consumption during the reaction compared to reactions occurring at lower temperatures. Furthermore, the extension of the redox reaction is large by the elevation of the working temperature^[27].

7.2.5.5. Sensing supercapacitor based on PEDOT/PVA hybrid film



In order to prove that the PEDOT/PVA film acts as a simultaneous sensing motor, we investigated the supercapacitor application of the PEDOT/PVA while capable of sensing its surrounding environment by utilizing the same electrochemical reaction^[28].

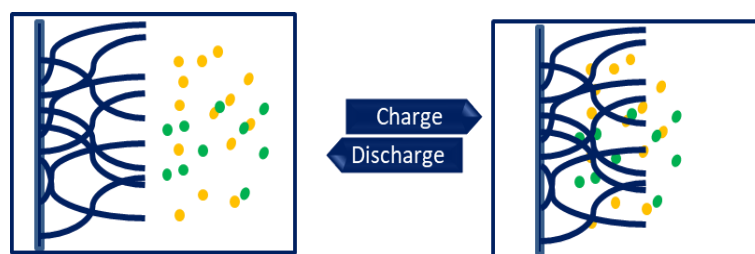
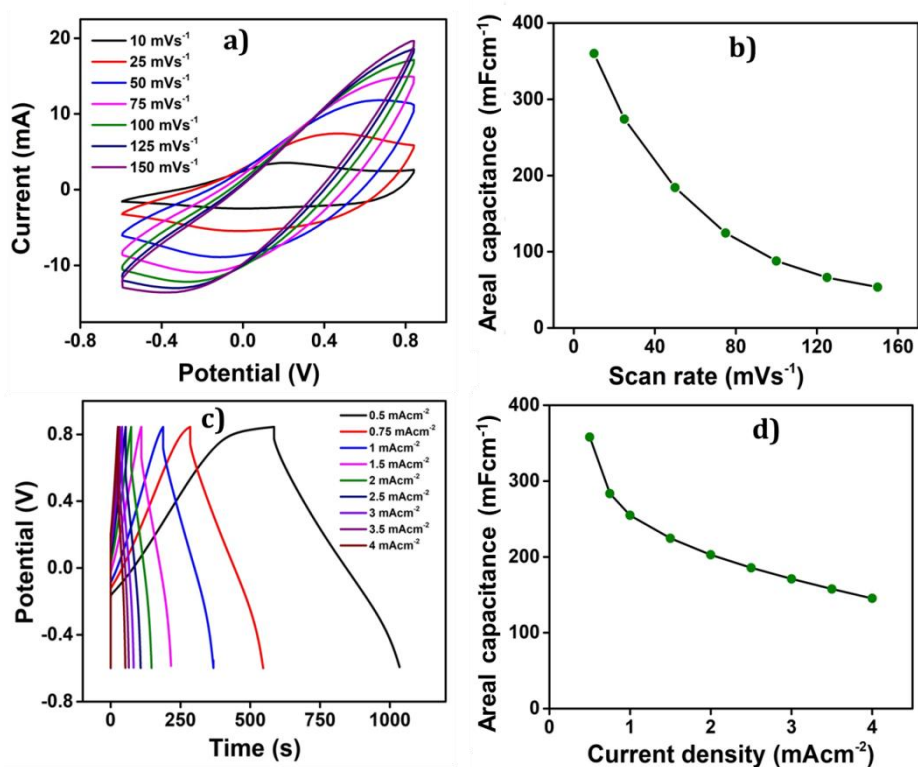


Figure 7.23 Schematic representation of charging and discharging in PEDOT/PVA film-based supercapacitor

7.2.5.5.1. Super capacitance performance of PEDOT/PVA film

We have investigated the charge storage capacity of the PEDOT/PVA film by analyzing its areal capacitance using CV and galvanostatic charge-discharge (GCD) methods^[29]. A schematic representation of the charging and discharging of the supercapacitor is shown in Figure 7.23. In order to calculate the areal capacitance of the PEDOT/PVA film, the CVs were recorded for different scan rates in 1 M NaCl at room temperature. The results are shown in Figure



7.24(a). From the figure, it is clear that the CVs have non-rectangular

Figure 7.24 (a) CVs of PEDOT/PVA film at different scan rates. **(b)** GCD of PEDOT/PVA film at different current densities. **(c)** Variation of areal capacitance to the scan rates. **(d)** Variation of specific capacitance with the current densities

shapes revealing the oxidation-reduction peaks. Film's faradaic pseudo-capacitive behavior due to faradaic reaction. The areal capacitance of the film was calculated from the CV data at different scan rates using equation 2.5. The results are presented in Table 7.2. The variation of the capacitance with the scan rates is shown in Figure 7.24(b). It can be seen that the capacitance decreases with increasing the scan rates. This is due to the fact that at higher scan rates lesser number of ions are penetrating the polymer chain relatively shorter time is available for the faradaic reaction takes place.

Table 7.2 Areal capacitance of PEDOT/PVA film at different scan rates

Scan rate (mVs ⁻¹)	Areal capacitance(mFcm ⁻²)
10	359.98
25	274.05
50	184.08
75	124.56
100	87.88
125	66.05
150	53.52
175	43.89
200	34.25

The areal capacitance of the PEDOT/PVA film was also calculated from GCD curves. Before recording the GCD, the potential range was fixed (-0.6 V to 0.845 V), which was obtained from the voltammetric

responses. Figure 7.24(c) shows the GCD curves for different current densities. A nonlinear charge-discharge curve was obtained, which confirms the pseudo-capacitive nature of the PEDOT/PVA film. Almost symmetrical GCD curves indicate the film's electrochemical reversibility and coulombic efficiency. The absence of an IR drop in the GCD curve is due to fast electron and ion transfer rates. The fast diffusion of ions takes place between the film and electrolyte due to the fast relaxation and compaction of the polymer chain. This minimizes the IR drop and enhances the electrochemical performance. The areal capacitance of the PEDOT/PVA film for different current densities was calculated using equation 2.8. The results are presented in Table 7.3. The relationship between capacitance and current densities is shown in Figure 7.24(d). The figure reveals that capacitance increases as current density decreases. Lower current densities allow sufficient time for the counter anions to diffuse into the active center into the polymer chain for efficient Faradaic reaction.

Table 7.3 Areal capacitance of PEDOT/PVA film at different current densities

Current density (mAcm ⁻²)	Areal capacitance(mFcm ⁻²)
0.5	357.99
0.75	283.49
1	254.77
1.5	224.53
2	202.77
2.5	185.64

3	170.97
3.5	157.68
4	145.33

Cyclic stability

The cyclic stability of the PEDOT/PVA film was studied by recording CV for up to 1500 cycles at a scan rate of 100 mVs^{-1} . Generally, CPs exhibit limited cyclic stability due to the continuous insertion and ejection of anions during their redox reaction, along with reversible conformational relaxation and compaction of the polymer chain. This results in the reduced cyclic stability of CP based supercapacitors [30]. However, in this investigation, the PEDOT/PVA film maintains 95.8% of its initial areal capacitance even after 1500 cycles as shown in Figure 7.25. This improved cyclic stability may be

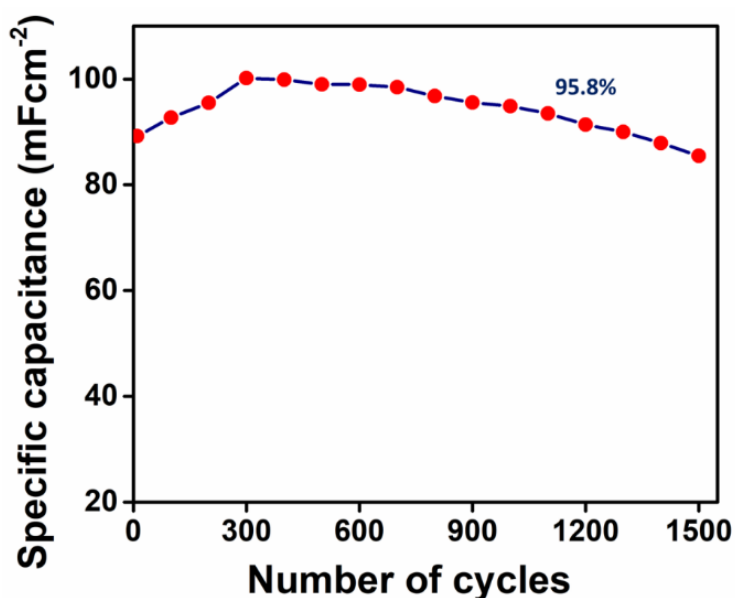


Figure 7.25 Cyclic stability of PEDOT/PVA film for 1500 cycle

attributed to the improved mechanical stability of the PEDOT chains due to its interaction with PVA which limits polymer degradation. It also expected that a controlled conformational movement of the PEDOT chain has been occurred due to the strong interaction between PVA and PEDOT polymer chains in the hybrid film.

7.2.5.5.1.1. PEDOT/PVA film as sensing supercapacitor

In order to prove the PEDOT/PVA film acts as a sensing supercapacitor, the simultaneous reactive sensing ability of the film during discharging was studied. The same discharging curve from GCD for different current densities is used after normalizing to explore the sensing characteristics toward the electrical working condition of the film. Figure 7.26(a) shows the normalized discharge curves obtained from the GCD curves for different current densities (Figure 7.24(b)). The electrical energy consumed during the reaction was calculated by integrating this normalized discharge curve. A linear relationship between the consumed electrical energy

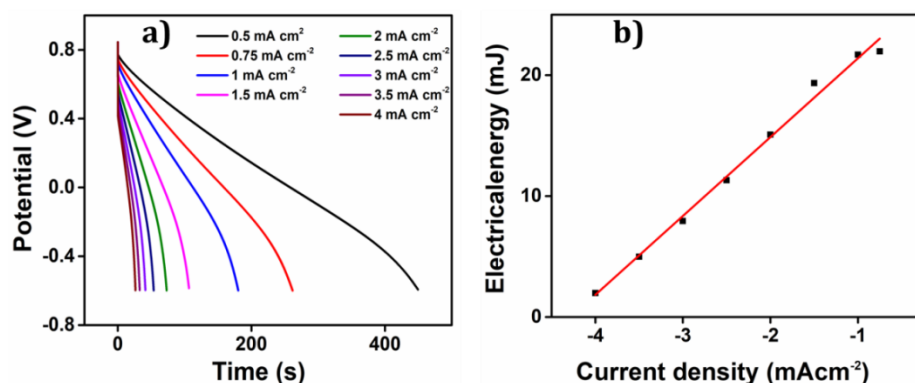


Figure 7.26 (a) Normalized discharge curve from GCD of PEDOT/PVA film for different current densities **(b)** consumed electrical energy as a function of applied current (R^2 is the correlation factor)

and the applied current densities was obtained as shown in Figure 7.26(b). This indicates that the film can sense the electrical working condition, i.e., applied current densities during the discharging process, without the need for additional connectivities. This result confirms that the PEDOT/PVA film can act not only as a supercapacitor but also as a reactive sensor of its electrical working conditions. Therefore it can act as a sensing supercapacitor.

7.2.5.6. Symmetric supercapacitor device based on PEDOT/PVA film

A symmetric supercapacitor device using PEDOT/PVA film was fabricated to check its applicability as a simultaneous sensing macromolecular motor. The details of the device fabrication are discussed in detail in Chapter 2. The electrochemical behavior and its role as a sensing supercapacitor were examined through CV, GCD, Chronopotentiometry, and electrochemical impedance spectroscopy (EIS) techniques.

In order to study the charge storage property, the CVs of the device were recorded for different scan rates at room temperature. The potential was cycled between 0 V to 1.445 V. The results are shown in Figure 7.27(a). From the figure, it can be seen that the CVs are non-rectangular in shape. The areal capacitance of the device was calculated from the CV data using equation 2.5 and listed in Table 7.4. The variation in capacitance with the scan rates is depicted in Figure 7.27(b). The figure reveals that the capacitance increases the scan rate decreases. This is because of the extended reaction time at lower scan rates.

Table 7.4 Areal capacitance of the supercapacitor device at different scan rates

Scan rate (mVs ⁻¹)	Areal capacitance(mFcm ⁻²)
10	311.41
25	207.6
50	128.72
75	106.11
100	83.04
125	69.20
150	63.43

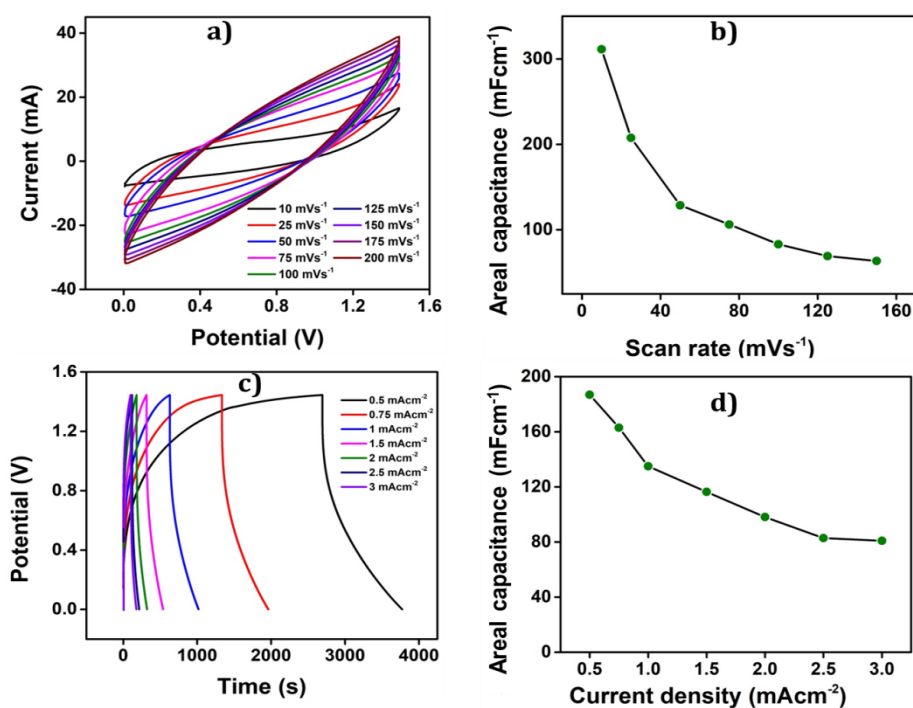


Figure 7.27 (a) CVs of supercapacitor device at different scan rates. (b) GCD curves at different current densities. (c) Variation of specific capacitance with respect to the scan rates. (d) Variation of specific capacitance with respect to different current densities

The areal capacitance of the supercapacitor device was also calculated from the GCD curves. The GCD curves of the device at a fixed potential range (0 V to 1.445 V) for different current densities are shown in Figure 7.27(c). The areal capacitance was then calculated from the GCD curves using the equation 2.8. The device exhibited a high areal capacitance of 186.85 mFcm⁻² at a current density of 0.5 mAcm⁻². The variation in capacitance with current densities is shown in Figure 7.27(d). It can be seen from the figure that the capacitance decreases as the current density increases. This is due to the insufficient time available for the ions to penetrate the polymer with the active sites of the polymer. The areal capacitances for various current densities are shown in Table 7.5.

Table 7.5 Specific capacitance of supercapacitor device at different current densities

Current density (mAcm⁻²)	Areal capacitance(mFcm⁻²)
0.5	186.85
0.75	162.90
1	134.95
1.5	116.32
2	98.09
2.5	82.78
3	80.86

The basic electrochemical characteristics of the device were also examined using EIS analysis. Figure 7.28 shows the Nyquist plot of the device. The figure shows the presence of a semi-circle in the high-frequency region and an approximately distorted straight line

in the low-frequency region. The semi-circle indicates the charge transfer occurring between the electrolyte and the immediate vicinity of the film. The point of intersection between the semi-circle and the real axis in the high-frequency zone corresponds to the equivalent series resistance (ESR). This encompasses various resistances, including the intrinsic resistance of the material, solution resistance, and the contact resistance of the electrode and electrolyte.

The effective connection between the electrode and the electrolyte is responsible for the optimum ESR value. The size of the semi-circle diameter signifies the impedance related to charge migration and transfer resistance. The presented Nyquist plot (Figure 7.28) indicates that a smaller diameter of the semi-circle in the high-frequency region suggests smoother charge transfer between the

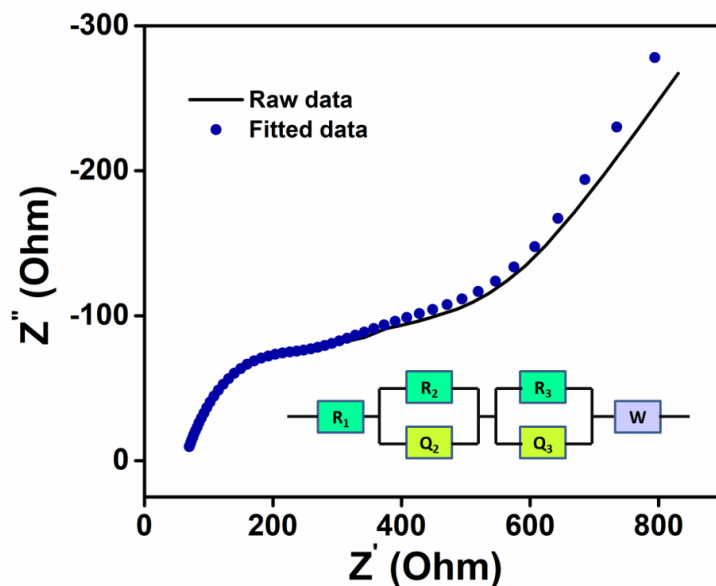


Figure 7.28 Nyquist plot of solid-state device

electrode and the electrolyte. The distorted linear segment corresponds to ion transfer governed by diffusion to the film. The slope of the line determines the diffusion rate. It is evident from Figure 7.28 that the device exhibits a commendable diffusion rate due to the highly porous nature of the films and the exceptional interaction between the electrolyte separator and the interposed films within the device.

The cyclic stability of the device holds significant importance for its practical application. Figure 7.29 shows the cyclic stability of the device obtained at the scan rate of 100 mVs^{-1} for 1700 cycles. The supercapacitor device maintains 92.14% of its initial capacitance value even after completing 1700 cycles, which underscores the device's robust and enduring electrochemical stability over extended periods.

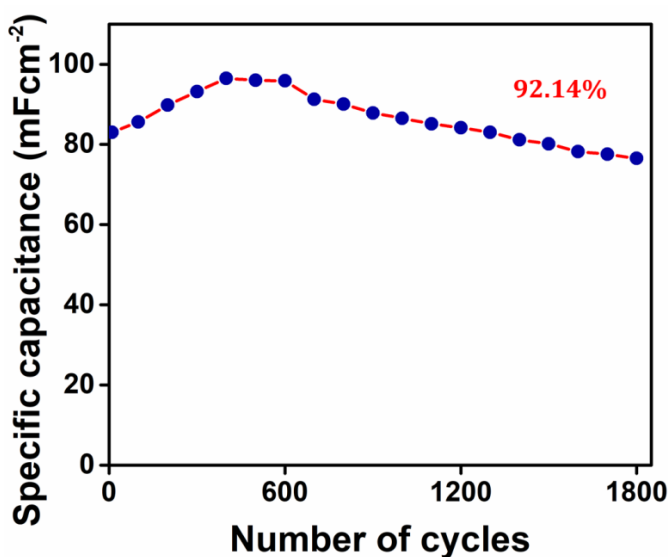


Figure 7.29 Cyclic stability of solid-state device for 1700 cycle

7.2.5.6.1. Reactive sensing characteristics of the PEDOT/PVA supercapacitor device

The reactive sensing capability of the symmetric supercapacitor device, towards electrical and thermal working conditions was investigated by recording the chronopotentiogram at a constant charge of ± 6 mC using the two-electrode method.

Supercapacitor device as a current sensor

The ability of the supercapacitor device to sense its electrical working condition was explored by applying different constant

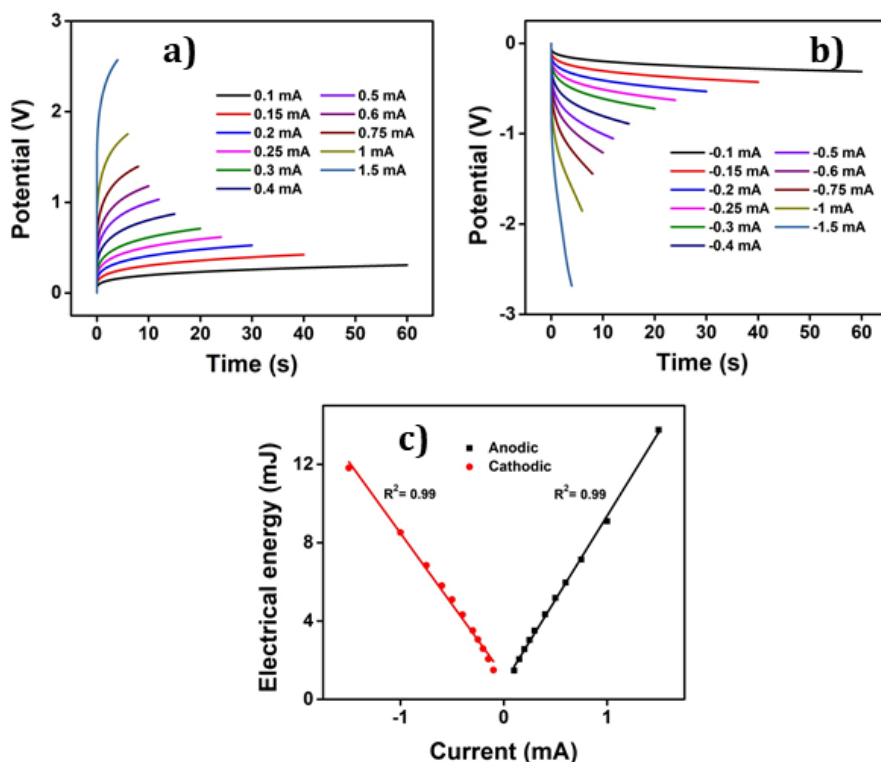


Figure 7.30 Chronopotentiograms obtained when different constant (a) anodic and (b) cathodic currents were applied to the supercapacitor device by passing a constant charge of 6 mC (c) Electrical energy consumed by the device as a function of applied current (R^2 is the correlation factor)

currents ranging from ± 0.1 mA to ± 1.5 mA at a constant charge of 6 mC. Figures 7.30(a) and (b) show the normalized chronopotentiograms. The electrical energy consumed during the reaction exhibited a linear relationship with both anodic and cathodic applied currents, as shown in 7.30(c). This confirms that the device can sense its electrical working condition while working without the need for any other additional connectivities. The consumed electrical energy is the sensing parameter. This is

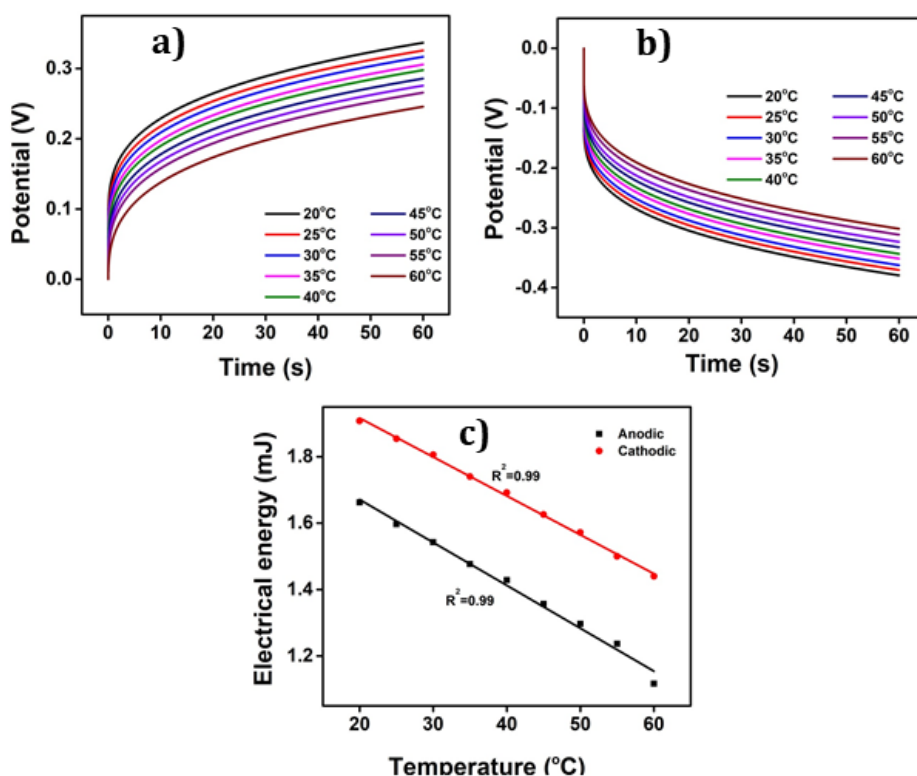


Figure 7.31 Chronopotentiogram obtained from different experimental temperatures when (a) +0.1 mA and (b) -0.1 mA of current were applied to the supercapacitor device for 60 s. (c) The variation of electrical energy consumed during the anodic and cathodic processes with temperature

analogous to the sensing ability of the biological muscles toward the electrical signals generated by the brain while working through the same neuronal connectivities.

Supercapacitor device as temperature sensor

The normalized chronopotentiograms at different temperatures for both anodic and cathodic processes at a constant charge of 6 mC were recorded to explore whether the supercapacitor device can act as a temperature sensor while working the sensing ability of the PEDOT/PVA supercapacitor device towards its thermal working condition. The results are presented in Figures 7.31(a) and (b). Figure 7.31(c) shows the linear relationship between the consumed electrical energy during the reaction and the working temperature. This result confirms that the device can sense the working temperature with the electrical energy as the sensing parameter. Similar to the current sensing capability, this supercapacitor device also senses the working temperature while working without the need of other any additional connectivities as biological muscles do.

7.2.5.6.2. PEDOT/PVA supercapacitor device as a simultaneous sensing supercapacitor

In order to prove the PEDOT/PVA symmetric device can act as a simultaneous sensing supercapacitor, the simultaneous reactive sensing ability of the device toward its electrical working condition during discharging was studied. The electrical energy consumed during the reaction was calculated from the normalized discharging curve from the same GCD for different current densities. Figure 7.32(a) shows the normalized discharging curves. The electrical

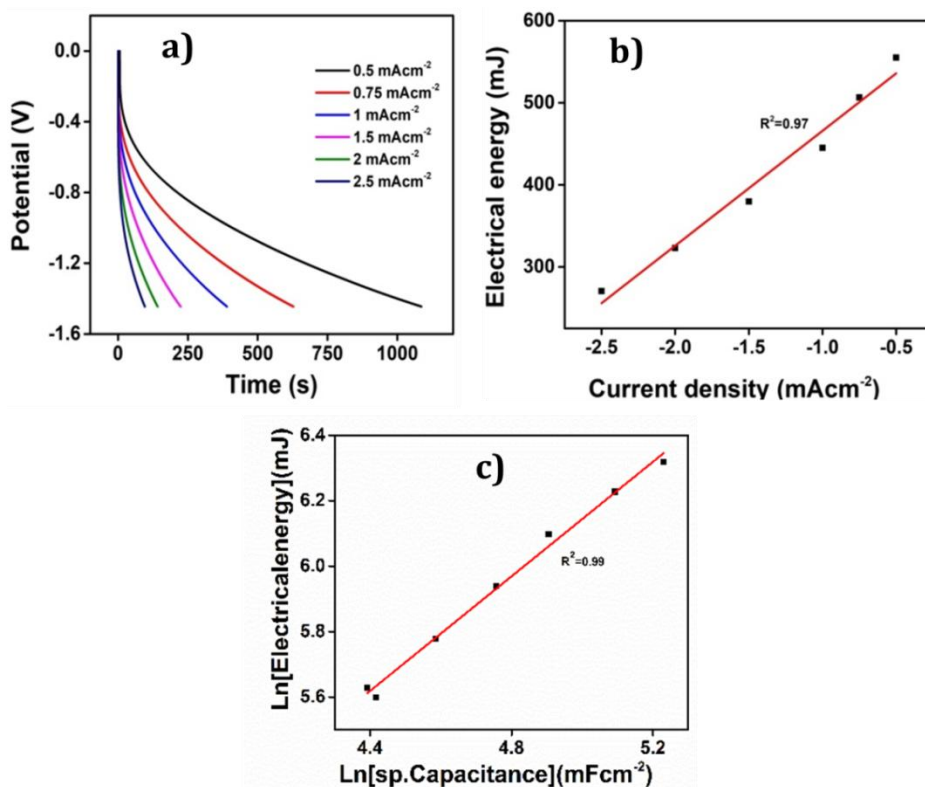


Figure 7.32 (a) Normalized discharge curve from GCD of the PEDOT/PVA supercapacitor device of PEDOT/PVA film for different current densities (b) Electrical energy consumed by the supercapacitor device as a function of applied current (R^2 is the correlation factor). (c) Logarithmic relation of specific capacitance with consumed electrical energy

energy consumed during the reaction shows a linear relationship with the applied current densities as shown in Figure 7.32(b). A logarithmic relation between the specific capacitance and the consumed electrical energy during the reaction is obtained as shown in Figure 7.32(c). The results confirm that the supercapacitor device can sense the electrical energetic condition simultaneously while working using the same two connecting wires. These results

underscored that the supercapacitor device made of PEDOT/PVA film can act as a sensing motor that can mimic the simultaneous sensing characteristics of biological muscles.

7.3. Conclusion

A flexible and mechanically stable electroactive PEDOT/PVA hybrid film was fabricated through in situ polymerization of EDOT using PVA film as a template and studied for its applicability as a macromolecular sensing motor. The hybrid film was characterized using FTIR-ATR, TGA, FE-SEM, EDX, and UTM analysis. Its electrochemical characteristics were thoroughly studied using CV, QV, GCD, and chronopotentiometry with a special emphasis on its biomimetic sensing characteristics and energy storage characteristics. The charge consumed during the reaction or the extension of the redox reaction was calculated from QV.

The biomimetic reactive sensing property of the PEDOT/PVA hybrid film towards its working energetic condition was explored using chronopotentiometric studies. The rate of the electrochemical reaction of the film under the application of constant square current waves was impacted by environmental factors such as electrical, chemical, and thermal. Any variation in these experimental variables was found to influence the potential evolution of the film during the reaction. The consumed electrical energy during this process was proved to act as the sensing parameter with respect to its working energetic conditions during the reaction.

As a result of the electrochemical reactions, the PEDOT/PVA film becomes a dense gel constituted by macromolecular polymer chains

ions and water. This dense gel is proven to mimic the basic components of those cells whose reactions originate the biological functions. The PEDOT/PVA film was used here as a model reactive material for the parallel exploration and quantification of biological functions.

The reaction energy includes, at any reaction time, quantitative information about, and sensing information of, any chemical, thermal, electrical, or mechanical variable acting on the reaction rate. This instantaneous quantitative information is provided by the evolution of the material potential in these artificial systems. This is similar to biological functions as the quantitative information about the sensing signal transferring to the brain.

The cooperative actuation of the PEDOT/PVA film during the reaction and the influence of the working energetic conditions on this cooperative actuation was also explored. The QV is employed to assess the extension/charge consumption during the film's conformational movements. The logarithmic relationship of the consumed charge with the scan rate and the electrolyte concentration and the semi-logarithmic relationship with the inverse of temperature confirm that the film can act as a sensor of its working energetic conditions. This corroborates the theoretical equations. The consumed charge is the sensing parameter. This cooperative actuation of PEDOT/PVA film is analogous to the muscle sarcomere actuation while changing the environmental variables. We argue that the cooperative actuation of the sarcomere is the origin of the sensing property of the biological muscles.

The charge storage property of the PEDOT/PVA film was explored further using CV and GCD curves. The areal capacitance was calculated at different scan rates and current densities. It is proved that the film could act as a supercapacitor with an areal capacitance of 359.98 mFcm⁻² and 357.99 mFcm⁻² for 10 mVs⁻¹ scan rate and 0.5 mAcm⁻² current density respectively. The film shows 95.8% cyclic stability even after 1500 cycles of CV responses.

The simultaneous sensing property of the PEDOT/PVA film was explored. The sensing ability towards the electrical energetic condition while discharging was analyzed and the consumed electrical energy during the discharge process was calculated. The linear relationship of consumed electrical energy with the applied current density confirms that the PEDOT/PVA film can sense the working electrical condition while working as the biological muscle does through the same two connecting wires.

A symmetric supercapacitor device made of PEDOT/PVA film was fabricated by sandwiching two symmetric PEDOT/PVA films with an electrolyte separator consisting of filter paper/PVA/NaCl. The device was studied for its potential application as a simultaneous sensing supercapacitor. The charge storage characteristics of the device are explored using CV and GCD curves. The basic electrochemical characteristics of the device were also verified using EIS analysis, which revealed the charge transfer property of the device. The device showed a cyclic stability of 92.18% even after 1700 cycles. The reactive sensing ability of the supercapacitor device towards its electrical and thermal working conditions was

explored and proved that the supercapacitor can act as a simultaneous current sensor as well as a temperature sensor using consumed electrical energy as the sensing parameter. The results proved that the PEDOT/PVA supercapacitor device can act as macromolecular sensing motors while working without any additional connectivities similar to the biological muscles sensing their surrounding environment while working.

References

- [1] aP. Železnik, A. Jelen, K. Kalc, D. G. Behm, Ž. Kozinc, *European Journal of Applied Physiology* **2024**, *124*, 1005-1014; bM. Badiola-Mateos, T. Osaki, R. D. Kamm, J. Samitier, *Scientific Reports* **2022**, *12*, 21318.
- [2] G. H. Rutherford, Z. D. Mobbille, J. Brandt-Trainer, R. Follmann, E. Rosa, Jr., *American Journal of Physics* **2020**, *88*, 918-923.
- [3] aN. Gao, J. Yu, Q. Tian, J. Shi, M. Zhang, S. Chen, L. Zang, *Chemosensors* **2021**, *9*, 79; bD. Cheng, X. Kan, *Journal of Electroanalytical Chemistry* **2020**, *857*, 113741.
- [4] aM. P. Sidheekha, L. Rajan, Y. A. Ismail, *Materials Chemistry and Physics* **2022**, *279*, 125769; bM. P. Sidheekha, K. Nufaira, A. K. Shabeeba, L. Rajan, Y. A. Ismail, *Materials Today: Proceedings* **2022**, *51*, 2286-2292.
- [5] Z. Fan, J. Ouyang, *Advanced Electronic Materials* **2019**, *5*, 1800769.
- [6] aA. F. Al Naim, S. S. Ibrahim, A. gamal El-Shamy, *Polymer* **2021**, *226*, 123792; bJ. Yin, Y. Bai, J. Lu, J. Ma, Q. Zhang, W. Hong, T. Jiao, *Colloids and Surfaces A: Physicochemical and Engineering Aspects* **2022**, *643*, 128791.
- [7] aN. Alexandre, J. Ribeiro, A. Gaertner, T. Pereira, I. Amorim, J. Fragoso, A. Lopes, J. Fernandes, E. Costa, A. Santos-Silva, *Journal of biomedical materials research Part A* **2014**, *102*, 4262-4275; bO. Azhar, Z. Jahan, F. Sher, M. B. K. Niazi, S. J. Kakar, M. Shahid, *Materials Science and Engineering: C* **2021**, *126*, 112127.
- [8] aL. Rajan, A. Shabeeba, M. P. Sidheekha, Y. Ismail, *Chemistry-An Asian Journal* **2023**, e202300742; bL. Rajan, M. P. Sidheekha, A. Shabeeba, Y. A. Ismail, *Materials Chemistry Frontiers* **2022**, *6*, 1706-1718.
- [9] aA. K. Shabeeba, M. M. Manikandan, M. P. Sidheekha, L. Rajan, Y. A. Ismail, *Materials Today: Proceedings* **2022**, *51*, 2293-2299; bL.

- Rajan, M. P. Sidheekha, A. Shabeeba, S. C. Unnikrishnan, Y. A. Ismail, *Res. Chem. Intermed.* **2022**, *48*, 4313-4329.
- [10] aT. F. Otero, *PCCP* **2017**, *19*, 1718-1730; bT. F. Otero, *Journal of Materials Chemistry B* **2013**, *1*, 3754-3767.
- [11] aY. Peng, B. Yan, Y. Li, J. Lan, L. Shi, R. Ran, *Journal of Materials Science* **2020**, *55*, 1280-1291; bA. Babaie, B. Bakhshandeh, A. Abedi, J. Mohammadnejad, I. Shabani, A. Ardeshiryajimi, S. R. Moosavi, J. Amini, L. Tayebi, *European Polymer Journal* **2020**, *140*, 110051.
- [12] Q. Gao, M. Wang, X. Kang, C. Zhu, M. Ge, *Composites Communications* **2020**, *17*, 134-140.
- [13] aP. AJENG, Pukyong National University **2022**; bM. Mumtaz, E. Ibarboure, C. Labrugère, E. Cloutet, H. Cramail, *Macromolecules* **2008**, *41*, 8964-8970.
- [14] Q. Xu, Y. Li, W. Feng, X. Yuan, *Synthetic Metals* **2010**, *160*, 88-93.
- [15] C. B. Tran, T. F. Otero, J. Travas-Sejdic, Q. B. Le, R. Kiefer, *Synthetic Metals* **2023**, *299*, 117466.
- [16] aT. F. Otero, *The Chemical Record* **2018**, *18*, 788-806; bL. Rajan, M. P. Sidheekha, A. Shabeeba, T. F. Otero, Y. A. Ismail, *Journal of Materials Chemistry A* **2024**, *12*, 4583-4600.
- [17] S. N. J. Syed Zainol Abidin, S. Mamat, S. Abdul Rasyid, Z. Zainal, Y. Sulaiman, *J. Polym. Sci., Part A: Polym. Chem.* **2018**, *56*, 50-58.
- [18] T. F. Otero, J. G. Martinez, K. Hosaka, H. Okuzaki, *Journal of electroanalytical chemistry* **2011**, *657*, 23-27.
- [19] J. G. Martinez, B. Berruoco, T. F. Otero, *Frontiers in bioengineering and biotechnology* **2015**, *3*, 15.
- [20] Y. A. Ismail, J. G. Martínez, A. S. Al Harrasi, S. J. Kim, T. F. Otero, *Sensors and Actuators B: chemical* **2011**, *160*, 1180-1190.
- [21] aA. Dhaka, V. Viswanath, A. Patapoutian, *Annu. Rev. Neurosci.* **2006**, *29*, 135-161; bG. M. Story, A. M. Peier, A. J. Reeve, S. R. Eid, J. Mosbacher, T. R. Hricik, T. J. Earley, A. C. Hergarden, D. A. Andersson, S. W. Hwang, *Cell* **2003**, *112*, 819-829.
- [22] T. F. Otero, *Electrochim. Acta* **2021**, *368*, 137576.
- [23] M. E. M. Mashat, G. Li, D. Zhang, *Scientific reports* **2017**, *7*, 11001.
- [24] aC. Poggese, C. Tesi, R. Stehle, *Pflügers Archiv* **2005**, *449*, 505-517; bB. C. W. Tanner, T. L. Daniel, M. Regnier, *PLoS computational biology* **2007**, *3*, e115.
- [25] T. F. Otero, S. Beaumont, *Electrochim. Acta* **2017**, *258*, 1293-1303.
- [26] T. F. Otero, S. Beaumont, *Sensors and Actuators B: Chemical* **2018**, *263*, 493-501.
- [27] T. F. Otero, S. Beaumont, *Electrochim. Acta* **2017**, *257*, 403-411.
- [28] M. P. Sidheekha, A. Shabeeba, L. Rajan, M. S. Thayyil, Y. A. Ismail, *Engineered Science* **2023**, *23*, 890.

- [29] X. Han, J. Sun, Q. Li, X. He, L. Dang, Z. Liu, Z. Lei, *ACS Sustainable Chemistry & Engineering* **2023**, *11*, 2938-2948.
- [30] M. F. Jimoh, M. F. El-Kady, G. S. Carson, M. B. Anderson, Q. Duong, R. B. Kaner, *Energy Storage Materials* **2023**, 102850.

Chapter 8

Summary and future outlook

This chapter offers a comprehensive summary of the primary discoveries and noteworthy aspects of the current study. In addition, this chapter explores the future outlook of the ongoing work. We have carried out in-depth electrochemical studies of PIN and PEDOT to understand their structural electrochemical characteristics and their connection with the conformational changes occurring during their electrochemical reaction. Further, we have explored their biomimetic reactive sensing characteristics. One of the objectives of this study is to establish the fact that, the reactive sensing capabilities with respect to the surrounding working conditions are a general property of all CPs. Studies in this direction have been extensively carried out on PPY-based materials. Very recently a few studies have been reported on PANI and PANI-based materials but no such studies have been carried out on PIN and PEDOT. One of the oldest dreams of scientists and engineers is to design a motor, capable of sensing itself without additional connectivities. Till now, there is no technological parallel exists for the development of such a self-sensing motor without additional connectivities. The only way to design such a system is by looking for a material model system capable of mimicking biological function leading to the design of self-sensing macromolecular motors using the same two connectivities by taking PIN and PEDOT as model materials to prove the above-mentioned concept.

Our group has already established this capability in PPY and PANI, and it is crucial to investigate other conducting polymers to verify their universality. Hence, we have selected PIN and PEDOT for this study. Investigating their reactive sensing capability necessitates a comprehensive understanding of their electrochemistry and structural changes during the reaction. Only by comprehending the various conformational states throughout the Faradaic process and identifying the potential limit at which the redox reaction occurs without parallel irreversible processes, we can calculate the redox charge and electrical energy expended during the reaction. These quantitative and qualitative details, along with their relationships with surrounding working conditions, serve as the sensing parameters for the working conditions. The major electrochemical tools used for all studies were centered on CV, QV, chronopotentiometry, GCD, and EIS.

Initially, we investigated the structural faradaic process of PIN, synthesized through chemical oxidative polymerization. The electrochemical redox reaction of PIN revealed four distinct structural processes such as reduction-shrinking, reduction-compaction, oxidation-relaxation, and oxidation-swelling.

We have optimized the redox reaction potential window of PIN without any parallel irreversible processes and found it to be within the range of -0.2V to 0.75V. Additionally, parallel irreversible reduction and oxidation processes were identified by recording voltammograms at various cathodic and anodic potential limits.

We have thoroughly examined the structural Faradaic process of PIN and are leveraging this understanding in its potential application as a biomimetic reactive sensor of surrounding environmental working conditions. The reactive sensing capabilities of PIN in response to various environmental variables (electrical, chemical, and thermal) were investigated using CV and chronopotentiometry. We proved that the redox charge and the electrical energy consumed during the reaction can act as sensing parameters. Consequently, the Faradaic redox reactions of PIN could emulate some of the biological functions, leading to the sensing of surrounding variables without any additional connectivity as the driving and the sensing signals are confined in the same two connecting wires at any point of the reaction.

The challenges associated with PIN powder, such as limited processability which is hindering its applications, were addressed by fabricating a free-standing flexible hybrid film of PIN using PVA as a template. Through an in situ chemical polymerization technique, we fabricated a conductive PIN/PVA hybrid film. The study delves into the reactive sensing capability and the cooperative actuation, i.e., reversible conformational movement of the film, examining its self-sensing property under various working conditions. Consequently, the PIN/PVA film demonstrates an ability to emulate the simultaneous sensing properties of biological muscles using only two connecting wires.

Our group has previously proved the reactive sensing characteristics of PPY and PANI. In the preceding chapters, we have

demonstrated this property for PIN. To validate that, reactive sensing is a general property of all CPs, we have chosen another notable conducting polymer, PEDOT.

We investigated the reactive sensing ability of chemically synthesized PEDOT, analyzing the structural Faradaic process induced by the electrochemical reaction of the polymer. Similar to PIN, four distinct conformational states were identified using QV. The redox charge and electrical energy were calculated from QV and chronopotentiometry. The potential window for the redox reaction of PEDOT, excluding any parallel irreversible processes, was optimized to be within the range of -0.6 V to 0.8 V.

We fabricated a highly electroactive, free-standing flexible film of PEDOT by chemically coating EDOT onto a pre-fabricated PVA film using in situ polymerization technique, similar to the approach employed for PIN/PVA. This PEDOT hybrid film exhibited greater electroactivity than the PIN/PVA film. We observed its sensing behavior under varying working conditions and explored the cooperative actuation of the polymer chain in different environmental conditions.

The logarithmic relationship of the consumed charge with the scan rate and the electrolyte concentration and the semi-logarithmic relationship with the inverse of temperature proved that the PIN, PEDOT, and their films can act as a sensor of its working energetic conditions by using consumed charge as the sensing parameter. The consumed electrical energy followed a linear relationship with the applied current, temperature, and log concentration, which proves

that the consumed electrical energy also can act as the sensing parameter. The theoretical equations are also derived.

To achieve our objective of designing a biomimetic self-sensing macromolecular motor, the charge storage characteristics and its applicability to act as a supercapacitor electrode material were explored using PEDOT/PVA hybrid film. The areal capacitance was calculated at different scan rates and current densities. It is proved that the film could act as a supercapacitor with an areal capacitance of 359.98 mFcm⁻² and 357.99 mFcm⁻² for 10 mVs⁻¹ scan rate and 0.5 mAcm⁻² current density respectively. The film shows 95.8% cyclic stability even after 1500 cycles of CV responses.

Subsequently, we developed a self-sensing symmetric solid-state supercapacitor device using this flexible film. The charge storage property of the device was also explored. Further, the self-sensing capability of the device towards the electrical and thermal energetic working conditions was explored. The results showed that the device could sense its electrical condition during working using the same electrochemical reaction and without requiring any additional connectivity. This unified use of the same connecting wire for both charge storage and sensing applications enables the device to function as a self-sensing macromolecular motor or a sensing supercapacitor, akin to biological muscles.

Our studies further prove that the reactive sensing characteristic is a general property of all CPs. The CPs can actuate and store charges by following commands from a computer, simultaneously providing feedback signals about the working environment to the computer

through the same connecting wire, resembling the sensing property of biological muscles.

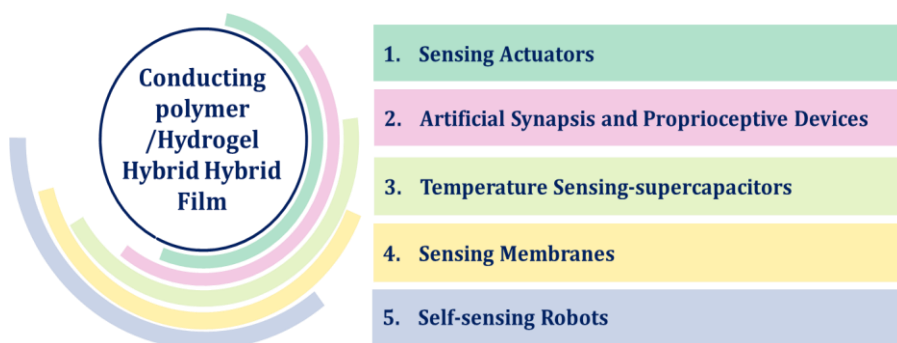
Future outlook

The current research has established the biomimetic reactive sensing characteristics of materials based on PIN and PEDOT. We have successfully fabricated flexible PIN/PVA and PEDOT/PVA hybrid films capable of acting as a freestanding electrode material. The outstanding electrochemical characteristics and mechanical stability of these materials especially PEDOT/PVA film present a broad range of possibilities for designing various types of biomimetic sensing macromolecular motors. In this study, we showcase the fabrication of a simultaneous sensing supercapacitor device, specifically a symmetric solid-state self-sensing motor using the PEDOT/PVA film that can sense the electrical conditions throughout the charging and discharging cycles apart from storing charges efficiently at various working temperatures. Consequently, the device functions as a supercapacitor with integrated temperature-sensing capabilities also, i.e., a sensing motor that functions based on the same electrochemical reaction.

Biological muscles inherently possess a self-sensing ability towards their working environment, using the same neuronal connectivities. This is possible through a distinctive electrochemical reaction taking place within the inter-cellular matrix. This self-awareness is referred to as proprioception. The scientific world has been trying for the last many years to develop an artificial proprioceptive device capable of self-sensing its surroundings using the same connecting

wires. Based on our results, we suggest that the best material model system for designing such proprioceptive devices is the CPs. The combination of CP chain, water, and ions represents the most basic material model system capable of mimicking biological functions. The electrochemical reactions of CPs in aqueous solutions involving electrons, ions, and water molecules that flow between the CP/electrolyte interface resulting in conformational movements, mimic similar events taking place in the biological cells, leading to its self-sensing property.

This similarity of the composition of CPs with the biological cells and simultaneous sensing capability during working can be exploited to mimic the synaptic communication observed in muscles. This is known as artificial synapsis. The simultaneous charge storage and sensing ability of CPs can also be exploited for developing self-sensing energy storage devices like sensing batteries, sensing supercapacitors, etc. They can also be used for the development of

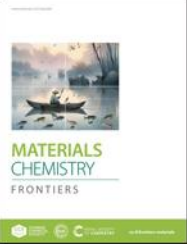
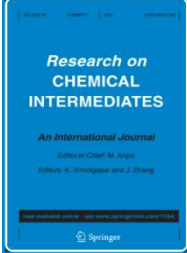



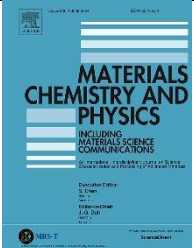

sensing membranes and self-sensing robots. Various future applications discussed in this context are succinctly presented in the following figure.

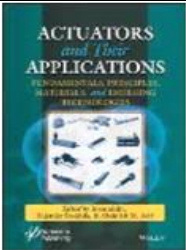

Through this work, we have detailed the properties of CPs in wet states which can lead to a wide range of possibilities for designing proprioceptive devices that can revolutionize future technologies.

LIST OF PUBLICATIONS

International Journals

	<p>L. Rajan, M.P. Sidheekha, A. Shabeeba, T.F. Otero, Y.A. Ismail, Structural electrochemistry of poly(3,4-ethylenedioxythiophene) and its applicability as simultaneous sensor of environmental surroundings: self-sensing electrical, thermal, and chemical working conditions, <i>Journal of Materials Chemistry A</i> 12(8) (2024) 4583-4600</p>
	<p>L. Rajan, M.P. Sidheekha, A. Shabeeba, Y.A. Ismail, Conducting polymers as bio-mimetic multistep macromolecular sensors of working conditions: polyindole/polyvinyl alcohol hybrid film senses electrical and chemical working ambient, <i>Materials Chemistry Frontiers</i> 6(12) (2022) 1706-1718</p>
	<p>L. Rajan, A. Shabeeba, M.P. Sidheekha, Y.A. Ismail, Reaction Induced Conformational Change in Polyindole: Polyindole/PVA Film as Biomimetic Sensors of Temperature and Electrical Energetic Conditions, <i>Chemistry - An Asian Journal</i> 18(22) (2023) e202300742.</p>
	<p>L. Rajan, M.P. Sidheekha, A.K. Shabeeba, S.C. Unnikrishnan, Y.A. Ismail, Reactive sensing capability towards the working electrical and chemical conditions of poly (aniline -co-o-toluidine) copolymers, <i>Res. Chem. Intermed.</i> 48 (2022) 4313 - 4329</p>

	<p>A. Shabeeba, L. Rajan, M.P. Sidheekha, M.S. Thayyil, Y.A. Ismail, Polypyrrole/hydrogel hybrid films as multi sensing supercapacitor electrodes, Journal of Energy Storage 55 (2022) 105724</p>
	<p>M.P. Sidheekha, A.Shabeeba, L. Rajan, M. S. Thayyil, Y.A. Ismail, Conducting Polymer/Hydrogel Hybrid Free-Standing Electrodes for Flexible Supercapacitors Capable of Self-Sensing Working Conditions: Large-Scale Fabrication Through Facile and Low-Cost Route, Engineered Science 23(7) (2023) 890.</p>
	<p>M.P. Sidheekha, L. Rajan, Y.A. Ismail, Reaction driven biomimetic sensing characteristics of polyaniline/chitosan hybrid film: Sensing chemical and electrical reaction conditions, Materials Chemistry and Physics (2022)</p>
	<p>A. Shabeeba, M.P. Sidheekha, L. Rajan, Y.A. Ismail, Flexible hybrid film of polypyrrole incorporated chitosan as a biomimetic multistep electrochemical sensor of working temperature: a potentiodynamic study, RSC Advances 12(49) (2022) 31911-31922</p>
	<p>A. Ajayan, L. Rajan, S. Prakash, Y.A. Ismail, Macromolecular sensing motors from conducting polymers: Polyaniline/methylcellulose composites as stable current sensing supercapacitors, International Journal of Biological Macromolecules 279 (2024) 135312</p>

	<p>Y. A. Ismail, A. K Shabeeba, M. P. Sidheekha, L. Rajan, Conducting polymer/hydrogel systems as soft actuators, <i>Actuators: Fundamentals, Principles, Materials and Applications</i>, Wiley-Scrivener publishers, (2020) 211-252</p>
	<p>Y. A. Ismail, A. Shabeeba, M. P. Sidheekha, L. Rajan, Electroactive Polymer Actuators, <i>Encyclopedia of Polymer Science and Technology</i>, Wiley publishers (2022)</p>
<h3>LIST OF PRESENTATIONS</h3>	
<p>1. Paper presentation (poster) in Advanced Materials and Manufacturing Technologies (AMMT 2023), National Conference organized by the National Institute for Interdisciplinary Science and Technology (NIIST), Thiruvananthapuram, Kerala</p>	
<p>2. Paper presentation (poster) in Frontiers in Chemical Sciences (FCS 2022), International Conference organized by the Department of Chemistry, University of Calicut</p>	